



U.S. Department  
of Transportation  
**Federal Highway  
Administration**

Publication No. FHWA-HIF-23-050

March 2023

Hydraulic Engineering Circular No. 19



# Highway Hydrology: Evolving Methods, Tools, and Data

*Page Intentionally Left Blank*

# Technical Report Documentation Page

1. Report No. FHWA HIF-23-050	2. Government Accession No.	3. Recipient's Catalog No.	
4. Title and Subtitle  Highway Hydrology: Evolving Methods, Tools, and Data		5. Report Date March 2023	
		6. Performing Organization Code	
7. Author(s) Roger Kilgore, A. Tamim Atayee, David Curtis, Jeff Harris, George "Rudy" Herrmann, David Thompson		8. Performing Organization Report No.	
9. Performing Organization Name and Address Kilgore Consulting and Management 2963 Ash Street Denver, CO 80207		10. Work Unit No. (TRAIS)	
		11. Contract or Grant No. DTFH61-17-D-00035	
12. Sponsoring Agency Name and Address Office of Bridges and Structures Federal Highway Administration 1200 New Jersey Avenue, S.E. Washington, D.C. 20590		13. Type of Report and Period Covered Reference Manual September 2020 – June 2022	
		14. Sponsoring Agency Code	
15. Supplementary Notes Project Manager: Stan Woronick, National Highway Institute; Cynthia Nurmi, National Highway Institute Technical Reviewers: Megan Frye, Luis Calderon, Daniel Sharar-Salgado, Joe Krolak Technical and Editorial Assistance: Liberty Smith, Muhammad Sinjar			
16. Abstract This reference manual (HEC-19) provides practical information in the evolving highway hydrology field. The information supports more resilient bridge and roadway design. Understanding of hydrologic behavior also can inform planning, design, operations, and maintenance. Following introductory material in Chapter 1 and policy context for hydrology in Chapter 2, Chapter 3 describes sources of nonstationarity and tools to identify and address changing land use and climate conditions. Chapter 4 provides information on established and emerging low flow metrics and tools that inform a broad range of potential transportation hydrology applications including estimating channel forming discharge, aquatic organism passage, ecosystem assessment, and water quality. The chapter also introduces hyporheic flows and continuous simulation tools. Chapter 5 addresses coincident flooding techniques that consider the combined risk of two sources of flooding at a site. This includes coincident flooding at the confluence of two streams and coastal compound flooding resulting from riverine flooding and storm surge near the coast. Chapter 6 introduces spatially distributed precipitation data sources and analysis tools that support more detailed watershed modeling. Chapter 7 focuses on topics that are of particular interest in specific areas of the country including the effects of wildfires on runoff, karst areas, and paleohydrology.			
17. Key Words Hydrology, Nonstationarity, Low Flow, Channel Forming Discharge, Coincident Flooding, Compound Flooding, Spatially Distributed Precipitation, Wildfire Runoff, Karst Hydrology, Paleohydrology		18. Distribution Statement Unlimited distribution	
19. Security Classification (of this report)  Unclassified	20. Security Classification (of this page) Unclassified	21. No. of Pages  191	22. Price  N/A
Form DOT F 1700.7 (8-72)		Reproduction of completed page authorized	

*Page Intentionally Left Blank*

## Table of Contents

Technical Report Documentation Page.....	i
Table of Contents.....	iii
List of Figures .....	vii
List of Tables .....	xi
Acknowledgments.....	xiii
Notice .....	xiv
Non-Binding Contents.....	xiv
Quality Assurance Statement.....	xiv
Glossary.....	xv
Abbreviations .....	xix
Chapter 1 - Introduction .....	1
1.1 Purpose and Scope .....	1
1.2 Organization .....	3
1.3 Target Audience .....	4
1.4 Units in this Manual .....	4
Chapter 2 - Federal Policy for Hydrology.....	5
2.1 Federal Highways and Hydrology: National Overview.....	5
2.2 FHWA Statutes and Regulations .....	5
2.2.1 FHWA Statute .....	6
2.2.2 FHWA Regulations.....	8
2.3 Other Federal Agency Statutes and Regulations .....	10
2.3.1 Rivers and Harbors Act [33 U.S.C. § 401 and § 403] .....	10
2.3.2 General Bridge Act [33 U.S.C. § 525 through 533].....	10
2.3.3 Department of Transportation Act [Public Law 89-670].....	10
2.3.4 National Environmental Policy Act [42 U.S.C. § 4321, et seq.] .....	11
2.3.5 Clean Water Act [33 U.S.C. § 1251-1387].....	11
2.3.6 Endangered Species Act [16 U.S.C. § 1531-1544].....	11
2.3.7 National Historic Preservation Act [54 U.S.C. 300101 et seq.].....	12
2.3.8 National Flood Insurance Act [42 U.S.C. § 4001 et seq.].....	12
2.3.9 Wild and Scenic Rivers Act [16 U.S.C. § 1271 et seq.].....	12
2.3.10 Fish and Wildlife Coordination Act [16 U.S.C. §§ 661-666c].....	13
2.3.11 Migratory Bird Treaty Act [16 U.S.C. § 703 et seq.].....	13

Chapter 3 - Nonstationarity .....	15
3.1 What is Nonstationarity? .....	15
3.2 Methods for Detecting Nonstationarity .....	18
3.2.1 Nonstationarity in Stream Gage Data .....	18
3.2.1.1 Mann-Kendall Test as Implemented in PeakFQ .....	18
3.2.1.2 USGS Integrated Water Availability Assessment Tool .....	19
3.2.1.3 U.S. Army Corps of Engineers Nonstationarity Detection Tool .....	20
3.2.2 Developing Tools for Nonstationarity Detection .....	22
3.3 Attribution of Nonstationarity .....	24
3.3.1 Watershed Changes .....	24
3.3.2 Climate .....	26
3.4 Assessing the Impact of Nonstationarity on Design Flows .....	26
3.4.1 Levels of Analysis Approach .....	26
3.4.2 Frequency Analysis with a Time-Varying Mean .....	27
3.4.3 Projecting Changes in Precipitation .....	31
3.5 Subdaily Precipitation Projections .....	34
Chapter 4 - Low Flow Hydrology .....	37
4.1 Low Flow Statistical Analysis .....	38
4.1.1 Flood Frequency Curves .....	38
4.1.2 Statistics on Low Flows .....	40
4.1.3 Low Flow Regression Equations .....	41
4.1.4 Flow Duration Analysis .....	44
4.2 Channel Forming Discharge .....	45
4.2.1 Bankfull Discharge .....	46
4.2.2 Specific AEP Discharge .....	48
4.2.3 Effective Discharge .....	48
4.3 Rainfall-Runoff Modeling .....	51
4.3.1 Single Event Modeling .....	52
4.3.2 Continuous Simulation Modeling .....	53
4.3.3 Rainfall-Runoff Software .....	54
4.3.3.1 Hydrologic Modeling System (HEC-HMS) .....	54
4.3.3.2 Storm Water Management Model (SWMM) .....	54
4.3.3.3 Precipitation-Runoff Modeling System (PRMS) .....	54
4.3.3.4 Gridded Surface Subsurface Hydrologic Analysis (GSSHA) .....	54

4.4	AOP/Ecosystem Design Flows .....	55
4.5	Water Quality and First Flush .....	55
Chapter 5 - Coincident Frequency.....		59
5.1	Multivariate Analysis .....	61
5.2	Flooding at River Confluences .....	62
5.2.1	Coincident Flooding Design at Confluences .....	64
5.2.2	Design Examples .....	72
5.2.3	Total Probability Theorem .....	81
5.3	Riverine/Storm Surge (Compound) Flooding .....	84
Chapter 6 - Spatially Distributed Precipitation .....		89
6.1	Point Rainfall Measurement.....	89
6.2	Spatially Distributed Rainfall Measurement.....	91
6.2.1	Radar Rainfall .....	92
6.2.2	Satellite Rainfall .....	93
6.3	Rainfall Estimation .....	94
6.3.1	Basic Principles.....	95
6.3.2	Radar Beam Polarization .....	100
6.4	Multi-Sensor Rainfall Estimation .....	101
6.5	Design Storm Development Using Gridded Precipitation .....	104
6.5.1	Creating Design Storms .....	105
6.5.2	Depth Area Reduction Curves.....	105
6.6	Sources for Historical Precipitation Data.....	108
6.6.1	National Center for Environmental Information.....	109
6.6.2	State and Regional Networks .....	109
6.6.3	MesoWest.....	111
6.6.4	NEXRAD Stage IV Data .....	112
6.6.5	NWS Analysis of Record for Calibration (AORC) Archive.....	112
6.6.6	PRISM .....	112
6.6.7	Private Sector .....	112
6.7	Application of Gridded Precipitation to Hydrology and Hydraulics Models.....	112
6.7.1	Gridded Precipitation Data Sources .....	113
6.7.2	Application to Hydrologic Models .....	114
6.7.3	Application to Integrated Hydrologic and Hydraulic Models .....	117

Chapter 7 - Special Topics .....	119
7.1    Wildfires and Runoff .....	119
7.1.1    Wildfire Effects on Hydrology .....	121
7.1.1.1    Infiltration Reduction .....	121
7.1.1.2    Sediment Bulking.....	122
7.1.2    Methodologies and Analytical Approaches .....	124
7.1.3    Mitigation and Countermeasures.....	126
7.2    Karst Terrain.....	129
7.2.1    Estimating Runoff.....	131
7.2.2    Mitigation.....	135
7.3    Paleohydrology .....	137
7.3.1    The Science of Paleohydrology .....	138
7.3.2    Historical Floods, Paleofloods, and Statistical Analyses .....	142
7.3.3    Scientific Techniques .....	143
7.3.3.1    Dendrochronology .....	143
7.3.3.2    Radiocarbon Dating.....	143
7.3.3.3    Optically Stimulated Luminescence .....	144
7.3.3.4    Speleothems .....	145
7.3.4    Limitations and Conditions .....	145
7.3.5    Case Study .....	146
Literature Cited .....	153
Appendix A - Units .....	163
Appendix B - Introduction to Multivariate Analysis .....	165
B.1    General Formulation of the Problem .....	165
B.2    Multivariate Distributions.....	166
B.3    Copulas .....	167



## List of Figures

Figure 1.1. Balancing economic, social, and environment aspects for sustainability. Source: Department of Environment Farming, and Rural Affairs United Kingdom. ....	1
Figure 3.1. Annual peak streamflow series from Pond Creek, Kentucky (USGS 03302000).....	16
Figure 3.2. Annual peak streamflow series from Mercer Creek, Washington (USGS 1212000). ....	17
Figure 3.3. Annual peak streamflow series from Newaukum Creek, Washington (USGS 12108500). ....	17
Figure 3.4. USGS IWAA web portal, displaying portions of Washington State. ....	20
Figure 3.5. Stream gage and watershed information and details of a trend analysis for the annual peak streamflow series for Mercer Creek near Bellevue, Washington (USGS 12120000). ....	21
Figure 3.6. Results from application of the USACE Nonstationary Detection Tool on annual peak streamflows from Mercer Creek near Bellevue, Washington (USGS 12120000). ....	22
Figure 3.7. Trend analysis produced by USACE Nonstationary Detection Tool for annual peak streamflow data from Mercer Creek near Bellevue, Washington (USGS 1212000). ....	23
Figure 3.8. Results from Pettit Test using the USACE Nonstationary Detection Tool on annual peak streamflow data from Mercer Creek near Bellevue, Washington (USGS 1212000). ....	24
Figure 3.9. Annual peak flow series from Pond Creek, Kentucky, illustrating nonstationarity.....	25
Figure 3.10. Annual peak streamflow series from Stockley Branch at Stockley, Delaware (USGS 01484500). ....	30
Figure 3.11. Ten-step process for projecting 24-hour precipitation quantiles. ....	32
Figure 4.1. HEC-SSP annual peak flow frequency curve for the Cosumnes River at Michigan Bar (USGS 11335000).....	39
Figure 4.2. Low flow tool selection flowchart. Source: USEPA (2018). ....	42
Figure 4.3. Example flow duration curve. Source: FHWA (2022). ....	45
Figure 4.4. Bankfull stage estimation from width-depth ratio. ....	47
Figure 4.5. Bankfull stage estimation from a rating curve. Source: after FISRWG (1998). ....	47
Figure 4.6. Effective discharge/channel forming flow. ....	49
Figure 4.7. Downstream daily flow duration curve, River Wye, UK, 1937-1962. Source: Hey (1975) used by permission. ....	50
Figure 4.8. Sample single event time window. ....	52
Figure 4.9. Sample continuous simulation time window. ....	53
Figure 5.1. Confluence of the Big Sioux River with the Missouri River at Sioux City, Iowa. ....	59

Figure 5.2. The Ashley, Cooper, and Wando Rivers entering Charleston Harbor (South Carolina).....	60
Figure 5.3. Influence reach schematic.....	63
Figure 5.4. Schematic illustrating backwater extent.....	65
Figure 5.5. Hypothetical flow frequency curves. ....	71
Figure 5.6. Confluence of the Nisqually River and Mineral Creek, Washington. ....	73
Figure 5.7. Confluence of the Raritan River and Middle Brook, New Jersey.....	77
Figure 5.8. Hypothetical probability density function.....	82
Figure 5.9. Hypothetical cumulative distribution function. ....	83
Figure 6.1. Rainfall map created from Thiessen polygon interpolation. ....	91
Figure 6.2: Rainfall map created from radar rainfall estimates.....	91
Figure 6.3. NWS WSR-88D radar network. Source: NWS.....	92
Figure 6.4. NWS radar image, Nashville, Tennessee.....	93
Figure 6.5. NWS national radar rainfall (left) and NOAA national satellite rainfall (right). Source: NWS. ....	94
Figure 6.6. Comparison of gage interpolated (left) and radar rainfall data (right). ....	94
Figure 6.7. Conceptualization of radar detection of rainfall.....	95
Figure 6.8. Conceptualization of radar “slice” during a volumetric scan.....	96
Figure 6.9. Typical NWS NEXRAD radar dome. Source: NWS. ....	96
Figure 6.10. Single versus multi-radar mosaic. Source: NWS. ....	97
Figure 6.11. Example NWS radar mosaic. Source: NWS. ....	98
Figure 6.12. Examples of radar coverage issues. Source: University Corporation for Atmospheric Research.....	98
Figure 6.13. Radar coverage quality over Sopori Wash watershed near Tucson, Arizona.....	99
Figure 6.14. Conceptualization of single polarization radar. Source: NWS.....	100
Figure 6.15. Conceptualization of dual polarization radar. Source: NWS.....	101
Figure 6.16. Example radar–gage comparison (storm total).....	103
Figure 6.17. Cumulative rainfall comparison (inrastorm). ....	104
Figure 6.18. Example nested design storm. ....	106
Figure 6.19. Conceptual diagram of hydrologic application to develop design flows. Source: NWS. ....	106
Figure 6.20. Depth area reduction factor from TP 29. Source: NWS. ....	107
Figure 6.21. Comparison of 1-hour DARFs. Source: NWS.....	108
Figure 6.22. Regional climate centers. Source: NOAA. ....	109
Figure 6.23. Florida water management districts. Source: Florida Department of Environmental Projection. ....	111

Figure 6.24. Watershed with individual radar pixels shown. ....	115
Figure 6.25. Watershed with sub-watershed averages shown.....	116
Figure 6.26. Gridded precipitation across the Sopori Wash watershed. ....	118
Figure 6.27. Accumulated precipitation across the Sopori Wash watershed.....	118
Figure 7.1. Placerita Canyon Road after the Foothill Fire, October 10, 2004. Source: Los Angeles County Department of Public Works.....	120
Figure 7.2 Diamond Mountain Road near Antelope Lake, California. Source: U.S. Forest Service.....	122
Figure 7.3. Post-wildfire 2010 debris flow from San Gabriel Mountains, California. Source: NRCS (2016). ....	123
Figure 7.4. Clearing of a post-wildfire debris flow that closed I-70 in Glenwood Canyon, Colorado, in 2021. ....	124
Figure 7.5. Example of bulked flow hydrograph.....	125
Figure 7.6. Temporary emergency mitigation to prevent further post-wildfire sediment and rock flow onto I-70 in Glenwood Canyon Colorado.....	126
Figure 7.7. Debris basin. Source: Los Angeles County Department of Public Works.....	127
Figure 7.8. Rail and timber structure. Source: Los Angeles County Department of Public Works. ....	128
Figure 7.9. Crib dam. Source: USGS. ....	129
Figure 7.10. Karst and potential karst areas in soluble rock in the contiguous United States. Source: Epstein and Johnson (2003). ....	130
Figure 7.11. Karst and potential karst areas in soluble rock in (A) Alaska, (B) Hawaii, and (C) Puerto Rico and the Virgin Islands. Source: Weary and Doctor (2014). ....	131
Figure 7.12. Seco sinkhole entrance, Edwards Aquifer, Texas. Source: Edwards Aquifer Authority (2022). ....	132
Figure 7.13. Karst cave system, Texas. Source: Desert Sky Engineering and Hydrology and used by permission. ....	132
Figure 7.14. Burd Run watershed, south central Pennsylvania. Source: Hawkins and Weichel (2015).....	134
Figure 7.15. Big Spring Creek watershed, south central Pennsylvania. Source: Hawkins and Weichel (2015).....	134
Figure 7.16. Sinkhole repair with an impervious cover. Source: PennDEP (2012).....	136
Figure 7.17. Sinkhole repair with a pervious cover. Source: PennDEP (2012). ....	137
Figure 7.18. Relationship of paleoflood hydrology to related sciences. ....	139
Figure 7.19. Potential PSI in a flood deposit: a tree branch protruding from a dark sediment layer. Source: Desert Sky Engineering and Hydrology and used by permission.....	141
Figure 7.20. Potential PSI in a flood deposit: interspersed coarse and fine sediment layers indicating different flood deposits. Source: Desert Sky Engineering and Hydrology and used by permission. ....	141

Figure 7.21. Speleothems, stalagmites, and stalactites. Source: Desert Sky Engineering and Hydrology and used by permission. ....	146
Figure 7.22. View of the lower of the rock shelters (#1). Image used by permission of Desert Sky Engineering and Hydrology. ....	148
Figure 7.23. Rock shelter #2. Image used by permission of Desert Sky Engineering and Hydrology. ....	148
Figure 7.24. Canyon wall, including an inaccessible ledge, and showing crevices and unoccupied shelters with overhangs. Image used by permission of Desert Sky Engineering and Hydrology.....	149
Figure 7.25. Stage/discharge curve at the former gage location, with stage translated from the tributary canyon to the gage. Source: Desert Sky Engineering and Hydrology and used by permission. ....	151
Figure B.1. Example of a joint probability surface for the Gumbel-Hougaard copula. ....	168

## List of Tables

Table 3.1. Flood frequency estimates for Stockley Branch with and without adjusting for nonstationarity. ....	31
Table 4.1. Low flow methods and applications. ....	38
Table 4.2. StreamStats results for ungaged Linda Creek at Hazel Avenue, Orangevale, California. ....	43
Table 5.1. Influence reach determination options. ....	66
Table 5.2. Watershed categories. ....	67
Table 5.3. Return period combinations for the 10-year joint return period. ....	68
Table 5.4. Return period combinations for the 25-year joint return period. ....	68
Table 5.5. Return period combinations for the 50-year joint return period. ....	69
Table 5.6. Return period combinations for the 100-year joint return period. ....	69
Table 5.7. Return period combinations for the 500-year joint return period. ....	70
Table 5.8. Nisqually/Mineral regression constants. ....	73
Table 5.9. Nisqually/Mineral flow range. ....	74
Table 5.10. Nisqually/Mineral influence reach determination. ....	74
Table 5.11. Nisqually/Mineral flows. ....	75
Table 5.12. Nisqually/Mineral flow combinations. ....	76
Table 5.13. Stage and velocity for Nisqually/Mineral combinations. ....	76
Table 5.14. Raritan/Middle Brook regression constants. ....	78
Table 5.15. Raritan/Middle Brook watershed data. ....	78
Table 5.16. Raritan/Middle Brook flow range. ....	78
Table 5.17. Raritan/Middle Brook influence reach determination. ....	79
Table 5.18. Raritan/Middle Brook flows. ....	80
Table 5.19. Raritan/Middle Brook flow combinations. ....	80
Table 5.20. Stage and velocity for Raritan/Middle Brook combinations. ....	81
Table 5.21. AEP bins. ....	83
Table 6.1. Example radar–gauge comparison. ....	102
Table 6.2. Statewide mesonets. Adapted from Mahmood et al. (2017). ....	110
Table 6.3. Gridded precipitation data sources. ....	113
Table 7.1. Coefficients for USGS regression equation (Flippo 1977). ....	133
Table 7.2. Karst loss coefficients (Laughland 1996). ....	135
Table 7.3. Gage heights and flows. ....	150

*Page Intentionally Left Blank*

## Acknowledgments

The cover image is the Eagles Nest Canyon (Texas). (Source: Ancient Southwest Texas Project, Texas State University. Used by permission.)

Unless noted otherwise, the authors developed all photographs and graphics in this document and give permission for their use in this document.

In Figures 5.1, 5.2, 5.6, and 5.7, the base images are the copyright property of Google® Earth™ and can be accessed from <https://www.google.com/earth> (Google 2020). Overlays and annotations were developed by the authors. Third party data providers acknowledged by Google include: Maxar Technologies and CNES/Airbus (Figures 5.1, 5.2, 5.6, and 5.7).

Images used from the public domain are designated by their source.

## **Notice**

This document is disseminated under the sponsorship of the U.S. Department of Transportation (USDOT) in the interest of information exchange. The U.S. Government assumes no liability for the use of the information contained in this document. This manual does not constitute a standard, specification, or policy.

The U.S. Government does not endorse products or manufacturers. Trademarks or manufacturers' names appear in this report only because they are considered essential to the objective of the document. They are included for informational purposes only and are not intended to reflect a preference, approval, or endorsement of any one product or entity.

## **Non-Binding Contents**

The contents of this document do not have the force and effect of law and are not meant to bind the public in any way. This document is intended only to provide clarity to the public regarding existing requirements under the law or agency policies.

## **Quality Assurance Statement**

The Federal Highway Administration (FHWA) provides high-quality information to serve Government, industry, and the public in a manner that promotes public understanding. The FHWA uses standards and policies to ensure and maximize the quality, objectivity, utility, and integrity of its information. The FHWA periodically reviews quality issues and adjusts its programs and processes to ensure continuous quality improvement.



## Glossary

4B3:	Partial-duration analysis to determine the lowest 4-day average flow that occurs (on average) once every 3 years.
7Q10:	Annual duration analysis to determine the lowest 7-day average flow that occurs (on average) once every 10 years.
Annual Duration:	Based on analysis of the annual peak values for each year of record.
Annual Exceedance Probability:	The probability that the magnitude of the random variable (e.g., annual maximum flood peak) will be equaled or exceeded each year.
Archaeology:	The study and reconstruction of past human life and activities.
Bed Gradation:	The percentage breakdown of riverbed material usually listed by the distribution of particle size found in the bed material.
Bulking:	Increasing the water flow to account for high concentrations of sediment in the flow.
Coincident Flow:	The combination of peak flows or flow hydrographs at a confluence.
Confluence:	The junction of two or more streams.
Debris:	Floating or submerged material, such as logs, other vegetation, and trash, transported by a stream.
Debris Flow:	Fluid flow controlled primarily by the composition of the sediment/debris mixture. Debris flow contains approximately 40 to 50 percent sediment by volume.
Denuded:	Stripped of its coverings and made bare.
Drainage Basin:	An area confined by drainage divides, often having only one outlet for flow (catchment, watershed).
Flashy Stream:	Stream characterized by rapidly rising and falling hydrograph stages. Typically associated with mountain streams, highly urbanized catchments, and arid environments.
Flood Frequency Curve:	A graph indicating the probability of occurrence that the annual flood flow equals or exceeds a given magnitude, or the recurrence interval corresponding to a given magnitude.
Floodplain:	Nearly flat, alluvial lowland bordering a stream or coastal waterbody that is subject to frequent inundation by floods.
Flow Duration Curve:	A plot showing the percentage of time that a certain flow in the river is equaled or exceeded.
Fluvial geomorphology:	The science dealing with the morphology (form) and dynamics of streams and rivers.
Hydrograph:	The graph of stage or flow over time.

Hydrology:	The science concerned with the occurrence, distribution, and circulation of water on the Earth.
Hydrophobicity:	Tendency to resist wetting or infiltration of moisture.
Joint Probability:	The probability of occurrence of two or more events. The events may be independent or may be correlated.
Karst:	A landscape and its subsurface characterized by flow through dissolutionally modified bedrock and characterized by irregular limestone with sinks, underground streams, and caverns.
Least Squares Regression:	A procedure for fitting a mathematical function that minimizes the sum of the squares of the differences between the predicted and measured values.
Level of Significance:	A statistical concept that equals the probability of making a specific error, namely of rejecting the null hypothesis when, in fact, it is true. The level of significance is used in statistical decision-making.
Maximum Likelihood Estimation:	A mathematical method of obtaining the parameters of a probability distribution by optimizing a likelihood function that yields the most likely parameters based on the sample information.
Mesonet	Observation network configured to observe mesoscale events.
Mesoscale	Relating to a meteorological phenomenon of intermediate size (approximately 6.2 to 620 miles (10 to 1000 kilometers) in horizontal extent).
Method-of-Moments Estimation:	A method of fitting the parameters of a probability distribution by equating them to the sample moments.
Moving-Average Smoothing:	A statistical method of smoothing a time or space series in which the nonsystematic variation is eliminated by averaging adjacent measurements. The smoothed series represents the systematic variation.
Nonhomogeneity:	A characteristic of time or space series that indicates the moments are not constant throughout the length of the series.
Nonparametric Statistics:	A class of statistical tests that do not require assumptions about the population distribution.
Nonstationarity:	A characteristic of time series data where statistical parameters of the series change over time. Such changes over time complicate the use of historical data for estimating future conditions.
Order-Theory Statistics:	A class of statistical methods in which the analysis is based primarily on the order relations among the sample values.

Return Period:	Over the long-term, the average length of time between occurrences in which the value of a random variable (e.g., flood magnitude) is equaled or exceeded. The return period is the inverse of the annual exceedance probability.
Paleoclimatology:	The study of ancient climates, prior to the widespread availability of instrumental records.
Paleohydrology:	The scientific study of the movement, distribution, and quality of water on Earth during previous periods of its history.
Parametric Statistics:	A class of statistical tests in which their derivation involved explicit assumptions about the underlying population.
Partial-duration Analysis:	A frequency analysis method that uses all floods of record above a threshold to derive a probability function to represent the data.
Risk:	The consequences associated with hazards considering the probabilities of those hazards. More specifically for this document, risks are the consequences associated with the probability of flooding including interactions with encroachments.
Runoff:	The portion of a rainfall event discharged from a watershed into the stream network during and immediately following the rainfall of either perennial or intermittent form.
Tidally-dominated River:	A river location where the flow and stage are affected by the astronomical tides including flow reversals under normal tidal conditions.
Tidally-influenced River:	A river location where the flow and stage are modulated by the astronomical tides but where the flow does not reverse under normal tidal conditions.

*Page Intentionally Left Blank*

## Abbreviations

AASHTO	American Association of State Highway and Transportation Officials
ACWI	Advisory Committee on Water Information
AEP	Annual Exceedance Probability
AMS	Annual Maximum Series
AOP	Aquatic Organism Passage
AORC	Analysis of Record for Calibration Temperature and Precipitation Records
ARI	Annual Recurrence Interval
ARS	Agricultural Research Service
BAER	Burned Area Emergency Response
BF	Bulking Factor
BFE	Base Flood Elevation
BFI	Base Flow Index
BMP	Best Management Practice
CDF	Cumulative Distribution Function
CDR	Climate Data Record
CFR	Code of Federal Regulations
CHS	Coastal Hazards System
CLOMR	Conditional Letter of Map Revision
CMIP	Coupled Model Intercomparison Project
CMORPH	Climate Prediction Center Morphing Technique satellite-based precipitation
CN	Curve Number
CWA	Clean Water Act
DARF	Depth Area Reduction Factor
DEM	Digital Elevation Model
DOT	Department of Transportation
DSS	Hydrologic Engineering Center Data Storage System
EMA	Expected Moments Algorithm
EO	Executive Order
ERDC	Engineer Research and Development Center
FAHP	Federal-Aid Highway Program
FDC	Flow Duration Curve
FEMA	Federal Emergency Management Agency

FHWA	Federal Highway Administration
FIRM	Flood Insurance Rate Map
FIS	Flood Insurance Study
FTP	File Transfer Protocol
GARR	Gage Adjusted Radar Rainfall estimates
GCM	Global Climate Model
GDAL	Geospatial Data Abstraction Library
GIS	Geographic Information System
GPS	Global Positioning System
G/R	Gage/Radar ratio
GSSHA	Gridded Surface Subsurface Hydrologic Analysis
H&H	Hydrology and Hydraulics
HDG	Highway Drainage Guidelines
HDS	Hydraulic Design Series
HEC	Hydraulic Engineering Circular
HEC	Hydrologic Engineering Center
HEC-SSP	USACE Statistical Software Package
HMS	Hydrologic Modeling System
IDF	Intensity-Duration-Frequency
KFWS	Call sign for NWS WSR-99D Radar near Fort Worth, Texas
LTP	Long-Term Persistence
MetVue	Meteorological Visualization Utility Engine
MPE	Multisensor Precipitation Estimate
NASA	National Aeronautics and Space Administration
NCDC	National Climatic Data Center
NCEI	National Centers for Environmental Information
NCEP	National Centers for Environmental Prediction
NCHRP	National Cooperative Highway Research Program
NED	National Elevation Database
NEH	National Engineering Handbook
NEPA	National Environmental Policy Act
NEXRAD	Next-Generation Radar
NFIP	National Flood Insurance Program
NHI	National Highway Institute
NLDAS-v2	North American Land Data Assimilation System version 2

NOAA	National Oceanic and Atmospheric Administration
NPDES	National Pollutant Discharge Elimination System
NRC	National Research Council
NRCS	National Resources Conservation Service
NSS	National Streamflow Statistics
NWIS	National Water Information System
NWS	National Weather Service
O&M	Operations and Maintenance
ODFW	Oregon Department of Fish and Wildlife
OSL	Optically Stimulated Luminescence
OSU	Oregon State University
PDF	Probability Density Function
PeakFQ	USGS Peak Flow Frequency Analysis Software
PFDS	Precipitation Frequency Data Server
PM	Post Meridian
PRISM	Parameter-elevation Regressions on Independent Slopes Model
PRMS	Precipitation-Runoff Modeling System
PSI	Paleostage Indicator
Radar	Radio Detection and Ranging
RAS	River Analysis System
RCM	Regional Climate Model
RFC	Rainfall Frequency Curve
ROW	Right-of-Way
rpm	Revolutions per minute
SCS	Soil Conservation Service (now NRCS)
SELDM	Stochastic Empirical Loading and Dilution Model
SFHA	Special Flood Hazard Area
SIR	Scientific Investigation Report
STAR	Center for Satellite Applications and Research
SWMM	Storm Water Management Model
TC	Tropical Cyclone
TL	Thermal Luminescence
TP	Technical Paper
USACE	U.S. Army Corps of Engineers
USBR	U.S. Bureau of Reclamation

USDA	U.S. Department of Agriculture
USDOJ	U.S. Department of the Interior
USDOT	U.S. Department of Transportation
USEPA	U.S. Environmental Protection Agency
USFS	U.S. Forest Service
USFWS	U.S. Fish and Wildlife Service
USCG	U.S. Coast Guard
USGS	U.S. Geological Survey
VIC	Variable Infiltration Capacity
WMO	World Meteorological Organization
WRDA	Water Resources Development Act
WREG	Weighted-Multiple-Linear Regression Program
WSR-88D	Weather Surveillance Radar – 88D (88 indicates 1988 as the radar design year. D indicates Doppler.)



# Chapter 1 - Introduction

As the understanding of the interactions between roadway infrastructure and hydrology grows, transportation planners, designers, and engineers face new and evolving challenges. This manual provides technical information on evolving methods, tools, and data sources useful for highway hydrology. It complements the Federal Highway Administration (FHWA) manual, *Highway Hydrology*, Hydraulic Design Series Number 2 (HDS-2) (FHWA 2002). This chapter describes the purpose and scope, organization, target audience, and units used in the manual.

## 1.1 Purpose and Scope

This manual provides a general overview and information for development of hydrologic estimates to support design of resilient bridge and roadway transportation infrastructure. The manual covers new hydrologic tools that are becoming more widely available and new topic areas increasingly applicable to highway and bridge projects. Some of these topics represent challenges faced in specific areas of the country.

This manual supports planning, implementation, and stewardship of sustainable, resilient, and reliable transportation networks. The FHWA describes sustainability as considering three primary values or principles: social, environmental, and economic (FHWA 2022a). The goal of sustainability is the satisfaction of basic social and economic needs, both present and future, and the responsible use of natural resources, all while maintaining or improving the well-being of the environment on which life depends. Figure 1.1 illustrates these three values.

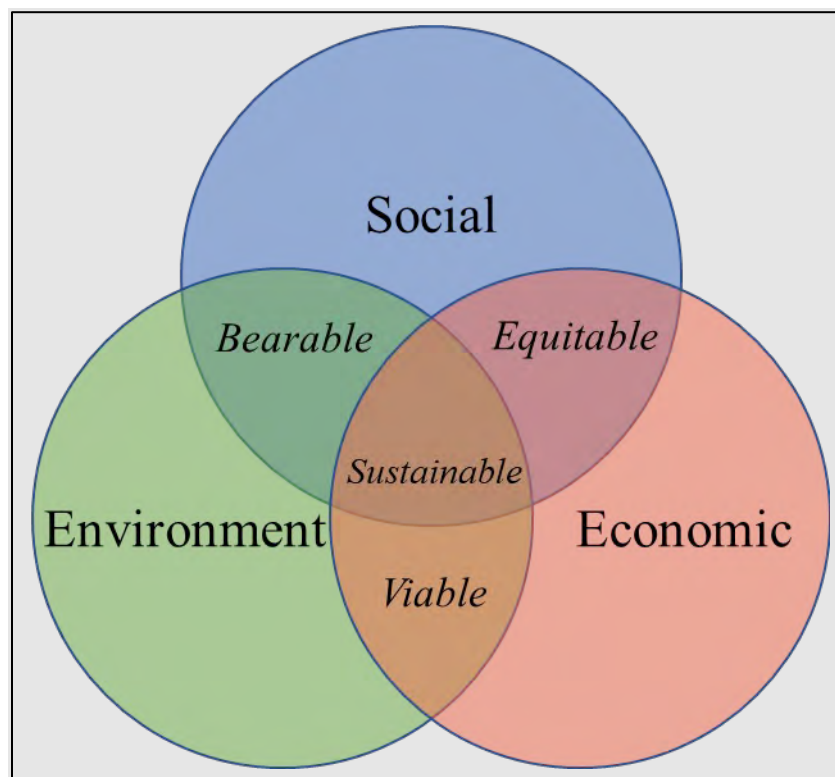


Figure 1.1. Balancing economic, social, and environment aspects for sustainability. Source: Department of Environment Farming, and Rural Affairs United Kingdom.

Commonly, society views sustainability through a lens of balancing the needs of the environment with the economic needs of roadway and bridge development. This balancing results in the identification of viability as shown in the figure, but this is only part of the picture. Balancing the environment with social values results in what is bearable, or acceptable, by both society and the environment, while balancing the social and economic results in what is equitable.

Sustainability results when all three values (social, environmental, and economic) are in balance. Planners and analysts sometimes refer to these three dimensions – economic, environment, and social – as the “triple bottom line” of sustainability. A sustainable approach to highways means helping decision makers make balanced choices among economic, social, and environmental values that will benefit current and future road users. For FHWA, a sustainable highway project satisfies basic social and economic needs, makes responsible use of natural resources, and maintains or improves the well-being of the environment.

This manual also addresses issues related to hydrologic modeling to facilitate more resilient and reliable hydraulic designs within which potential future hydrologic and meteorologic conditions are identified and accommodated. Reliability is tied to resilience because a resilient transportation network is safer and less susceptible to delays and failures.

FHWA Order 5520 (FHWA 2014) states that “it is FHWA’s policy to strive to identify the risks of climate change and extreme weather events to current and planned transportation systems. The FHWA will work to integrate consideration of these risks into its planning, operations, policies, and programs in order to promote preparedness and resilience; safeguard Federal investments; and ensure the safety, reliability, and sustainability of the Nation’s transportation systems.”

The United States Department of Transportation (USDOT) “Climate Action Plan” affirms that resilient and reliable designs are essential to addressing the significant and growing risk presented by climate change (USDOT 2021). Developed pursuant to Section 211 of Executive Order 14008 (86 FR 7619 (Jan. 27, 2021)), the Climate Action Plan presents USDOT’s plan to address the significant and growing risk presented by climate change. The FHWA Policy Framework on “Using Bipartisan Infrastructure Law Resources to Build a Better America” also highlights FHWA’s policy to make the transportation network more sustainable and resilient to a changing climate (FHWA 2021).

In the transportation context, this climate risk is many-faceted, including risks to the safety, effectiveness, equity, and sustainability of the Nation’s transportation infrastructure and the communities it serves. The USDOT recognizes that the United States has a “once-in-a-

### Resilience

With respect to a project, the FHWA defines “resilience” as a project with the ability to anticipate, prepare for, and or adapt to changing conditions and or withstand, respond to, and or recover rapidly from disruptions, including the ability: (A) to resist hazards or withstand impacts from weather events and natural disasters, or reduce the magnitude or duration of impacts of a disruptive weather event or natural disaster on a project; and (B) to have the absorptive capacity, adaptive capacity, and recoverability to decrease project vulnerability to weather events or other natural disasters. 23 U.S.C. § 101(a)(24) (added by Sec. 11103 of the Bipartisan Infrastructure Law (BIL), enacted as the Infrastructure Investment and Jobs Act, Pub. L. 117-58 (Nov. 15, 2021)). See also FHWA Order 5520 (FHWA 2014).

generation” opportunity to address this risk, which is increasing over time (USDOT 2021; see also [Executive Order 14008 on Tackling the Climate Crisis at Home and Abroad, 86 FR 7619 \(2021\)](#)).

Addressing the risk of climate change is also closely interlinked with advancing transportation equity because of the disproportionate impacts of climate change on vulnerable populations, including older adults, children, low-income communities, and communities of color. Past Federal transportation investments have too often failed to consider transportation equity for all community members, including traditionally underserved and underrepresented populations (USDOT 2022). “Underserved populations” include minority and low-income populations but may also include many other demographic categories that face challenges engaging with the transportation process and receiving equitable benefits. (See FHWA 2015.) The USDOT has committed to pursuing a comprehensive approach to advancing equity for all (USDOT 2022; see also FHWA 2021a; and Executive Order 13985, 86 FR 7009 (2021)). Equity in transportation seeks the consistent and systematic fair, just, and impartial treatment of all individuals, including individuals who belong to traditionally underserved communities or populations (USDOT 2022).

The FHWA encourages the advancement of projects that address climate change and sustainability (FHWA 2021). To enable this, FHWA encourages consideration of climate change and sustainability throughout the planning and project development process, including the extent to which Federal-aid projects align with the President’s greenhouse gas reduction, climate resilience, and environmental justice commitments.

The FHWA believes that this manual will be useful for aligning and integrating these concepts and components of sustainability within the context of highways and the riverine environment. Such alignments will consist of both direct and indirect interstices and situations.

## **1.2 Organization**

This manual consists of seven chapters, a glossary, list of acronyms, reference section, and two appendices. This chapter, **Chapter 1**, provides discussion of the purpose and scope, organization, target audience, and units.

**Chapter 2** provides an overview of Federal policy as it relates to highway hydrology. This context and the series of statutes and regulations on which it is based informs the hydrologic and hydraulic design of transportation infrastructure assets.

**Chapter 3** describes stationarity and nonstationarity. Historical use of hydrologic data assumes that past patterns of precipitation and flow will continue in the future (stationarity). The chapter describes identification of nonstationarity and how designers can address it.

**Chapter 4** outlines a range of hydrologic applications that use low flow hydrology and discusses tools for estimating low flows. Applications include bankfull flow estimates, sediment transport analyses, stream restoration projects, aquatic organism passage design, ecosystem assessment, and water quality analyses.

**Chapter 5** describes detailed methods and information for analyzing coincident flooding. The chapter addresses two primary types of coincident flooding: 1) flooding at confluent streams and 2) coincident occurrence of rainfall based flooding and coastal storm surge (known as coastal compound flooding).

**Chapter 6** outlines evolving sources of spatial precipitation data and tools for rainfall-runoff analysis using spatial precipitation.

**Chapter 7** describes topics of regional or special interest including wildfires and runoff, Karst terrain, and paleohydrology.

### **1.3 Target Audience**

The target audience includes Federal, State, and local highway agencies with responsibility for developing or using hydrology to support roadway and bridge planning, design, construction, and operations and maintenance. Others responsible for planning, operating, and maintaining roadways and bridges, as well as those interested in the environmental performance and resilience of transportation infrastructure, may also find this a useful reference.

This manual does not have the force and effect of law and it is not meant to bind the public in any way. The FHWA intends any descriptions of processes and approaches to provide illustrative insights into the underlying scientific and engineering concepts and practices rather than any proscribed guidance or requirements.

### **1.4 Units in this Manual**

This manual uses customary (English) units. However, in limited situations both customary units and SI (metric) units are used or only SI units are used because these are the predominant measure used nationwide and globally for such topics. In these situations, the manual provides the rationale for the use of units. Appendix A summarizes information on units and unit conversions.

## Chapter 2 - Federal Policy for Hydrology

Federal policy related to hydrology sets the context for planning, design, construction, and operations and maintenance of roadways and their associated stormwater drainage infrastructure. This chapter provides background on applicable FHWA specific statutes and regulations and provides an overview of other Federal statutes and regulations that may affect roadway projects and hydrology.

### Context for Roadways and Hydrology

Federal policy—in the form of statutes and regulations—establishes the context and parameters for the development of transportation infrastructure that serves to facilitate the movement of both people and goods. Taken together, these statutes and regulations, administered by multiple federal agencies, reflect national values for economic well-being and environmental stewardship. Hydrology plays a role in achieving the goals of these statutes and regulations. For example, hydrologic analyses are needed to establish the overtopping and base flood magnitudes as per 23 CFR Part 650.117 (content of design studies) and may be needed to evaluate habitat impacts under the Endangered Species Act.

### 2.1 *Federal Highways and Hydrology: National Overview*

The FHWA has the primary responsibility for Federal policy on highways. Legislation for the Federal road system dates back over a century. The Federal Aid Road Act of 1916 created the Federal-aid Highway Program, which funded State highway agencies so they could make road improvements “to get the farmers out of the mud.” This 1916 Act charged the Bureau of Public Roads with implementing the program. The growth of the Federal highway system, including the addition of the Interstate Highway System, led to concerns of the effect of highways on the environment, city development, and public mass transit. This led to the 1966 establishment of the U.S. Department of Transportation (USDOT) in the Department of Transportation Act of 1966 (Public Law 89-670). The same enabling legislation renamed the Bureau of Public Roads to the FHWA. Currently, the FHWA continues to administer Federal policy on highways, and also coordinates extensively with other Federal agencies on environmental policies and permits, floodplains, and other compliance issues related to highway program and project delivery.

Other agencies influence hydrology policy. At the Federal level, the Federal Emergency Management Agency (FEMA) oversees the National Floodplain Insurance Program (NFIP). The U.S. Fish and Wildlife Service (USFWS) and the National Oceanic and Atmospheric Administration (NOAA) National Marine Fisheries Service (NMFS) administer and enforce the Endangered Species Act (ESA). Almost every project involving work or activities in rivers is subject to the Clean Water Act (CWA) of 1972, which the U.S. Environmental Protection Agency (USEPA) administers in coordination with State governments.

### 2.2 *FHWA Statutes and Regulations*

The FHWA provides financial and technical assistance to State and local governments to ensure that U.S. roads and highways continue to be among the safest and most technologically sound in the world. The FHWA authority for the subject matter of this manual includes the following statutes

and regulations. The section below provides a synopsis of these various authorities as well as pertinent Congressional findings and statements, policy, and guidance.

### 2.2.1 FHWA Statute

The FHWA generally operates under the statutory authority of Title 23 (Highways) of the United States Code (U.S.C.). For the purposes of this manual, relevant sections include:

- **Standards [23 U.S.C. § 109].** It is the intent of Congress that federally funded projects to resurface, restore, and rehabilitate highways shall “be constructed in accordance with standards to preserve and extend the service life of highways and enhance highway safety.” [23 U.S.C. § 109(n)]. Designs for new, reconstructed, resurfaced, restored, or rehabilitated highways on the National Highway System must consider, among other criteria, the “constructed and natural environment of the area.” [Id. at (c)(1)(a)].
- **Maintenance [23 U.S.C. § 116].** Preventive maintenance is eligible for Federal assistance under Title 23 if a State Department of Transportation (SDOT) can demonstrate that it is a “cost-effective means of extending the useful life of a Federal-aid highway.” [23 U.S.C. § 116(e).]
- **National highway performance program [NHPP] [23 U.S.C. § 119].** The NHPP allows FHWA to provide Federal-aid funds for “construction, replacement ..., rehabilitation, preservation, and protection (including ... protection against extreme events) of bridges on the National Highway System.” [23 U.S.C. § 119(d)(2)(B)]. The NHPP also allows Federal-aid funds for “[construction, replacement ..., rehabilitation, preservation, and protection (including ... protection against extreme events) of tunnels on the National Highway System.]” [Id. at (d)(2)(C)].
- **Surface transportation block grant [STBG] program [23 U.S.C. § 133].** The STBG program allows FHWA to provide Federal-aid funds for protection of “bridges (including approaches to bridges and other elevated structures) and tunnels on public roads” including “painting, scour countermeasures, seismic retrofits, impact protection measures, security countermeasures, and protection against extreme events.” [23 U.S.C. § 133(b)(10)]. The STBG program also allows Federal-aid funds for “inspection and evaluation of bridges and tunnels and other highway assets.” [Id.]
- **Metropolitan transportation planning [23 U.S.C. § 134].** In the context of metropolitan transportation planning, Congress has found that it “is in the national interest ... to encourage and promote the safe and efficient management, operation, and development of surface transportation systems ... within and between States and urbanized areas” including taking “resiliency needs” into consideration. [23 U.S.C. § 134(a)(1)].
- **National bridge and tunnel inventory and inspection standards [23 U.S.C. § 144].** Congress has found that “continued improvement to bridge conditions is essential to protect the safety of the traveling public.” [23 U.S.C. § 144(a)(1)(A)]. Congress has further found that “the systematic preventative maintenance of bridges, and replacement and rehabilitation of deficient bridges, should be undertaken.” [Id. at (a)(1)(B)]. In addition, Congress has also declared that “it is in the vital national interest” to use a “data-driven, risk-based approach” toward meeting these ends.” [Id. at (a)(2)(B)]. Considering these findings and declarations, Section 144 requires FHWA to maintain an inventory of bridges and tunnels on public roads both “on and off Federal-aid highways.” [Id. at (b)]. The FHWA is also required to “establish and maintain inspection standards for the proper inspection and evaluation of all highway bridges and tunnels for safety and serviceability.” [Id. at (h)(1)(A).] Section 144 also provides an exception to the requirement to obtain a bridge

permit from the U.S. Coast Guard for certain bridges over a limited subset of navigable waters. [Id. at (c)(2)].

- **National goals and performance management measures [23 U.S.C. § 150].** Congress has declared that it is “in the interest” of the U.S. to focus the Federal-aid highway program on certain national transportation goals including Infrastructure Condition, or the objective to “maintain ... highway infrastructure in a state of good repair;” and System Reliability, or the objective to “improve the efficiency of the surface transportation system.” [23 U.S.C. § 150(b)].
- **PROTECT Program [23 U.S.C. § 176].** The Promoting Resilient Operations for Transformative, Efficient, and Cost-Saving Transportation (PROTECT) program allows the FHWA to provide grants for resilience improvements through: (i) formula funding distributed to States; (ii) competitive planning grants; and (iii) competitive resilience improvement grants. [23 U.S.C. § 176(b)] Eligible activities under the PROTECT program include, among others, “resurfacing, restoration, rehabilitation, reconstruction, replacement, improvement, or realignment of” certain existing surface transportation facilities and “the incorporation of natural infrastructure.” [23 U.S.C. §§ 176(c)(1) and 176(d)(4)(A)(ii)(II)]
- Bridge Replacement, Rehabilitation, Preservation, Protection, and Construction Program (or Bridge Formula Program) (Division J, title VIII, Highway Infrastructure Program heading, paragraph (1)). The Bridge Formula Program provides funding to help repair approximately 15,000 highway bridges. In addition to providing funds to States to replace, rehabilitate, preserve, protect, and construct highway bridges, the Bridge Formula Program has dedicated funding for Tribal transportation facility bridges as well as “off-system” bridges, which are generally locally-owned facilities not on the Federal-aid highway system.
- **Bridge Investment Program (23 U.S.C. § 124).** The Bridge Investment Program provides financial assistance for eligible projects with program goals to improve the safety, efficiency, and reliability of the movement of people and freight over bridges; improve the condition of bridges; and provide financial assistance that leverages and encourages non-Federal contributions from sponsors and stakeholders involved in the planning, design, and construction of eligible projects.
- **National Culvert Removal, Replacement, and Restoration Grants Program (49 U.S.C. §§ 6703)].** The National Culvert Removal, Replacement, and Restoration Grant program established an annual competitive grant program to award grants to eligible entities for projects for the replacement, removal, and repair of culverts or weirs that would meaningfully improve or restore fish passage for anadromous fish.
- **Research and technology development and deployment [23 U.S.C. § 503].** In carrying out certain highway and bridge infrastructure and research and development activities, FHWA must “study vulnerabilities of the transportation system to ... extreme events and methods to reduce those vulnerabilities.” [23 U.S.C. § 503(b)(3)(B)(viii)].
- **Statutory Definition of “Resilience.” [23 U.S.C. § 101(a)(24)].** Section 11103 of the Bipartisan Infrastructure Law (BIL), enacted as the Infrastructure Investment and Jobs Act, Pub. L. 117-58 (Nov. 15, 2021), added a definition of “resilience,” which applies throughout Title 23 of the U.S. Code. With respect to a project, “resilience” means a project with the ability to anticipate, prepare for, and or adapt to changing conditions and or withstand, respond to, and or recover rapidly from disruptions, including the ability: (A) to resist hazards or withstand impacts from weather events and natural disasters, or reduce the



magnitude or duration of impacts of a disruptive weather event or natural disaster on a project; and (B) to have the absorptive capacity, adaptive capacity, and recoverability to decrease project vulnerability to weather events or other natural disasters. 23 U.S.C. § 101(a)(24). See also FHWA Order 5520 (FHWA 2014b).

### 2.2.2 FHWA Regulations

The FHWA's regulations are found within the Code of Federal Regulations (CFR), Title 23, Highways (23 CFR). The FHWA requires compliance with all applicable Federal law and regulations, including the regulations in Chapter I, Subchapter A, Part 1 of 23 CFR for a project to be eligible for Federal-aid or other FHWA participation or assistance. [23 CFR § 1.36]. The following FHWA regulations apply to highway projects and actions interacting with and within rivers and floodplains (paraphrased for brevity):

**Scope of the statewide and nonmetropolitan transportation planning process [23 CFR § 450.206].** SDOTs must “carry out a continuing, cooperative, and comprehensive statewide transportation planning process that provides for consideration and implementation of projects, strategies, and services that will ... improve the resiliency and reliability of the transportation system.” [23 CFR § 450.206(a)].

**Asset Management Plans [23 CFR part 515].** Part 515 establishes processes that a SDOT must use to develop a transportation asset management plan (TAMP). Two notable sections include:

- **Section 515.7(b).** “A State DOT shall establish a process for conducting life-cycle planning for an asset class or asset sub-group at the network level (network to be defined by the State DOT). As a State DOT develops its life-cycle planning process, the State DOT should include future changes in demand; information on current and future environmental conditions including extreme weather events, climate change, and seismic activity; and other factors that could impact whole of life costs of assets.”
- **Section 515.7(c).** A State DOT shall establish a process for developing a risk management plan. This process shall, at a minimum, produce information including: Identification of risks that can affect condition of NHS pavements and bridges and the performance of the NHS, including risks associated with current and future environmental conditions, such as extreme weather events, climate change, seismic activity, and risks related to recurring damage and costs as identified through the evaluation of facilities repeated damaged by emergency events carried out under part 667 of 23 CFR. Additional information that must be produced is specified in the regulation at 23 CFR 515.7(c).
- In addition, BIL Section 11105 amended 23 U.S.C. Section 119(e)(4) to require State DOTs to consider extreme weather and resilience as part of the life-cycle planning and risk management analyses within a TAMP (FHWA 2022b).

**Design Standards [23 CFR part 625].** Part 625 describes structural and geometric design standards.

- **Sections 625.3(a)(1) , 625.3(b) and 625.4(b)(3).** The FHWA, in cooperation with SDOTs, has approved the American Association of State Highway and Transportation Officials (AASHTO) Load and Resistance Factor Design (LRFD) Bridge Design Specifications. Based on FHWA's approval, certain National Highway System (NHS) projects must follow those LRFD Specifications including sections related to hydrology, hydraulics, and bridge scour. Among other standards, policies, and specifications listed in 23 CFR 625.4, FHWA has also approved the AASHTO Policy on Geometric Design of Highways and Streets (AASHTO 2018).



- **Section 625.3(a)(2).** Non-NHS projects must follow SDOT standard(s) and specifications on drainage, bridges, and other topics.

**Location and Hydraulic Design of Encroachments on Flood Plains [23 CFR Part 650, Subpart A].** One of the FHWA’s most important river-related regulations, 23 CFR Part 650, Subpart A sets forth policies and procedures for location and hydraulic design of highway encroachments in base (1-percent chance) floodplains. Section 650.111 sets forth requirements for location hydraulic studies to identify the potential impact of the highway alternatives on the base floodplain; these studies are commonly used during the NEPA process. The regulations prohibit significant encroachment unless FHWA determines that such encroachment is the only practicable alternative. [23 CFR § 650.113(a)]. This finding must be included in the NEPA documents for a project and supported information including the reasons for the finding and considered alternatives. [Id.]. The procedures also provide minimum standards for Interstate Highways, set freeboard requirements to account for debris and scour, and require highway encroachments to be consistent with certain established design flow standards for hydraulic structures, including standards from FEMA and State and local governments related to administration of the National Flood Insurance Program (NFIP). [23 CFR § 650.115(a)]. Notably, the policies and procedures in this Subpart apply to encroachments in all base floodplains, not just the floodplains regulated by the Federal Emergency Management Agency (FEMA) in the NFIP. [23 CFR § 650.107]. Additionally, the Subpart incorporates a requirement for project-by-project risk assessments or analyses. [23 CFR § 650.115(a)(1)]. Notable sections include:

- **Section 650.103 [Policy].** This section states that “it is the policy of the FHWA: (a) To encourage a broad and unified effort to prevent uneconomic, hazardous or incompatible use and development of the Nation’s flood plains, (b) To avoid longitudinal encroachments, where practicable, (c) To avoid significant encroachments, where practicable, (d) To minimize impacts of highway agency actions which adversely affect base flood plains, (e) To restore and preserve the natural and beneficial flood-plain values that are adversely impacted by highway agency actions, (f) To avoid support of incompatible flood-plain development, (g) To be consistent with the intent of the Standards and Criteria of the National Flood Insurance Program, where appropriate, and (h) To incorporate “A Unified National Program for Floodplain Management” of the Water Resources Council into FHWA procedures.” [23 CFR § 650.103].
- **Section 650.115 [Hydraulic Design Standards].** This regulation applies to all Federal-aid projects, whether on the NHS or Non-NHS. Federal, State, local, and AASHTO standards may not change or override the design standards set forth under § 650.115 — although certain State and local standards must also be satisfied under that section. That section requires development of a “Design Study” for each highway project involving an encroachment on a floodplain. [23 CFR § 650.115(a)].
- **Section 650.117 [Content of Design Studies].** This regulation requires studies to contain the “hydrologic and hydraulic data and design computations.” [23 CFR § 650.117(b)]. As both hydrologic and hydraulic factors and characteristics lead to scour formation, data and computations applicable to scour should be provided as well. Project plans must show the water surface elevations of the overtopping flood and base flood (i.e., 100-year flood) if larger than the overtopping flood. [23 CFR §650.117(c)].

Executive Order 14030, Climate-Related Financial Risk, and Executive Order 13690, Establishing a Federal Flood Risk Management Standard and a Process for Further Soliciting and Considering Stakeholder Input (80 FR 6425). Project applicants should be aware that DOT and FHWA, as of 2023, are in the process of developing guidance and considering updates to floodplain orders,

regulations and associated requirements, including redefining the appropriate flood hazard area to account for future climate conditions.

**National Bridge Inspection Standards [23 CFR § 650 Subpart C].** This regulation implements requirements of 23 U.S.C. § 144. In addition to the inspection and inventory requirements, the regulation specifically focuses on scour at bridges.

**Mitigation of Impacts to Wetlands and Natural Habitat [23 CFR § 777].** This regulation provides policy and procedures for the evaluation and mitigation of adverse environmental impacts to wetlands and natural habitat resulting from Federal-aid funded projects.

## **2.3 Other Federal Agency Statutes and Regulations**

Civil engineering projects in the river environment are subject to numerous Federal laws, policies, and regulations. This section describes some of the common Federal statutes, regulations, and other authoritative guidance that may govern highway projects.

### **2.3.1 Rivers and Harbors Act [33 U.S.C. § 401 and § 403]**

River and coastal highway engineering projects are subject to Section 9 [33 U.S.C. § 401] and Section 10 [33 U.S.C. § 403] of the Rivers and Harbors Act of 1899. Section 9 of this act restricts the construction of any bridge, dam, dike, or causeway over or in U.S. navigable waterways. Except for bridges and causeways under Section 9 [33 U.S.C. § 401], the U.S. Army Corps of Engineers (USACE) is responsible for maintaining the standards set by and for issuing permits under the Rivers and Harbors Act. Authority to administer Section 9, applying to bridges and causeways, was redelegated to the U.S. Coast Guard under the provisions of the Department of Transportation Act of 1966 (as discussed below).

### **2.3.2 General Bridge Act [33 U.S.C. § 525 through 533]**

The General Bridge Act of 1946 requires the location and plans of bridges and causeways across the navigable waters of the United States be submitted to and approved by the U.S. Coast Guard prior to construction. [33 U.S.C. § 525]. The USACE may also impose conditions relating to maintenance and operation of the structure. [Id.]. The General Bridge Act of 1946 is cited as the legislative authority for bridge construction in most cases. Although the General Bridge Act of 1946 originally provided authority for issuing bridge permits to the USACE, subsequent legislation transferred these responsibilities from the USACE to the U.S. Coast Guard.

### **2.3.3 Department of Transportation Act [Public Law 89-670]**

The Department of Transportation Act of 1966 transferred the U.S. Coast Guard (USCG) to USDOT. One of USCG's newly assigned duties was to issue bridge permits. This, along with the Rivers and Harbors Act and General Bridge Act, made the USCG responsible for ensuring that bridges and other waterway obstructions do not interfere with the navigability of waters of the United States without express permission of the United States Government. Subsequent legislation amended 23 U.S.C. § 144 to provide certain exceptions to USCG's authority under 33 U.S.C. § 401 and 33 U.S.C. § 525 for bridges constructed, reconstructed, rehabilitated, or replaced using Federal-aid funds. [23 U.S.C. § 144(c)(2)]. As of 2003, the USCG moved to the Department of Homeland Security (DHS) pursuant to the Homeland Security Act of 2002 (Public Law 107-296).

### 2.3.4 National Environmental Policy Act [42 U.S.C. § 4321, et seq.]

The National Environmental Policy Act of 1969 (NEPA) establishes the continuing policy of the Federal government to use all practicable means and measures “to foster and promote the general welfare, ... create and maintain conditions under which man and nature can exist in productive harmony, and fulfill the social, economic, and other requirements of present and future generations of Americans.” [42 U.S.C. § 4331]. To achieve this goal, NEPA creates a requirement for Federal agencies to consider the environmental impacts of their actions before undertaking them. [42 U.S.C. § 4332(C)].

Section 102(2)(C) of NEPA requires that Federal agencies develop a detailed statement on proposals for major Federal actions significantly affecting the quality of the human environment. [42 U.S.C. § 4332(C)]. FHWA implements NEPA according to the Council on Environmental Quality (CEQ) NEPA regulations at 40 CFR Part 1500 et seq. and the FHWA-FRA-FTA joint regulations at 23 CFR Part 771.

### 2.3.5 Clean Water Act [33 U.S.C. § 1251-1387]

Almost every project involving work or activities in rivers is subject to the Clean Water Act (CWA) of 1972, which the U.S. Environmental Protection Agency (USEPA) administers in coordination with State governments. The CWA is the primary Federal statute governing protection of the Nation’s surface waters. Engineering of highways in the river environment is often subject to Section 404 of the CWA, which regulates the discharge of dredged or fill material in waters of the U.S., including wetlands. [33 U.S.C. § 1344]. This includes the use of dredged or fill material for development, water resource projects, and infrastructure development (e.g., roads, bridges, etc.). The USACE handles the day-to-day administration and enforcement of the Section 404 program, including issuing permits. In circumstances where Section 404 is triggered, permit applicants also obtain a Section 401 certification from the State in which the discharge of dredged or fill material originates. [13 U.S.C. § 1341]. The Section 401 certification assures that materials discharged to waters of the U.S. will comply with relevant provisions of the CWA, including water quality standards. In addition, Section 402 of the CWA establishes the National Pollutant Discharge Elimination System (NPDES) Program. [33 U.S.C. § 1342]. The NPDES Program requires a permit for discharges of pollutants into waters of the United States, including storm water discharges.

### 2.3.6 Endangered Species Act [16 U.S.C. § 1531-1544]

Highway engineering projects have the potential to impact federally-listed fish, wildlife, and plants. The purposes of the Endangered Species Act of 1973 (ESA) include conserving “the ecosystems upon which endangered species and threatened species depend” and providing “a program for the conservation of such endangered species and threatened species.” [16 U.S.C. § 1531]. It is the policy of Congress that all Federal agencies shall seek to conserve endangered and threatened species and shall utilize their authorities in furtherance of the purposes of the ESA [16 U.S.C. § 1531]. The U.S. Fish and Wildlife Service (USFWS) and the NOAA National Marine Fisheries Service (NMFS) administer the ESA. The USFWS and NMFS conduct consultations with the lead Federal agency when a proposed project may affect federally endangered or threatened species. USFWS or NMFS involvement in a project depends on the affected species and the nature and extent of anticipated impacts (direct and indirect) to that species and its designated critical habitat. If anticipating a “take” of a federally-listed species, USFWS or NMFS will issue a biological opinion, the terms and conditions of which are binding on the lead Federal agency. [16 U.S.C. § 1536.].

### 2.3.7 National Historic Preservation Act [54 U.S.C. 300101 et seq.]

River highway engineering projects are often subject to the National Historic Preservation Act of 1966 (NHPA). Section 106 of the National Historic Preservation Act (NHPA) (commonly called “Section 106”) requires Federal agencies to consider the impacts on historic properties of projects that they carry out, approve, or fund. [54 U.S.C. § 306108]. The implementing regulations for the Section 106 process are found in 36 CFR part 800. Those regulations provide that Federal agencies, in consultation with the Advisory Council on Historic Preservation, the State Historic Preservation Officers (SHPO), and certain other interested parties, identify and assess adverse effects to historic properties and seek ways to avoid, minimize, or mitigate those effects. [36 CFR § 800.4-800.6]. Under Section 106, “historic property” is defined as any prehistoric or historic district, site, building, structure, or object included in, or eligible to be included in, the National Register of Historic Places [36 CFR 800.16(l)(1); see also 54 U.S.C. 300311 and 302102]. The responsibilities of SHPOs are set forth at 54 U.S.C. § 302303.

In addition to Section 106, Section 4(f) of the U.S. Department of Transportation Act of 1966 [23 U.S.C. 138 and 49 U.S.C. 303] requires that FHWA not approve the use of historic sites for a project unless there is no prudent and feasible alternative and the project incorporates all possible planning to minimize harm, or any impacts to historic sites are determined to be *de minimis*. The FHWA’s regulations for implementation of Section 4(f) are found at 23 CFR part 774.

### 2.3.8 National Flood Insurance Act [42 U.S.C. § 4001 et seq.]

The National Flood Insurance Act of 1968 instituted the National Flood Insurance Program (NFIP) to help indemnify and reduce impacts associated with floods. The NFIP adopted the area subject to a 1 percent chance or greater of being flooded in any given year (also known as the 100-year flood) as the standard, or base flood, for mapping U.S. floodplains. See, e.g., 44 CFR § 9.4. The area inundated by the 100-year flood determines the Special Flood Hazard Area (SFHA) on Flood Insurance Rate Maps (FIRMs) developed by FEMA and used to determine flood insurance rates for structures. See, e.g., 44 CFR § 59.1 (defining “area of special flood hazard”). FEMA implements the NFIP using its regulations found in 44 CFR.

The FHWA’s policies require projects to be consistent with the Standards and Criteria in the NFIP, where appropriate. 23 CFR § 650.115(a)(5). To assist SDOTs in complying with this policy, FHWA developed coordination procedures for Federal-aid highway projects with encroachments in NFIP regulated floodplains. FEMA agreed to these procedures by signing a 1982 Memorandum of Understanding with FHWA.

### 2.3.9 Wild and Scenic Rivers Act [16 U.S.C. § 1271 et seq.].

The act establishes a policy to preserve designated rivers “in free-flowing condition” and to protect “their immediate environments ... for the benefit and enjoyment of present and future generations.” [16 U.S.C. § 1271]. Section 7(a) provides that “no department or agency of the United States shall assist by loan, grant, license, or otherwise in the construction of any water resources project that would have a direct and adverse effect on the values for which such river was established.” 16 U.S.C. § 1278(a). A water resources project is “any dam, water conduit, reservoir, powerhouse, transmission line, or other project works under the Federal Power Act... or other construction of developments which would affect the free-flowing characteristics of a Wild and Scenic River or Study River.” 36 CFR § 297.3. “Federal assistance means any assistance by an authorizing agency including, but not limited to,... [a] license, permit, or other authorization granted by the Corps of Engineers, Department of the Army, pursuant to the Rivers and Harbors Act of 1899 and section 404 of the Clean Water Act (33 U.S.C. 1344).” *Id.* Fish and Wildlife Coordination Act [16 U.S.C. §§ 661-666c].

### 2.3.10 Fish and Wildlife Coordination Act [16 U.S.C. §§ 661-666c]

The Fish and Wildlife Coordination Act (FWCA) requires consultation with the USFWS, the NMFS, and State wildlife agencies for activities that affect, control, or modify waters of any stream or bodies of water, to minimize the adverse impacts of such actions on fish and wildlife resources and habitat. This consultation is generally incorporated into the process of complying with Section 404 of the Clean Water Act, NEPA, or other Federal permit, license, or review requirements.

### 2.3.11 Migratory Bird Treaty Act [16 U.S.C. § 703 et seq.].

The protection of all migratory birds is governed by the Migratory Bird Treaty Act (MBTA) [16 U.S.C. §§ 703-712], which generally prohibits the take of any migratory bird or any part, nest, or eggs of any such bird. [16 U.S.C. § 703(a)]. Under the MBTA, it is illegal to “take, kill, possess, transport, or import migratory birds or any part, nest, or egg of any such bird” unless authorized by a valid permit from the USFWS. [Id.]. The regulation at 50 CFR 10.13 includes a list of migratory birds protected by the MBTA.

*Page Intentionally Left Blank*

## Chapter 3 - Nonstationarity

Engineers use a variety of technologies to estimate peak flows for design of drainage structures. In so doing, they use the concepts of both stationarity and nonstationarity, often without explicit acknowledgment. Engineers often assume that stationarity is appropriate, but nonstationarity is becoming increasingly important. This chapter describes the concepts of stationarity and nonstationarity, discusses how they affect the design process, and presents some techniques for analyzing nonstationary watersheds.

### 3.1 What is Nonstationarity?

A **stationary** time series is one that does not exhibit an underlying change in the process that generates the time series. Furthermore, the distribution parameters that describe data from the underlying process, such as mean, variance, skew, and higher-order parameters do not vary with time. Data from the past are representative of future values and can be used for analyzing future events. Such a process or time series is said to have the characteristic of **stationarity**.

In contrast, a time series that has a trend, abrupt change, or periodic variability is a **nonstationary** time series. The underlying process that generates the time series is variable. Such a nonstationary time series is said to have the characteristic of **nonstationarity**. Nonstationary patterns and trends from the past might not be valid for future events, and predictions based on past events might be subject to greater uncertainty than those from stationary time series.

Nonstationarity results from a variety of sources and can cause increased peak flows, decreased peak flows, and other changes to the annual peak streamflow series. The most common source of nonstationarity is change to the watershed land use and land cover. Engineers address this type of change routinely. Other sources of nonstationarity include construction or removal of dams, detention/retention facilities, stream diversion, climate change, and other changes within the watershed influencing watershed flooding.

A **trend** is a gradual change in the time series. Examples of this include a peak streamflow that increases or decreases gradually over time. The gradual development of a watershed, with commensurate increases in impervious area and reduction of the times of concentration, could result in such a trend. The impact of a trend on the sample parameters for the underlying process would be changing values of the mean, variance, and higher-order parameters. The variance might or might not increase. The same is true for higher-order parameters.

An **abrupt change** occurs over a short period of time. The watershed response to construction or removal of a dam or significant detention/retention facilities represents an abrupt change. This is especially apparent in the reach of a stream immediately downstream from the structure (or structures).

**Periodic variability** is a cycle of wet and dry periods in the time series. It results particularly from periodic variability in the regional climate.

A potential problem in trend detection in hydrologic time series is that the length of record is often short, sometimes only a few years of observations. Although statistical significance is indicated in measures such as the p-value computed as part of the statistical testing, engineers carefully review analyses developed from small datasets before drawing conclusions from the results. See Bulletin 17C (England et al. 2019) for more information about the use of short records and the inherent uncertainties associated with them.

Figure 3.1 depicts the annual peak streamflow series from Pond Creek near Louisville, Kentucky and illustrates the challenges in trend identification. A change in the peak flows begins in the mid-1950s and ends in the mid-1960s. Trend lines on the figure generally indicate no trend before the mid-1950s and no trend after the mid-1960s. This abrupt change in the annual peak series is attributed to a period of rapid development of the watershed. This development resulted in increased impervious area and decreased time of concentration for the watershed, which increased the peak flows. It is an example of an abrupt change to the processes that produce peak flow.

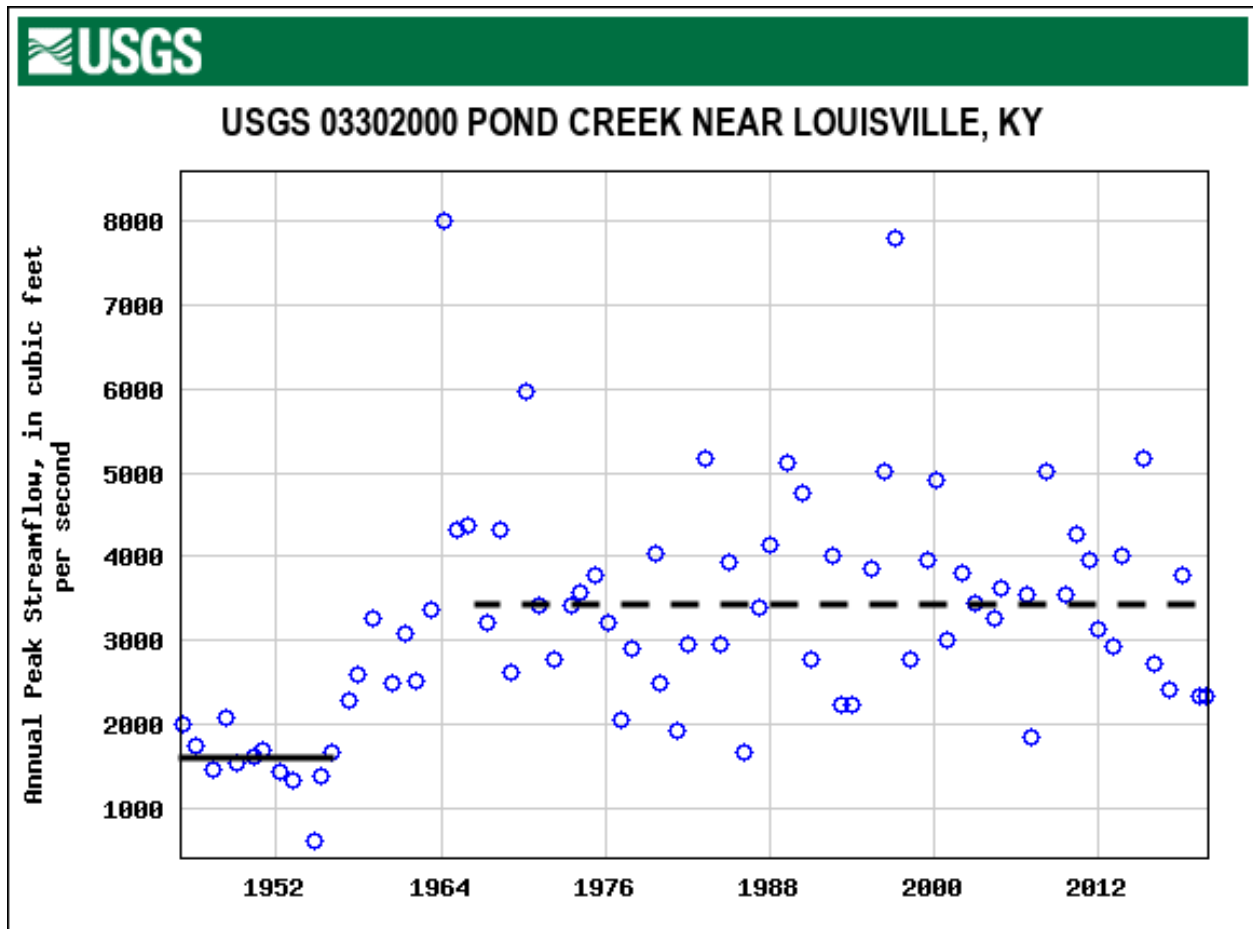


Figure 3.1. Annual peak streamflow series from Pond Creek, Kentucky (USGS 03302000).

Figure 3.2 depicts the annual peak streamflow series from Mercer Creek near Bellevue, Washington. Visually, the annual peak series is increasing with respect to time. That is, there is an apparent trend in the annual peak streamflow series data shown by the solid trendline in the figure.

In contrast, Figure 3.3 depicts the annual peak streamflow series from Newaukum Creek near Black Diamond, Washington. Although this watershed is in the same region as Mercer Creek, no trend, or possibly a decreasing trend, in the annual peak streamflow series is evident.



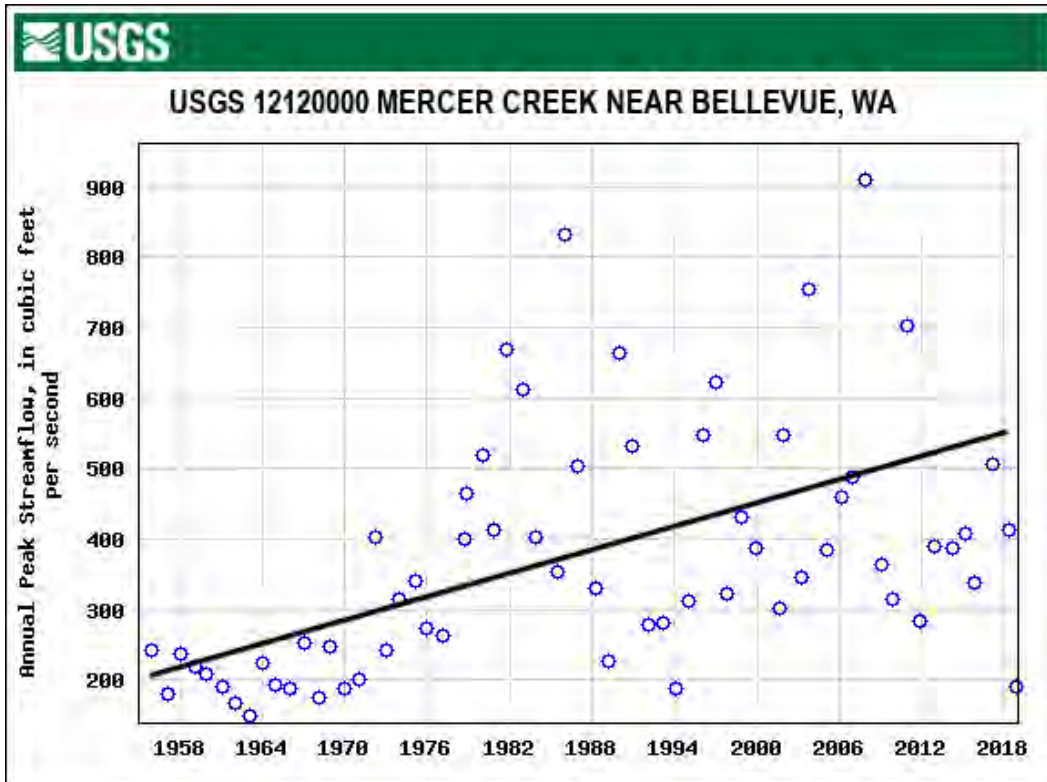


Figure 3.2. Annual peak streamflow series from Mercer Creek, Washington (USGS 1212000).

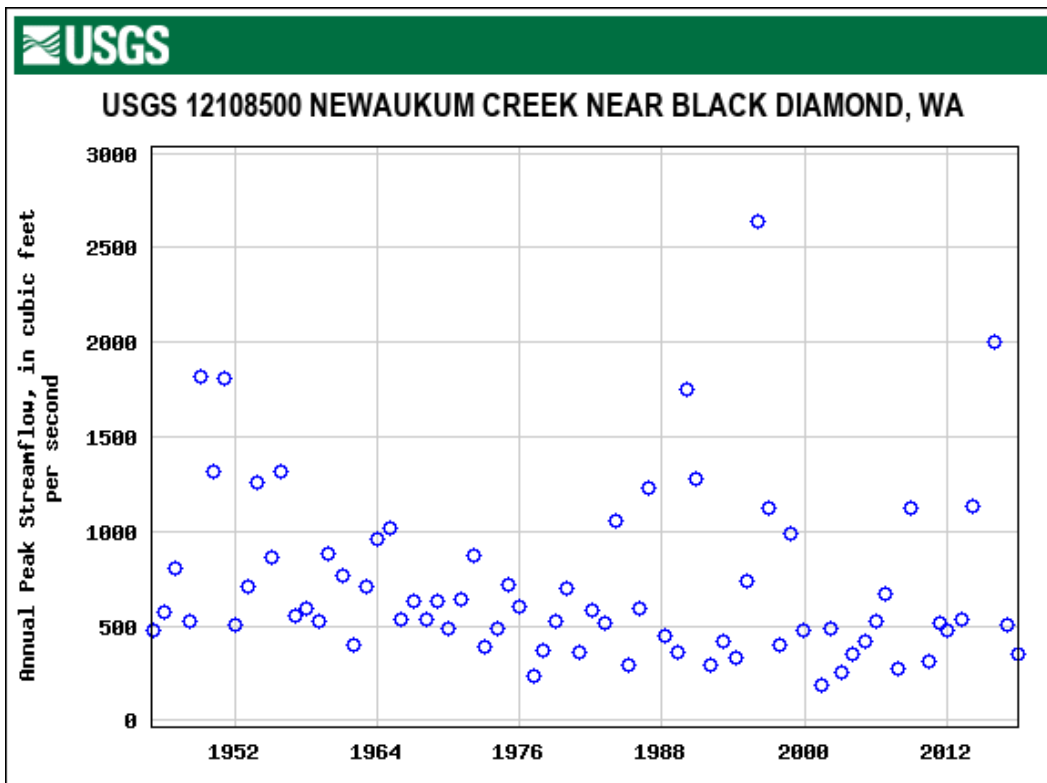


Figure 3.3. Annual peak streamflow series from Newaukum Creek, Washington (USGS 12108500).

## 3.2 Methods for Detecting Nonstationarity

Assuming stationarity when nonstationarity exists in a historical dataset can lead to significant errors in hydrologic analyses. This could, in turn, result in the design of roadway or bridge structures that are not protective of the public safety based on accepted flooding risks or more costly than justified by the same risks. Therefore, detecting nonstationarity in hydrologic data can be important for design. This section provides several methods for detecting nonstationarity.

### 3.2.1 Nonstationarity in Stream Gage Data

As described previously, nonstationarities in stream gage data can result from a number of causes. This section describes tools to detect nonstationarity in stream gage data. These techniques do not identify the cause of the nonstationarity.

#### 3.2.1.1 Mann-Kendall Test as Implemented in PeakFQ

HEC-17 (FHWA 2016) presents methods for detecting nonstationarity in streamflow data. The Mann-Kendall test (Helsel et al. 2020) can detect gradual changes. This test uses the Kendall tau statistic to measure the relation between peak flow and year (the time series of flow). Kendall's tau is nonparametric and does not depend on the actual streamflow values, but on the ranks of the streamflow values. The ranks of the observations are compared to determine if the series is increasing or decreasing (or neither at a desired level of significance,  $p$ ). The tau statistic has a range from -1 to 1.

The U.S. Geological Survey (USGS) PeakFQ program implements this test as of version 7.1 (Flynn et al. 2006). Kendall's tau is one of the outputs from a flood frequency analysis using PeakFQ. The following example illustrates the use of PeakFQ for trend analysis.

**Example 3.1:** Determine the presence or absence of a gradual trend in an annual peak streamflow series.

**Objective:** Use the PeakFQ software to assess whether the assumption of stationarity is reasonable for the annual peak streamflow series for Mercer Creek. Assume a 5-percent level of significance.

Input the data presented in Figure 3.2 into PeakFQ and run a flood frequency analysis for this gaging station.

*Step 1. Download the data from the USGS data portal for Mercer Creek (USGS 12120000).*

Using a web browser to access <https://nwis.waterdata.usgs.gov/usa/nwis/peak>, check the Site Number box and submit. Enter the station identifier (12120000) and then wait for the list of stream gages to be returned. Then select that number (12120000) in the result. Finally, select the Peakfq (watstore) format link to directly download the data. Save the results to a text file.

*Step 2. Input the data into PeakFQ (Version 7.1 or later).*

Open PeakFQ and input the file into the program. Use station skew and turn on the Urban/Reg Peaks switch.

*Step 3. Run PeakFQ for USGS 12120000 and examine the results.*

Run the PeakFQ analysis and then view the output file. Notice the Kendall's tau parameters table in the output file. For the gaged peaks,  $\tau = 0.386$ , the  $p$ -value is 0.000, the median slope is 3.911, and there are 64 peaks in the gage record. The slope is in  $\text{ft}^3/\text{s}$  per year.

**Solution:** Notice that Kendall's tau is 0.386 and the p-value is 0.000. That means the series is increasing with time and the test is statistically significant (at the 5-percent level of significance— $p$  is less than 0.05). This indicates a trend in the annual peak streamflow series.

### p-value?

The p-value for the sample in the example was 0.000. The p-value is the level of significance for the test statistic. Analysts compare it to the desired level of significance for the analysis. For example, if the analyst desires to evaluate the test at the 0.05 (5 percent) or 0.01 (1 percent) level they compare the p-value to the desired level of significance. In this example, since the p-value of 0.000 is less than both 0.05 and 0.01, the analyst considers the presence of an increasing trend to be statistically significant.

#### 3.2.1.2 USGS Integrated Water Availability Assessment Tool

Dudley et al. (2019, 2018) developed a program that performs a trend analysis of USGS streamflow data. Results are displayed at <https://iwaas.wim.usgs.gov/sw-flow-trends/>. Regional trends are useful for informing results from other analytical approaches and determining whether an adjustment for nonstationary peak streamflow is consistent with observations at other stream gages.

For example, the web portal screenshot in Figure 3.4 displays a portion of a map of Washington showing a number of stream gages with annual peak flow data. Stream gages with a statistically significant uptrend are demarked by the solid upward pointing triangles; those with a statistically significant downtrend are demarked by a solid downward pointing triangle. Many others have uptrends or downtrends that are not statistically significant, indicated by upward or downward pointing open triangles. This might indicate that additional attention is needed for determining design flows from gaging data in the region.

Figure 3.5 displays general information about Mercer Creek near Bellevue, Washington. (Note that Figure 3.2 displays data from this stream gage.) The screenshot shows the location, stream gage number, and a note that the analysis detected a statistically significant uptrend assuming the peak flow observations are independent.

Figure 3.5 also displays the detailed analysis of annual peak streamflow from Mercer Creek. The period of record 1966-2015 shows an uptrend in the annual peak streamflow series with a value of 3.9 ft<sup>3</sup>/s/yr. The p-value for this uptrend is 0.003, which is significant at the 5-percent level of significance. This indicates a statistically significant trend, although causation of the trend is not known at this stage of analysis.

The USGS tool is useful for examining the existence of trends at particular gaging stations and over an area of interest. The tool provides three different assumptions for time series testing: independence of events (INDE), short-term persistence (first-order autoregressive (AR1)), and long-term persistence (LTP). The documentation for the web portal and research by Hamed and Rao (1998), Cohn and Lins (2005), and Hamed (2008) present details for applying these assumptions.

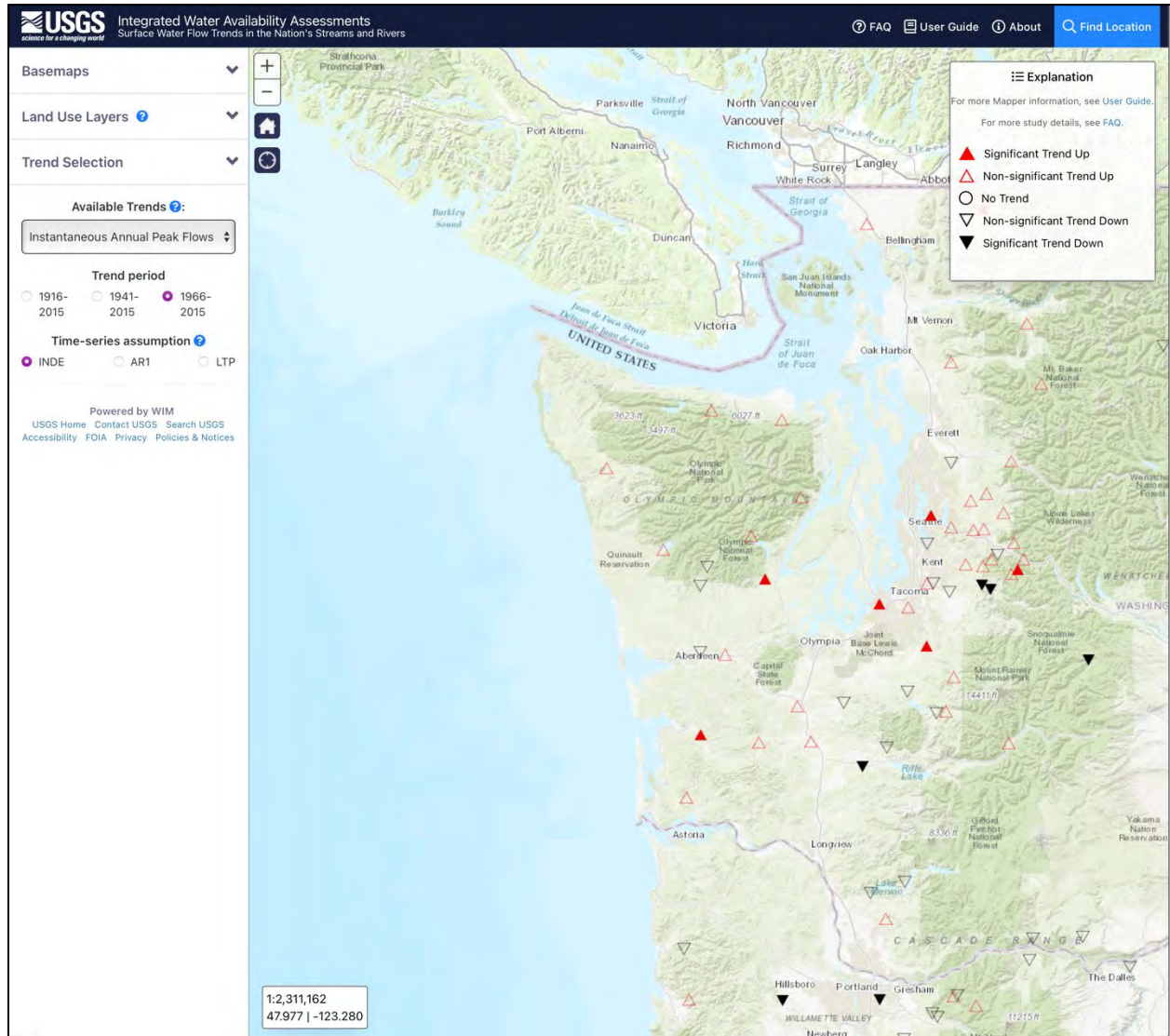


Figure 3.4. USGS IWAA web portal, displaying portions of Washington State.

### 3.2.1.3 U.S. Army Corps of Engineers Nonstationarity Detection Tool

The Mann-Kendall test used in PeakFQ evaluates gradual trends in annual peak flows. Some flow records may show an abrupt shift or change in the time series rather than a gradual trend. For example, there may be distinct periods exhibiting different flood characteristics before and after construction of flood control structures. For abrupt changes, the nonparametric (rank based) Pettitt test allows detection of changes in the mean (median) when the change point time is unknown (Pettitt 1979, Villarini et al. 2009). The Pettitt test identifies the year in which the maximum difference in ranks occurs across the full period of record. The construction of a flood detention structure or major channelization in a watershed is usually well documented and known to the analyst. However, the Pettitt test is useful for detecting episodic change if the analyst is unaware of the watershed history.

The U.S. Army Corps of Engineers (USACE) has prepared a Nonstationarity Detection Tool that facilitates identification of nonstationarities in annual peak flow series data from USGS gaging stations. The tool includes the Pettitt test among several techniques (Friedman et al. 2016). While the tool is complex and capable, the user will benefit from a background in statistics.



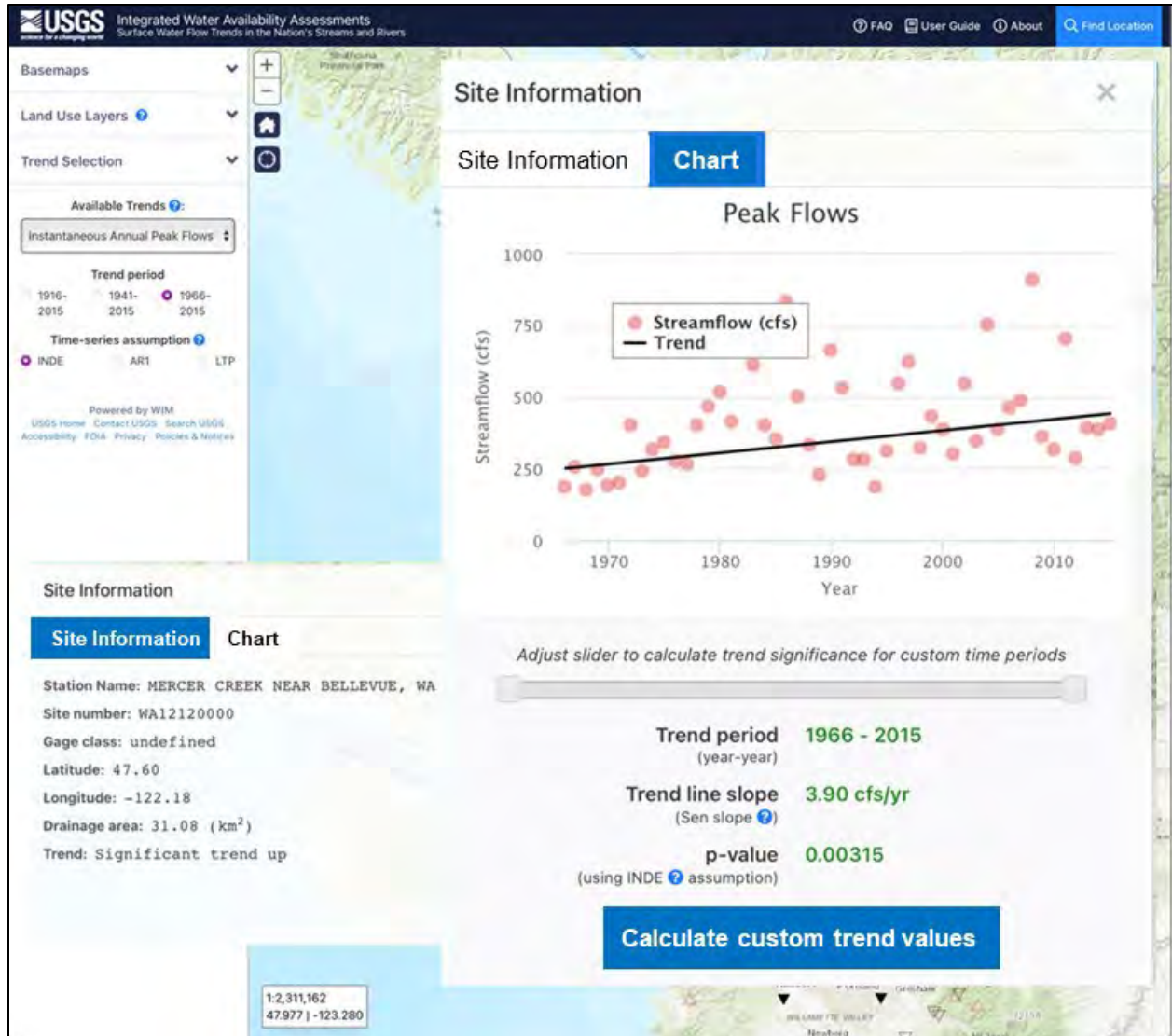


Figure 3.5. Stream gage and watershed information and details of a trend analysis for the annual peak streamflow series for Mercer Creek near Bellevue, Washington (USGS 12120000).

Figure 3.6 displays many results from analysis of annual peak streamflow data from Mercer Creek near Bellevue, Washington (USGS 1212000), using the USACE Nonstationary Detection Tool. The results show a change in watershed behavior from the late 1960s to the late 1970s. This is consistent with other descriptions of development of the watershed.

Figure 3.7 displays results from a monotonic trend analysis of the Mercer Creek data using the USACE tool. This analysis used the Mann-Kendall test, and the results are statistically significant at the 5-percent level of significance. This is similar to results from other tests for a trend.

Figure 3.8 shows the results from a Pettit test for an abrupt change in the annual peak streamflow series from Mercer Creek. The mean, standard deviation, and variance are all nonstationary (statistically significant).

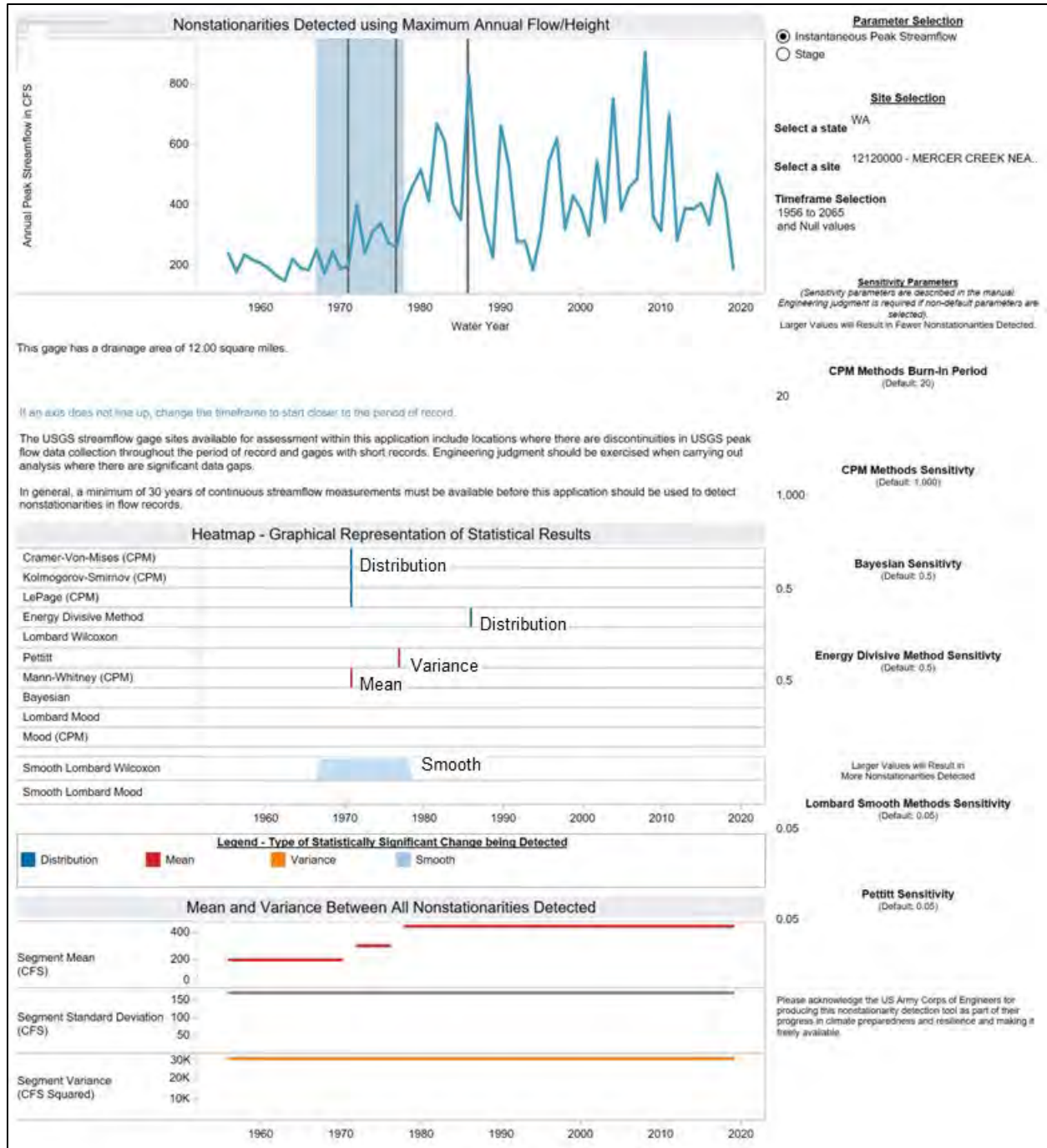


Figure 3.6. Results from application of the USACE Nonstationary Detection Tool on annual peak streamflows from Mercer Creek near Bellevue, Washington (USGS 12120000).

### 3.2.2 Developing Tools for Nonstationarity Detection

Detection of nonstationarity and its potential impact on hydrologic analysis and design continues to be an active area of applied research. Serinaldi et al. (2018) provide a caution on use of significance testing for detecting trends in hydrological time series. They provide an example and demonstrate how use of daily stream records (with the inherently larger database) can change the test outcomes over using annual series. This observation provides insight into why it is

important to consider additional time series assumptions, such as presented by Dudley et al. (2018, 2019) for the USGS Integrated Water Availability Assessments (IWAA).

Sarhadi and Soulis (2017) provided an analysis and methodology for detecting trends in extreme (hydrological) precipitation and then adjusting the intensity-duration-frequency (IDF) curves of the region around the Great Lakes of the United States and Canada. The process has potential application for adjustment of nonstationary IDF curves in other regions of the United States.

Konrad and Restivo (2021) approached detection of potential trends in annual peak streamflow using a quantile regression approach. The database comprised annual maximum streamflow data from 2,683 stations with at least 50 years of record. Data were transformed using the base 10 logarithm and estimates for the 0.1, 0.5, and 0.9 annual exceedance probability (AEP) quantiles. Regression was performed on each quantile to determine the presence of a trend. Trends were identified for the 0.5 quantile at 36 percent of the sites.

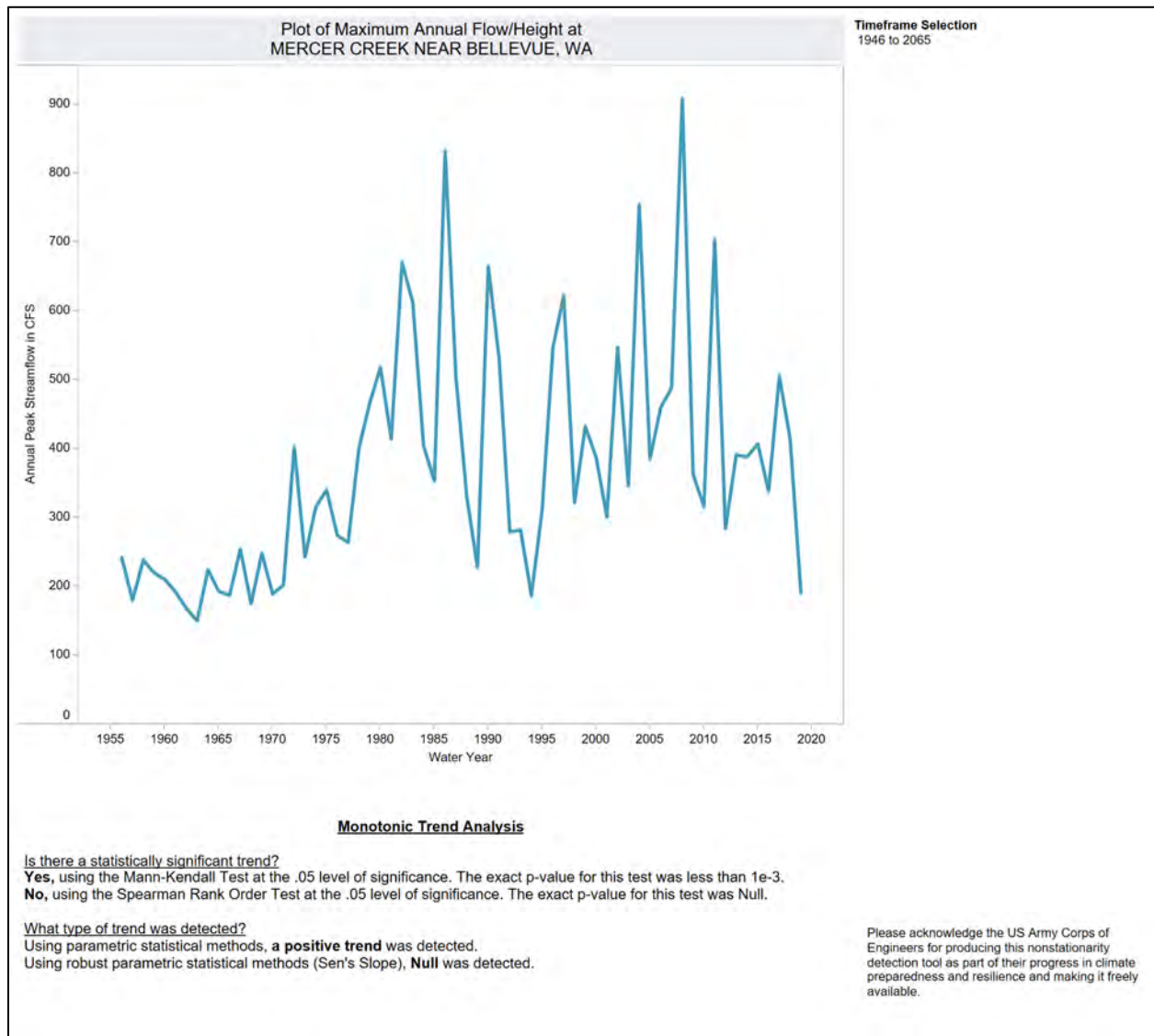


Figure 3.7. Trend analysis produced by USACE Nonstationary Detection Tool for annual peak streamflow data from Mercer Creek near Bellevue, Washington (USGS 1212000).

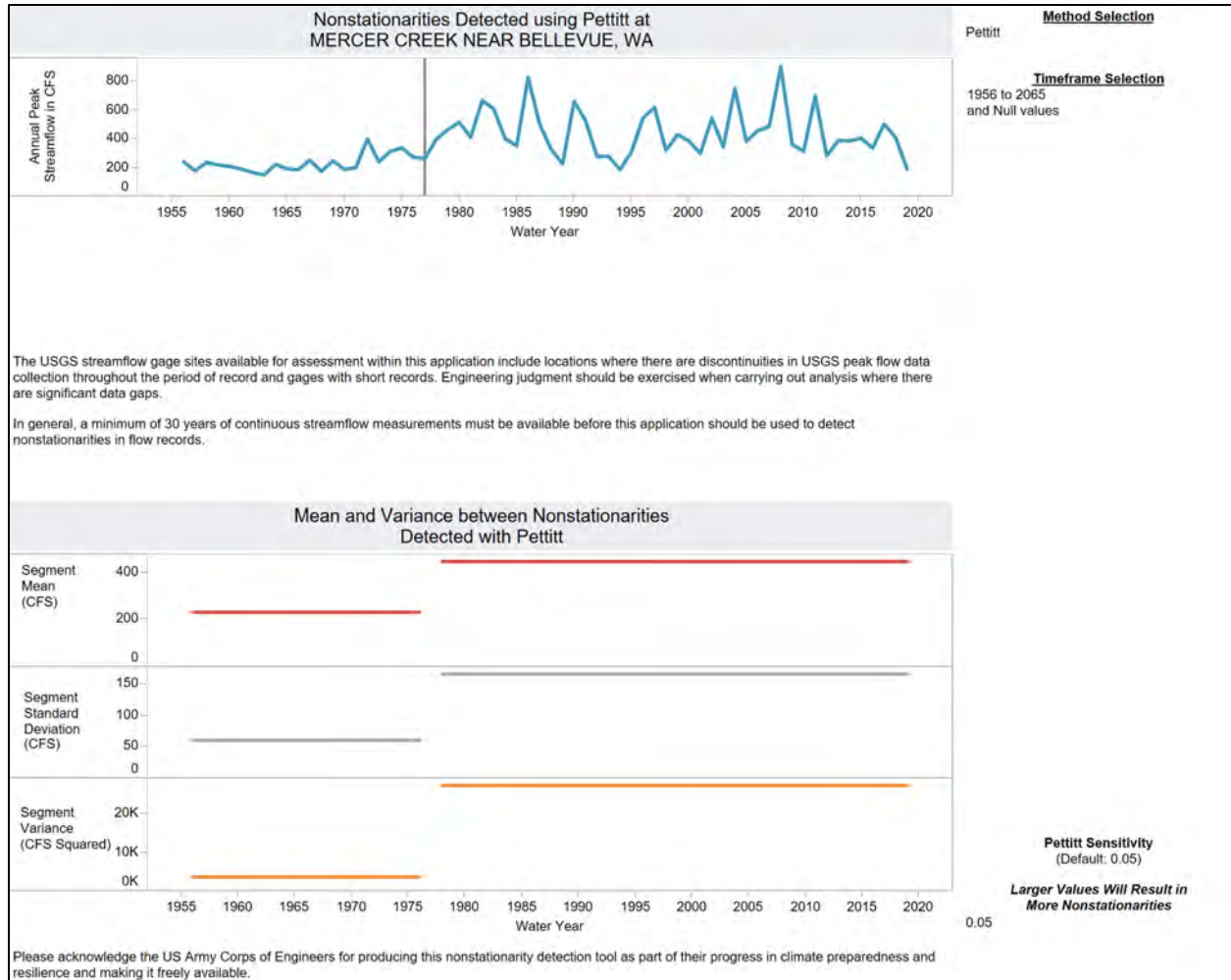


Figure 3.8. Results from Pettit Test using the USACE Nonstationary Detection Tool on annual peak streamflow data from Mercer Creek near Bellevue, Washington (USGS 1212000).

### 3.3 Attribution of Nonstationarity

Detecting nonstationarity is the first step to incorporate it projections regarding potential future conditions. The analyst identifies trend causes to assess whether they will continue into the future and to what degree the causes will continue to influence runoff. Analysts refer to this process of cause identification as **attribution**. This section briefly describes two causes of nonstationarity in runoff and flooding patterns—watershed changes and climate change.

#### 3.3.1 Watershed Changes

Nonstationarity commonly arises from changes in land use/land cover of the watershed, often associated with urban development. Changes in agricultural practices may also contribute to nonstationarity in rural areas. Engineers regularly address watershed changes when conducting hydrologic analyses. The typical impact is a reduction in the watershed timing parameter (runoff drains faster to the watershed outlet) and an increase in impervious area. Such changes include:

- Development that changes the runoff-producing capacity of the watershed landscape, including impervious area, culverts, and channel improvements.
- Construction of impoundments for agriculture.



- Introduction of agricultural drainage tiles.
- Addition of detention and retention facilities.
- Land cover changes from wildfires on the watershed.

Designers sometimes mitigate development impacts using detention or retention storage. These structures can reduce increases in the annual peak streamflow series (and therefore reduce the possibility for a trend).

Engineers can determine historical changes to the watershed landscape by analyzing historical aerial photographs. Records for jurisdictional authorities are sometimes available as well. It is beneficial to obtain this information when possible and for use in analyzing possible watershed flow trends.

Figure 3.9 depicts the impact of watershed changes on the annual peak runoff series from Pond Creek, Kentucky. For this watershed, urbanization caused an increase of impervious area and a decrease in the response time of the watershed. Therefore, peak flows from the latter part of the period of record are greater than those experienced before the changes occurred. This is an example of nonstationarity resulting from physical changes to the watershed.

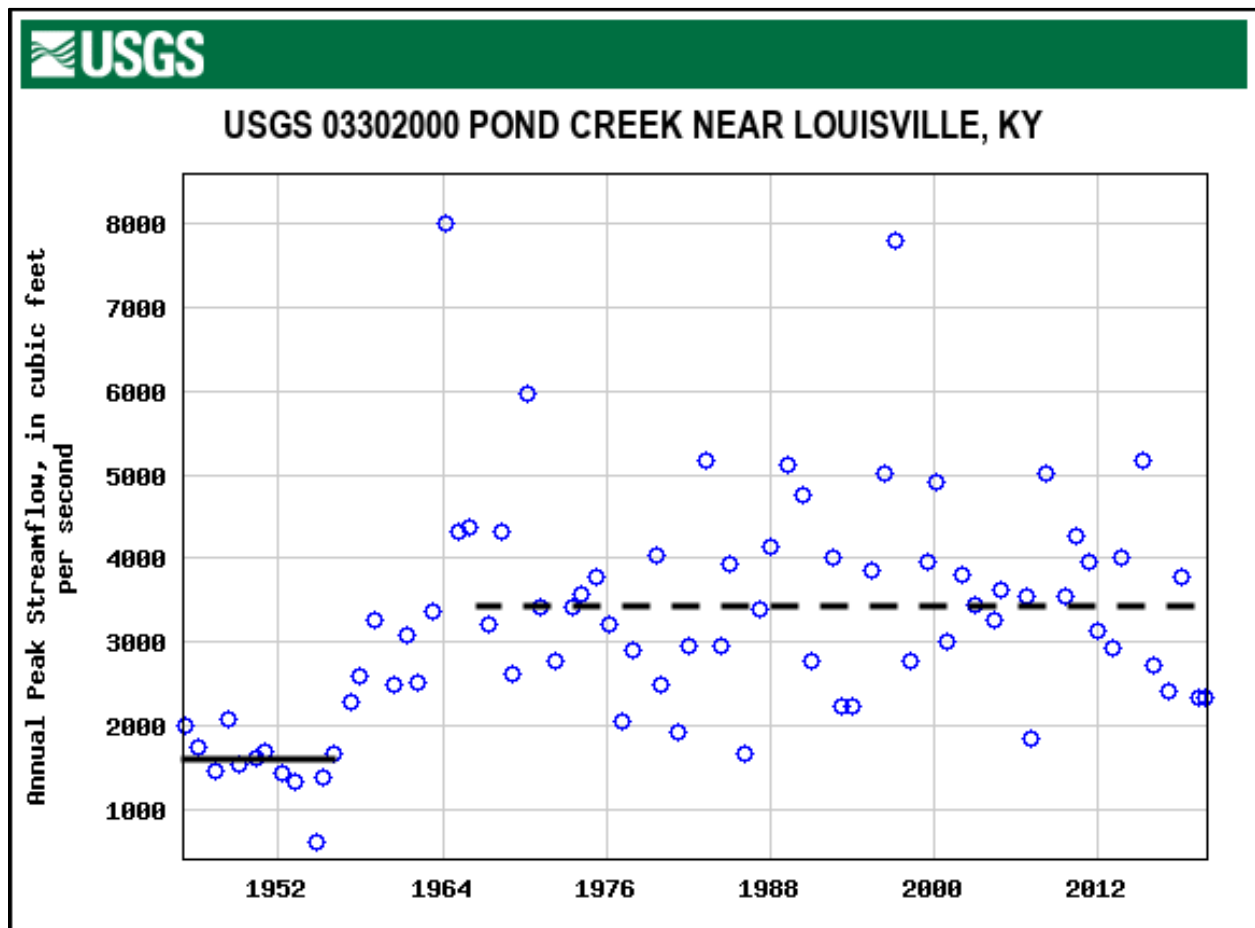


Figure 3.9. Annual peak flow series from Pond Creek, Kentucky, illustrating nonstationarity.

### 3.3.2 Climate

Changes in precipitation and temperature may also contribute to nonstationarity in streamflows. In some areas extreme precipitation may increase with increasing global temperatures resulting in more frequent flooding. In others, increasing droughts may occur resulting in less total runoff.

In areas where precipitation occurs as rain or snow, changing temperatures may result in less snowfall changing the accumulation of snowpack and spring runoff patterns. Changing temperatures could also influence rain-on-snow events changing local patterns of flooding.

Attributing future trends in streamflow patterns to a changing climate is challenging but researchers have developed tools to support the analysis and design of transportation infrastructure. The next section summarizes selected tools and resources.

## 3.4 Assessing the Impact of Nonstationarity on Design Flows

Tools and resources for assessing the impact of nonstationarity on design flows are available and continually evolving. HEC-17 (FHWA 2016) and NCHRP 15-61 (Kilgore et al. 2019) present information for analyzing nonstationary hydrologic processes and for developing hydraulic design estimates for watersheds with nonstationary hydrology. This section summarizes some of these tools, but more information is available in these reference documents.

### 3.4.1 Levels of Analysis Approach

Kilgore et al. (2019) describe a four-level design approach that includes consideration of climate change and its impact on highway drainage design. This approach refined the levels of analysis introduced in HEC-17 (FHWA 2016) that recognized that all projects are not equally sensitive to potential climate change and do not offer the same risks. The general framework is:

- **Level 1 – Design flow based on historical data.** At level 1, the design team estimates the design flow using typical hydrologic design techniques based on historical data. In addition, the design team qualitatively considers changes in the estimated design flow based on possible future changes in land use and climate.
- **Level 2 – Design flow based on historical data/confidence limits.** At level 2, the design team estimates the design flow based on historical data and qualitatively considers future changes in land use and climate as in level 1. In addition, the design team quantitatively estimates a range of flows (confidence limits) based on historical data to evaluate plan/project performance.
- **Level 3 – Design flow based on projected information/confidence limits.** At level 3, the design team develops projected land use and climate data, where possible. The design team performs hydrologic modeling using the projected land use and climate data to estimate projected design flows and confidence limits. At level 3, another element of analysis is introduced -- the analysis and use of output from climate models.

#### How Many Levels of Analysis?

HEC-17 (FHWA 2016) outlined five levels of analysis and the more recent research study (Kilgore et al. 2019) consolidated the levels to four. The FHWA is proceeding with four levels in its training materials and newer reference manuals. However, the most important concept to remember is not the number of levels but simply that different levels apply to different situations.

- **Level 4 – Design flow based on projected information/confidence limits with expanded evaluation.** At level 4, the design team performs the equivalent of the level 3 analyses based on custom projections of land use and climate. The design team also expands to include appropriate expertise in climate science, in land use planning, or both to secure site-specific custom projections.

Analysts consider varying levels of analysis to match the risk associated with a project. Risk is the product of the probability of an undesirable event and the consequences of the event. Risk analysis or assessment incorporates the concept of vulnerability and provides some measure of the costs and consequences (monetary and other) associated with damages and performance interruptions associated with the asset vulnerability to facilitate the comparison of alternatives. HEC-17 (FHWA 2016) provides additional information on risk analysis.

### 3.4.2 Frequency Analysis with a Time-Varying Mean

An approach for adjusting nonstationary peak flows is adjustment of the mean. The approach is based on development by Vogel et al. (2011) and Read and Vogel (2015) for the 2-parameter log-normal distribution. Kilgore et al. (2019) and FHWA (2016) extend this approach to adjust the mean of the log-Pearson type III distribution. The suggested procedure includes the following steps:

1. Estimate a time-varying mean of the logarithms of the annual peak streamflow series over the period of record and test the trend for statistical significance.
2. Develop a causal hypothesis for the trend, i.e., attribution. Use available information to evaluate the hypothesis for explaining the trend and its continuation into the future.
3. If the information developed in steps 1 and 2 confirm the presence and reasons for a historical trend to be continued, compute the involved statistics to develop an equation for estimating design flows.
4. Compute the design flow quantiles.

The following paragraphs expand the approach.

#### **Step 1. Assess whether a trend is present in the annual peak streamflow series.**

The assessment of a trend in the annual peak streamflow series begins with visual inspection of a plot of the time series data. It is appropriate to examine the entire period of record and the latter portion of the record for possible trends. If a potential trend is identified, then estimate the trend using linear regression on the logarithms of the series to fit:

$$\log_{10}(Q) = Y = \bar{L}\bar{Q}_0 + Bt \quad (3.1)$$

where:

- |                    |   |   |
|--------------------|---|---|
| Q                  | = | Annual peak flow, ft <sup>3</sup> /s (m <sup>3</sup> /s)    |
| t                  | = | Time from the beginning of the trend, years                 |
| $\bar{L}\bar{Q}_0$ | = | Intercept of the logarithms (at the beginning of the trend) |
| B                  | = | Slope of the trend  |

The slope B represents the magnitude of change in the logarithmic series and is tested for statistical significance. If PeakFQ is used to fit a flood frequency curve, then PeakFQ applies the Mann-Kendall test for a trend. If a typical statistical software (such as the R project) is used for the linear regression, then the statistical significance is computed as part of the regression

process. (Appendix 4 of Bulletin 17C (England et al. 2019) describes the Mann-Kendall test.) If the resulting trend slope is not statistically significant, then the engineer concludes that no trend exists, and further steps are not indicated.

Yu and Stedinger (2018) state that this procedure for adjusting quantiles for a time-varying mean is appropriate only for trends with a slope, i.e., the variable B, between 0.25 and 1.0 percent per year. They conclude that if the slope of the trend is less than 0.25 percent, then there is insufficient difference between the stationary and nonstationary flood frequency curve to justify the analysis. If the slope of the trend exceeds 1.0 percent per year, then the variance and skew of the distribution would likely benefit from being adjusted. Serago and Vogel (2018) provide discussion of these additional analytical processes.

### **Step 2. Validate the trend by examining historical information.**

In equation 3.1, the time variable is a surrogate for those factors driving the trend identified in step 1. If a trend is detected in the annual peak streamflow series, then it is important to validate use of the trend by examining the historical record for changes in land use, climate, or other factors. The objective is to explain the occurrence of the trend and determine whether continuation of the trend is expected.

Step 2 can include correlation analysis. However, correlation is not necessarily causation. The engineer using trend analysis to estimate design flows will want to have a solid rationale for the trend's cause and to justify applying this analysis.

### **Step 3. Compute the design quantiles of interest using the results of steps 1 and 2.**

With the trend analysis of step 1 and the rationale from step 2, the engineer computes the appropriate statistics including the trend to produce the equation incorporating the time-varying mean. Serago and Vogel (2018) present the following equation for this analysis:

$$\log_{10}(Q_x) = \bar{LQ} + B \left( t - \frac{n+1}{2} \right) + K_x S \quad (3.2)$$

where:

$\bar{LQ}$	=	Mean logarithm of the historical peak streamflow series
$Q_x$	=	Flow quantile associated with x annual exceedance probability
B	=	Slope of the trend line
S	=	Standard deviation of the residuals from the linear regression for equation 3.1
$K_x$	=	Pearson type III frequency factor
t	=	Time since the beginning of the record, years
n	=	Number of years in the record

The AEP is any quantile needed for the design. Examples are the 0.10 AEP (10-year) and the 0.01 AEP (100-year).

If the slope of the regression line is 0 or statistically insignificant, then equation 3.2 reduces to the stationary form of the design quantile equation. This suggests that three cases could be considered for the computation of design quantiles:

- Case 1. The stationary form of the design quantile equation is used to compute design estimates. These values serve as a basis for comparison with nonstationary estimates.
- Case 2. The engineer is less confident that the identified trend will continue past the historical record. In this case, t is set to n and the design estimates computed. The design

quantiles computed represent the quantiles at the end of the period of record (the historical period).

- Case 3. The engineer is sufficiently confident that the historical trend is likely to continue beyond the historical period. Therefore, the engineer computes design quantiles with  $t$  greater than  $n$  (an extrapolation beyond the period of record) to estimate future conditions. The engineer considers the uncertainty that the driver of the trend will continue to avoid extraordinarily conservative design estimates that might result in oversized structures. Kilgore et al. (2019) presents additional discussion of this case.

**Step 4. Compare the results of the stationary and nonstationary analysis and evaluate the results for application to the design.**

The design quantiles computed in step 3 are compared and evaluated for application. This is an opportunity to examine the projected impact of the trend on the design quantiles by comparing to the stationary case. This is also a critical check on the analysis.

The following example illustrates this four-step process for analyzing trends in a stream gage record.

**Example 3.2:** Application of the time-varying mean approach to analyzing a stream gage record.

**Objective:** Determine if a trend is present in an annual peak streamflow series. If so, estimate the impact of the trend on the 2-, 10-, and 100-year recurrence interval design flowrates.

Stockley Branch at Stockley (USGS 01484500), a rural five-square-mile watershed in southern Delaware. As shown in Figure 3.10 the period of record for Stockley Branch is 1943 through 2004, a total of 61 years of record.

PeakFQ was used to fit a log-Pearson type III distribution to the series. PeakFQ produced a value of Kendall's tau of 0.330 with a p-value of 0.000. Therefore, a statistically significant trend is present in the series.

**Step 1. Assess whether a trend is present in the annual peak streamflow series.**

Any statistical analysis tool can support this analysis. R project was used to perform linear regression on the logarithms of annual peak streamflow from the Stockley Branch data, but other statistical tools can be used to complete the analysis. The resulting values are:

Slope: 0.00657 (p-value of near zero, which is statistically significant at the 5 percent level of significance)

Intercept: 1.6551 (p-value near zero, which is statistically significant)

Therefore, the linear fit is appropriate for use in a trend analysis. The line is the dotted line through the datapoints of Figure 3.10.

**Step 2. Validate the trend in the data.**

There were no significant land use changes to the watershed over the period of record. The nonstationarity of the peak streamflow series is likely a result of increases in precipitation over the period of record. Because the analyst is not certain that the trend will continue past the historical period, then quantiles will be estimated using the mean logarithm at the end of the historical period.

Additional analysis of precipitation trends could be performed. A problem is that it is not known if a precipitation trend would be found in the annual rainfall or some other duration. Making that determination would involve further exploration.

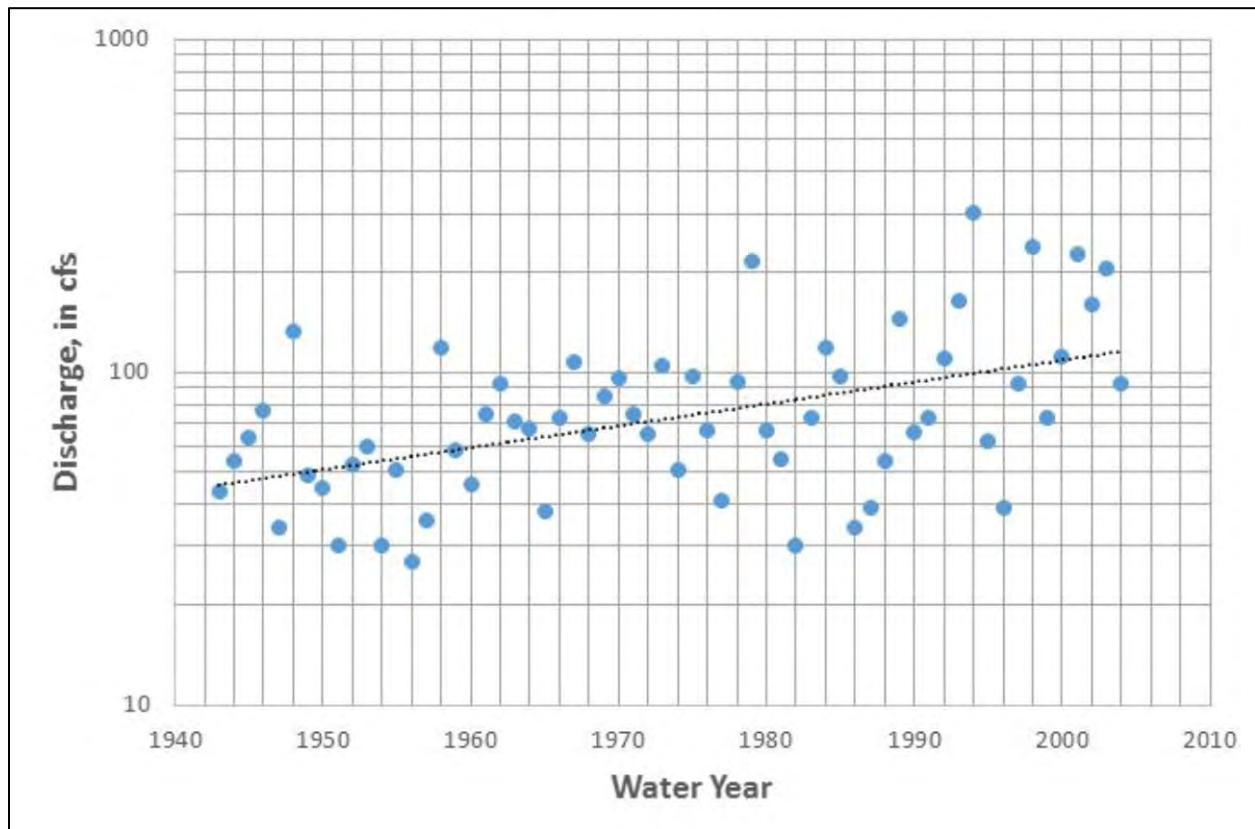


Figure 3.10. Annual peak streamflow series from Stockley Branch at Stockley, Delaware (USGS 01484500).

*Step 3. Compute the design quantiles.*

The statistics for the series (from PeakFQ) are:

Mean logarithm: 1.8623

Skew coefficient: 0.465

Standard deviation: 0.2123 (of the linear fit residuals)

$K_{0.50}$ : -0.07704

$K_{0.10}$ : 1.3204

$K_{0.01}$ : 2.6686

The quantiles of interest for the nonstationary are computed using equation 3.2:

$$\log_{10}(Q) = 1.8623 + 0.006557 \left( 61 - \frac{61+1}{2} \right) + 0.2123K = 1.6551 + 0.19671 + 0.2123K = 2.0590 + 0.2123K$$

The 0.50 AEP quantile is given by:

$$\log_{10}(Q) = 2.0590 + 0.2123(-0.07704) = 2.0426$$

$$Q_{0.5} = 10^{2.0426} = 103, \text{ say } 100 \text{ ft}^3/\text{s}.$$

The other quantiles are computed in the same way substituting the values for K. Table 3.1 summarizes the results.

*Step 4. Compare results for stationary and nonstationary analysis and evaluate the results.*

Table 3.1 lists with and without the adjustment for the trend. The increases are consistent with the slope of the regression line (about 0.6 percent per year) and that increase is within the bounds of 0.25 to 1 percent per year. Therefore, the analysis is useful to estimating the flood frequency curve from a time-varying mean.

Table 3.1. Flood frequency estimates for Stockley Branch with and without adjusting for nonstationarity.

AEP	Estimate Without Adjusting for Nonstationarity (ft <sup>3</sup> /s)	Estimate With Nonstationarity Adjustment (ft <sup>3</sup> /s)
0.50	70	100
0.10	150	220
0.01	320	420

**Solution:** For the most frequent event (0.5 AEP), the adjusted quantile is nearly 50-percent greater than the unadjusted. However, for the least frequent event (0.01 AEP), the increase is less, about one-third greater than the unadjusted event. The engineer could use these results to either design the structure, or to test the structure for resiliency.

### 3.4.3 Projecting Changes in Precipitation

Kilgore et al. (2019) provide an approach to estimate the potential changes to precipitation events useful for hydrologic analysis that is further refined by the approach in HEC-17 (FHWA 2016). This involves the use and processing of downscaled global climate model (GCM) output. The FHWA has developed a tool and user guide (FHWA 2021b) that facilitates the retrieval and processing of high-resolution climate projections using data from the Coupled Model Intercomparison Project (CMIP). This CMIP tool also performs many of the computational steps.

Figure 3.11 summarizes a 10-step method for estimating a future 24-hour duration rainfall frequency curve (RFC) for a range of AEPs or for estimating a single 24-hour quantile. The process is:

1. Determine the historical observed 24-hour precipitation RFC (or single AEP quantile, if only one quantile is appropriate) for the site.
2. Select baseline and future periods for analysis, as appropriate for the plan or project.
3. Identify the future scenarios and downscaled GCM outputs of interest from the most appropriate database of high-resolution climate projections, using the recommendations in Chapter 3 of Kilgore et al. (2019). Chapter 3 of Kilgore et al. discusses selection of downscaled climate data from GCMs and more.



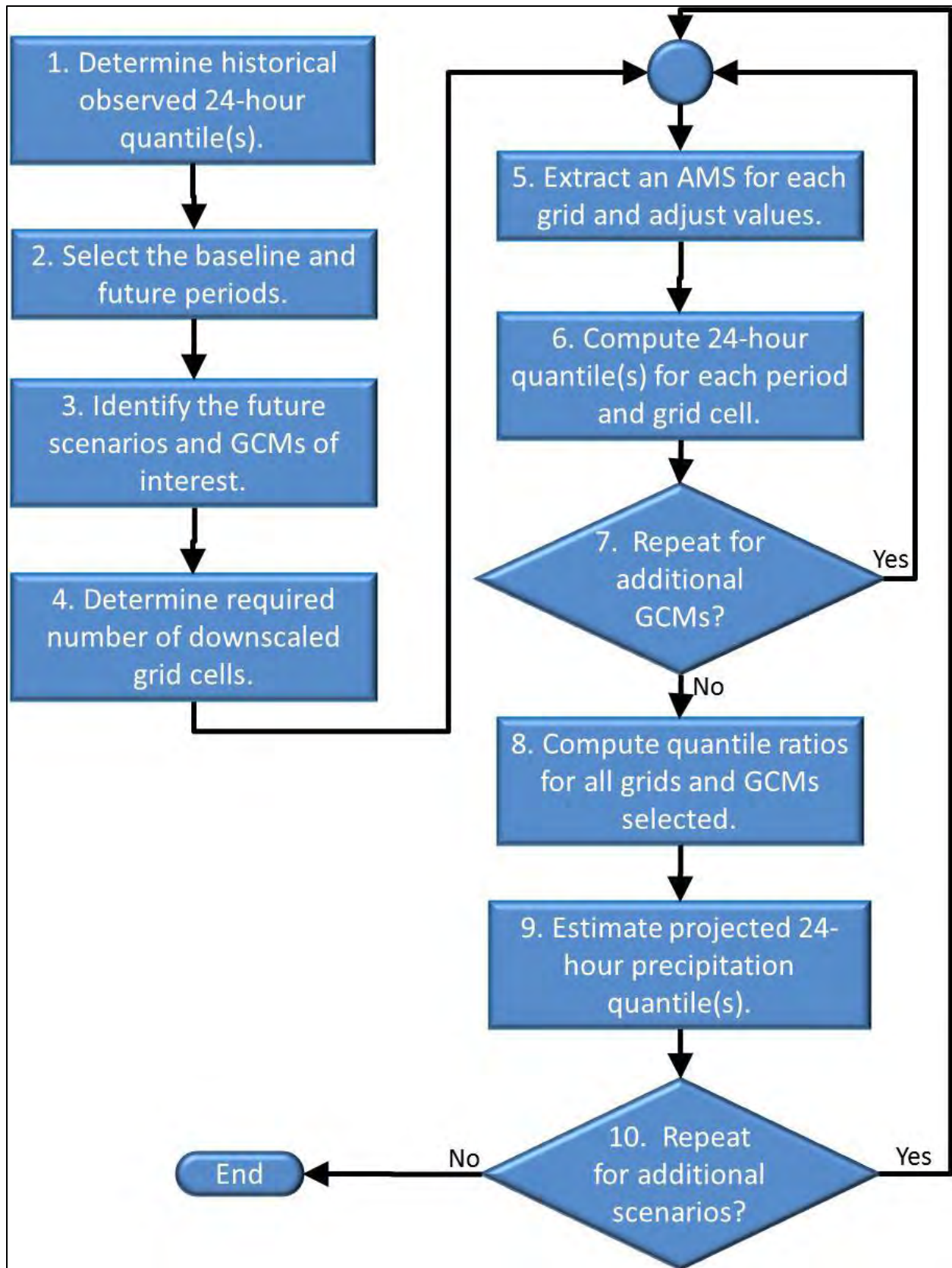


Figure 3.11. Ten-step process for projecting 24-hour precipitation quantiles.



4. Determine the number of grid cells that will adequately cover the watershed of interest.
5. Acquire the daily precipitation values and extract an annual maximum series (AMS) for each grid cell for the selected future scenario and downscaled GCM output dataset.
6. For each grid cell, compute the 24-hour precipitation RFC (or single AEP quantile) for the baseline period and for the future period from the AMS from step 5, using an appropriate statistical distribution.
7. Repeat steps 5 and 6 for each individual downscaled GCM output identified in step 3. The result of this step is a set of estimates for a 24-hour RFC (or single AEP quantile) for each grid cell and each downscaled GCM output for both the baseline and future periods for the selected scenario.
8. Compute the ratios of the modeled (downscaled GCM output) future 24-hour precipitation RFC (or single AEP quantile) to the modeled baseline 24-hour precipitation RFC (or single AEP quantile) for all grid cells and simulations.
9. Estimate the projected 24-hour precipitation RFC (or single AEP quantile) from the historical observed 24-hour precipitation RFC (or single AEP quantile) from step 1 and the ratio(s) from step 8.
10. Repeat steps 5 through 9 for each future scenario identified in step 3.

### Precipitation Value Adjustments

The 10-step procedure uses ratios of daily precipitation values. These modeled values are “constrained” daily values, i.e., midnight to midnight, rather than “unconstrained” 24-hour values that can shift to represent the largest rainfall in a 24-hour period. The modeled values also represent areal averages over the grid rather than point estimates. To use the modeled values directly, the engineer would need to adjust the AMS in step 5 to unconstrained point values with an areal reduction factor and an unconstrained 24-hour correction factor appropriate for the location (See Kilgore et al. 2019). However, since the 10-step procedure uses ratios, the adjustments cancel and are not needed.

In step 8, the engineer computes the ratio of the future and baseline modeled 24-hour quantiles for each grid cell and each simulation as:

$$RFB_{q,n} = \frac{PF_{q,n}}{PB_{q,n}} \quad (3.3)$$

where:

- $RFB_{q,n}$  = Ratio of the future to baseline 24-hour precipitation quantile (q) for grid (n)
- $PF_{q,n}$  = Future 24-hour precipitation quantile (q) for grid (n)
- $PB_{q,n}$  = Baseline 24-hour precipitation quantile (q) for grid (n)

In step 9, the engineer estimates the projected 24-hour precipitation quantile(s) by multiplying the historical precipitation quantile from step 1 by the ratio of future to baseline model estimates from step 8 as:

$$P_{q,p} = P_{q,h} (RFB_q) \quad (3.4)$$

where:

- $P_{q,p}$  = Projected 24-hour precipitation quantile (q).
- $P_{q,h}$  = Historical 24-hour precipitation quantile (q).
- $RFB_q$  = Ratio of the model future to model baseline 24-hour precipitation for quantile (q).

Equation 3.4 is not recommended for quantiles more extreme than the 0.1 AEP quantile, because the current ability of high-resolution climate datasets to represent precipitation extremes (in the engineering hydrology sense) is limited. Therefore, equation 3.5 is recommended for more extreme quantiles, including the 0.04 and 0.01 AEP quantiles. In this equation, the ratio associated with the 0.1 AEP quantile is substituted for the ratios estimated for the more extreme quantiles.

$$P_{q,p} = P_{q,h} (RFB_{0.1}) \quad (3.5)$$

where:

- $RFB_{0.1}$  = Ratio of the model future to model baseline for the 24-hour precipitation 0.1 AEP quantile

The engineer can consider the uncertainty in the estimate(s) of the projected 24-hour precipitation quantile(s). This will provide insight into the potential variation in these estimates resulting from scientific uncertainty based on the ensemble of GCMs. Knowledge of and the ability to select the appropriate climate change scenario is also part of the process. Kilgore et al. (2019) and Thomas et al. (2020) present detailed examples of this process.

### 3.5 Subdaily Precipitation Projections

Stormwater management systems depend on IDF curves as a common design tool. However, due to climate change, the extreme precipitation quantiles represented by IDF curves will be subject to alteration over time. Many current tools, including the methodology described in the previous section, use daily precipitation because that is available from many high-resolution climate datasets. Subdaily durations, e.g., 15-minute, 1-hour, or 6-hours are generally not widely available though this is changing. Several researchers have tested methods for projecting subdaily precipitation.

Kilgore et al. (2019) developed an approach that estimates subdaily durations based on projected 24-hour quantiles and the historical ratios of subdaily to 24-hour precipitation depths for a given location. The approach assumes that the historical ratios are reasonable approximations for future ratios. While this assumption of stationarity is limiting, the method provides a basis for projecting IDF curve information to support design.

#### GCM Variability

GCM outputs vary because of the assumptions about the driving physics used to simplify the real world, the underlying data used in each model, and the focus of the particular developer (and user base). Outputs from groups of GCMs can be aggregated (averaged) to produce a central tendency and a range of variability useful for understanding what the future might look like. Kilgore et al. (2019) provides information on GCM variations and ensembles.

Others have explored other methods. For example, Fadhel et al. (2017) observed that many adaptation approaches adopt a single benchmark period for bias correction. They assess the expected changes between the IDF curves of the current climate and those of a projected future climate and the uncertainties associated with such curves. To provide future IDF curves, daily precipitation data simulated by a 1-km Regional Climate Model (RCM) were temporally bias-corrected by using eight reference periods with a fixed length of 30 years and a moving window of 5 years between the cases for the period 1950–2014. Then the bias-corrected data were further disaggregated into ensemble of 5-min series by using an algorithm which combines the Nonparametric Prediction (NPRED) model and the method of fragments (MoF) framework. The algorithm uses the radar data to resample the disaggregated future rainfall fragments conditioned to the daily rainfall and temperature data. The disaggregated data were then aggregated into different durations based on concentration time.

### Bias Correction

GCMs are complex models that simulate physical processes to calculate resulting changes in the Earth's climate system including temperature, precipitation, and other variables. When compared with historical data, they sometimes exhibit biases, either systematically overestimating or underestimating certain variables. The bias correction process adjusts model outputs to better match the data.

The results suggest that uncertainty in the percentage of change in the projected rainfall compared to the rainfall in the current climate varies significantly depending on which of the eight reference periods are used for the bias correction. Both the maximum projection of rainfall intensity and the maximum change in future projections are affected by using different reference periods for different frequencies and durations. Such an important issue has been largely ignored by the engineering community and this study has shown the importance of including the uncertainty of benchmarking periods in bias-correcting future climate projections.

### NOAA Atlas 14 and Nonstationarity

NOAA (2022) presented results of research into nonstationary analysis of precipitation data and downscaled global climate model (GCM) outputs. The research is highly technical, but indicates a direction for NOAA regarding production of precipitation-frequency data, e.g., NOAA Atlas 14 for use in design activities.

NOAA intends to replace the current L-moment approach with a generalized maximum likelihood (GMLE) approach for estimating distribution parameters. The GMLE approach permits inclusion of nonstationary parameters in the fitted distributions with information from the Coupled Model Intercomparison Project (CMIP). NOAA also endorsed using ratios from downscaled GCMs of precipitation projections, as described in HEC-17 (FHWA 2016) and NCHRP 15-61 (Kilgore et al. 2019), rather than using absolute numbers from the climate datasets.

When implemented, these findings (and others) can provide designers charged with examining the potential impact of climate change on drainage design with valuable insights.

Wang et al. (2019) developed probability based IDF curves for the Department of Defense to construct and manage its infrastructure in a changing climate. Their objectives were to: 1) develop an innovative approach for considering rainfall nonstationarity in developing such IDF curves and 2) apply this approach to the State of Virginia. In this regard, they used the observed data on 15-min rainfall at 57 gages and the precipitations projected by 12 pairs of RCMs and GCMs. For a given gage or watershed, in terms of fitting the empirical exceedance probabilities, the authors chose a best-fit statistical distribution and then used it to create the existing, projected historic, and projected future IDF curves. For a given return period, the authors compared projected historic IDF curves with the existing ones to determine the lower and upper limits of the future IDF curve. The most-probable future IDF curve was determined as the average of the 12 curves responding to the GCM-RCM models. In addition, for a given duration and return period, the authors used the responding rainfall intensities to create a probability based IDF curve. Further, the areal precipitations for each of the 53 watersheds were used to create the watershed-level future IDF curves.

While many methods are not broadly actionable, much research is ongoing. A recent example is Miro et al. (2021), in which a tool for projecting the IDF curve for the Chesapeake Bay watershed was developed. Therefore, additional literature review, synthesis, and analysis will be valuable to determine what new technology is available and actionable or can be extended to tools useful to the design community.

## Chapter 4 - Low Flow Hydrology

The full range of flows informs the design of highway drainage facilities. Low flow and any structures that influence it can be particularly important for their relation to the maintenance of habitat and the survivability of species dependent on that habitat. For example, if the slope of a culvert generates a flow velocity greater than the fish species can swim through, that fish species may not survive at that location.

The *International glossary of hydrology* (WMO 1974) describes low flow as “flow of water in a stream during prolonged dry weather.” Prolonged dry weather can occur at various times during the year depending on geographical region. For example, in the Western United States, most rainfall occurs between November and April. In many locations, little precipitation occurs between May and October. The prolonged periods of low flow typical of this period result from low precipitation. In areas of the United States with cold winters, precipitation may occur in the form of snow. Persistent cold weather without snow melt can cause prolonged periods of low flow.

Because of natural variability, low flows and high flows differ in a stream from year to year. Any particular year can be an anomaly relating to when low flow occurs and if it even does. Magnitude and duration of low flow can vary greatly from year to year.

This chapter discusses several techniques for estimating low flows important the hydrologic design of roads and bridges:

- Low flow statistical analysis, including annual exceedance probability quantiles, multiday statistics, and flow duration curves.
- Bankfull indicators.
- Rainfall-runoff modeling, including event simulation and continuous simulation.

Applications for these tools include:

- Designing for aquatic organism passage (AOP) and evaluation of ecosystems.
- Managing and mitigating stormwater quality runoff.
- Designing stream restoration improvements.
- Assessing sediment transport.
- Performing geomorphological assessments.

### Low Flow versus Drought

Drought and low flow are sometimes considered synonymous; however, they are not the same. Drought is more general than low flow and can be characterized by more than just low flow in streams. Droughts are classified by their meteorological and atmospheric impacts. Generally, drought is described in terms of water availability for various uses. Simply put, the difference between low flow and drought relates to low flow being generally a seasonal phenomenon and an important part of the regular flow regime in a river. Drought generally results from an extended period of below average precipitation.

This chapter also describes channel forming discharge, a concept used in many applications including stream restoration, sediment transport, and geomorphological assessment. As discussed in this chapter, engineers can estimate channel forming discharge using several low flow tools. Table 4.1 cross-references low flow hydrology tools and their potential applications as discussed in this chapter.

Table 4.1. Low flow methods and applications.

Application	Low Flow Hydrology Method					
	AEP Quantiles	Multiday Statistics	Flow Duration Curve	Bankfull Indicators	Event Runoff Depth	Continuous Simulation Runoff
Aquatic Organism Passage/ Ecosystem Evaluation	X	X	X	X	X	X
Stormwater Runoff Quality		X			X	X
Stream Restoration*	X		X	X		X
Sediment Transport*	X		X	X		X
Geomorphological Assessment*	X		X	X		X

\*These applications may use the channel forming discharge, which can be estimated using the indicated tools.

## 4.1 Low Flow Statistical Analysis

This section describes low flow statistics and their computation. Engineers develop low flow statistics in two general ways: 1) extending flood frequency curves to commonly occurring values and 2) computing statistics based on low rather than high flows.

### 4.1.1 Flood Frequency Curves

Some situations, such as fish passage, may call for low flows based on a fraction of the 0.5 annual exceedance probability (AEP) (2-year) flood. The “Guidelines for Determining Flood Flow Frequency—Bulletin 17C” (England et al. 2019) is the primary reference on performing a flood frequency analysis. It primarily focuses on performing frequency analysis using homogenous unregulated, gaged flows.

Typically, engineers use Bulletin 17C analyses to generate rare event flows, such as the 0.01 AEP (100 year) flood. Bulletin 17C analyses also generate the statistics of the annual peak flows (mean, skew, and standard deviation). These statistics represent the entire frequency curve including the more frequent events, such as 0.99 AEP, which is essentially a peak flow that can be statistically expected to occur annually. Figure 4.1 depicts a flood frequency curve showing the 0.5 and 0.99 AEP lower flow values estimated from peak flow frequency analysis.

Engineers typically use PeakFQ (USGS 2006) and HEC-SSP (USACE 2019) at locations where recorded instantaneous annual maximum peak flows are available. Both applications provide



estimates of instantaneous annual maximum peak flows having a range of AEPs. Both also use the Pearson type III frequency distribution to fit the logarithms of instantaneous annual peak flows following Bulletin 17C procedures. Figure 4.1 displays an annual peak flow frequency analysis from HEC-SSP.

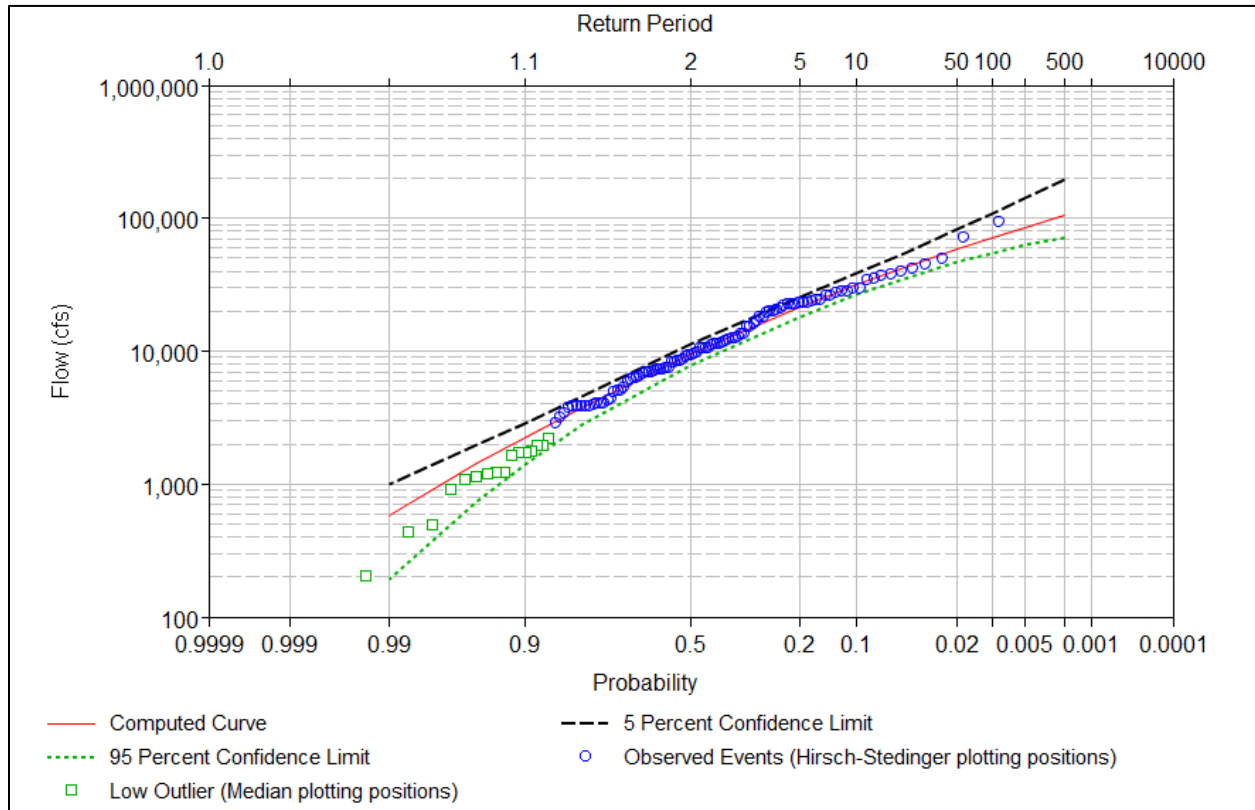


Figure 4.1. HEC-SSP annual peak flow frequency curve for the Cosumnes River at Michigan Bar (USGS 11335000).

Many engineers use HEC-SSP or PeakFQ to develop a 0.99 AEP flow based on annual peak flows. Additionally, a 0.99 AEP can be computed based on an annual maximum series based on mean daily flows. (The mean daily flow is the average streamflow during a day.) The highest mean daily flow in a year is lower than the instantaneous annual peak flow except for large watersheds where the two values become approximately equal.

Both software packages also compute the 5 and 95 percent confidence limits. These limits provide the 90 percent chance envelope about the computed frequency curve. The 95 percent limit is

#### Annual or Partial Duration Series for Small Magnitude Flows?

Estimates of small magnitude flows (more frequent than a 0.5 AEP magnitude) from flood frequency curves likely differ when based on annual versus partial duration series. Estimates can also differ between partial duration series using different thresholds and fit to different probability distributions. In general, partial duration series provide better estimates of small magnitude flows (Karim et al. 2017). The need for the low probability flow informs selection of the “right” partial duration series.

the low limit meaning that there is just a 5 percent chance the flow could be lower than the value given for the 95 percent limit. The engineer accounts for the low outlier tests within this software since the test may remove some low flows which could result in a slightly higher flow value at the 0.99 AEP. This test is used to remove the effects that low outlier flows may have on the computation of less frequent events (Cohn et al. 2013).

#### 4.1.2 Statistics on Low Flows

Hydrological or biological drivers generally determine an appropriate low flow value for an application. Determining which is important depends on the location and context of the project. An area with high environmental impact would most likely use a biological flow. Engineers express both hydrologic and biologic low flows in terms of their averaging period and their frequency of exceedance. The averaging period, or duration is generally given in days, for example, a 4-day average flow or a 7-day average flow but could also be in hours.

For hydrologic low flows, engineers employ the same statistical processes to compute a low flow as they do to compute a high (flood) flow quantile, e.g., a log-Pearson type III flow estimating technique. The two differences are: 1) an exceedance is a value lower than the quantile value and 2) the value is averaged over a period of days rather than an instantaneous maximum. Hydrologic low flows are designated as XQY. For example, a common hydrologic low flow is the 7Q10, that is, the lowest 7-day average flow that occurs on average once in every 10 years.

To compute hydrologic high flows, the engineer creates an annual maximum series of the highest instantaneous value recorded at a gage. Then, by fitting to an appropriate probability distribution, the engineer determines the value of a flood quantile that has a given AEP (or return period), for example the 0.01 AEP (100-year return period) flood.

Similarly, to compute a hydrologic low flow, the engineer creates an annual maximum series of the lowest x-day average in a given year and fits the annual series of values to an appropriate probability distribution. Finally, the engineer selects the appropriate exceedance return period for the design situation. For the 7Q10 statistic, the averaging period is 7 days (x equals 7), and the return period is 10 years. That is, the annual probability of experiencing a 7-day flow less than the 7Q10 is 0.1. The hydrologic low flow method was initially developed to answer questions relating to water supply, such as “On average, in how many years out of 10 will the flow be below a certain level?”

The hydrologic method does not consider the biological effects of multiple occurrences of low flows in a year. To address this limitation, the U.S. Environmental Protection Agency (USEPA) Office of Research and Development developed the biologically based design flow method (USEPA 1986, USEPA 2021). This approach was developed to answer questions relating to the exposure of aquatic organisms and humans to contaminants, such as “How many days can an aquatic organism be exposed to a certain contaminant before its survival is threatened?” The biological method counts all low flow events below a given threshold within a period of record, even if several occur in one year and

#### What is the difference between 4B3 and 4Q3?

The 4B3 is a biologically based four-day average flow event occurring (on average) once every three years. The 4B3 is often used as a basis for USEPA chronic aquatic life criteria. The 4Q3 is a hydrologically based design flow four-day average flow event occurring (on average) once every three years, but it does not equate to the 4B3. The 4Q3 is based on one value in each year while the 4B3 is based on all values in a year below a certain threshold value.



does not use probability distributions. Rather, the analyst counts each occurrence of crossing a threshold to examine the actual frequency of biological exposure.

Biologic low flows are designated as XBY. For example, the 4B3 is the biologic low flow where, on average, a lower 4-day average flow is experienced every three years. USEPA aquatic life criteria for water quality specify the averaging period and allowed number of exceedances depending on the pollutants and other considerations. USEPA uses the 1B3 for acute toxicity and the 4B3 for chronic effects. The biologic method is adaptable to other averaging periods and frequencies that might be selected for specific pollutants (e.g., ammonia) or site-specific criteria.

Although the field of hydrology and State water quality standards have extensively used the extreme value analytical techniques to calculate hydrologic design flows, these methods do not capture the cumulative nature of low flow event effects. These methods only consider the most extreme low flow in any given year. By considering all low flow events with a year, the biologic design flow method accounts for the cumulative nature of the biological effects related to low flow events.

The *Manual on Low-flow Estimation and Prediction* from the World Meteorological Organization (WMO) (WMO 2009) provides suggested analytical procedures for estimating and predicting low river flows at all sites, regardless of the availability of observed data. The manual does not discuss specific software.

HEC-SSP also enables users to perform a hydrologic low flow analysis such as the 7Q10. Using what is called a “volume frequency analysis” HEC-SSP allows users to aggregate multi-day averages and fit annual series of minimum values to probability distributions. HEC-SSP computes the hydrologic statistic using the annual minimum values for a given duration (e.g., 1 day, 3 days, 7 days, 15 days) for a given recurrence, e.g., 10-year, directly from data recorded at a stream gage. Because a multi-day average can be thought of as a volume, the volume frequency analysis applies.

HEC-SSP can also compute a biological statistic (e.g., 1B3, 4B3). However, since the biological statistics are based on a partial-duration minimum series rather than an annual minimum series, the analyst preprocesses the data before using HEC-SSP. For example, for the 1B3, the analyst retains all the daily flow values lower than a preselected low flow threshold and excludes adjacent values not considered statistically independent. Then, the analyst inputs the data to HEC-SSP and records the magnitude of the value associated with the 3-year recurrence interval. For a multi-day biologic statistic, such as the 4B3, the analyst computes a rolling average series of 3-day durations and retains values less than the preselected threshold. The analyst deletes adjacent values that are not statistically independent and applies HEC-SSP to the remaining dataset.

The SWToolbox (USGS 2019a) allows users to compute n-day frequency analyses (i.e., 1Q10 or 7Q10) and biologically based flows (i.e., 1B3 or 4B3). It also facilitates the use of USGS National Water Information System (NWIS) streamflow data, as well as user-provided data files. This tool applies at locations with recorded flow data.

#### 4.1.3 Low Flow Regression Equations

In choosing the type of low flow statistic and the tools to estimate the low flow estimate, the engineer considers the application and the available data. The USEPA created the *How-To Handbook for National Pollutant Discharge Elimination System (NPDES) Permit Writers* (USEPA 2018) with detailed examples of when conditions may warrant the use of either StreamStats, WREG, or SWToolbox to compute low flows. Figure 4.2 presents a flowchart of conditions that users may consider.

The USGS has developed numerous equations nationwide for estimating low flows. The National Streamflow Statistics (NSS) program includes these equations and the USGS developed regression equations for estimating flood frequency statistics in the United States, as well as equations for estimating other streamflow statistics in many States (USGS 2019b). NSS relies on manual entry of the basin characteristics used as explanatory variables in the equations and then solves the equations to estimate the statistics. Reports on the NSS website document all the equations in NSS for every State, the Commonwealth of Puerto Rico, and a number of metropolitan areas in the United States. The reports also describe limitations for their use.

The USGS integrated NSS into StreamStats, which includes several tools for statistical analysis for flow data. The web-based StreamStats application provides access to an assortment of geographic information system (GIS) tools for water resources planning and management, as well as engineering and design purposes (USGS 2017a). Engineers use StreamStats for mapping and exploring the drainage area and stream gages near a flow location of interest. StreamStats provides flows at an ungaged location.

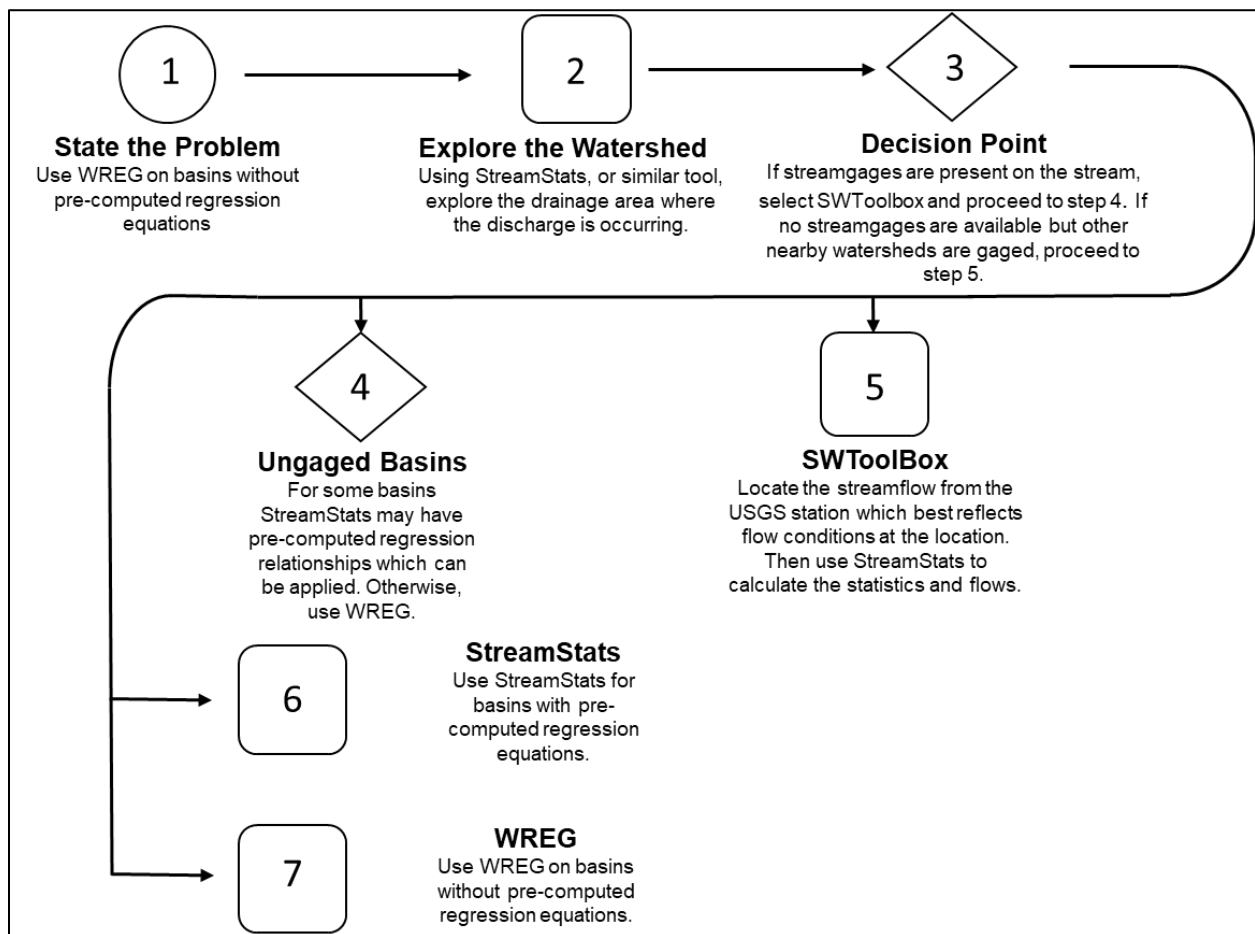


Figure 4.2. Low flow tool selection flowchart. Source: USEPA (2018).

In some situations, engineers may choose to develop new regional low flow regression equations using the Weighted-Multiple-Linear Regression Program (WREG) software (USGS 2017b). Engineers can apply these estimates at ungaged basins or use them to improve the corresponding estimate at continuous-record streamflow gages with short records. The regional estimation equation results from a multiple-linear regression relating observable basin characteristics, such as drainage area, to streamflow characteristics.

The following example illustrates a process for estimating a low flow statistic using StreamStats results.

**Example 4.1: Extrapolation of StreamStats results.**

**Objective:** Extrapolate StreamStats results to generate the 0.99 AEP flow.

As discussed above, the 0.99 AEP flow can be used as a low flow value at a location. StreamStats provides a simple method to generate a flow frequency curve at essentially any location. However, the lowest exceedance generated by StreamStats is the 0.5 AEP. Therefore, a procedure to extrapolate the StreamStats results to the 0.99 AEP can be useful. Table 4.2 presents a sample of StreamStats results for an actual location. This example will extrapolate results in Table 4.2 down to the 0.99 exceedance. An engineer working on a drainage facility could use this procedure to generate the 0.99 exceedance flow.

Table 4.2. StreamStats results for ungaged Linda Creek at Hazel Avenue, Orangevale, California.

AEP	Flow (ft <sup>3</sup> /s)
0.5	260
0.2	600
0.1	820
0.25	1,060
0.02	1,230
0.01	1,390
0.005	1,520
0.002	1,690

Appendix 5 in Bulletin 17B (IACWD 1982) provides three equations (numbered 5-3, 5-4, and 5-5 in that text) to generate a skew, standard deviation, and mean, respectively, from a computed frequency curve. These are reproduced here as:

$$G_s = -2.50 + 3.12 \frac{\text{Log}(Q_{0.01} / Q_{0.1})}{\text{Log}(Q_{0.1} / Q_{0.5})} \quad (4.1)$$

$$S_s = \frac{\text{Log}(Q_{0.01} / Q_{0.5})}{K_{0.01} - K_{0.5}} \quad (4.2)$$

$$\bar{X}_s = \text{Log}(Q_{0.5}) - K_{0.5} S_s \quad (4.3)$$

Although Bulletin 17C has superseded and improved some computational methods in Bulletin 17B, these equations remain valid.

**Step 1. Compute skew.**

Use equation 4.1:

$$G_s = -2.50 + 3.12 \frac{\text{Log}(Q_{0.01} / Q_{0.1})}{\text{Log}(Q_{0.1} / Q_{0.5})} = -2.50 + 3.12 \frac{\text{Log}(1390 / 820)}{\text{Log}(820 / 260)} = -1.07$$

Using a table of frequency factors (K) for the log-Pearson type III distribution values, such as in HDS-2, interpolate between skew values of -1.0 and -1.1 at the exceedance probability values of 0.01 and 0.5 to compute the standard deviation. In this case the K values are 1.5392 and 0.17497, respectively.

**Step 2. Compute standard deviation and mean.**

From equations 4.2 and 4.3, the standard deviation and mean are 0.533 and 2.317, respectively.

**Step 3. Compute 0.99 Exceedance flow.**

Using the following equation:

$$\text{Log}Q = \bar{X}_s + K_{0.99} S_s \quad (4.4)$$

where:

- Q = Flow, ft<sup>3</sup>/s
- $\bar{X}_s$  = Mean computed from equation 4.3
- K<sub>0.99</sub> = Frequency factor for the 0.99 exceedance probability
- S<sub>s</sub> = Standard deviation from equation 4.2

$$\text{Log}Q = \bar{X}_s + K S_s = 2.317 + (-3.069)(0.533) = 0.68$$

$$Q = 10^{0.68} = 4.8 \text{ ft}^3 / \text{s}$$

**Solution:** The 0.99 exceedance probability is estimated as 4.8 ft<sup>3</sup>/s.

It would be worth testing the statistics generated using equations 4.1 through 4.3 to see how well they reproduce the StreamStats results. Equation 4.4 can be used. A separate frequency factor (K) would be used for each exceedance probability. The 0.99 exceedance flow can be used in a hydraulic model to determine impacts of the drainage structure.

#### 4.1.4 Flow Duration Analysis

How much water flows in a watercourse and how long those flow conditions persist can be critical information for planning, designing, building, and maintaining transportation infrastructure in the river environment. Figure 4.3 illustrates a flow duration curve (FDC) which is a plot showing the percentage of time that flow is equaled or exceeded during the period of interest. Common analysis periods include annual, seasonal, monthly, and specific construction periods. Depending on the purpose, hydrologists working on a transportation infrastructure project develop FDCs to reflect maximum, average, or minimum annual or monthly flow conditions.

When designing transportation infrastructure, engineers often use FDCs to estimate the channel forming discharge (see Section 4.2) and mean annual sediment transport capacity used to

evaluate annualized, reach-scale aggradation or degradation trends. They also use this information to identify hydrologic conditions for aquatic organism passage, including fish, as discussed in Section 4.4. Flow duration curves characterizing likely flow conditions during construction and operation also inform the work of those planning and preparing for in-water construction and maintenance activities. HEC-16 (FHWA 2023) provides additional detail on flow duration curves.

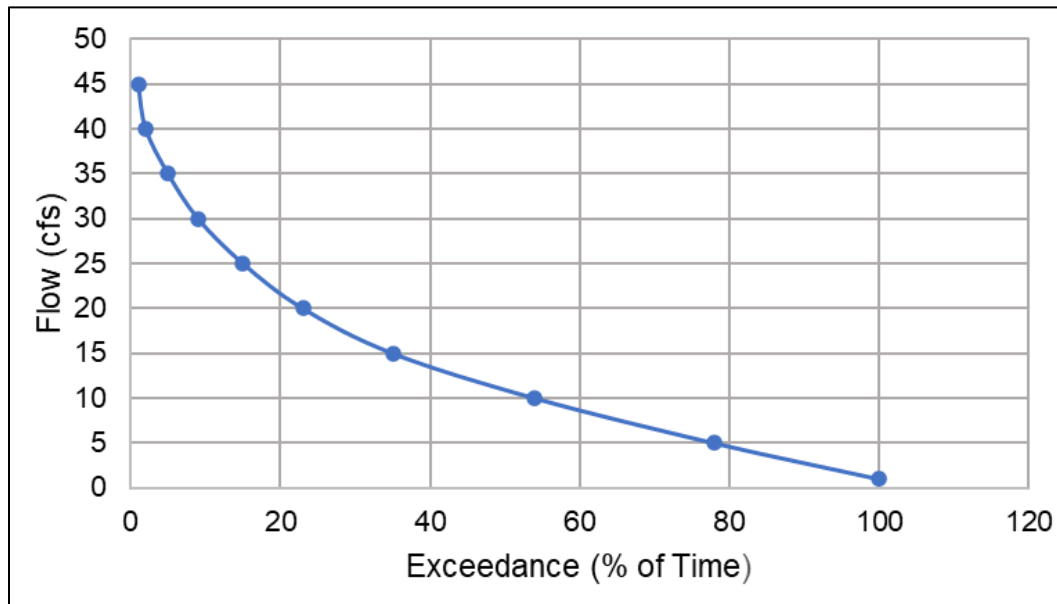


Figure 4.3. Example flow duration curve. Source: FHWA (2022).

## 4.2 Channel Forming Discharge

The channel forming discharge concept emerges from the idea that for any alluvial channel geometry, a single steady flow exists, which, given enough time, would produce channel dimensions equivalent to those shaped by the natural long-term hydrograph. The concept of channel forming discharge is now a cornerstone of many river channel restoration designs, particularly when the design includes floodplains or depends on selecting stable channel geometries. This section discusses channel forming discharge and how it relates to transportation drainage design.

Engineers working on transportation drainage facilities use an estimate of the channel forming discharge for several purposes:

- Assessment and design of alternative channel configurations and conveyance characteristics.
- Evaluation of the expected long-term stability and potential adjustments for a given channel reach. For example, they could use the channel forming discharge in a sediment transport model to understand the relative trend of a reach for dynamic stability, aggradation, or degradation.
- Evaluation of how pre- and post- construction channel velocities compare to the velocity associated with the channel forming discharge.
- Assessment and design of water crossings passable to fish (see Barnard et al. 2013).

Engineers commonly use one or a combination of the following three methods to estimate the channel forming discharge for a stable alluvial channel:

- Estimation of the bankfull discharge using field geomorphic indicators. (See HEC-16 (FHWA 2023) for an introductory discussion.)
- Estimation of the AEP for a flow that fills the channel before spilling onto the active floodplain.
- Determination of the effective discharge based on flood frequency and sediment transport relationships.

Using two or more methods provides a cross-check to reduce uncertainty in the final estimate. The three methods above are considered deterministic, not theoretical, because their values can be determined from calculations following a designated procedure. Rather than assuming any of these deterministic flows are the channel forming discharge, it is important to confirm them using field indicators of geomorphic significance (Copeland et al. 2000).

Another alternative is for analysts to perform a “sediment continuity” or “sediment impact” analysis. This analysis considers a broader range of information and is an alternative for stable channel design for most alluvial channels. National Cooperative Highway Research Program (NCHRP) Research Report 853 (Bledsoe et al. 2017) explores this alternative approach.

#### 4.2.1 Bankfull Discharge

The bankfull discharge is the maximum flow that a channel can convey without spilling onto its adjacent active floodplain. Engineers consider this flow to have morphological significance because it represents the breakpoint between the processes of channel formation and floodplain formation.

Engineers determine bankfull discharge by identifying the bankfull stage and then determining the flow associated with that stage. Several approaches for identifying bankfull stage exist. These approaches include channel width-depth ratios, stage-discharge break points and geomorphic indicators (Knighton 1984, FISRWG 1998). Geomorphic indicators defining bankfull stage include breaks in slopes between the channel and adjacent floodplains, the highest elevation of depositional features (e.g., point bars), changes in sediment gradations from coarse to fine, vegetation changes, and exposed plant roots (Wolman and Leopold 1957, Dunne and Leopold 1978).

Figure 4.4 illustrates bankfull stage as the elevation where the width to depth ratio is a minimum (Knighton 1984). This approach is systematic and relies only on accurate field surveys. Figure 4.5 illustrates determination of bankfull discharge at a distinct break in the stage-discharge rating curve from floodplain conveyance based on measured data or hydraulic modeling. The accuracy of the rating curve used in the bankfull discharge estimation depends on the uncertainties associated with assigned hydraulic roughness coefficients and the cross-section geometry. Uncertainty is greatest when the stage-discharge rating curve is estimated from a single cross-section. The FHWA’s HEC-16 (FHWA 2023) describes the use of geomorphic indicators for bankfull discharge estimates.

The concept of bankfull discharge is most relevant for watercourses with a discernible floodplain and assumes channel stability. Measurements of bankfull stage indicators in an unstable (degrading or aggrading) or non-alluvial stream reach, are therefore not valid. Similarly, bankfull stage indicators in ephemeral alluvial streams in arid environments or highly urbanized watersheds can be absent or uncertain.

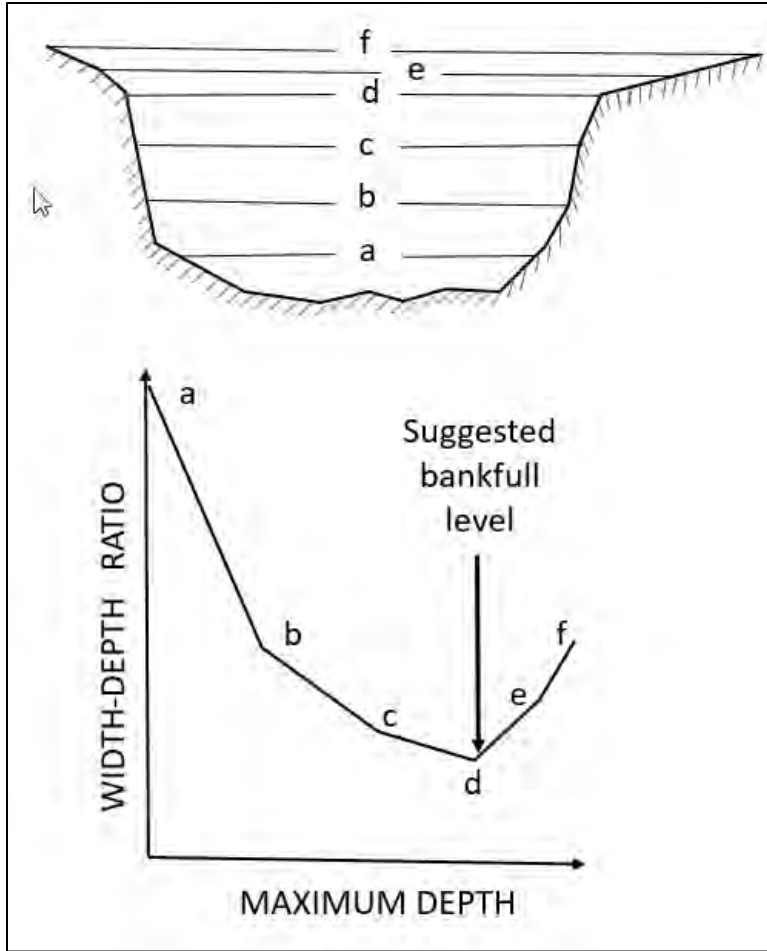


Figure 4.4. Bankfull stage estimation from width-depth ratio.

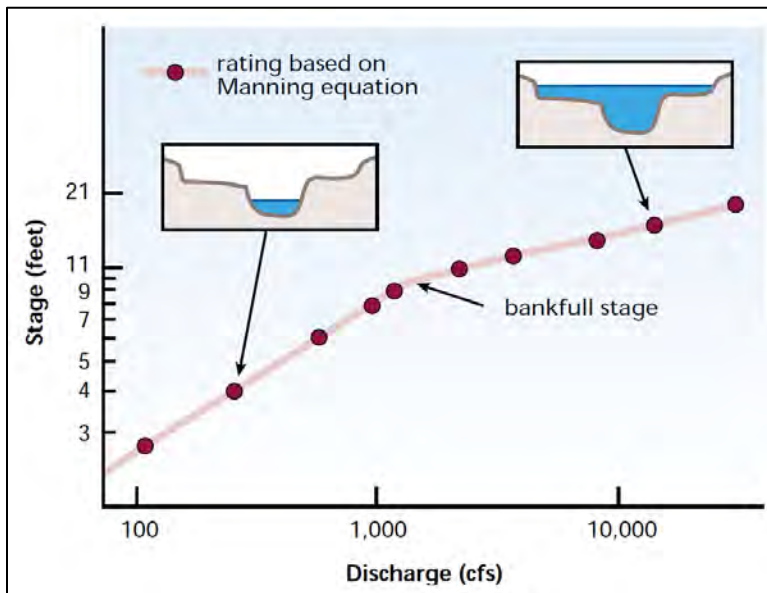


Figure 4.5. Bankfull stage estimation from a rating curve. Source: after FISRWG (1998).

### 4.2.2 Specific AEP Discharge

When identification of bankfull stage and discharge is difficult or not applicable, researchers have related the channel forming discharge to a specific AEP discharge. In general, bankfull discharge in stable channels has been found to correspond to a return period of approximately 1.01 to 2.5 years (99 percent and 40 percent AEP). Leopold (1994) concluded that the 1.5-year (67 percent AEP) flow is a representative mean of many streams.

However, in some situations, the channel forming discharge does not fall within the 1.01- to 2.5-year range, e.g., for channels with flashy hydrology. Williams (1978) found that out of 35 floodplains he studied in the United States, the bankfull discharge varied between the 1.01- and 32-year (0.99 and 0.031 AEP) respectively). Williams also found that only about a third of those streams had a bankfull discharge AEP between 1.01- and 5-years (0.99 and 0.2 AEP, respectively). In a similar study, Pickup and Warner (1976) determined that bankfull AEP ranged from 4 to 10 years (0.25 and 0.1 AEP, respectively). Because of such discrepancies, many researchers have concluded that AEP approaches tend to generate poor estimates of bankfull discharge.

Although the assumption that the channel forming discharge has an AEP ranging between 1.01 and 2.5 years (0.99 and 0.4 AEP, respectively) is sufficient for reconnaissance-level studies, for design purposes, it is important to verify in the field that the selected flow reflects morphologically significant features. Field verifications can be performed through inspection of reference reaches, data collection, and comparison with other bankfull discharge estimates. This is especially true for highly modified streams such as in urban or mined areas, as well as for ephemeral streams in arid and semiarid areas.

### 4.2.3 Effective Discharge

Andrews (1980) describes effective discharge as the mean of the flow increment that transports the largest fraction of the annual sediment load over a period of years. Wolman and Miller (1960) further describe effective discharge as a function of both the magnitude of the event and its frequency of occurrence. Engineers calculate the effective discharge using the flow frequency distribution and the bed material load rating curve. Bed material is the part of the total sediment flow composed of grain sizes found in the riverbed. Figure 4.6 illustrates the relationship between sediment transport, frequency of the transport, and the effective discharge. The peak of curve III marks the flow that most effectively transports sediment and, therefore, that researchers hypothesize does the most work in forming the channel. Biedenharn et al. (2000) provides a detailed explanation with examples of how to calculate the effective discharge. As illustrated in the figure, the procedure includes three steps.

#### **Step 1. Derivation of the flow frequency distribution.**

Engineers typically use mean daily flows to construct the FDC. However, for smaller streams with flood events that may last only a few hours, hourly or sub-hourly time series may be appropriate. Engineers can develop the FDC from gage data or from physiographically similar watersheds. To provide the flow frequency distribution, engineers divide the FDC into flow increments, calculating an occurrence frequency for each increment.

When gage data exist, engineers can use them directly to construct the FDC, if watershed conditions have remained unchanged during the selected historical flow period. An appropriate period of record is sufficiently long to include a wide range of morphologically significant flows, but not so long that changes in climate, land use, or runoff characteristics produce significant changes with time in the data. A reasonable minimum period of record for an effective discharge



calculation is about 10 years, with 20 years of record providing more certainty that the data fully represent the range of morphologically significant flows.

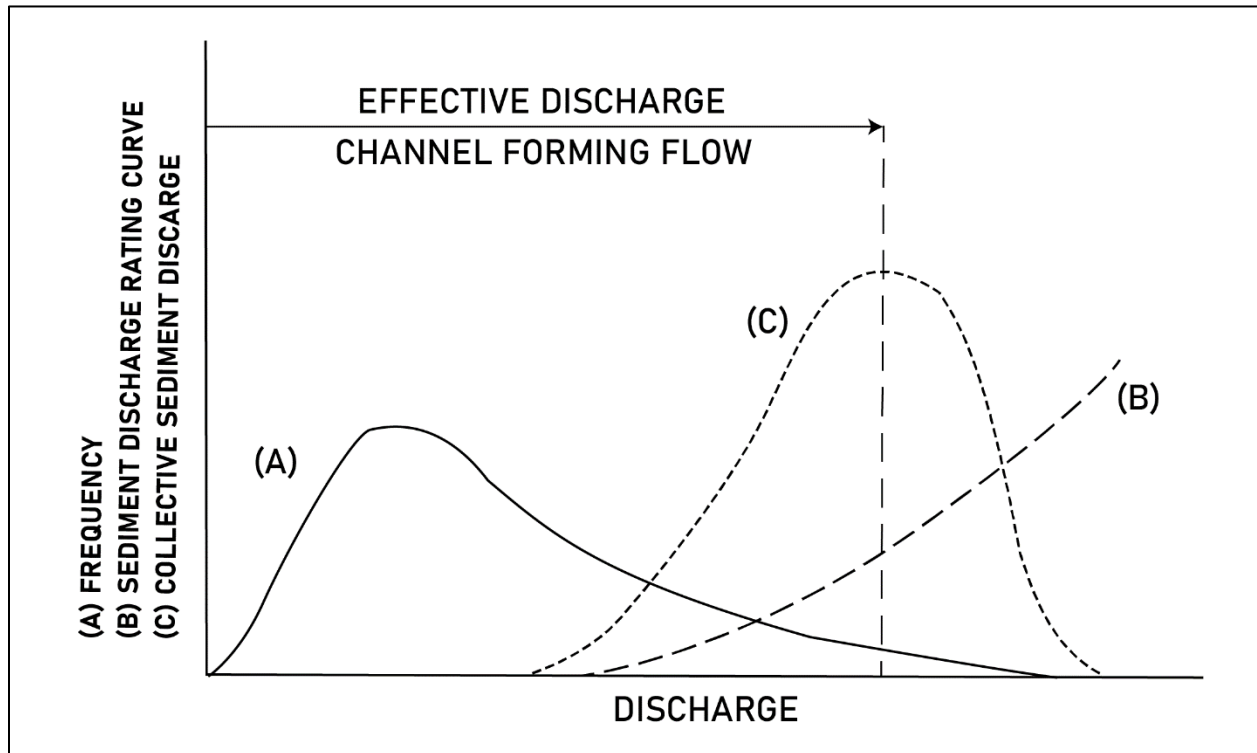


Figure 4.6. Effective discharge/channel forming flow.

When gage data are not available, two possible methods can be followed to develop the FDC: 1) use records from nearby gaging stations within the same drainage basin, or 2) develop a regionalized FDC.

The drainage basin flow duration method relies on the availability of gaging station data at several sites on the project stream. Flow duration curves for each gaging station are derived for the longest possible common period of record. Provided there is a regular downstream decrease in the flow per unit watershed area, then a graph of flow for a given exceedance duration against upstream drainage produces a power function with insignificant scatter about the best-fit regression line. Figure 4.7 shows an example of the drainage basin flow duration method applied to the River Wye in the United Kingdom (Hey 1975). This method enables the FDC at an ungaged site on that river to be determined as a function of its upstream watershed area.

The regional-scaling method relies on the availability of data from watersheds with similar characteristics and the existence of regional regression equations. The first step in creating a regional FDC is developing flow ratios from an appropriate gaged watershed. Watson et al. (1997) suggest using the 2-year flow  $Q_2$  to normalize a flow duration curve from a similar, gaged watershed as  $Q/Q_2$  to create a dimensionless FDC. If more than one similar gaged site is available, an average dimensionless flow duration curve for all the sites can be developed. In the second step the engineer computes the  $Q_2$  for the ungaged site using a regression equation or any appropriate method. Finally, the engineer calculates the flow duration curve for the ungaged site by multiplying the dimensionless flow duration curve (step 1) by the ungaged  $Q_2$  (step 2).

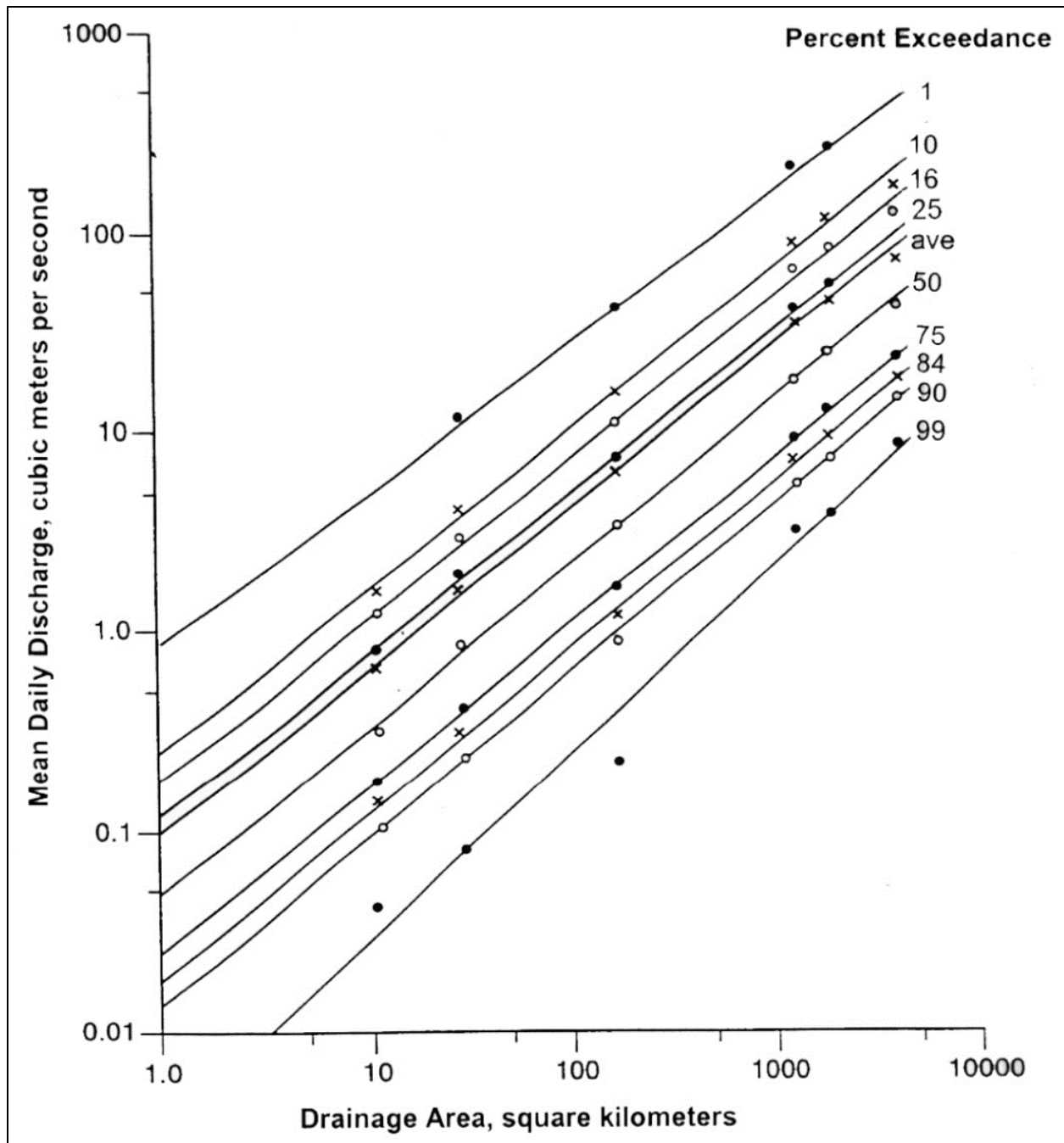


Figure 4.7. Downstream daily flow duration curve, River Wye, UK, 1937-1962. Source: Hey (1975) used by permission.

### Step 2. Derivation of the bed material load rating curve.

Sediment data are used to generate the bed material load rating curve. These data may be obtained from measurements at a gaging station if the gage is near the project reach and if size-class fractions are provided so that the bed material portion of the measured load can be determined. If the bed material load moves both as bed load and suspended load, then both bed load and suspended load measurements are used to determine the bed material load.

In streams dominated by suspended load, a best-fit regression curve fitted to the data may be adequate to produce a bed material load function. Frequently, this takes the form of a power function:

$$Q_s = aQ^b \quad (4.5)$$

where:

$Q_s$	=	Bed material load
$Q$	=	Water flow
$a$	=	Regression coefficient
$b$	=	Regression exponent

However, a power function may not be appropriate in all cases. Sometimes, at high flows the rate of increase in sediment concentration with flow begins to decrease, especially for the finer sand sizes. In this case a different curve fitting function may be indicated. In coarse bed streams, a coarse surface layer is likely to develop at lower flows, significantly reducing sediment transport potential. This process involves both hydraulic sorting of the streambed and hiding of small particles behind bigger particles. Typically, calculated sediment transport rating curves developed from a single bed gradation will overestimate sediment transport at low flows.

If measured data are insufficient to estimate a bed material load rating curve, use of sediment transport equations or modeling may be appropriate as described in HEC-16 (FHWA 2023). The HEC-RAS software (USACE 2021c) or the SRH-D software (USBR 2020) can be used to estimate a bed material load rating curve or perform sediment transport simulations at the reach of interest. A sediment transport rating curve can be also constructed estimating the sediment capacity for several flows following the procedure outlined in NCHRP 24-40 study (NASEM 2017)

### **Step 3. Derivation of the bed material load histogram.**

The flows used to generate the bed material load histogram are the mean flows of each flow increments (classes) in the flow frequency distribution. The histogram is generated by using the representative flows and the bed material load rating curve to find the bed material load for each flow class and multiplying this load by the frequency of occurrence of that flow class. The results are plotted as a histogram representing the total amount of bed material load transported by each flow class during the period of record.

As shown in Figure 4.6, the bed material load histogram will display a continuous distribution with a single mode (peak) in many cases. In this case, the effective discharge corresponds to the mean flow for the modal class (the peak of the histogram). If the modal class cannot be readily identified, the effective discharge can be estimated by drawing a smooth curve through the tops of the histogram bars and interpolating the effective discharge from the peak of the curve. If the modal class of the bed material load histogram is the lowest flow class, it is likely that the indicated effective discharge is erroneous. In this case it may be appropriate to modify the procedure by either increasing the number of flow classes or modifying the bed material rating curve, noting the cautions to be exercised in each case.

## **4.3 Rainfall-Runoff Modeling**

Low flow statistical methods (Section 4.1) or channel forming discharge methods (Section 4.2) may provide sufficient detail to generate a flow at the location of interest. However, sometimes modeling a location with a rainfall-runoff model provides more detailed information relating to runoff at the location. Computed runoff is also an important input for hydraulic software when

determining the hydraulic impacts, such as velocity changes or sediment impacts, resulting from a new drainage facility.

When engineers develop models for project locations, either single event or continuous models may be appropriate. The type of simulation selected depends on project goals. Generally, model developers use event-based simulations to evaluate flood risk reduction project measures and alternatives. Engineers infrequently use event-based models for computing a low flow value for a location. However, since single event simulation models are generally applied more widely than continuous simulation models, they are included here to provide the comparison to continuous simulation. Rainfall duration and time step depend on the response time of the basin above the location. A short response would indicate that short time step data are appropriate. A long response, on the order of days, indicates longer time step data can be used.

Model calibration is critical to have confidence that the model can reproduce an observed event. Because low flows are of interest, calibrating the model to correctly reproduce periods of low flow is important.

#### 4.3.1 Single Event Modeling

Engineers create single event models to reproduce a specific short term runoff event. These events are typically represented by a runoff hydrograph rising and falling over a period of days and might be specified as the June 2003 event or December 1964 event.

Figure 4.8 depicts a flood event. The event tends to be characterized by the time from the start of the rising limb of the hydrograph to the end of the hydrograph recession. Engineers typically use an event-based model to reconstruct observed flood events. They would then calibrate the model to multiple events and the model is used to predict hypothetical runoff events such as the 1 in 100-year event. Engineers have multiple methods from which to choose in building the model (USACE 2021a).

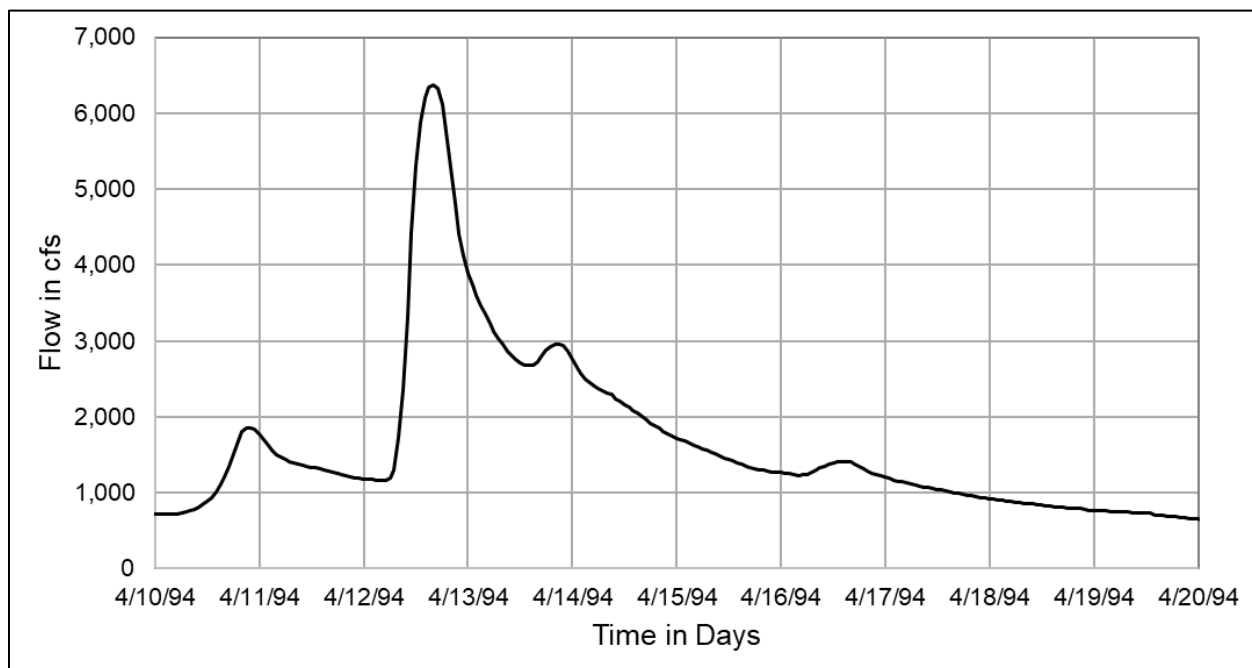


Figure 4.8. Sample single event time window.

Rainfall-runoff models depend on rainfall as a primary input. The National Weather Service (NWS) National Oceanic and Atmospheric Administration (NOAA) Atlas 14 Precipitation Frequency Data Server (PFDS) available from the NOAA website provides precipitation data engineers can use to compute low flow at a location for a single (design) event. The analyst can select the location of interest and the website will return precipitation values for varying AEPs based on annual maxima series or annual recurrence interval (ARI) for partial-duration series. By selecting an AEP or ARI for a frequent precipitation event, the rainfall-runoff model will generate a low flow. If the analyst determines that the NOAA 14 data do not adequately represent rainfall at the project location, a frequency analysis of local rainfall could be performed to determine rainfall values to use in the model.

#### 4.3.2 Continuous Simulation Modeling

Continuous simulation models can extend over a period of multiple days, months, or even years. The period modeled may include both high runoff periods and low flow periods. Engineers sometimes use these models when evaluating areas of environmental concern. Because continuous simulation models entail considerable data inputs, the engineer first determines whether the project warrants the involved effort compared to an estimate derived from a method described in Section 4.1 or Section 4.2.

Engineers use continuous simulation models to reproduce high and low flows that typically occur over a long period and to assess how a project may impact flows or how flows may impact a project over the same period. It is important that models over long time periods contain simulation methods that allow the soil to absorb water during times of precipitation as well as dry during periods of no precipitation. This is typically called soil moisture accounting. Figure 4.9 depicts a long-term period that could be modeled as a continuous simulation.

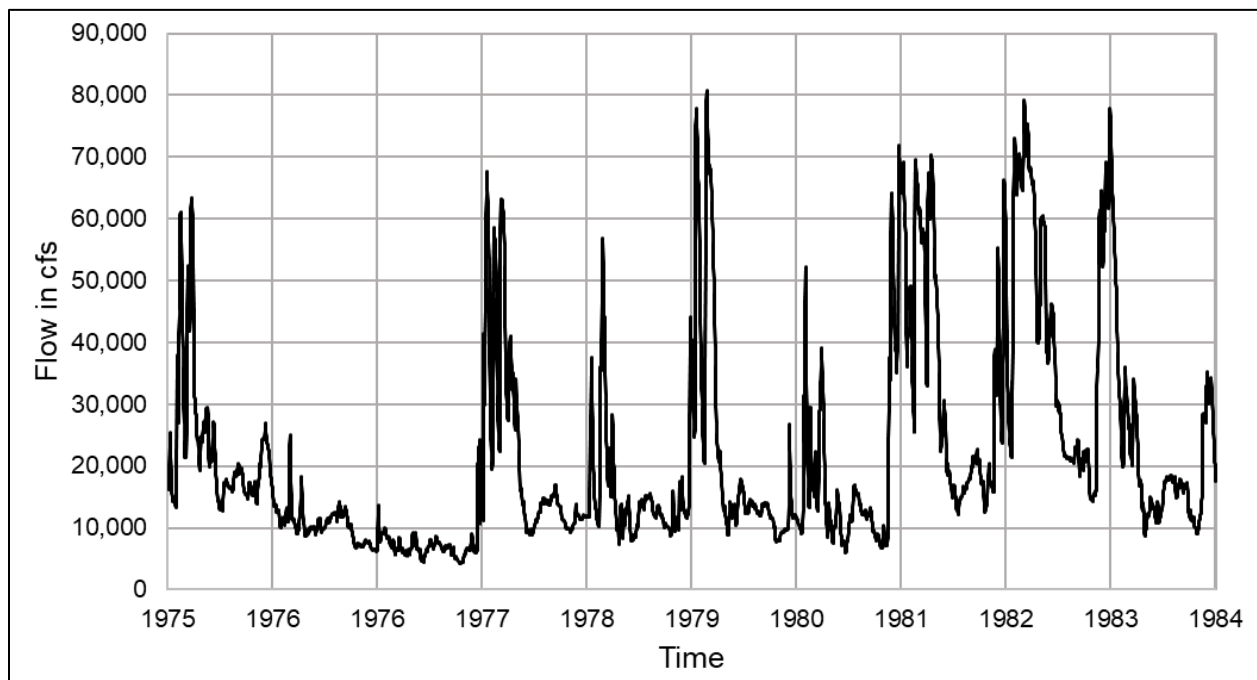


Figure 4.9. Sample continuous simulation time window.

As an example, if a location has two or three years of observed flows and rainfall, the engineer could build and calibrate a continuous simulation model for the two or three years of available data. The modeler could then use longer term precipitation data (e.g., 30 years) to apply the

precipitation to the model and run it for the 30-year predictive period. The low flows predicted by this model, between times of precipitation, could be used to estimate a low flow for the location.

### 4.3.3 Rainfall-Runoff Software

Software implementation of event-based and continuous simulation models have been developed by the USGS, USACE, USEPA, and many others. This section highlights examples of commonly used tools in the public domain. Each example has multiple modeling capabilities and can be used for single event or continuous simulation. To select the appropriate application for a given project location, the engineer will want to understand how the software would handle specific situations. The websites for each organization provide detailed capabilities of the software.

#### 4.3.3.1 Hydrologic Modeling System (HEC-HMS)

The Hydrologic Engineering Center office of the USACE developed HEC-HMS, which can be downloaded, along with its documentation, from the HEC website (USACE 2021a). HEC-HMS simulates the precipitation-runoff processes of dendritic watershed systems. It applies in a wide range of geographic areas to solve the widest possible range of problems. This includes both large river basin water supply and flood hydrology and small urban or natural watershed runoff. Engineers can use hydrographs produced by the program directly or in conjunction with other software for studies of water availability, urban drainage, flow forecasting, future urbanization impact, reservoir spillway design, flood damage reduction, floodplain regulation, and systems operation.

#### 4.3.3.2 Storm Water Management Model (SWMM)

Developed by the USEPA, SWMM and associated documentation can be downloaded from the USEPA website (USEPA 2020). SWMM is a dynamic rainfall-runoff simulation model used for single event or long-term (continuous) simulation of runoff quantity and quality from primarily urban areas. The runoff component of SWMM operates on a collection of sub catchment areas that receive precipitation and generate runoff and pollutant loads. The routing portion of SWMM transports this runoff through a system of pipes, channels, storage/treatment devices, pumps, and regulators. SWMM tracks the quantity and quality of runoff generated within each sub catchment, and the flow rate, flow depth, and quality of water in each pipe and channel during a simulation period comprised of multiple time steps.

#### 4.3.3.3 Precipitation-Runoff Modeling System (PRMS)

Developed by the USGS, PRMS (USGS 2021) and associated documentation can be downloaded from the USGS website. PRMS is a deterministic, distributed-parameter, physical process-based modeling system developed to evaluate the response of various combinations of climate and land use on streamflow and general watershed hydrology. PRMS can simulate hydrologic processes including evaporation, transpiration, snow accumulation and melt, runoff, infiltration, and interflow. PRMS provides several options for computing these processes determined by the energy and water budgets of the plant canopy, soil zone, and snowpack based on distributed climate information (maximum and minimum air temperature, precipitation, potential evapotranspiration, solar radiation, humidity, and wind speed).

#### 4.3.3.4 Gridded Surface Subsurface Hydrologic Analysis (GSSHA)

The Engineer Research and Development Center (ERDC) office of the USACE developed GSSHA (USACE 2021b). GSSHA and associated documentation can be downloaded from the GSSHA Wiki page. GSSHA is a physics-based, distributed, hydrologic, sediment and constituent fate and transport model. Features include two-dimensional (2D) overland flow, one-dimensional

(1D) streamflow, 1D infiltration, 2D groundwater, and full coupling between the groundwater, shallow soils, streams, and overland flow. Sediment and constituent fate and transport are simulated in the shallow soils, overland flow plane, and in streams and channels. GSSHA can be used as an episodic or continuous model where soil surface moisture, groundwater levels, stream interactions, and constituent fate are continuously simulated. The fully coupled groundwater to surface water interaction allows GSSHA to model basins in both arid and humid environments.

#### 4.4 AOP/Ecosystem Design Flows

As discussed in HEC-26 (FHWA 2010), historical culvert design methods focused on hydraulic conditions resulting from the design flood, frequently taken as the 0.04, 0.02, and 0.01 AEP event. By not explicitly considering a full spectrum of streamflows, including low flows, the resulting designs have resulted in hydraulic barriers (velocity, depth, or jump) and sedimentation issues at some road crossings.

##### Oregon Low Flows

According to the Oregon Department of Fish and Wildlife (ODFW), low flow design for some applications (ODFW 2004) considers either:

- The 0.5 AEP (2-year), seven consecutive day (7Q2) low flow discharge.
- The 95 percent exceedance flow.

Aquatic organism passage and other ecosystem design methods emphasize lower flows that occur more frequently than typical design floods. Depending on the type of AOP road crossing selected for design, it may be appropriate to determine the flow rate for certain frequently occurring flows, such as the 0.5 AEP flow or lower to consider the changes in depth for the lowest expected flow occurring when the target species is present. Many States have adopted specific low flow statistics for AOP design (see box). As mentioned previously, stream simulation techniques attempt to mimic natural stream velocities and depths over a range of flows reducing the need to examine target species specifically or a single design flow.

Stream gage data, if available, provide the most accurate way to calculate AOP flow rates but because comparatively few streams are gaged, the project site

is unlikely to have gaging data. Therefore, engineers frequently estimate AOP streamflow using a hydrologic method like those described in Section 4.1.

Because of the uncertainty of these methods, and because of importance of velocity for assessing AOP conditions, analysts consider the uncertainty associated with these estimates and perform sensitivity analyses. Engineering judgment is important for AOP flow estimates in steeper watersheds and urbanized or urbanizing watersheds, where land use and basin hydrology changes during the life of the project may affect maximum and minimum flows.

#### 4.5 Water Quality and First Flush

Transportation agencies address water quality effects of stormwater runoff from highways, roads, bridges, and other transportation facilities. The construction, operation, and maintenance of roadways affect stormwater runoff quality from highways. Runoff from road surfaces contains sediment, oil, grit, and other contaminants. Suspended sediment increases water turbidity and pollutants tend to attach to fine sediment particles. Both processes negatively affect water quality.

Implementing innovative best management practices (BMP) and encouraging cooperation between highway and other water-related agencies helps protect water quality related to roadway projects. NASEM (2006) provides a thorough overview of water quality, BMP, and first flush for



highway applications. The California Department of Transportation provides a detailed characterization of the first flush phenomenon (Stenstrom and Kayhanian 2005).

National and State-specific standards and runoff estimation methods are useful for water quality mitigation. The USEPA compilation of State stormwater standards gives a thorough overview of the practices, including first flush treatment, in each of the 50 States and the District of Columbia (USEPA 2011). HEC-16 (FHWA 2023) also contains a section on water quality that provides an overview of the extensive water quality work FHWA has sponsored with the USGS.

The highest concentration of pollutants during a single storm event is typically generated in the first period of runoff and is known as the “first flush.” In arid and semi-arid regions, the first rainfall of the wet season tends to cause the most pollutant-concentrated runoff. This “seasonal first flush” washes out the pollutants accumulated during the dry season.

Identifying and quantifying the storm and seasonal first flushes presents an opportunity to better mitigate water quality. Effectively treating the higher concentrations of the first flush may be a more cost-effective approach than a uniform treatment of the entire runoff volume. Treatment cost relates to volume of water; trapping and removal efficiency increases with higher pollutant concentrations.

Engineers can estimate a first flush volume based on a runoff depth, such as 0.5 or 0.75 inches, which implicitly corresponds to a frequency of occurrence, and multiplied by the drainage surface area. The Los Angeles Municipal Stormwater Permit, for example, calls for treatment of the first 0.75 inch of runoff, which it estimates is approximately equivalent to the 85<sup>th</sup> percentile. Similarly, engineers can estimate the first flush volume based on a specific rainfall depth, such as one inch, and a runoff volume fraction:

$$V = APC_R \quad (4.6)$$

where:

V	=	Runoff volume, ft <sup>3</sup> (m <sup>3</sup> )
A	=	Drainage surface area, ft <sup>2</sup> (m <sup>2</sup> )
P	=	Precipitation, ft (m)
C <sub>R</sub>	=	Runoff volume fraction

Another approach to estimating water quality runoff volumes is applying continuous simulation models. As discussed in Section 4.3.2 and in other manuals, e.g., the Washington Department of Transportation (WSDOT 2019), continuous simulation models can be effective in replicating long duration low flows in cases of environmental concern, which is relevant to this application. As discussed earlier, higher concentration of pollutants tends to occur in low flows. Hence, designers typically size runoff treatment facilities based on the runoff volume resulting from higher frequency flows, examples of which are the 2-year recurrence interval and the 85<sup>th</sup> or 90<sup>th</sup> percentile flows.

The pollutant load is a relationship between runoff volume and pollutant concentration:

$$L = \frac{cV}{\alpha} \quad (4.7)$$

where:

L	=	Pollutant load, lb (kg)
c	=	Pollutant concentration, mg/L
V	=	Runoff volume, ft <sup>3</sup> (m <sup>3</sup> )
α	=	Unit conversion constant, 16,000 in CU (1,000 in SI)



This relation applies to each pollutant source and the sum of the pollutant loads is the total pollutant load. With the estimated runoff volume and pollutant load, an engineer can select an appropriate BMP that can effectively remove a significant portion of the pollutant load.

Water quality and first flush modeling software can typically model water quality indicators, such as suspended solids, biological oxygen demand (BOD), chemical oxygen demand (COD), total nitrogen (TN), total phosphorous (TP), and E. coli. For example, the USEPA SWMM is a dynamic rainfall-runoff simulation model used for single event or long-term (continuous) simulation of runoff quantity and quality from primarily urban areas (Rossman 2015). Originally developed in 1971, SWMM pioneered water quality modeling and evolved into one of the most widely used stormwater management modeling tools. In addition to the public domain version, many proprietary versions have added graphical and user-friendly functionality.

The Stochastic Empirical Loading and Dilution Model (SELDL), developed by USGS in cooperation with FHWA, is a planning-level tool that estimates mean concentrations, flows, and pollutant loads in stormwater runoff (Granato 2013). SELDL is a stochastic model that assesses the risk for adverse effects of runoff on receiving waters, the potential need for mitigation measures, and the potential effectiveness of such management measures for reducing these risks.

Model for Urban Sewers (MOUSE) simulates urban stormwater systems and was developed by the Danish Hydraulic Institute (DHI) (DHI 2003). The MOUSE is one of the computational engines of the hydraulic modeling software, MIKE URBAN. Its capabilities include modeling of water quality and sediment transport in stormwater systems, and it is comparable to SWMM. SWMM is generally more frequently used in North America, whereas MOUSE is more frequently used outside of North America.

*Page Intentionally Left Blank*

## Chapter 5 - Coincident Frequency

This chapter describes tools and approaches for estimating floods at stream confluences and where riverine and coastal storms interact. Stream confluences pose unique challenges for the design of transportation infrastructure upstream, around, and downstream of the confluence. This is because roads may be affected by events in either waterway, or by the combined effects of events in both confluent waterways. Differences in hydrology, size, terrain, shape, and degree/type of development between the contributing drainage basins may create several design challenges. Tributary-mainstem interactions center on the confluence but their influences and effects extend along both the mainstem and the tributary waterway.

Figure 5.1 shows the confluence where the smaller Big Sioux River joins the much larger Missouri River at Sioux City, Iowa. Interstate 29 crosses the Big Sioux River approximately 1.5 miles upstream of the confluence. In the early morning of April 1, 1962, the 556-foot upstream (westbound) I-29 bridge collapsed. The engineering evaluation of the collapse concluded that high flows on the Big Sioux River combined with relatively low flows (and stage) on the Missouri River contributed to high velocities at the I-29 crossing that scoured away supporting material at the bridge piers causing the failure (Erickson 1962).

In the Big Sioux River I-29 collapse, the coincident events were a high hydrologic event on the tributary and a low event on the mainstem. Coincident high flows on both the tributary and the mainstem also could have created unanticipated flooding conditions. Engineers use coincident frequency analysis techniques to analyze the risks associated with such events.



Figure 5.1. Confluence of the Big Sioux River with the Missouri River at Sioux City, Iowa.



Figure 5.2 illustrates where a different type of coincident event, commonly called coastal compound flooding, may occur. Rainfall driven flooding of the Ashley, Cooper, or Wando rivers combined with high storm surge driven into Charleston Harbor could create flooding levels greater than either event occurring separately.

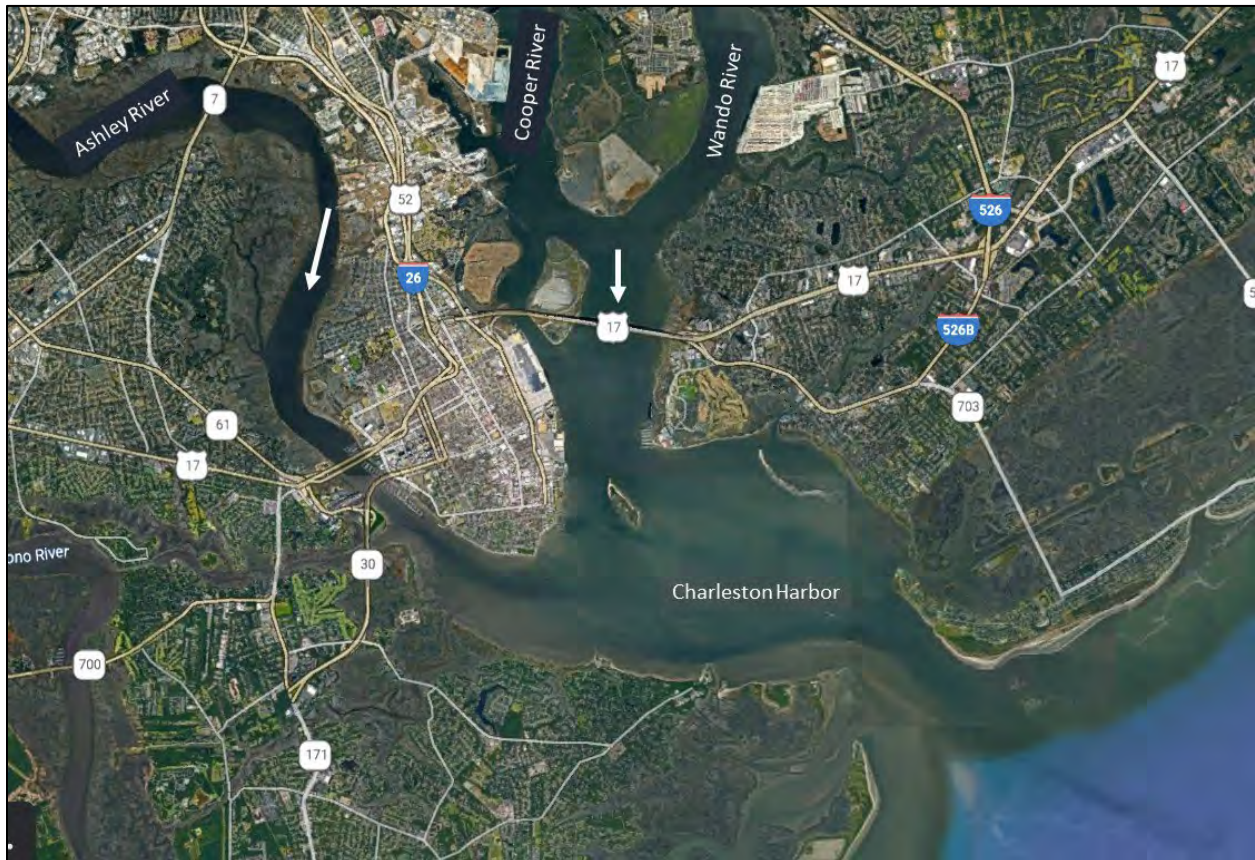


Figure 5.2. The Ashley, Cooper, and Wando Rivers entering Charleston Harbor (South Carolina).

Both examples of coincident flooding are characterized by two events that may have some degree of correlation with each other. In the first case, the two events are flooding on a tributary and flooding on a mainstem at a river confluence. In the second case, the two events are riverine flooding and coastal storm surge.

If there is no correlation between the two events, then they are independent and coincident frequency analysis is not indicated. If there is correlation, coincident frequency analysis quantifies the dependence (correlation) between the events. Dependence often results because there is a physical relationship between the two events or because they can both result from the same cause. For example, confluent flooding in Sioux City, Iowa (Figure 5.1), can result from a rainstorm that is sufficiently large spatially to cause flooding on both watersheds. Other storms may be too small, spatially, to affect both confluent rivers. Similarly, coastal compound flooding at Charleston Harbor (Figure 5.2) might result from a hurricane carrying sufficient rainfall and timed so that riverine flooding occurs at the same time winds push storm surge into the harbor.

Coincident frequency analysis, as described in this chapter, provides tools to describe the frequency distributions of each event acting individually and to characterize the dependence

between them. Both the individual frequency distributions (called marginal distributions) and their interdependence vary with location, meteorology, topography, and other watershed conditions.

Because these problems involve two variables, multivariate analysis is used to develop tools for engineers. Beyond these examples, coincident frequency analysis can include more than two variables depending on the needs and complexities of a situation. Bensi et al. (2019) reported on efforts to develop more general approaches to probabilistic assessment of what they called “multi-mechanism” floods (MMF). They introduced a generalized MMF assessment framework to describe the distinctions among various types of flood-forcing phenomena and flood mechanisms.

This chapter focuses on tools and approaches currently available for bivariate assessment of coincident flooding situations like those illustrated in Sioux City, Iowa (confluence flooding), and Charleston, South Carolina (coastal compound flooding). The following section introduces multivariate analysis. The subsequent sections describe tools for confluence and coastal compound flooding relevant for the roads and bridges in riverine and coastal settings.

## 5.1 *Multivariate Analysis*

Engineers perform many statistical analyses of hydrologic variables with univariate random variables, for example, analyses of the frequency distribution of annual peak flows from a watershed or the distribution of rainfall depth over a fixed duration at a rain gage. The FHWA (2022) provides descriptions of the normal, log-normal, Gumbel extreme value, and log-Pearson type III frequency distributions.

However, coincident frequency analysis and other hydrologic problems involve two or more random variables. In these cases, engineers use either a simplifying assumption to reduce the complexity to something treatable with univariate statistics, or more complex analyses involving multivariate statistics.

Multivariate analysis typically includes two components: 1) establishing the marginal distributions of each variable and 2) describing the dependence between variables. The marginal distribution of a random variable is the probability distribution of that variable independent of any other value. That is, it is the univariate distribution. As described previously, the dependence relates to how one variable contributes to the other variable or how both variables can result from a common source. Multivariate distributions and copulas express dependency in different ways. See Appendix B for additional information on multivariate analysis and these tools.

**Bivariate distributions** are a subset of multivariate distributions involving two random variables. A bivariate distribution is characterized by a distribution function, which is a scalar-valued function of a vector-valued random variable (in this case two random variables). In the limit of each random variable, a univariate distribution function results, termed the marginal distribution. So, for a distribution function  $H(x,y)$  there are two marginal distributions,  $F(x)$  and  $G(y)$ . Bivariate distributions have the same type of marginal distributions, that is, the same distribution function, although with different parameter values. Examples of bivariate distributions include the bivariate normal distribution and the bivariate Gumbel distribution. The latter can be developed in several forms. Appendix B includes additional information on bivariate distributions.

**Copulas** are a more general approach to bivariate (or multivariate) problems. The term copula refers to a function, called the dependence function, used to link two univariate distributions in such a way as to represent the bivariate (or multivariate) dependence between the two random variables. The potential of a copula is realized in that the copula is independent from the form of the univariate marginal distributions. That is, the marginal distributions of a copula are uniformly distributed on the interval (0,1). Therefore, the marginal distributions can be chosen such that they provide a best-fit of the univariate random variables, with the copula used to model the

dependence behavior. Engineers can apply many copulas to bivariate (and multivariate) random variables. Section 5.2 describes a tool for coincident flooding at river confluences based on copulas. Appendix B includes additional information on copulas.

As with univariate analyses, fitting multivariate probability distributions with historical data generally assumes stationarity in the data. When stationarity is a reasonable assumption, engineers can use these fitted distributions to assess risk for infrastructure over its anticipated lifespan. However, a changing climate, a changing watershed, or both may alter historical probability distributions of extreme events, or it may alter the dependence structure or both.

Hao and Singh (2020) examined the historical record of the dependence structure of two types of compound events, finding changes. They indicate that this history of alterations suggests further changes are possible. Wahl et al. (2015) also observed an increase in coastal compound flooding events over the past century, noting that future increases in that trend may be expected.

Coincident frequency analyses for confluent streams (section 5.2) and for coastal compound flooding (section 5.3) are challenging because of the many factors that contribute to flooding and the dependence structure with other flooding mechanisms. To the extent that nonstationarity changes these relationships, the process is further complicated. However, coincident frequency analysis of combined risks remains an important tool for understanding potential infrastructure consequences and safety with or without climate change.

## 5.2 Flooding at River Confluences

This section describes copula-based tools for estimating the joint probability of flooding at river confluences (Kilgore et al. 2013). Highway drainage structures are often located near the confluence of two streams where they may be subject to inundation by high flows from either stream. Engineers design stream crossings to meet performance objectives for floods of a specified return period, e.g., the 100-year flood, as specified by the applicable design criteria. Because the flooding of structures on one stream can be affected by high flows on the other stream, engineers seek to understand the relationship between the joint exceedance probability of the confluent stream pair, i.e., the **joint probability** of the coincident flows, with the individual exceedance probability on each stream.

The joint probability question arises when a structure is located where the hydraulic behavior of some combination of the main and tributary streams may result in critical hydraulic design conditions. The portion of the tributary stream that is influenced by both the flow of the tributary stream and the backwater caused by the mainstem is the **influence reach** (Kilgore et al. 2013). The location of the structure within the influence reach, as well as the joint hydrologic behavior of the confluent streams, determines the importance of the confluent streams on the appropriate design conditions for the structure.

Figure 5.3 illustrates the concept of an influence reach with three possible alternative structure locations relative to the influence reach. For any given confluent pair of streams, there is a distance upstream of the confluence within which the flow from both streams will influence the hydraulic conditions at the structure. This distance ( $X_{max}$ ) varies with the magnitude of the flow. If the distance of the structure location above the confluence ( $x$ ) is less than  $X_{max}$ , then the structure is located in the influence reach and joint probability analysis may be appropriate to design a cost-effective and reliable structure. Although the figure shows the structure location and influence reach on the tributary stream, the analysis is the same if the structure and influence reach are on the mainstem.

For a structure located very close to the confluence of the main and tributary streams (location A in Figure 5.3), the structure is sufficiently close to the confluence that the critical design condition

is determined by the backwater at the confluence. This case essentially reduces to an analysis of the flow at the confluence, and joint probability analysis may not be justified. A designer unsure whether the site is sufficiently close, will want to apply the joint probability design procedure.

For a structure located a significant distance from (or at a much higher elevation than) the confluence (location C in Figure 5.3), the structure is beyond the influence reach and joint probability analysis is not indicated. This case represents the typical riverine hydraulic design condition.

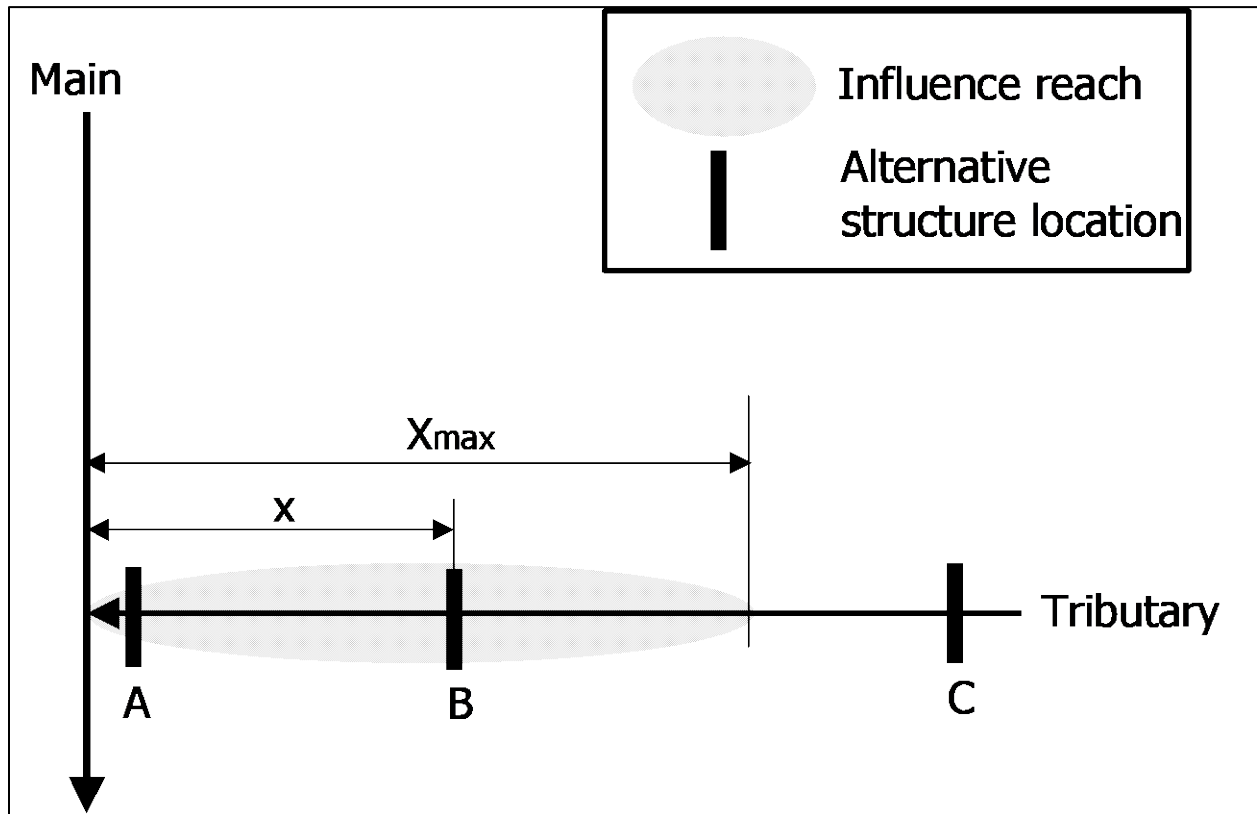


Figure 5.3. Influence reach schematic.

Alternative location B in Figure 5.3 represents the joint probability problem where the distance of the structure from the confluence,  $x$ , is less than  $X_{max}$  and the structure is within the influence reach. The hydraulic conditions, e.g., depth and velocity for a structure at location B, are a function of the flow at the confluence (establishing the downstream control elevation) and the flow in the tributary (determining the water surface profile from the downstream control to the design location). More simply put, the hydraulic conditions at location B can be considered a function of the main and tributary streamflows.

In a typical riverine situation (one stream) engineers generally follow a three-step design procedure:

1. Select an appropriate design return period.
2. Estimate the flow rate associated with that return period.
3. Apply that flow rate to a hydraulic analysis of the structure.

For confluent streams, engineers still use the appropriate design return period for the site but refer to it as the joint probability return period. Then, engineers perform additional analyses to

determine the appropriate return periods to use on the mainstem and the tributary stream such that the joint probability is as intended. This section presents two approaches for analyzing this problem, a copula-based technique and the total probability theorem.

### 5.2.1 Coincident Flooding Design at Confluences

This section presents a step-by-step procedure that can be useful for analyzing coincident flooding at stream confluences. The approach applies to many design situations and objectives. However, for situations of high sensitivity or vulnerability either for the infrastructure itself or for the traveling public, the designer may wish to review the full NCHRP report (Kilgore et al. 2013) to understand the foundation of this method and to review the application procedures in more detail.

Kilgore et al. (2013) indicate that this design procedure only applies to stream confluence pairs satisfying three conditions:

- Neither watershed in the pair is substantially affected by regulation.
- The sum of the watershed drainage areas is less than 9,000 mi<sup>2</sup>.
- The drainage area of the smaller watershed of the pair exceeds 1 mi<sup>2</sup>.

The latter two bullets imply drainage area ratio limits between the two confluent watersheds.

Engineers using joint probability analysis for a site potentially affected by confluent streams typically follow six basic steps (described in more detail below):

1. Specify the design condition.
2. Compute the flow range of interest.
3. Determine if the site is within the influence reach.
4. Determine potential hydrologic combinations.
5. Estimate flows for each potential hydrologic combination.
6. Perform hydraulic analyses for each hydrologic combination.

#### **Step 1. Specify the design condition.**

The designer chooses the appropriate annual design condition appropriate for the site and type of structure, e.g., bridge, culvert, etc. This step is the same for any waterway crossing or other channel work, with or without the joint probability problem. The designer first establishes annual exceedance probability (AEP) and relevant design parameters. The design AEP might range from 0.1 to 0.002, corresponding to return periods from 10-yr to 500-yr. At this stage, a cost-benefit analysis frequently includes examination of a range of design conditions.

The designer also chooses whether the site and design objectives will benefit from a representative (best-fit) or envelope analysis. For this methodology, the representative approach uses the best-fit estimate, while the envelope approach provides a more conservative estimate based on applying a design envelope around the underlying data. In most design situations, the representative approach is appropriate as it will result in the statistically most likely estimate of conditions at the site. If, however, there is reason to be more conservative, the engineer can choose the envelope approach.

This distinction can be compared to application of U.S. Geological Survey (USGS) regression equations for estimating flows. In most situations, engineers use the estimate from the equation as the statistically most likely value. However, the equation also comes with information on the



standard error of the equation that provides a basis for evaluating the design for sensitivity to the uncertainty in the design flow.

### Step 2. Compute flow range of interest.

Four flows—two on the mainstem and two on the tributary stream—establish the range of flows of interest. For both the main and tributary streams the engineer estimates the 2-yr and design condition flows. The 2-yr flow represents the lower end of the range. The design condition is the return period selected in step 1 and represents the higher end of the range. For example, if the engineer chooses a 100-yr design condition, the engineer calculates the 2-yr and 100-yr events for the two confluent streams.

Joint probability analysis does not involve special hydrological techniques to estimate flow from a watershed. Depending on the watershed and applicable guidance, the engineer selects any appropriate peak flow or hydrograph technique. For example, if USGS regression peak flow techniques apply to a given situation for a typical riverine setting, that technique would also be acceptable in a joint probability context.

### Step 3. Determine influence reach.

Joint probability design techniques are useful only if the project site is within the influence reach. To determine this, the designer creates a hydraulic model for the site using HEC-RAS or other appropriate tool. To properly capture the interaction between the confluent streams, it is important to extend the hydraulic model downstream of the confluence. For the stream with the hydraulic structure, the engineer extends it upstream of the hydraulic structure to the same extent that they would in a typical riverine situation, that is, at least upstream of the anticipated extent of backwater as shown in Figure 5.4. For the confluent stream, the engineer only extends the model upstream sufficiently so that the boundary condition does not influence the water surface elevation at the confluence. For the typical (subcritical) flow condition this is just upstream of the confluence.

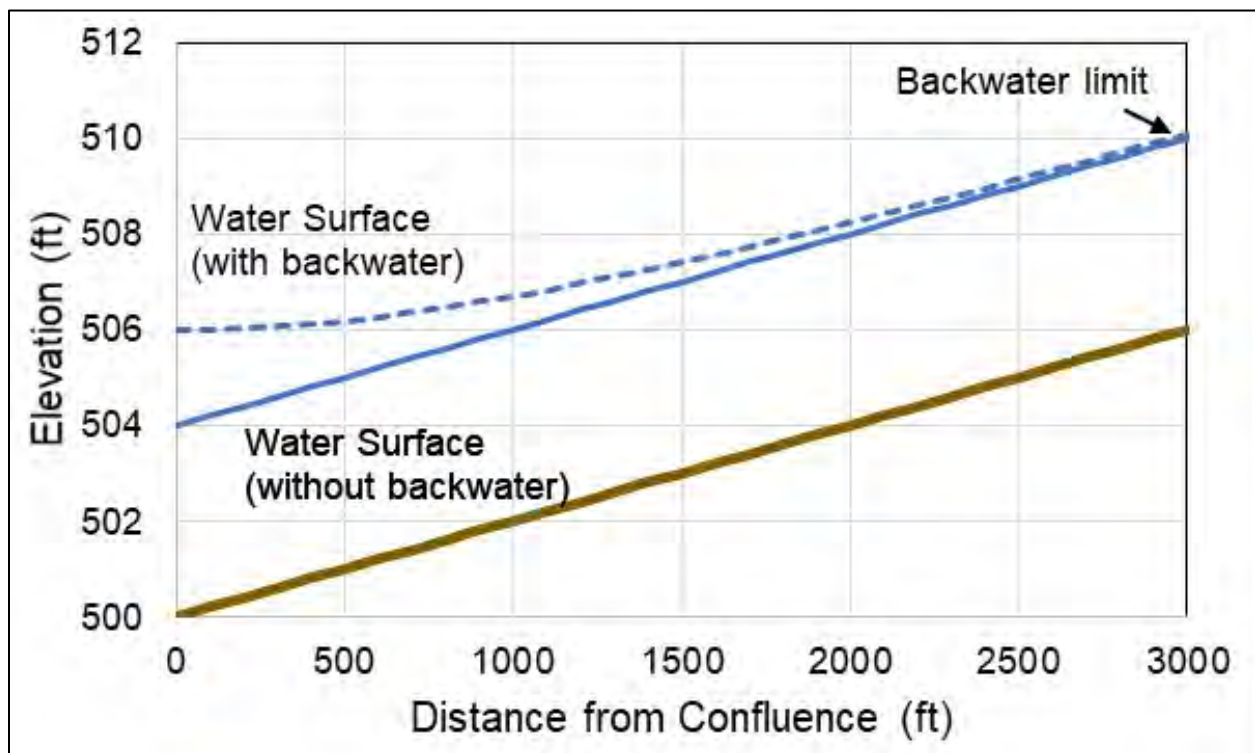


Figure 5.4. Schematic illustrating backwater extent.

Once the hydraulic model is set up, the engineer runs two hydrologic scenarios to determine if the structure is within the influence reach. Table 5.1 summarizes the scenarios. Both use the 2-yr return period flow for the stream with the hydraulic structure. Scenario I includes the 2-yr return period flow on the other stream and scenario II includes the design return period flow on the other stream.

Table 5.1. Influence reach determination options.

Scenario	Stream Where Hydraulic Structure Is Located	Confluent Stream
I	2-yr	2-yr
II	2-yr	design return period

The engineer compares the water surface elevations at the hydraulic structure site for the two scenarios. If the water surface elevations at the project site are the same between the two scenarios, the project site is outside the influence reach (not affected by backwater from the confluent stream) and joint probability techniques are not indicated. If the water surface elevations are not the same between the two scenarios, the site is within the influence reach and the engineer can choose to apply this joint probability design procedure.

Assessing whether hydraulic conditions are different between scenario I and scenario II involves determining how close the two conditions would be to be considered the same. Defining this involves considering many factors including the purpose of the analysis, the potential for error in the flow estimates, and the sensitivity of the hydraulic conditions to the flow estimates. Equation 5.1 provides a rule of thumb for making this determination (Kilgore 2013). If the equation is true, the engineer considers that the site is within the influence reach.

$$WSE_{II} - WSE_I \geq \max(H, WSE_{I+10\%} - WSE_I) \quad (5.1)$$

where:

- $WSE_I$  = Water surface elevation at site for scenario I, ft (m)
- $WSE_{II}$  = Water surface elevation at site for scenario II, ft (m)
- $WSE_{I+10\%}$  = Water surface elevation at site for scenario I with flow rates on both streams increased by 10 percent, ft (m)
- $H$  = Reference elevation change set at 0.2 ft (0.06 m)

$WSE_{I+10\%}$  represents the water surface elevation at the site under scenario I when the flows on both confluent streams are increased by 10 percent. This provides an indicator of the sensitivity of the water surface elevation to the flow estimates. The reference elevation change,  $H$ , is a constant that provides a minimum rule of thumb value for those situations where the system is less sensitive to flow. When in doubt about the use of this rule of thumb, the designer typically assumes that the site is within the influence reach and proceeds with the joint probability analysis.

When setting up the HEC-RAS or other hydraulic model, the designer applies the respective flows for the main and tributary to those reaches above the confluence. The flow below the confluence is the sum of the flows on the confluent streams.

#### Step 4. Determine hydrologic combinations.

Appropriate combinations of flow to be considered for a pair of confluent streams depend on the degree to which their flood flow patterns are correlated. Based on the research database and analyses on which this method is based, engineers can estimate this correlation by the ratio of the watershed areas and the combined watershed area. The drainage area ratio,  $R_A$ , is computed by dividing the drainage area of the larger watershed by the drainage area of the smaller watershed (Kilgore et al. 2013). The total watershed area ( $A_{TOT}$ ) is computed by summing the two drainage areas. Table 5.2. summarizes the categories derived from Kilgore et al. (2013) by analyzing their database for observable breakpoints.

Table 5.2. Watershed categories.

Drainage Area Ratio	Total Watershed Area	
	$A_{TOT} < 350 \text{ mi}^2$	$A_{TOT} \geq 350 \text{ mi}^2$
$RA < 7$	SS	SL
$RA \geq 7$	LS	LL

The category label is a two-letter code. The first letter references the drainage area ratio. If it is less than 7, the ratio is considered to be small and is indicated by an "S." If it is greater than or equal to 7 then the ratio is considered to be large and is indicated by an "L." Similarly, the second letter in the code references the total watershed area. If the total watershed area is less than 350  $\text{mi}^2$ , the letter "S" is assigned for small. If not, the letter "L" is assigned for large.

Kilgore et al. (2013) developed combinations of individual return period flows on the tributary and mainstems for the 10-, 25-, 50-, 100-, and 500-yr joint design frequency events summarized in Table 5.3 through Table 5.7. The designer selects the table corresponding to the joint design return period and finds the watershed category within that table. Then, depending on whether the representative approach or envelope approach has been adopted, a series of return period combinations are listed. For the 10- and 25-year joint return periods there are three combinations while for the 50-, 100-, and 500-year joint return periods five combinations are listed.

Table 5.3. Return period combinations for the 10-year joint return period.

Category	Approach	Location	Combination		
			1	2	3
SS	Representative	Tributary	3	8	10
		Main	10	8	3
	Envelope	Tributary	5	9	10
		Main	10	9	5
SL	Representative	Tributary	2	7	10
		Main	10	7	2
	Envelope	Tributary	4	8	10
		Main	10	8	4
LS	Representative	Tributary	3	8	10
		Main	10	8	3
	Envelope	Tributary	5	9	10
		Main	10	9	5
LL	Representative	Tributary	1.25	6	10
		Main	10	6	1.25
	Envelope	Tributary	2	7	10
		Main	10	7	2

Table 5.4. Return period combinations for the 25-year joint return period.

Category	Approach	Location	Combination		
			1	2	3
SS	Representative	Tributary	6	19	25
		Main	25	19	6
	Envelope	Tributary	13	22	25
		Main	25	22	13
SL	Representative	Tributary	3	17	25
		Main	25	17	3
	Envelope	Tributary	10	21	25
		Main	25	21	10
LS	Representative	Tributary	6	19	25
		Main	25	19	6
	Envelope	Tributary	13	22	25
		Main	25	22	13
LL	Representative	Tributary	1.25	14	25
		Main	25	14	1.25
	Envelope	Tributary	3	17	25
		Main	25	17	3

Table 5.5. Return period combinations for the 50-year joint return period.

Category	Approach	Location	Combination				
			1	2	3	4	5
SS	Representative	Tributary	11	31	38	43	50
		Main	50	43	38	31	11
	Envelope	Tributary	25	39	43	46	50
		Main	50	46	43	39	25
SL	Representative	Tributary	5	26	34	40	50
		Main	50	40	34	26	5
	Envelope	Tributary	20	36	41	45	50
		Main	50	45	41	36	20
LS	Representative	Tributary	11	31	38	43	50
		Main	50	43	38	31	11
	Envelope	Tributary	25	39	43	46	50
		Main	50	46	43	39	25
LL	Representative	Tributary	2	19	27	35	50
		Main	50	35	27	19	2
	Envelope	Tributary	4	25	33	40	50
		Main	50	40	33	25	4

Table 5.6. Return period combinations for the 100-year joint return period.

Category	Approach	Location	Combination				
			1	2	3	4	5
SS	Representative	Tributary	20	62	75	86	100
		Main	100	86	75	62	20
	Envelope	Tributary	50	77	86	92	100
		Main	100	92	86	77	50
SL	Representative	Tributary	9	52	67	81	100
		Main	100	81	67	52	9
	Envelope	Tributary	39	72	83	91	100
		Main	100	91	83	72	39
LS	Representative	Tributary	20	62	75	86	100
		Main	100	86	75	62	20
	Envelope	Tributary	50	77	86	92	100
		Main	100	92	86	77	50
LL	Representative	Tributary	2	37	54	70	100
		Main	100	70	54	37	2
	Envelope	Tributary	7	50	66	79	100
		Main	100	79	66	50	7

Table 5.7. Return period combinations for the 500-year joint return period.

Category	Approach	Location	Combination				
			1	2	3	4	5
SS	Representative	Tributary	98	308	376	429	500
		Main	500	429	376	308	98
	Envelope	Tributary	249	385	430	462	500
		Main	500	462	430	385	249
SL	Representative	Tributary	39	257	336	402	500
		Main	500	402	336	257	39
	Envelope	Tributary	200	361	414	453	500
		Main	500	453	414	361	200
LS	Representative	Tributary	98	308	376	429	500
		Main	500	429	376	308	98
	Envelope	Tributary	249	385	430	462	500
		Main	500	462	430	385	249
LL	Representative	Tributary	5	182	269	349	500
		Main	500	349	269	182	5
	Envelope	Tributary	30	246	327	395	500
		Main	500	395	327	246	30

**Step 5. Estimate flows for combinations.**

Next, the engineer estimates the flows corresponding to the combination return periods using the hydrologic method applied in step 2. Because the set of combinations includes return periods not directly estimated using common methods, the engineer interpolates in those cases. Figure 5.5 displays example flow frequency curves for hypothetical main and tributary streams. The plotted points represent the return periods generally available from various hydrologic techniques: 2-, 10-, 25-, 50-, and 100-yr. The curves represent the range of values between the plotted points.

When the situation calls for use of a different return period, for example, a 77-year return period flow, the engineer obtains it by interpolating between the 50-year and 100-year values using equations 5.2 and 5.3.

$$\log Q_x = \frac{\log T_x - \log T_L}{\log T_H - \log T_L} (\log Q_H - \log Q_L) + \log Q_L \quad (5.2)$$

$$Q_x = 10^{\log Q_x} \quad (5.3)$$

where:

- $Q_x$  = Flow at return period  $x$ ,  $\text{ft}^3/\text{s}$  ( $\text{m}^3/\text{s}$ )
- $Q_H$  = Known flow at return period higher than  $x$ ,  $\text{ft}^3/\text{s}$  ( $\text{m}^3/\text{s}$ )
- $Q_L$  = Known flow at return period lower than  $x$ ,  $\text{ft}^3/\text{s}$  ( $\text{m}^3/\text{s}$ )
- $T_x$  = Return period of interest, years
- $T_H$  = Return period of  $Q_H$ , years
- $T_L$  = Return period of  $Q_L$ , years

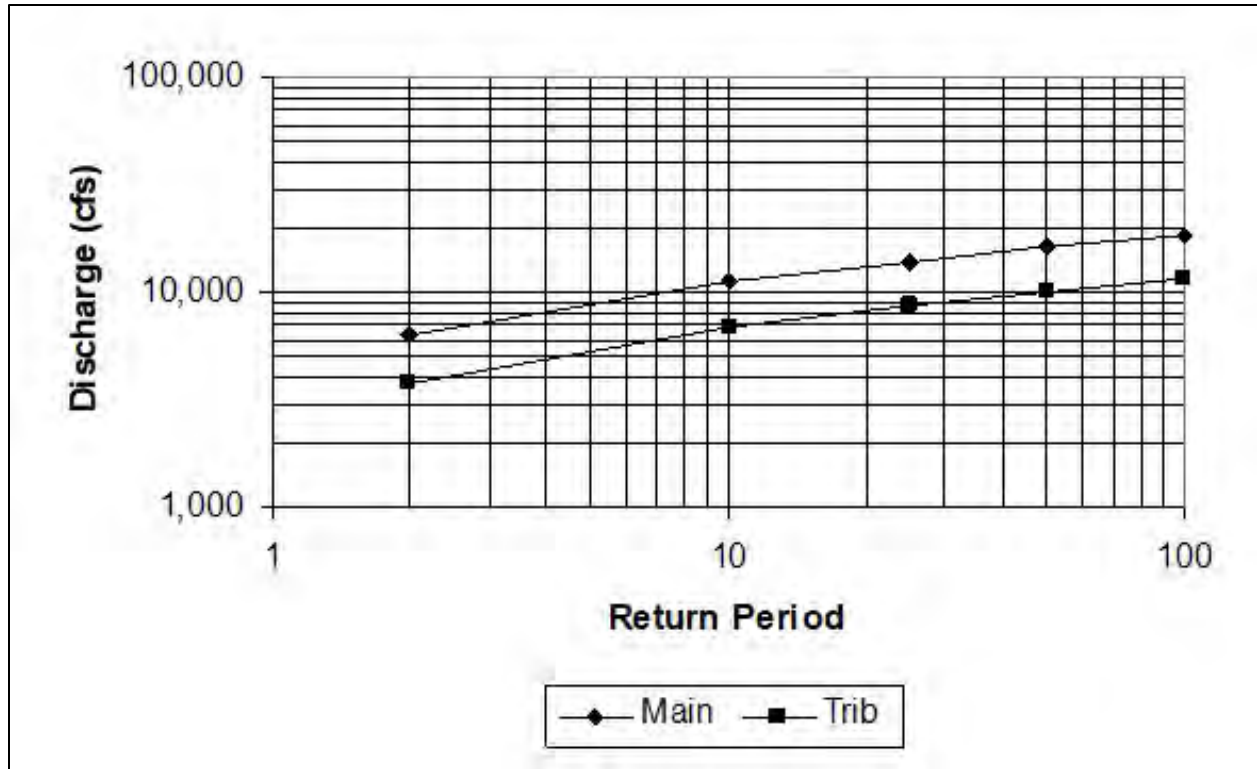


Figure 5.5. Hypothetical flow frequency curves.

Linear interpolation in log-log space described in equation 5.2 approximates the estimated flows at intermediate return periods. In most cases, this approximation is appropriate for identifying the flow combinations as described previously. However, the engineer can choose to substitute the 2-yr for the 1.25-yr value rather than use the equation if the use of the higher flow results in a conservative hydraulic condition. Recall that higher flow can be conservative in terms of water depth but not necessarily for velocity.

For the LL watershed category using the representative approach, the engineer uses an estimate of the 1.25-yr return period flow for the 10-year (Table 5.3) and 25-year (Table 5.4) return periods. The 1.25-yr return period flow can be calculated by extrapolating from the 2-yr and 10-yr flows as follows:

$$Q_{1.25} = 10^{1.292\log Q_2 - 0.292\log Q_{10}} \tag{5.4}$$

where:

- $Q_{1.25}$  = 1.25-yr flow, ft<sup>3</sup>/s (m<sup>3</sup>/s)
- $Q_2$  = 2-yr flow, ft<sup>3</sup>/s (m<sup>3</sup>/s)
- $Q_{10}$  = 10-yr flow, ft<sup>3</sup>/s (m<sup>3</sup>/s)

Linear extrapolation in log-log space described in equation 5.4 approximates the estimated flows at the 1.25-yr return period. In most cases, this approximation is appropriate for identifying the flow combinations from step 3. The engineer can choose to evaluate the effect on the flow using other curve fitting interpolation schemes.



**Step 6. Analyze combinations.**

After developing flow pairs for the potential combinations, the engineer uses the same hydraulic model applied in step 3 for each flow combination. Depending on the design objective (stage or velocity) and site location within the influence reach, one of the combinations will yield the extreme condition for a given design objective.

When flood elevations are a concern, the engineer selects the combination with the highest elevation to evaluate impacts. Similarly, velocity at the site is a concern, the engineer selects the combination with the highest velocity to evaluate impacts. For scour analyses, which depend on stage and velocity, the engineer estimates scour using each combination and uses the maximum scour for design. The extreme condition for the appropriate design objective is considered the design condition corresponding to that joint return period. A different combination might be the design condition for stage, velocity, and scour.

**5.2.2 Design Examples**

This section provides two design examples to illustrate the joint probability analysis procedure for confluent streams. They are based on actual watersheds in the States of Washington and New Jersey. In addition to the hydrologic analyses, completion of a joint probability analysis depends on application of HEC-RAS or another hydraulic model. However, because the implementation of riverine hydraulic models in the context of joint probability analyses is not unique, these examples do not feature actual HEC-RAS analyses. Rather, they provide realistic, but synthetic, data representative of hydraulic model outputs to illustrate the procedures.

**Example 5.1: Joint probability analysis of confluent streams.**

**Objective:** Estimate the joint probability combinations associated with the 50-year design criteria for a hypothetical bridge proposed over Mineral Creek upstream of the confluence with the Nisqually River in Washington State.

**Given:** Drainage area for Mineral Creek: 70.3 mi<sup>2</sup>.  
Drainage area for the Nisqually River: 133 mi<sup>2</sup>.

Figure 5.6 provides an aerial view of the confluence.

**Step 1. Specify the design condition.**

The appropriate joint probability return period is the same as the return period for the type of structure being evaluated in a typical riverine situation. This example uses the 50-year return period. Therefore, the 50-year return period is selected as our specified design condition for the joint probability.

Since the proposed project involves no features that justify a more conservative approach, the representative approach is selected.

**Step 2. Compute the flow range of interest.**

The flow range of interest is from the 2-year to the 50-year (design condition) events. The engineer estimates these values using an acceptable hydrologic methodology for the site. One acceptable method for this location is the USGS regression equations for the area (Sumioka et al. 1998). The watershed pair is located in USGS region 2 for which the following regression equation applies:

$$Q_T = aA^{b_1}P_M^{b_2}$$



where:

- $Q_T$  = Design flow for return period, T,  $ft^3/s$
- $A$  = Drainage area,  $mi^2$
- $P_M$  = Mean annual precipitation, inch
- $a, b_1, b_2$  = Regression constants



Figure 5.6. Confluence of the Nisqually River and Mineral Creek, Washington.

Table 5.8 provides the regression constants. The mean annual precipitation for Mineral Creek and the Nisqually River is 98 and 94 inches, respectively. Table 5.9 summarizes results from the USGS equations for the site-specific data.

Table 5.8. Nisqually/Mineral regression constants.

Return Period	Regression Constants		
	a	$b_1$	$b_2$
2	0.090	0.877	1.51
10	0.129	0.868	1.57
25	0.148	0.864	1.59
50	0.161	0.862	1.61
100	0.174	0.861	1.62

Table 5.9. Nisqually/Mineral flow range.

Return Period	Flow (ft <sup>3</sup> /s)	
	Nisqually River	Mineral Creek
2	6,260	3,810
50	16,400	10,100

**Step 3. Determine if site is within influence reach.**

The engineer sets up a HEC-RAS hydraulic model appropriate for the site. Since the proposed bridge is to be located on Mineral Creek, the following two scenarios are analyzed in the hydraulic model:

- Scenario I with the 2-year flow on the Nisqually River and the 2-year flow on Mineral Creek.
- Scenario II with the 50-year flow on the Nisqually River and the 2-year flow on Mineral Creek.

The engineer extracts the water surface elevations at the proposed bridge site from the two scenario runs and computes the difference ( $WSE_{II} - WSE_I$ ). Table 5.10 summarizes these data. The difference in water surface elevation between scenarios I and II is 0.5 feet. Referring to equation 5.1, this difference is greater than the reference elevation change, H, which is 0.2 ft. Therefore, equation 5.1 is true and the site is within the reference reach.

Based on this conclusion, scenario I is not run again with the flows increased by 10 percent. However, for illustrative purposes, Table 5.10 summarizes the results from running scenario I+10% with hypothetical water surface elevation results. Equation 5.1 remains true for this site; the site is within the influence reach for the flow range of interest. (There is no harm in performing a joint probability analysis for a site beyond the influence reach in terms of the results as one of the flow combinations is equivalent to the typical riverine situation.)

Table 5.10. Nisqually/Mineral influence reach determination.

Scenario	Mineral Creek Return Period	Nisqually River Return Period	Mineral Creek Flow (ft <sup>3</sup> /s)	Nisqually River Flow (ft <sup>3</sup> /s)	Water Surface Elevation (ft)
I	2-year	2-year	3,810	6,260	28.0
II	2-year	50-year	3,810	16,400	28.5
I+10%	2-year + 10%	2-year + 10%	4,190	6,890	28.1

**Step 4. Determine hydrologic combinations.**

For this example, the drainage area ratio,  $R_A$ , is equal to  $133/70.3 = 1.9$  and  $A_{TOT}$  is equal to  $133 + 70.3 = 203$  mi<sup>2</sup>. From Table 5.2, it is apparent the site falls within category SS.

For the joint design return period of 50-years, the relevant potential hydrologic combinations are found in Table 5.5. With a watershed category of SS and using the representative approach, it is evident that there are five potential combinations. Combination 1 uses the 11-year return period on Mineral Creek and the 50-year return period on the Nisqually River. Combinations 2 through 5 progressively increase the return period on Mineral Creek while decreasing the return period on the Nisqually River. All combinations represent the 50-yr joint return period.

**Step 5. Estimate flows for hydrologic combinations.**

For the example, the 11-, 31-, 38-, 43-, and 50-year flows on both Mineral Creek and the Nisqually River will be estimated. Previously, the 50-year flows were estimated using the applicable USGS equations in step 2. The same set of USGS equations is used to estimate the 10- and 25-year flows. Interpolation is then used to derive the 11-, 31-, 38-, and 43-yr flows. Table 5.11. provides the results of applying the applicable USGS equations.

Table 5.11. Nisqually/Mineral flows.

Return Period	Nisqually River Flow (ft <sup>3</sup> /s)	Mineral Creek Flow (ft <sup>3</sup> /s)
10	11,300	6,920
25	13,900	8,550
50	16,400	10,100

Flows for the intermediate values are computed using equations 5.2 and 5.3. For example, the flow corresponding to a 38-yr return period for the Nisqually River used for combination 3 is calculated as follows:

$$\log Q_{38} = \frac{\log(38) - \log(25)}{\log(50) - \log(25)} (\log(16,400) - \log(13,900)) + \log(13,900)$$

$$\log Q_{38} = \frac{1.580 - 1.398}{1.699 - 1.398} (4.215 - 4.143) + 4.143 = 4.186$$

$$Q_{38} = 10^{\log Q_{38}} = 10^{4.186} = 15,346 = 15,300$$

Using the same procedure, the remaining flows are computed and summarized in Table 5.12.

Table 5.12. Nisqually/Mineral flow combinations.

Combination	Mineral Creek Return Period (yrs)	Nisqually River Return Period (yrs)	Mineral Creek Flow (ft <sup>3</sup> /s)	Nisqually River Flow (ft <sup>3</sup> /s)
1	11	50	7,070	16,400
2	31	43	9,000	15,800
3	38	38	9,460	15,300
4	43	31	9,740	14,600
5	50	11	10,100	11,500

*Step 6. Perform hydraulic analyses for each combination.*

After development of flow pairs for the hydrologic combinations, each pair is applied to the hydraulic model developed for step 3. Table 5.13. summarizes the stage and velocity at the structure site for each combination of flows.

Table 5.13. Stage and velocity for Nisqually/Mineral combinations.

Combination	Stage (ft)	Velocity (ft/s)
1	28.7	14.2
2	29.6	11.1
3	30.2	10.2
4	30.4	9.5
5	29.8	11.7

**Solution:** The most extreme results for the variables of interest are taken as the 50-year joint probability design conditions. For freeboard, stage is the driving variable; maximum stage is derived from combination 4. For scour, the designer takes the results from all five combinations and performs a scour computation for each. The maximum scour is used for design.

It is important to remember that the most extreme values for depth, velocity, or scour may not come from the same combination. Results from different combinations are not combined. In this example, the designer does not take the maximum depth from combination 4 and the maximum velocity from combination 1 to compute scour. These do not occur under the same conditions and are not evaluated as if they did.

**Example 5.2:** Joint probability analysis of confluent streams with a large area ratio.

**Objective:** Estimate the joint probability combinations for a hypothetical culvert installation proposed on the West Branch of Middle Brook upstream of the confluence with the Raritan River in New Jersey.

**Given:** Drainage area for the West Branch of Middle Brook: 2 mi<sup>2</sup>.  
Drainage area of the Raritan River: 784 mi<sup>2</sup>. Approximately 11 square miles of the Raritan River watershed is noncontributing, making the effective drainage



area 773 square miles. Figure 5.7 shows an aerial view of the confluence of Middle Brook with the Raritan River. The West Branch and the East Branch join forming Middle Brook.

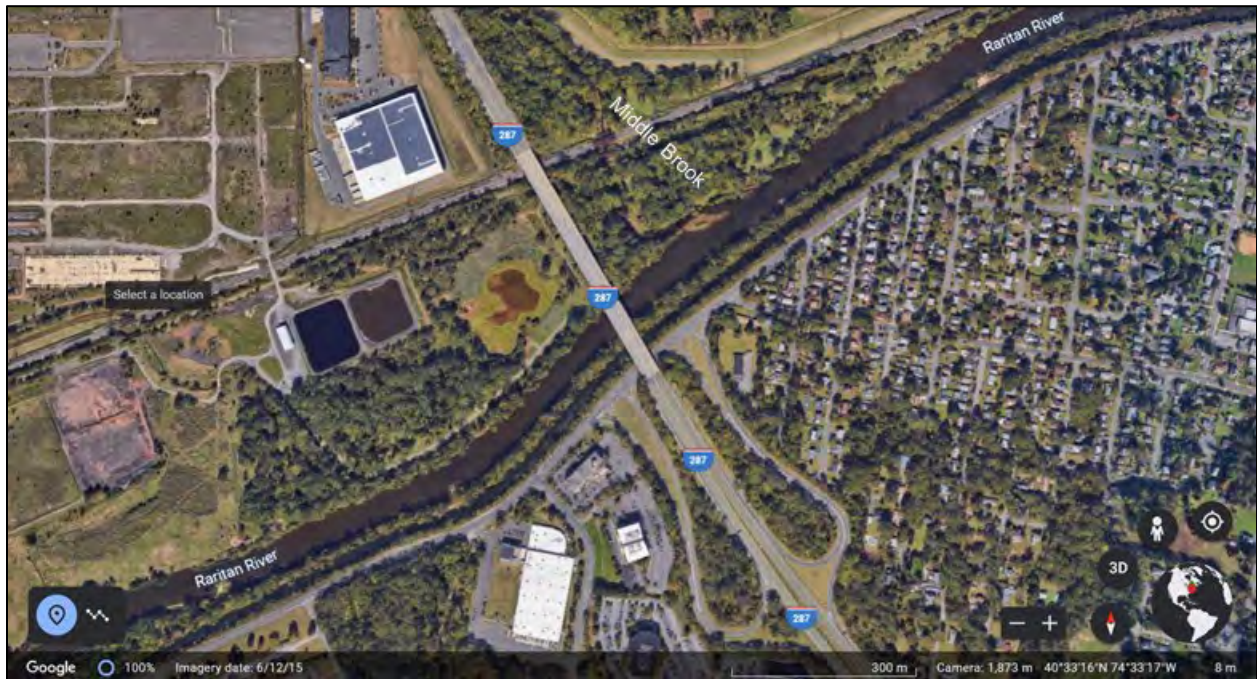


Figure 5.7. Confluence of the Raritan River and Middle Brook, New Jersey.

**Step 1. Specify the design condition.**

The appropriate joint probability return period is the same as the return period for the type of structure being evaluated in a typical riverine situation. For this example, the 25-year return period is appropriate. Therefore, the 25-year return period is selected as the specified design condition for the joint probability.

Since the proposed project involves no features that justify a more conservative approach, the representative approach is selected.

**Step 2. Compute the flow range of interest.**

The flow range of interest is from the 2-year to the 25-year (design condition) events. These values are estimated using an acceptable hydrologic methodology for the site. One acceptable method for this location is the USGS regression equations for the area (Watson and Schopp 2009). The watershed pair is located in the unglaciated piedmont region of New Jersey for which the following regression equation applies:

$$Q_T = aA^{b_1} (ST + 1)^{b_2} S^{b_3} (D + 1)^{b_4}$$

where:

- $Q_T$  = Design flow for return period, T, ft<sup>3</sup>/s
- $A$  = Drainage area, mi<sup>2</sup>
- $ST$  = Percentage of basin covered by streams, lakes, and wetlands
- $S$  = Basin slope, ft/mi

D = Population density, persons/mi<sup>2</sup>  
 a,b<sub>1</sub>,b<sub>2</sub>,b<sub>3</sub>,b<sub>4</sub> = Regression constants

Table 5.14 provides the regression constants and Table 5.15 summarizes additional data for the watersheds. Applying USGS equations to the site-specific data yields the flow range summarized in Table 5.16.

Table 5.14. Raritan/Middle Brook regression constants.

Return Period	A	b <sub>1</sub>	b <sub>2</sub>	b <sub>3</sub>	b <sub>4</sub>
2	37.8	0.753	-0.054	0.251	0.127
5	75.3	0.741	-0.084	0.254	0.104
10	108	0.736	-0.104	0.258	0.092
25	159	0.732	-0.127	0.263	0.079
50	204	0.729	-0.144	0.267	0.070
100	256	0.728	-0.158	0.271	0.062

Table 5.15. Raritan/Middle Brook watershed data.

Data Type	Raritan River	Middle Brook
Area (mi <sup>2</sup> )	773	2
Storage (percent)	14.6	22.3
Slope (ft/mi)	11.0	70.2
Pop. Density (persons/ mi <sup>2</sup> )	523	765

Table 5.16. Raritan/Middle Brook flow range.

Return Period	Raritan River Flow (ft <sup>3</sup> /s)	Middle Brook Flow (ft <sup>3</sup> /s)
2	19,700	360
25	45,000	920

**Step 3. Determine if site is within influence reach.**

The engineer sets up a HEC-RAS hydraulic model appropriate for the site. Since the proposed bridge is to be located on the West Branch of Middle Brook, the following two scenarios are analyzed in the hydraulic model:

- Scenario I with the 2-year flow on the Raritan River and the 2-year flow on Middle Brook.
- Scenario II with the 25-year flow on the Raritan River and the 2-year flow on Middle Brook.

The water surface elevations at the proposed bridge site are extracted from the two scenario runs and the difference is computed ( $WSE_{II} - WSE_I$ ). Table 5.17 summarizes these data with hypothetical water surface elevation results. The difference in water surface elevation between scenarios I and II is 0.4 feet. Referring to equation 5.1, this difference is greater than the reference elevation change, H, which is 0.2 ft. Therefore equation 5.1 is true and the site is within the reference reach.

Table 5.17. Raritan/Middle Brook influence reach determination.

Scenario	Middle Brook Return Period	Raritan River Return Period	Middle Brook Flow (ft <sup>3</sup> /s)	Raritan River Flow (ft <sup>3</sup> /s)	Water Surface Elevation (ft)
I	2-year	2-year	360	19,700	43.8
II	2-year	25-year	360	45,000	44.2
I+10%	2-year + 10%	2-year + 10%	400	21,700	43.9

Based on this conclusion scenario I is not run again with the flows increased by 10 percent. However, for illustrative purposes, Table 5.17 summarizes the results from running scenario I+10%. Equation 5.1 remains true for this site; the site is within the influence reach for the flow range of interest. (There is no harm in performing a joint probability analysis for a site beyond the influence reach in terms of the results as one of the flow combinations is equivalent to the typical riverine situation.)

**Step 4. Determine hydrologic combinations.**

For this example, the drainage area ratio,  $R_A$ , is equal to  $773/2 = 386$  and  $A_{TOT}$  is equal to  $773 + 2 = 775$  mi<sup>2</sup>. From Table 5.2, it is apparent the site falls within category LL.

For the joint design return period of 25-years, Table 5.4 summarizes the relevant hydrologic combinations. With a watershed category of LL and using the representative approach, it is apparent that there are three combinations. Combination 1 uses the 1.25-year flow on Middle Brook and the 25-year flow on the Raritan River. Combination 2 employs the 14-yr event on both streams; combination 3 uses the 25-year event on the Middle Brook and the 1.25-year event on the Raritan River. All combinations represent the 25-yr joint return period.

**Step 5. Estimate flows for hydrologic combinations.**

For the example, the 1.25-, 14-, and 25-year flows on both Middle Brook and the Raritan River are estimated. The 25-year flows were previously estimated using the applicable USGS equation in step 2. To estimate the 14-yr flow the same set of USGS equations is used to estimate the 10- and 25-year flows and then interpolate. Table 5.18 provides the results of applying the applicable USGS equations.

Table 5.18. Raritan/Middle Brook flows.

Return Period	Raritan River Flow (ft <sup>3</sup> /s)	Middle Brook Flow (ft <sup>3</sup> /s)
2	19,700	360
10	35,800	720
25	45,000	920

Flows for the 14-year event are computed using equations 5.2 and 5.3. For example, the flow corresponding to a 14-yr return period for the Raritan River for combination 2 is calculated as follows.

$$\log Q_{14} = \frac{\log(14) - \log(10)}{\log(25) - \log(10)} (\log(45,000) - \log(35,800)) + \log(35,800)$$

$$\log Q_{14} = \frac{1.146 - 1.000}{1.398 - 1.000} (4.653 - 4.554) + 4.554 = 4.590$$

$$Q_{14} = 10^{\log Q_{14}} = 10^{4.590} = 38,905 = 38,900$$

Using the same procedure, the 14-year flow on Middle Brook is also computed.

The 1.25-year event is estimated using equation 5.4. For the Raritan River, the calculation is as follows:

$$Q_{1.25} = 10^{1.292 \log Q_2 - 0.292 \log Q_{10}} = 10^{1.292 \log(19,700) - 0.292 \log(35,800)} = 16,500$$

Table 5.19 summarizes all relevant flows.

Table 5.19. Raritan/Middle Brook flow combinations.

Combination	Middle Brook Return Period (yrs)	Raritan River Return Period (yrs)	Middle Brook Flow (ft <sup>3</sup> /s)	Raritan River Flow (ft <sup>3</sup> /s)
1	1.25	25	290	45,000
2	14	14	790	38,900
3	25	1.25	920	16,500

**Step 6. Perform hydraulic analyses for each combination.**

After developing flow pairs for the hydrologic combinations, each pair is applied to the hydraulic model developed for step 3. Table 5.20. summarizes the stage and velocity at the structure site for each combination of flows.



Table 5.20. Stage and velocity for Raritan/Middle Brook combinations.

Combination	Stage (ft)	Velocity (ft/s)
1	44.2	4.9
2	44.8	10.8
3	45.0	11.8

**Solution:** The most extreme results for the variables of interest are taken as the 25-year joint probability design conditions. Each combination has the same probability of occurrence, that is, 45.0 ft is the 25-year stage and 11.8 is the 25-yr velocity. These do not necessarily occur in the same combination as they did for this example.

For consideration of freeboard, stage is the driving variable; maximum stage is derived from combination 3. For consideration of scour, the designer takes the results from all three combinations and performs a scour computation for each. The maximum scour is used for design. However, in this case, the maximum stage and velocity are both from combination 3. Therefore, that combination is the governing case for scour.

Although not true in this example, it is important to remember that the most extreme values for depth, velocity, or scour may come from different combinations. If that is the case, as in the first example, results from different combinations are not combined.

### 5.2.3 Total Probability Theorem

The total probability theorem has been applied at river confluences (e.g., Dyhouse 1985, Pingel and Ford 2004). Engineers apply the total probability method for joint probability using the procedure described in EM 1110-2-1415 (USACE 1993). The method is also available in the USACE computer program HEC-SSP. The objective of the method, as applied in this section, is to produce a cumulative distribution function for tributary stage to evaluate flooding of a road crossing on the tributary affected by both the downstream mainstem water surface elevation and the tributary flow.

The foundation of the total probability method is the total probability theorem:

$$P[B] = \sum_{i=1}^n P[B | A_i] P[A_i] \quad (5.5)$$

where:

- $P[B]$  = Probability that B will occur
- $P[B|A_i]$  = Probability that B will occur given  $A_i$  has occurred
- $P[A_i]$  = Probability that  $A_i$  will occur

For continuous variables, equation 5.5 is written as:

$$P[B] = \int_A P[B | A] P[A] dA \quad (5.6)$$

Application of equation 5.5 or 5.6 over the range of values for the variable B results in a probability density function (PDF) for B as shown in Figure 5.8. The shape of the PDF in the figure is hypothetical; the actual shape depends on the statistical nature of the variable.

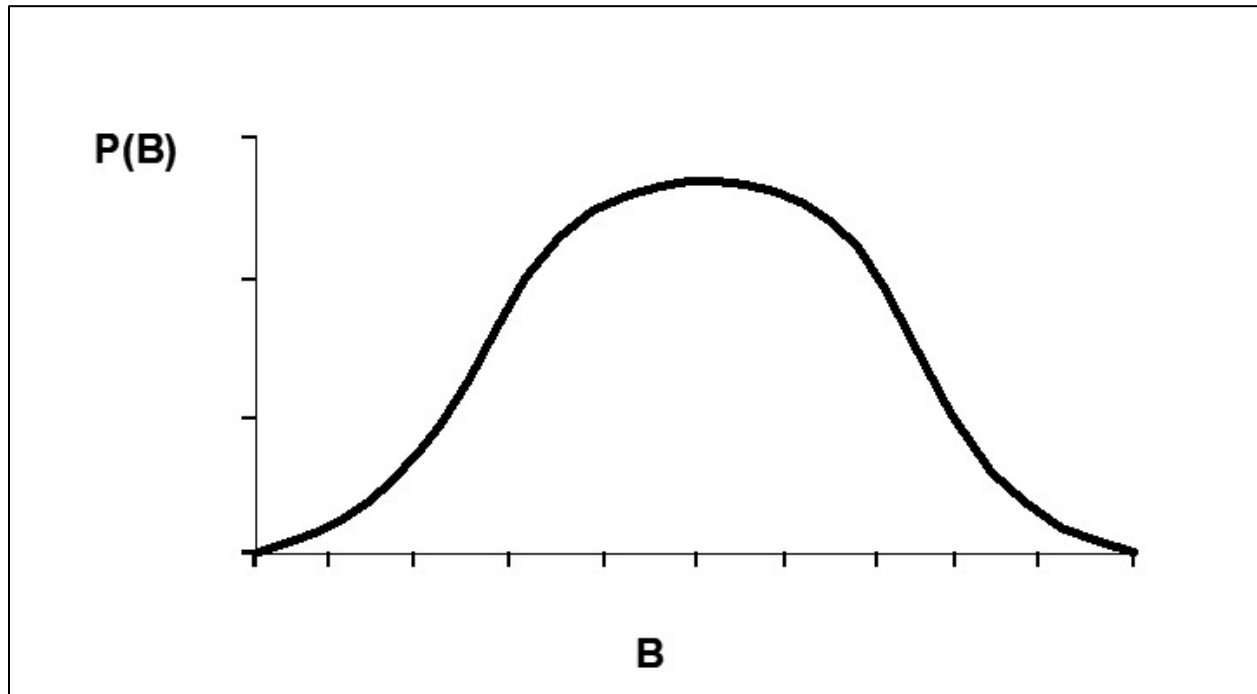


Figure 5.8. Hypothetical probability density function.

The PDF is transformed into the cumulative distribution function (CDF) by estimating the probability of nonexceedance for each value of B. Conceptually, the probability of nonexceedance is the area under the PDF to the left of the value of B. Performing this analysis over the range of B results in a CDF as shown in Figure 5.9. Again, the shape in the figure is hypothetical and depends on the shape of the PDF.

It is often desirable to express the CDF in terms of probability of exceedance,  $P_e$ , rather than probability of nonexceedance  $P_{ne}$ . It is straightforward to achieve this transformation since  $P_e + P_{ne} = 1$ . Figure 5.9 shows the result of this relation by the addition of the second vertical axis ( $P_e$ ) with the numerical values reversed from the first vertical axis ( $P_{ne}$ ).

As stated previously, the application of the total probability method of interest for this application is to develop the CDF for stage of the tributary at a site of interest. Therefore, the variable B in the previous discussion is tributary stage,  $y_T$ . Equation 5.5 becomes:

$$P[y_T] = \sum_{i=1}^n P[y_T | Q_{M,i}] P[Q_{M,i}] \quad (5.7)$$

where:

- $P[y_T]$  = Probability that stage  $y_T$  will occur
- $P[y_T | Q_{M,i}]$  = Probability that stage  $y_T$  will occur given flow on the mainstem,  $Q_{M,i}$  has occurred
- $P[Q_{M,i}]$  = Probability that mainstem flow,  $Q_{M,i}$  will occur

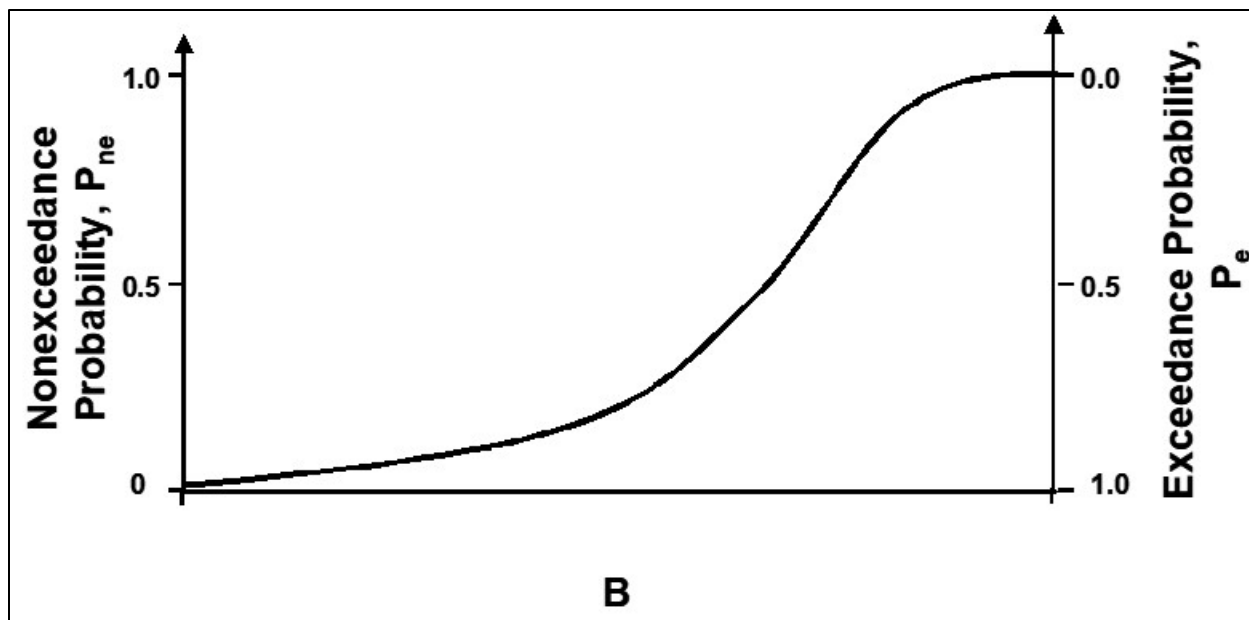


Figure 5.9. Hypothetical cumulative distribution function.

Because the tributary stage,  $y_T$ , is a function of both the mainstem flow ( $Q_M$ ) and the tributary flow ( $Q_T$ ), equation 5.7 might have been stated with  $Q_T$  rather than  $Q_M$ . The preferred representation depends on which of the two flows is considered the “dominant” variable. Close to the confluence,  $Q_M$  may be the dominant variable while closer to the upstream end of the influence reach,  $Q_T$  may be the dominant variable.

The subscript,  $i$ , represents an index ranging from 1 to  $n$  where  $n$  is the number groups (bins) into which the variable  $Q_M$  is divided.  $Q_{M,i}$  represents the index value for that bin. Bins for this analysis are selected based on AEPs of interest to the designer analyzing coincident flooding. Table 5.21 summarizes seven bins by an index value and range. The “bin AEP Index Value” value is the average of the logs (base 10) of the upper and lower bounds of the bin AEP range. Bin number 3, for example, includes flows that range from an AEP of 0.063 to an AEP of 0.141 with the index value being AEP equal to 0.1. In terms of return period, bin number 3 includes flows that range from a 16-yr return period to a 7-yr return period with an index value of the 10-yr flow.

Table 5.21. AEP bins.

Bin number	Bin AEP (Index Value)	Bin AEP range	$P[Q_{M,i}]$
1	0.500	0.316 > AEP >= 1.000	0.684
2	0.200	0.141 > AEP >= 0.316	0.175
3	0.100	0.063 > AEP >= 0.141	0.078
4	0.040	0.028 > AEP >= 0.063	0.035
5	0.020	0.014 > AEP >= 0.028	0.014
6	0.010	0.004 > AEP >= 0.014	0.010
7	0.002	0.000 > AEP >= 0.004	0.004

To apply equation 5.7, the engineer estimates  $P[Q_{M,i}]$  and  $P[y_T|Q_{M,i}]$ . For this illustration, Table 5.21 provides estimates  $P[Q_{M,i}]$  calculated as the range of the AEP bin. For example, the probability of a flow falling in bin 3 is equal to the width of the range ( $0.141-0.063 = 0.078$ ).

$P[y_T|Q_{M,i}]$  is the conditional probability of experiencing a stage of  $y_T$  given a flow on the mainstem in bin  $i$ . However, with coincident flows  $y_T$  is a function of both  $Q_M$  and the flow on the tributary,  $Q_T$ . Referred to as a “linking relationship,” there is some function used to calculate the tributary stage,  $y_T$ . Typically, this linking relationship is provided with a HEC-RAS model of the confluence with  $Q_T$  and  $Q_M$  as inputs. Functionally, the relation is expressed as follows:

$$y_T = f(Q_T, Q_M) \quad (5.8)$$

where:

$y_T$	=	Tributary stream stage
$Q_T$	=	Tributary streamflow
$Q_M$	=	Mainstem flow

Although critical to application of the total probability theorem, the linking relationship does not provide the conditional probability,  $P[y_T|Q_{M,i}]$ . Particular applications call for development of the conditional probabilities (conditional probability matrices). Kilgore et al. (2013) provides conditional probability matrices applicable to many situations in the United States and provides an example application.

### 5.3 Riverine/Storm Surge (Compound) Flooding

Coastal compound flooding relates to the interaction of coastal storm surge and runoff from rainfall on watersheds near the coast (FHWA 2020). Combined hydrologic, hydraulic, and hydrodynamic simulations of flow and water levels reveal that rainfall-runoff can significantly affect coastal water levels and that the presence of storm surge generally results in higher flood levels in tidally-influenced or tidally-dominated rivers than would otherwise exist. Topography of the watershed, particularly elevation gain from coastal elevations, as well as the time lag between the rainfall and the storm surge influence the coincidence of flooding causes commonly called coastal compound flooding (FHWA 2020).

The environment of a tidally-influenced or tidally-dominated river differs from that in a purely fluvial watercourse. Tidally-dominated rivers are subject to (FHWA 2021a):

- Tidally-driven changes in water level and reversals in flow direction.
- Weather-related wave action that varies daily, seasonally, and decadal (due to El Niño on the west coast or North Atlantic Oscillation on the east coast).
- Coastal flooding resulting from storm surges.

Tidally-influenced rivers differ in that flow is mostly unidirectional, and normal tidal fluctuations reduce the riverine flow duration parts of the tidal cycle rather than reverse it. However, tidally-influenced rivers can also be subject to long-term, weather-related wave action and coastal flooding, leading to occasional flow reversals during these extreme events. The hydraulic forces associated with coastal storm induced water fluxes, currents, and waves may be greater than those experienced in the fluvial reaches of a watercourse, potentially affecting bridges miles from the coast. The elevated coastal water levels act as a downstream control for storm related rainfall-runoff within coastal watersheds. Until the surge recedes, it creates a higher backwater condition for the rainfall-runoff increasing flood elevations compared with what they would be without the

storm surge. Depending on the coastline bathymetry and topography, large volumes of freshwater runoff can also contribute to higher water levels at the coast than would occur with storm surge alone.

As with the coincident riverine flooding discussed in Section 5.2, the possibility of coastal compound flooding depends on the correlation between the rainfall and storm surge events. This dependence relates to the characteristics of the storm (e.g., size, speed, direction, type) causing the rainfall and surge as well as the coastal topography and bathymetry. Superimposed on these factors are the regular ebb and flow associated with the regular tidal cycles.

Quantitative assessment of coastal compound flooding is primarily scenario driven because of the large number of contributing factors. Gori et al. (2020) loosely coupled hydrologic, hydraulic, and hydrodynamic models to analyze six coastal compound flooding events from tropical cyclone events making landfall near the Cape Fear Estuary, North Carolina. They identified combinations of direct rainfall, river runoff, and storm surge that raised river levels by up to 1.2 ft in some areas. Many others have confirmed coastal compound flooding effects, including those in the San Francisco Bay/Napa River (Herdman et al. 2018), Sabine Lake, Texas (Santos et al. 2021), and the Shoalhaven Estuary in Southeastern Australia (Kumbier et al. 2018). Kumbier et al. (2018) hypothesized that large watersheds with quick response times to rainfall increase coastal compound flooding risks.

Nadal-Caraballo et al. (2022) quantified the joint hazards of tropical cyclones and Mississippi River flooding in the Greater New Orleans area with additional hazard analysis of tropical cyclones over a wider area off the coast of Louisiana. They applied a Probabilistic Coastal Hazard Analysis Framework integrating:

- Regional storm climatology characterization.
- Marginal distributions of tropical cyclone (TC) atmospheric forcing parameters.
- Development of synthetic TCs.
- Dependence modeling of TC parameters.
- Joint probability analysis of atmospheric forcing and hydrodynamic responses.
- High resolution numerical model simulation.
- Metamodeling prediction of storm responses.
- Quantification of uncertainty associated with the randomness of events.

This intensive modeling approach generated hurricane-induced still water levels and other parameters for AEPs ranging from 0.1 to 0.0001.

### What Have We Learned?

The research described in this section uses several approaches to deepen the understanding of the complex phenomenon of compound flooding. These approaches include:

- Modeling hypothetical future scenarios of storm surge and rainfall events.
- Analyzing historical compound flooding events and their effects.
- Conducting regional or national statistical studies of historical data.

This research also shows that compound flooding is more complicated than adding the effects of the components—surge and rainfall—because timing and other factors also influence outcomes.

Hendry et al. (2019) examined the historical record of coastal compound flooding events in the United Kingdom to identify patterns that could be useful in evaluating future risks. Their first objective was to map the dependence between storm surge and river flow, comparing different methods for quantifying the dependence between these two variables. They showed that spatial variability in the dependence and number of joint occurrences of high skew surges and high river flow is driven by meteorological differences in storm characteristics. They found that on the western coast of the United Kingdom, the storms that generate high skew surges and high river flow are typically similar and track across the United Kingdom on comparable pathways. In contrast, they found that on the eastern coast, the storms that typically generate high skew surges are mostly distinct from the types of storms that tend to generate high river flow. They found that high skew surges tend to occur more frequently with high river flow at watersheds with a lower base flow index (BFI), smaller watershed area, and steeper elevation gradient. In watersheds with a high BFI, large watershed area, and shallow elevation gradient, the peak river flow tends to occur several days after the high skew surge. Findings such as these might not apply directly to the U.S. coast, but a similar analysis could be conducted to assess risks to the United States.

Petroliagkis et al. (2016) explored the explicit use of joint probability methods in coastal flood hazard component calculations, since flood risk is rarely a function of just one source variable but usually two or three variables such as river flow, storm surge, wave, etc. They specifically analyzed combinations of: 1) surge and wave, 2) surge and flow, and 3) wave and flow. The analysis focused on over 32 locations selected to cover a variety of coastal environments along European riverine and estuary areas. In the absence of coincident long-term measurements, they simulated data observations resulting in a set of hindcasts for surge, wave height, and flow. Overall, they found moderate correlations and dependencies between surge and river flow in most locations but with a time lag to experience coastal compound flooding with surge leading flow values. As with the Hendry et al. (2019) study, these results might not directly apply to the United States, but they indicate the type of analysis that could be conducted and possible outcomes of such a study.

Wahl et al. (2015) assessed the co-occurrence of storm surge and heavy precipitation in the United States. They took a national approach to estimate the likelihood of joint occurrence of these two phenomena for the contiguous United States and showed that the risk of coastal compound flooding is higher for the Atlantic and Gulf coasts than for the Pacific coast. They also provided evidence that the number of compound events has increased significantly over the past century at many of the major coastal cities. For example, New York City has experienced an increase in compound events attributed to a shift toward storm surge weather patterns that also favor high precipitation (Wahl et al. 2015).

### What's That?

Attempts to understand compound flooding can lead to developing potentially unfamiliar parameters such as:

- Skew surge: the difference between the maximum observed high water and the maximum predicted (astronomical) high water, in each tidal cycle.
- Base flow index: the proportion of river runoff derived from stored sources (Gustard et al. 1992), a potential indicator of watershed flashiness (how quickly a river responds to precipitation).

Without considering the potential for coastal compound flooding (storm surge with precipitation driven riverine flooding) engineers may underestimate flooding risks in coastal areas. Because coastal compound flooding is influenced by many meteorological and topographical factors, engineering assessment of coastal compound flooding typically involves site-specific modeling of possible scenarios. As summarized in this section, some resources provide broad insights to the risks of coastal compound flooding nationally, but do not replace site-specific analyses.

*Page Intentionally Left Blank*



## Chapter 6 - Spatially Distributed Precipitation

Understanding how rainfall is distributed spatially is fundamental to hydrologic design. It is essential for accurate volumetric estimation of watershed rainfall. For modeling, hydrologists traditionally measure rainfall data at precise locations with rain gages. Hydrologists use these data, known as point data, to describe rainfall over a much larger area such as a watershed. However, networks of rain gages rarely have sufficient density to characterize rainfall variability over a watershed.

In recent years, new methods of rainfall estimation have rapidly advanced that provide more context to the spatial distribution of rainfall. Engineers and hydrologists now commonly use radar estimated rainfall in hydrologic applications. This chapter provides insights engineers and hydrologists can use to understand how spatially distributed datasets are derived and used.

This chapter discusses point rainfall measurement along with methods to convert networks of point measurements into watershed scale estimates of rainfall. Next, it introduces methods for directly estimating the spatial distribution of rainfall, such as weather radar and satellites. The chapter covers basic principles of radar rainfall estimation along with basic methods for combining data from multiple measurement technologies (e.g., rain gage and radar) to improve rainfall estimates. The chapter concludes with discussions of the application of spatially distributed data to hydrologic models and the implications of spatially distributed data in the development of hydrologic design storms. Common sources of spatially distributed data are noted.

### Precipitation versus Rainfall

Many use the terms “precipitation” and “rainfall” synonymously. Technically, precipitation is more general, describing all forms of water falling from the sky, including rain, hail, sleet, snow, etc. Rain is a liquid form of precipitation in which water falls from the sky as droplets.

### 6.1 Point Rainfall Measurement

Volumetric outflows from a contributing watershed represent the hydrologic response to volumetric inflows, namely precipitation. Hydrologists often use a network of precipitation gages scattered across the watershed to measure precipitation at each gage location or point. Collecting point estimates allows hydrologists to infer the total volume of precipitation entering the watershed.

Gages measure precipitation falling through an orifice that may range from 1 to 12 inches in diameter. A 12-inch-diameter gage measures precipitation falling on a hydrologically tiny area of 0.000000282 mi<sup>2</sup>. Even with a dense network of one gage per 10 mi<sup>2</sup>, a gage network measures rainfall at a resolution of parts per billion.

To determine the average precipitation depth over a watershed, the hydrologist combines point estimates to create a precipitation “surface” by interpolation for each time step in a storm event. Multiplying the average precipitation depth over the watershed by the watershed area yields total volume at each time step. Common interpolation schemes have included the Thiessen polygon (or nearest neighbor) approach, the inverse distance squared weighting technique, and the isohyetal method (Viessman and Lewis 2003). Software tools, such as HEC-HMS, implement these interpolation schemes.

The Thiessen polygon approach applies the precipitation value measured at the closest gage to the point of interest. The collection of points closest to each specific gage in a gage network forms a Thiessen polygon. The result is a set of irregularly shaped polygons covering the watershed. Each polygon is associated with an individual rain gage. Figure 6.1 presents an example of the Thiessen polygon interpolation approach for a network of eight gage locations, each labeled with a four-digit identifier. All points within polygon number 2083 are closer to gage number 2083 than to any other gage in the network. Similarly, all points within polygon number 7244 are closer to gage number 7244 than any other gage. Watershed average rainfall is determined by weighting each rain gage value by the amount of area for each gage's polygon contained within the watershed boundary.

The resolution of the resulting precipitation surface depends entirely on the density of the gage network. Given the complex nature of natural precipitation, gage networks rarely have sufficient density to accurately estimate the true influx of precipitation. Further, gage networks are static and unmoving. The interpolated surface reflects the geometry of the rain gage network at each time step rather than the intricate evolution of a storm event.

In contrast to the Thiessen polygon rainfall distribution shown in Figure 6.1, Figure 6.2 shows the rainfall distribution from the same storm as estimated from radar. The differences are clear. Radar based rainfall shows that a band of heavy rain fell, largely unobserved between the gages in the eastern third of the watershed. Further, radar-based rainfall shows much lower rainfall amounts in the central and western portions of the watershed. In this case, the Thiessen polygon interpolation distorts both the location and amounts of rainfall in the watershed.

Another common interpolation scheme is inverse distance squared weighting. Inverse distance squared weighting estimates precipitation at a point using a weighted average of gages in the network. The hydrologist weights each gage observation by  $1/d^2$  where  $d$  is the distance between the point estimate location and each rain gage. Closer gages are given more weight than gages further away. As with Thiessen polygons, the resolution of the resulting precipitation surface depends on gage network density.

Other interpolation methods such as inverse distance weighting, a generalized version of  $1/d^2$ , spline, linear regression, and kriging in various forms, are used to interpolate rainfall. Inverse distance squared and Thiessen polygon methods are used in HEC-HMS. Broader selections of interpolation methods are found in Geographical Information Systems.

Often rainfall interpolation schemes produce over-simplified and distorted rainfall patterns that depict the wrong rain in the wrong place at the wrong time. When applied to hydrologic models, engineers expect the models to accurately reproduce an observed watershed response based on the observed rainfall inputs. When engineers find the results do not fit observed results, they "calibrate" the model to force it to reproduce observed hydrologic results. In some cases, engineers may be calibrating the hydrologic model to compensate for poorly established rainfall inputs rather than other watershed factors.

Understanding how rainfall is distributed spatially is fundamental to hydrologic design. Where thunderstorms dominate, interpolating point measurements can produce excessive data smoothing leading to storms with heavy rainfall spread over too large an area. This can result in overdesigned and unnecessarily costly infrastructure.

Newly available technologies attempt to improve the spatial distribution of rainfall and the resulting volumetric estimates of watershed input. Radar and satellite instrumentation can fill the gaps between gages at resolutions sufficient to resolve the complex variations in precipitation in both time and space.

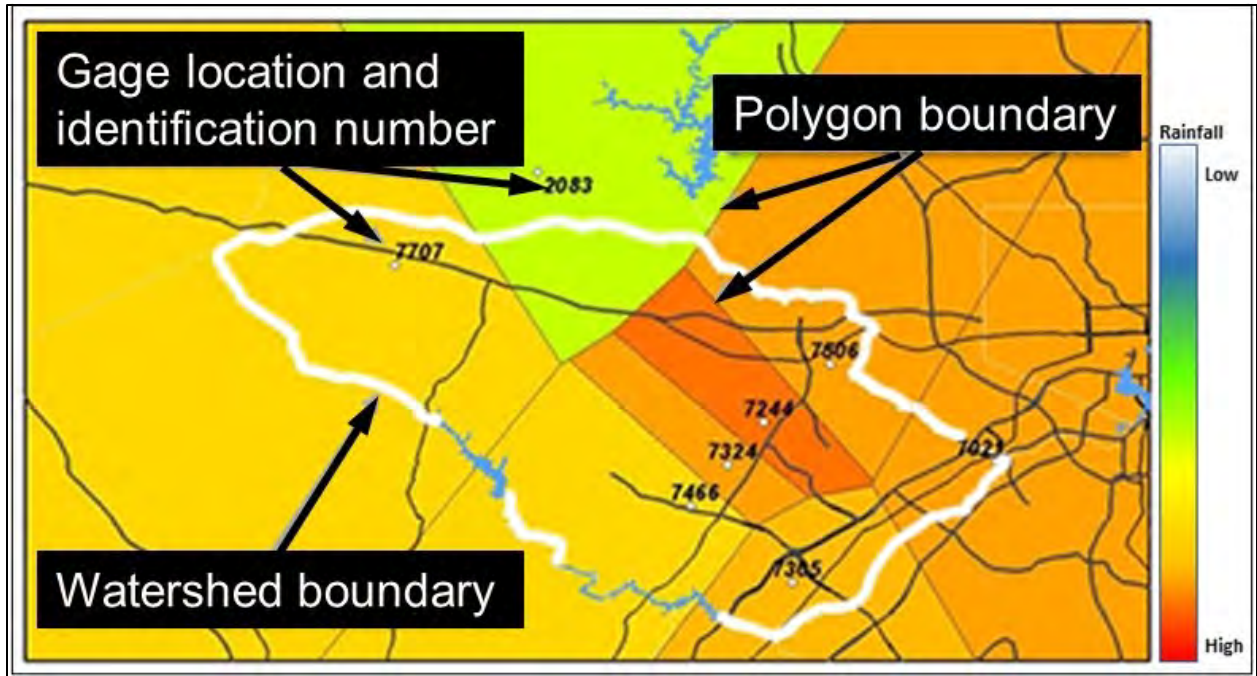


Figure 6.1. Rainfall map created from Thiessen polygon interpolation.

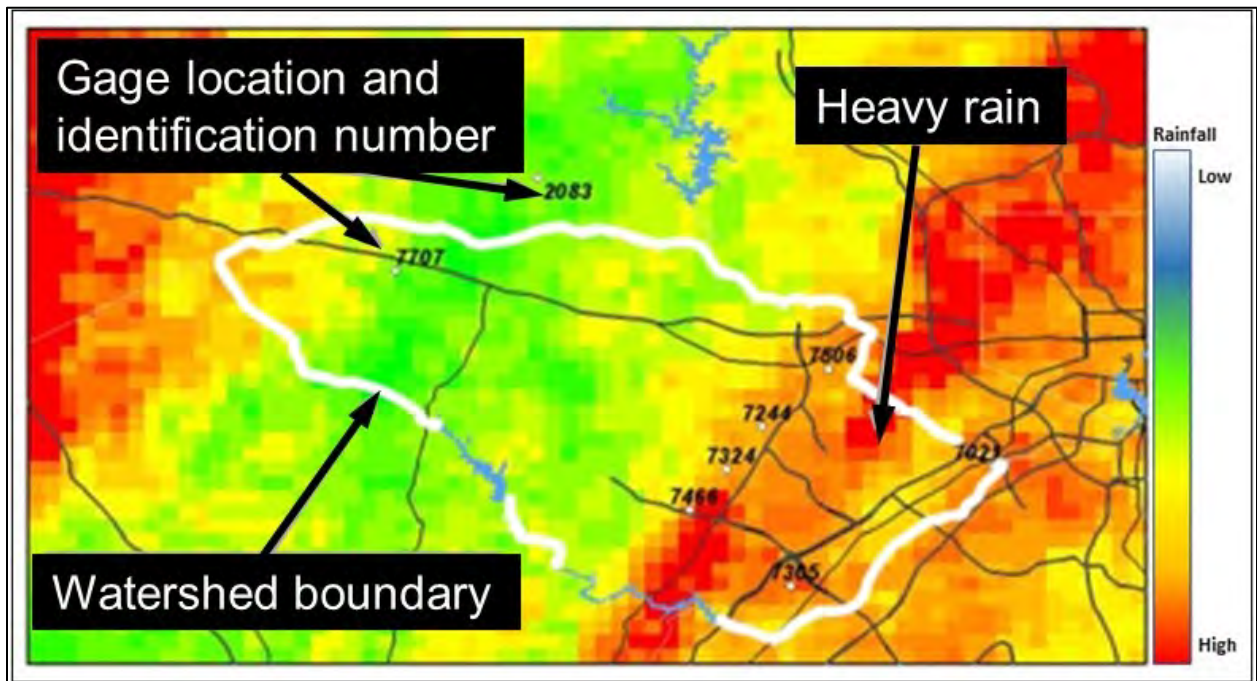


Figure 6.2: Rainfall map created from radar rainfall estimates.

## 6.2 Spatially Distributed Rainfall Measurement

Complex distributions of rainfall are often beyond the ability of rain gage networks to fully resolve, potentially creating inaccurate input for hydrologic analyses. Radar and satellite technology platforms are filling that need. The U.S. National Weather Service (NWS) weather radar network is an important source of spatially distributed rainfall data.

### 6.2.1 Radar Rainfall

Scientists recognized the meteorological applications of radar in World War II when they found precipitation interfered with detection of aircraft flying across the English Channel to England. After another 50 years of development, radar became a valuable tool for hydrologic applications in the United States with the introduction of the NWS WSR-88D in the 1990s. With the deployment of a network of approximately 140 radars across the United States as shown in Figure 6.3, rainfall estimates at a 1-kilometer square resolution in 5-minute time steps became available.

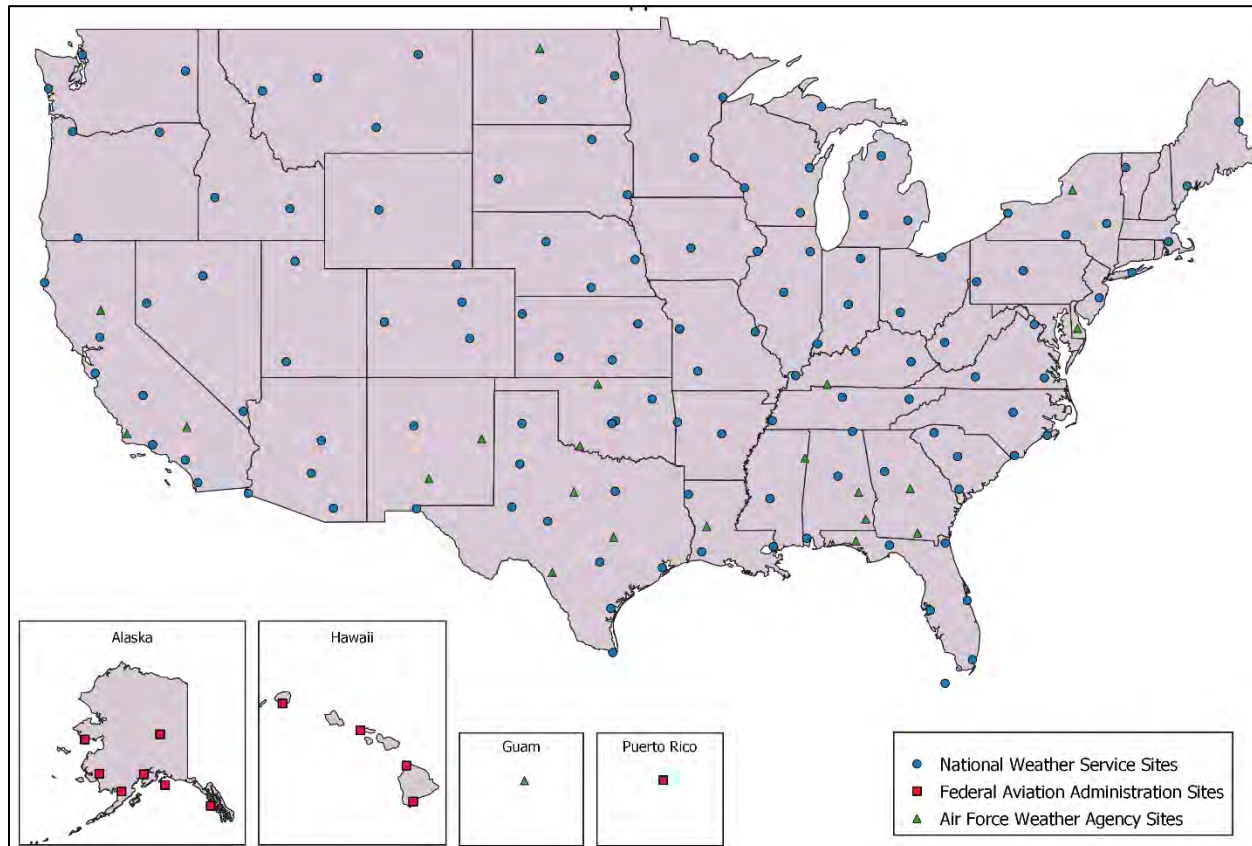


Figure 6.3. NWS WSR-88D radar network. Source: NWS.

Radar data resolutions continue to improve. Data resolution on the order of 0.5 km x 0.5 km is now available, which yields precipitation estimates every 60 to 70 acres.

The radar image from the NWS radar in Nashville, Tennessee, presented in Figure 6.4, shows an area of intense rainfall moving through Nashville metropolitan area. The complex details of the spatial distribution of rainfall over the region is more evident from the increased resolution.



### 6.2.2 Satellite Rainfall

Satellites, whether polar-orbiting or geostationary orbiting, represent another technology platform for estimating the spatial distribution of rainfall. Satellites offer complete coverage of the United States and territories. Typically, hydrologists derive rainfall estimates from sensors tuned to infrared wavelengths measuring cloud top temperatures. Colder temperatures indicate higher well-developed cloud structures associated with heavier rainfall.

**Polar versus Geostationary Orbiting**

Polar orbiting satellites constantly circle the Earth at approximately 520 miles above the Earth's surface, passing near the north and south poles on each orbit.

Geostationary satellites orbit the Earth at approximately 22,300 miles above the surface. The satellites orbit in the equatorial plane matching the speed of the Earth's rotation, remaining stationary above a fixed point on the ground.

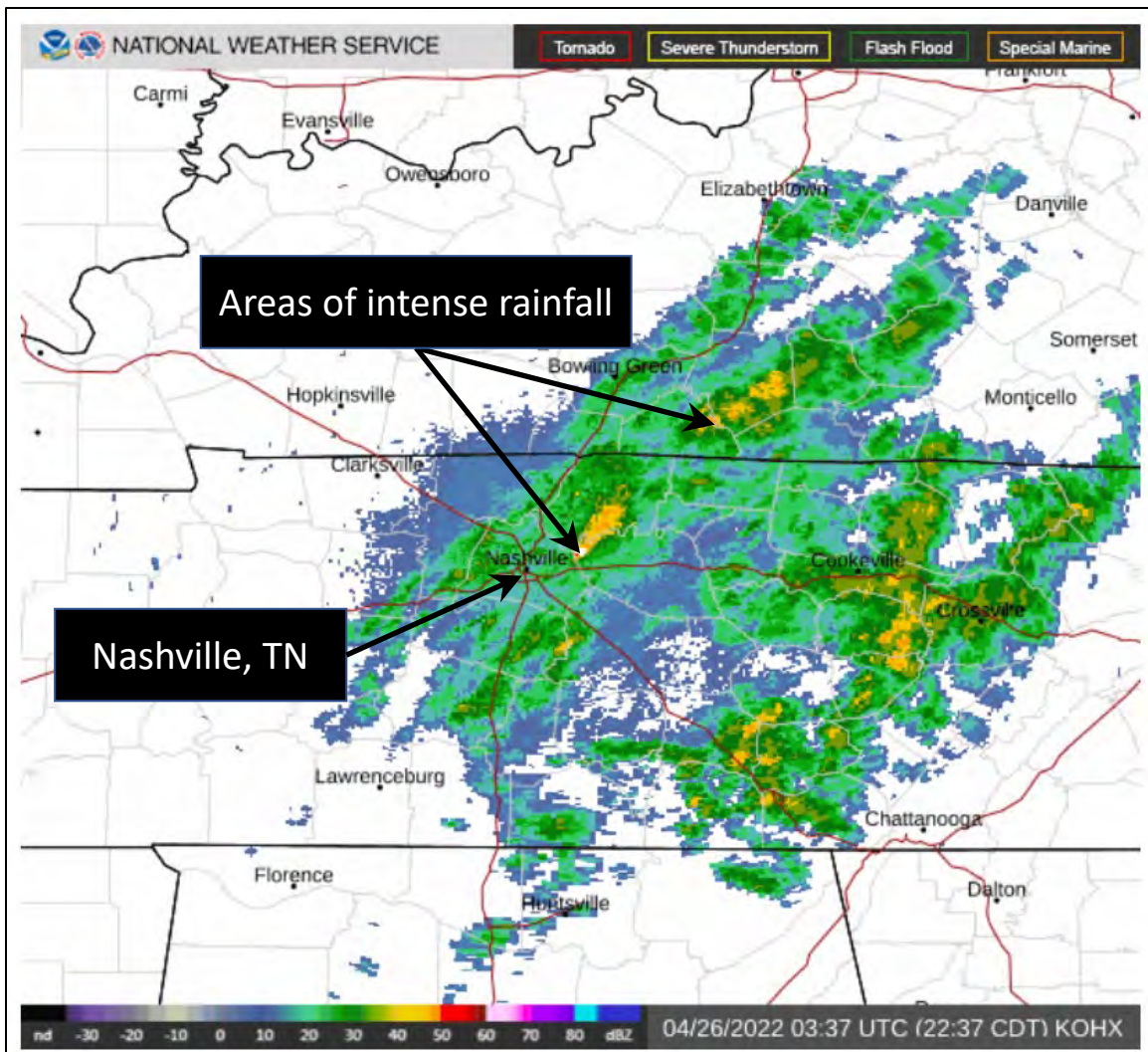


Figure 6.4. NWS radar image, Nashville, Tennessee.

Satellite rainfall estimation accuracy still trails the current accuracy, spatial resolution, and data latency (the amount of time between a data observation and its arrival at its destination) of both NWS Next-Generation Radar (NEXRAD) radar and rain gauges. Figure 6.5 compares a national map of NEXRAD rainfall intensity estimates (left) to a national map of experimental near real-time satellite-based estimates of rainfall intensity from the National Oceanic and Atmospheric Administration (NOAA) Center for Satellite Applications and Research (STAR). Visual inspection shows broad agreement with the general location of rainfall but large differences at watershed scales. Despite the shortcomings, satellite data are a valid option for locations lacking gage and radar data, as in the mountainous regions of the Western United States and much of Alaska.

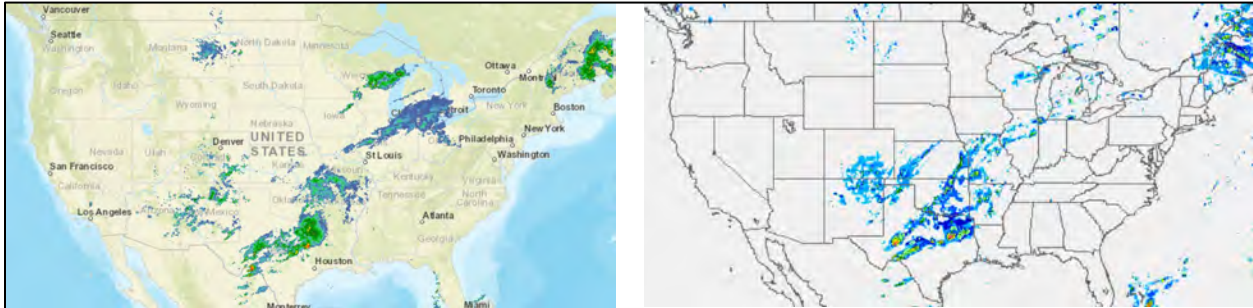


Figure 6.5. NWS national radar rainfall (left) and NOAA national satellite rainfall (right). Source: NWS.

### 6.3 Rainfall Estimation

From a hydrologic perspective, radar estimated rainfall data provide the key benefit of improved estimates of the spatial signature of precipitation. Figure 6.6 compares the gage interpolated rainfall image from Figure 6.1 with the rainfall distribution estimated from NWS radar for the same storm (Figure 6.2). Note the increased fidelity of the radar image. The image reveals the complex nature of the storm event in ways that a gage network cannot. The stark differences can lead to significantly different results from a hydrologic model. More accurate placement of rainfall in the watershed allows engineers to focus on calibrating the hydrology of an event rather than compensating for poorly delimited rainfall inputs.

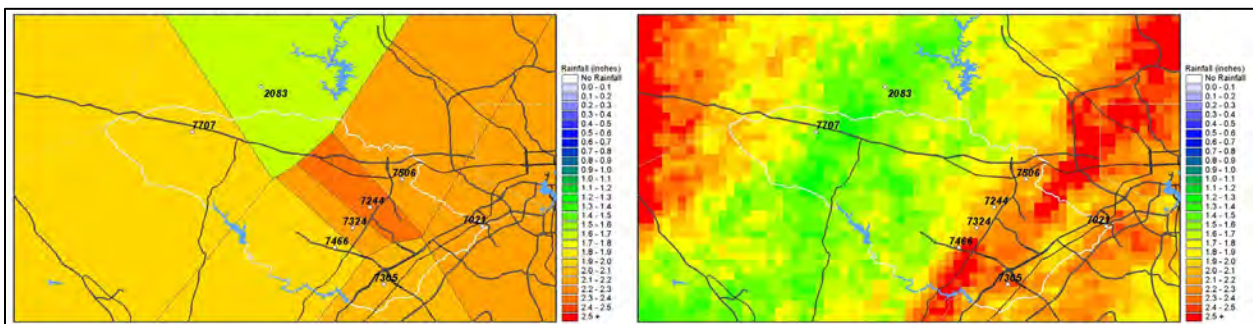


Figure 6.6. Comparison of gage interpolated (left) and radar rainfall data (right).

In-depth coverage of radar rainfall estimation exceeds the scope of this manual. However, understanding several concepts and basic principles will benefit practicing engineers. For more details on weather radar principles, see Bringi and Chandrasekar (2001) and Rinehart (2010).

### 6.3.1 Basic Principles

Gages (e.g., tipping buckets, weighing gages, etc.) measure rainfall directly. Radar measures rainfall indirectly. The radar antenna transmits radio signals of an appropriate frequency and wavelength into the atmosphere. Along the transmission pathway, the signal scatters when encountering raindrops, snowflakes, hail, or other forms of precipitation. Some of the signal reflects back to the originating radar antenna. Figure 6.7 illustrates a conceptualized view of this process.

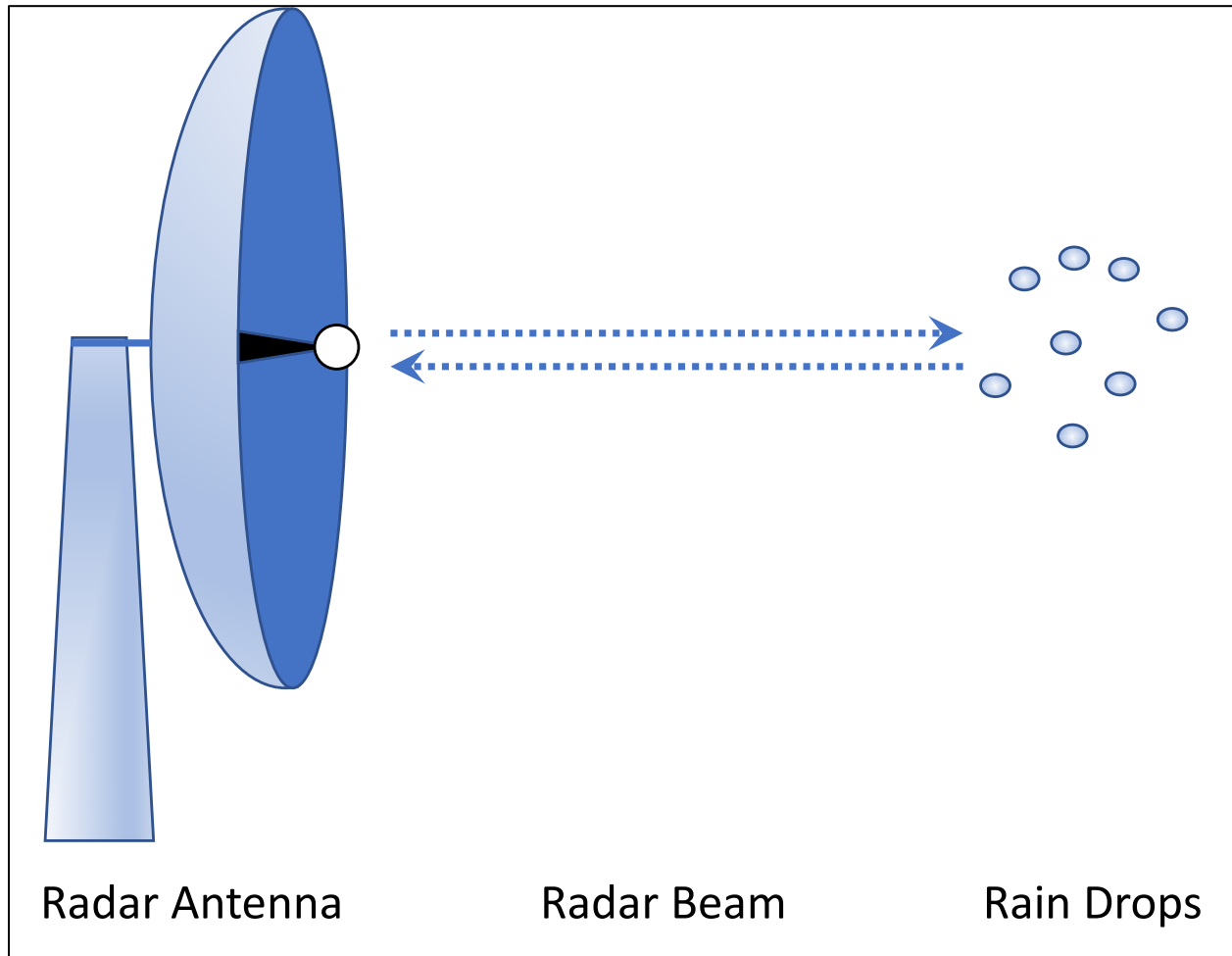


Figure 6.7. Conceptualization of radar detection of rainfall.

The radar antenna rotates around its vertical axis at approximately 5 rpm to scan a slice of the atmosphere starting with a center beam elevation  $0.5^\circ$  above horizontal. After completing one elevation scan, the beam elevation increases successively for scan elevations up to  $19.5^\circ$  above horizontal. Figure 6.8 provides a conceptualized representation of a slice of the atmosphere scanned at  $0.5^\circ$  elevation. The volume directly above the radar location (the “cone of silence”) cannot be physically monitored by current generation NEXRAD radars.

Depending on weather conditions, NWS employs several different combinations of volume scan elevations and scan frequencies. In the presence of precipitation, NEXRAD radars generate 14 volume slices every 5 to 6 minutes.



A waterproof spherical structure called the radar dome houses the radar antenna. It is constructed of material offering minimal interference potential for the transmitted and returned signals. Figure 6.9 shows a typical NWS radar dome.

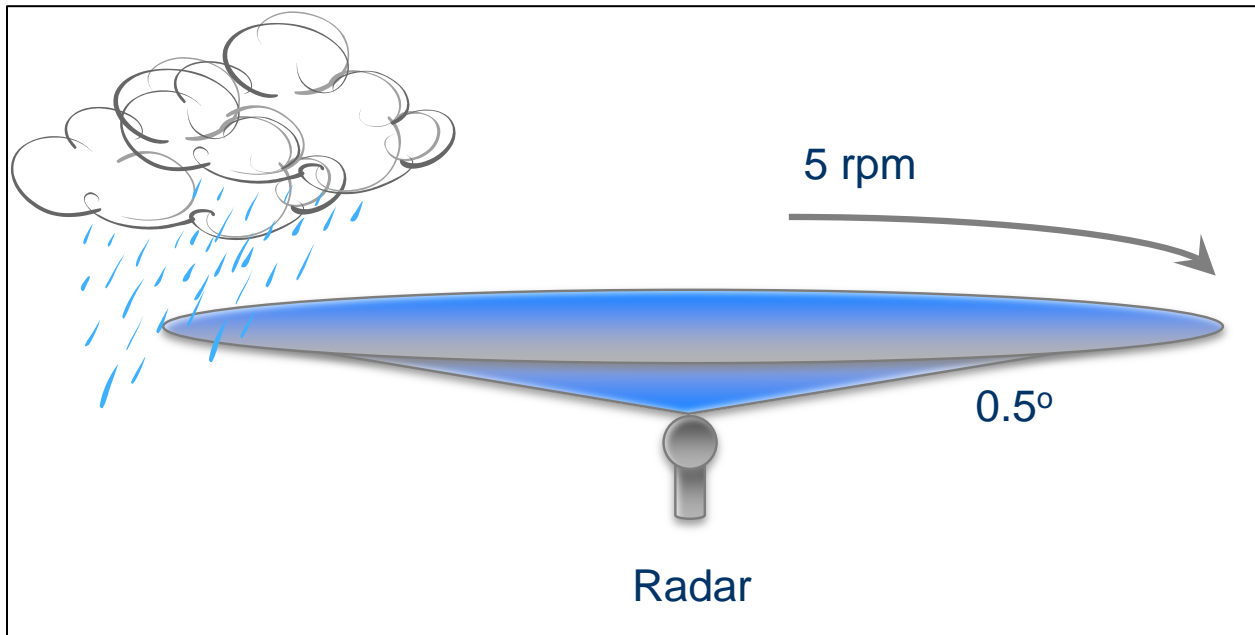


Figure 6.8. Conceptualization of radar "slice" during a volumetric scan.



Figure 6.9. Typical NWS NEXRAD radar dome. Source: NWS.



Algorithms convert the strength, timing, and direction of the returning signal to an estimate of the instantaneous precipitation intensity and its location. Precipitation intensity is assumed uniformly distributed across a small measurement area, known as a radar pixel, corresponding to the resolution of the radar. Radar resolutions of  $1^\circ$  azimuth (angular measure) by 1 km range (i.e., radial distance from the radar transmitter) or  $0.5^\circ$  azimuth by 0.5 km range are currently common resolutions.

The conical radar beam expands in size as it moves away from the radar transmitter. Close in, it has high radar resolution, with small resulting pixels. Further out, it has larger pixels, hence lower resolution as shown in Figure 6.10, left.

Since radio signals tend to travel in a straight line and the Earth surface is curved, the radar beam height above ground gets higher with distance from the radar. Eventually the beam is higher than the location of the rain in the atmosphere. The range limit for hydrologic applications is about 230 km from the radar.

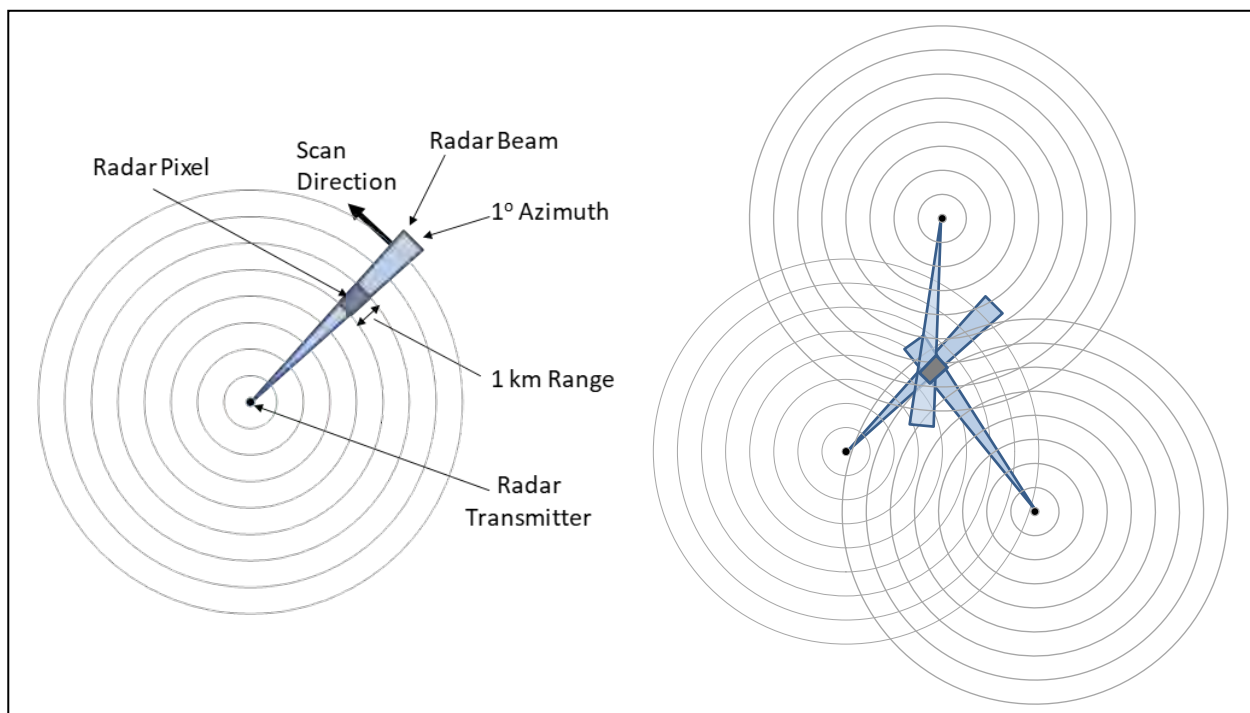


Figure 6.10. Single versus multi-radar mosaic. Source: NWS.

To overcome range limitations of a single radar, the NWS formed radar networks such that scan regions of individual radars overlap as shown in Figure 6.10, right. The NWS converts individual scans from a cylindrical coordinate system (azimuth, range) to a rectangular grid system ( $x$ ,  $y$ ). Then, they combine individual radar images into a common grid to form the mosaic of radar rainfall images from multiple radars. Because they provide a more complete picture of rainfall distribution, hydrologists generally prefer mosaiced radar rainfall images, especially for larger watersheds.

Radar mosaics, like the one shown in Figure 6.11, represent instantaneous rainfall intensities. The hydrologist determines accumulations by averaging estimated rainfall intensity at each pixel and integrating over time. This typically yields grids of estimated 5-minute rainfall amounts.

Design hydrologists using radar rainfall estimates will also benefit from understanding several other limitations of radar estimated radar. Figure 6.12 illustrates several common issues of concern. First, Figure 6.12 shows a rainstorm at the radar location. As noted earlier, current

generation NEXRAD radars cannot transmit vertically, producing the cone of silence in the immediate vicinity above the radar. Heavy precipitation falling directly on the radar dome can attenuate the radar signal, causing underestimation. On the left side of Figure 6.12, complex terrain blocks the radar signal from reaching precipitation within radar range. On the right side of Figure 6.12, the radar beam overshoots a rain event with little vertical development. Further to the right, the beam intersects the precipitation high in the rain cloud. In this case, overshooting can occur and under-report rainfall amounts. Lower-level winds can also direct precipitation away from the indicated location by the time precipitation reaches the ground.



Figure 6.11. Example NWS radar mosaic. Source: NWS.

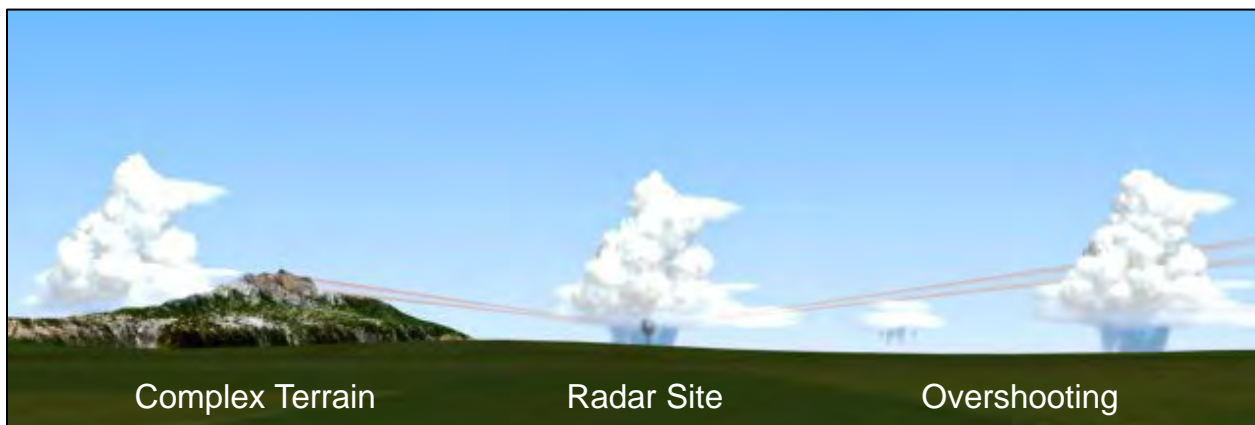
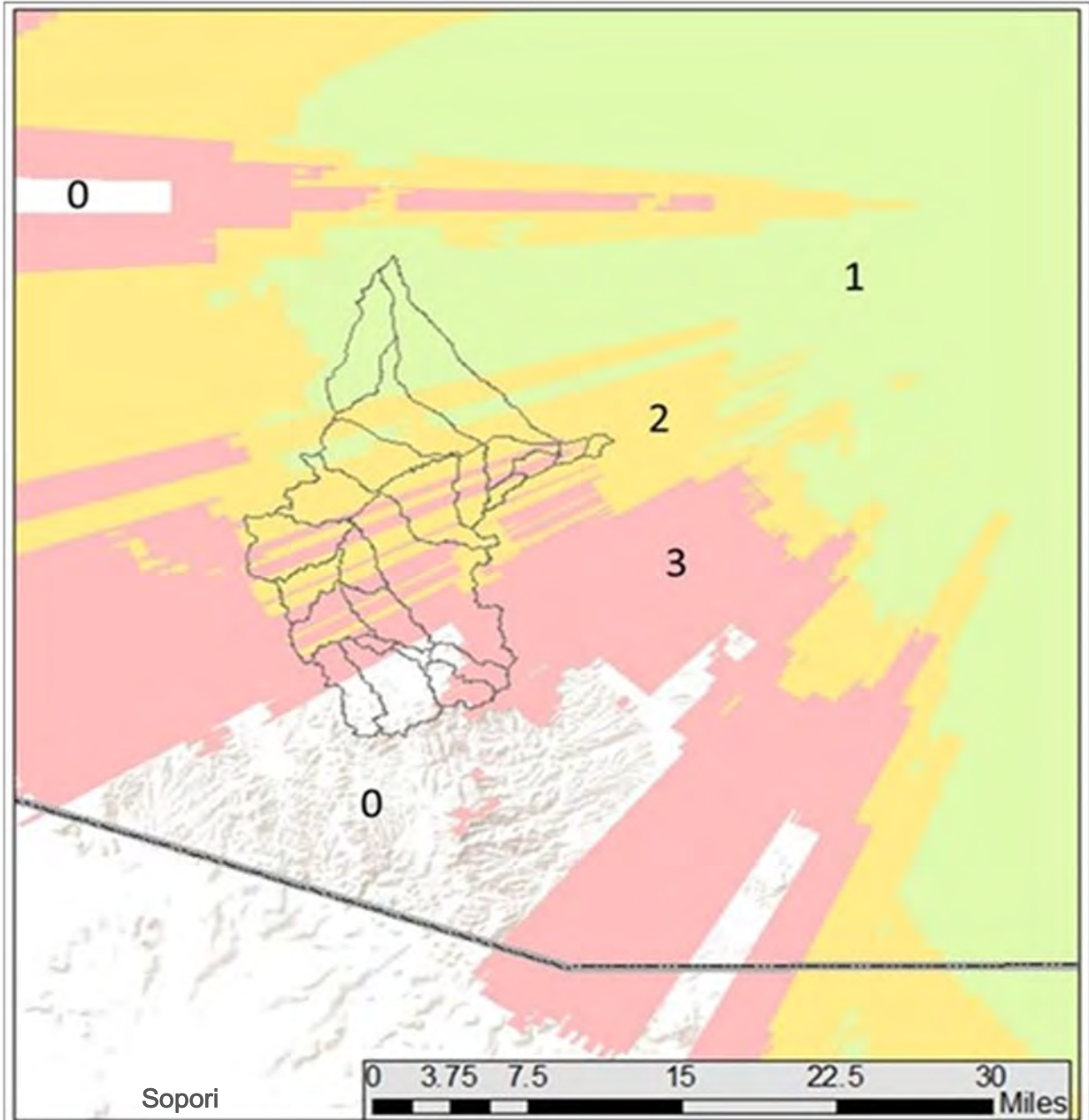


Figure 6.12. Examples of radar coverage issues. Source: University Corporation for Atmospheric Research.

Figure 6.13 shows a more nuanced view of radar coverage quality when complex terrain affects radar. The National Center for Environmental Information (NCEI) provides coverage quality information for each NEXRAD radar. Figure 6.13 shows regions of varying coverage quality from the Tempe, Arizona, NEXRAD. Located in the vicinity of Sopori Wash, a tributary of the Santa

Cruz River southwest of Tucson, Arizona, this radar just north of the United States-Mexico border contends with rugged terrain. The shaded areas represent coverage quality, with “1” indicating best coverage, “2” indicating better coverage, “3” indicating poor coverage, and “0” indicating areas of no reliable coverage.



**Legend**




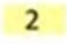

-  Sopori Wash HEC1 Sub-basins
-  State Boundary
-  1 Radar best coverage
-  2 Radar better coverage
-  3 Radar fair coverage

Figure 6.13. Radar coverage quality over Sopori Wash watershed near Tucson, Arizona.



Coverage qualities derive from simple geometry of a radar beam relative to the terrain. However, coverage quality also depends on storm type and atmospheric conditions. Strong vertical development of thunderstorms may provide useful rainfall estimates even in areas designated as poorly covered. Other storms with rain producing processes in the lowest portions of the atmosphere may yield poor estimates in all areas, especially as the distance from the radar increases. A watershed of interest in an area of no reliable coverage, may not have radar data usable for accurate rainfall estimation. When possible, the hydrologist can assess radar data quality by comparing radar rainfall estimates to rain gage observations.

### 6.3.2 Radar Beam Polarization

Electromagnetic radiation such as radio waves has both electric and magnetic fields. Polarization refers to the orientation of the electrical field relative to the Earth's surface. If parallel to the Earth's surface, the radar beam has horizontal polarization. If oriented vertically with respect to the Earth's surface, the beam has vertical polarization.

When the NWS first deployed NEXRAD radars in the early 1990s, the radar beams were polarized in the horizontal plane only, as shown in Figure 6.14. Horizontally polarized beams provide a good sense of the horizontal dimension (i.e., width) of a rain drop, hail stone, or snowflake. They have less ability to sense the vertical dimensions of their targets. Limited to one preferred direction, horizontally polarized beams have less ability to discriminate between precipitation types and assumed rain drop volumes. This limitation has a significant impact on radar rainfall estimate accuracy.

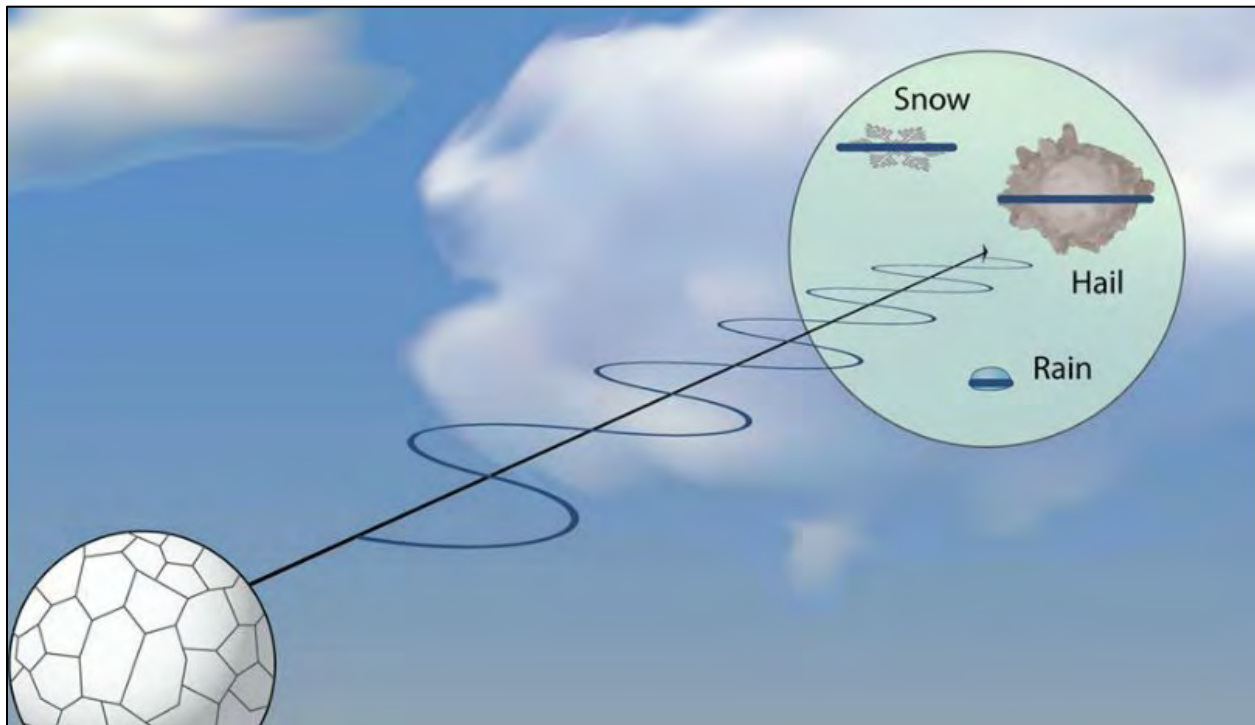


Figure 6.14. Conceptualization of single polarization radar. Source: NWS.

As shown in Figure 6.15, dual polarized radars transmit and receive beams with both horizontal and vertical components, enabling improved detection of the size, shape, and type of atmospheric targets. Dual polarized radars also enable improved ability to reject signals from non-meteorological sources in the atmosphere such as birds, bats, insects, etc.

In 2011, the NWS began the NEXRAD network upgrade from horizontally polarized radars to dual polarized configurations, completing the transition of the entire NEXRAD radar network in 2013. When reviewing historical radar rainfall estimates, practitioners will want to keep this transition timeline in mind if they note changes in data quality in the radar rainfall record.

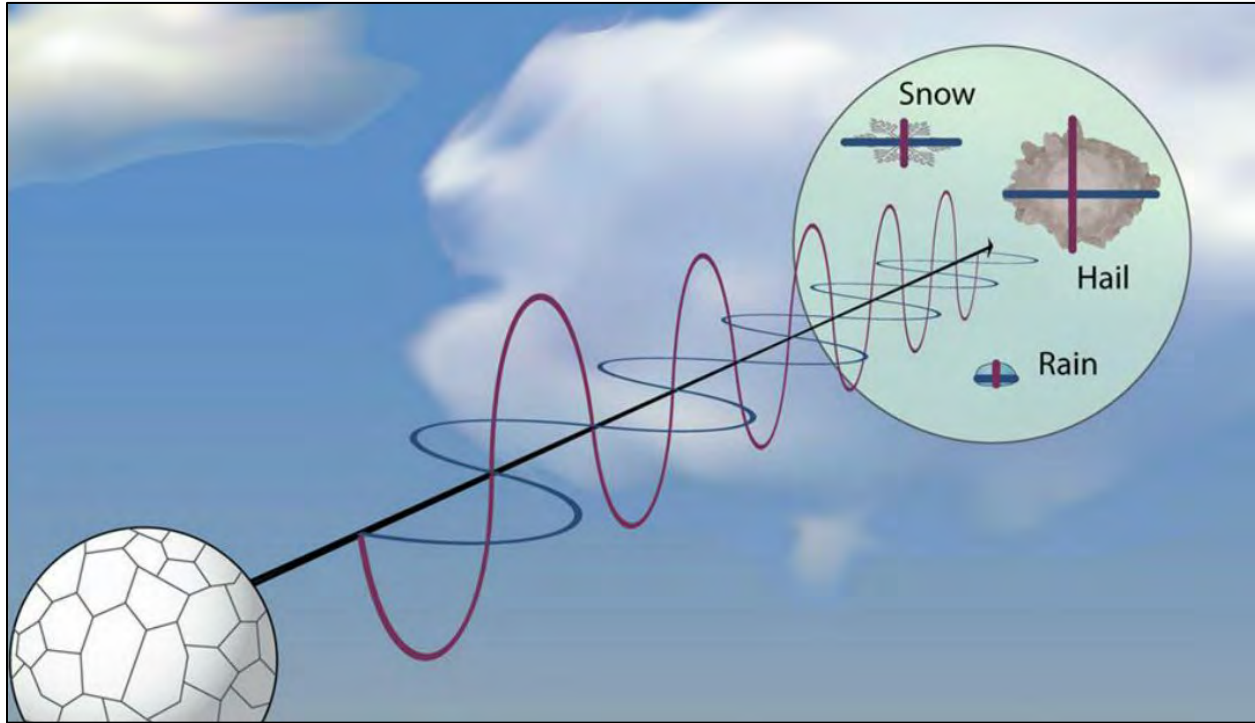


Figure 6.15. Conceptualization of dual polarization radar. Source: NWS.

#### 6.4 Multi-Sensor Rainfall Estimation

The strength of a rain gage is its ability to measure rainfall with a high degree of accuracy at a point. In this case, the point is the rain gage orifice, commonly ranging from 1 to 12 inches in diameter. Rain gages provide little information about rain falling between gages miles or tens of miles apart.

Conversely, radar excels at identifying the spatial signature of rainfall, which is useful to accurately estimate the volume of rain falling on a watershed. However, compared to rain gage observations, radar less consistently estimates the amount of rain falling at a point. Hydrologists commonly call the difference between rain gage observations and radar rainfall estimates at gage locations “bias.” Radar rainfall estimates consistently lower than gage observations have a low bias. A high bias means that radar rainfall estimates are consistently higher than the corresponding gage observations.

To improve rainfall estimation quality, hydrologists commonly combine rainfall from multiple sensor platforms, e.g., rain gages, radar, and satellite. Merging estimates from multiple platforms leverages strengths of each platform (i.e., the point accuracy of rain gages and the spatial acuity of radars). At the same time, it mitigates their weaknesses (i.e., that rain gages do not “see” rain falling between the gages and that radars can misrepresent rainfall amounts at a point). Overall, the merged product better estimates rainfall in time and space.

The most common multi-sensor rainfall product available to practicing engineers and hydrologists combines radar and rain gage data. The merged product is called gage adjusted radar rainfall

data (GARR). The spatial signature of radar rainfall replaces spatial interpolation schemes like Thiessen polygons or inverse distance weighting used with rain gage-only analyses. GARR tends to provide a more realistic estimate of the true distribution of rainfall over a watershed, thereby improving estimates of the location and volume of rain entering a watershed at any given time. Putting the right rain at the right place at the right time leads to improved estimates of hydrologic response.

When using radar rainfall estimates, a critical step involves comparing radar estimates and rain gage observations to determine the reasonableness of the radar data. The hydrologist compares the gage observation and the rainfall estimate for the radar pixel containing the rain gage location. GIS tools makes identifying the appropriate radar pixels relatively easy.

Table 6.1 presents an example of four storm total rain gage observations with associated radar rainfall estimates at those locations. The average radar rainfall estimate equals 5.21 inches while the average gage observation equals 4.15 inches. In this case, the radar data have a high bias.

Table 6.1. Example radar–gage comparison.

Location	Radar (inches)	Gage (inches)	GARR (inches)
Gage #1	5.55	4.47	4.42
Gage #2	5.46	4.20	4.35
Gage #3	4.84	4.12	3.85
Gage #4	4.99	3.82	3.98
Average	5.21	4.15	4.15

The simplest adjustment procedure to correct biased radar estimates computes the ratio of the average gage observation with the average of the radar estimates at the gage locations. The resulting ratio is commonly called the gage/radar ratio (G/R ratio). The G/R ratio for the example in Table 6.1 equals 0.80. The hydrologist adjusts the radar rainfall estimates by multiplying each radar rainfall estimate in the entire radar data field by the G/R ratio. Called the mean field bias adjustment, the procedure raises or lowers the entire radar data field such that the adjusted radar data are consistent with the rain gage observations.

Returning to the example in Table 6.1, the hydrologist would multiply each radar rainfall estimate by the G/R ratio, i.e., 0.80, with the results displayed in the column labeled GARR. Now, the average GARR value exactly equals the average gage observation, resulting in an average bias of zero.

Figure 6.16 shows the mean field bias adjustment procedure graphically. The filled circle symbols represent gage and radar data pairs from Table 6.1. If the radar data were unbiased, the gage-radar data pairs would plot along the diagonal line in Figure 6.16. A simple visual inspection clearly shows that the radar data values have a high bias in this example.

The triangle symbols shown in Figure 6.16 represent the rain gage and GARR data pairs from Table 6.1. The four triangle symbols cluster around the diagonal line in Figure 6.16, indicating that the bias was eliminated.

Perfect agreement between gage and GARR is not expected and there are no generally accepted standards on GARR quality in terms of how good is good enough. A challenge for use of GARR is that GARR can be made to exactly fit the gage data or any other +/- percent agreement between

gauge and radar data. A relevant measure of GARR quality is whether GARR enables a hydrologic model to reproduce observed streamflow.

Individual radar estimates represent averages over the radar pixel area. Even within a small radar pixel, rainfall can vary significantly above or below the pixel average. The rain gauge observation depends on where the gauge is located within the pixel; the point observation likely differs from the pixel average. Further, rain gauge observations themselves involve uncertainties that make exact agreement with radar estimates unlikely. A perfect or near-perfect match between GARR datasets and gauge observations may indicate that the GARR data were forced to fit the observed gauge data. This can artificially and unrealistically distort the spatial distribution of the rainfall, thereby producing inaccurate or misleading hydrologic results.

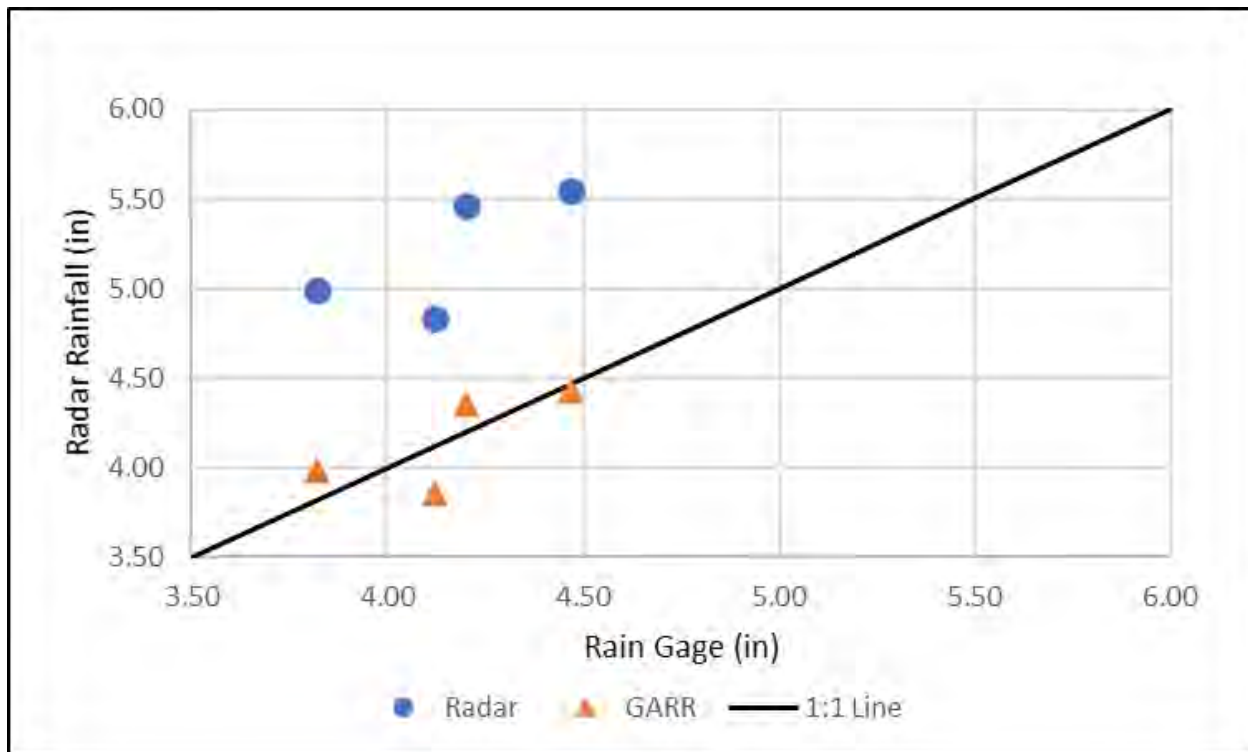


Figure 6.16. Example radar-gauge comparison (storm total).

Beyond storm totals, practitioners will also want to check the performance of intrastorm adjustments by comparing intrastorm radar estimates with intrastorm gauge measurements. Storms evolve over time. Intrastorm meteorological conditions change, potentially affecting accuracy of rainfall estimation at different times within the storm event. For example, radar signals returned from raindrops falling through the atmosphere are extremely sensitive to the distribution of rain drop sizes. Characteristic drop sizes can change over time as the storm evolves and the drop size distribution can change spatially as the storm moves. For these reasons and a host of others, it is important to examine intrastorm performance of radar estimates relative to gauge measurements.

Figure 6.17 presents examples comparing the cumulative gaged rainfall with cumulative radar rainfall at four gauge locations. In example 1, the radar underestimated the gauge total. However, radar rainfall estimates were high in the first half of the storm but underestimated rainfall relative to the gauge in the second half of the storm. In example 2, the radar consistently tracked the gauge observations throughout the event. In example 3, the radar estimates closely tracked the intrastorm gauge observations in the first half of the storm but slightly underestimated rainfall in the



second half. For example 4, radar rainfall estimates track the gage observations closely during the first part of the storm but underestimates rainfall in the second half of the storm.

The intrastorm performances shown in Figure 6.17 may be acceptable for hydrologic modeling applications depending on the importance of total rainfall volume and its distribution. However, sometimes intrastorm performance shows far more pronounced biases than shown in Figure 6.17. These cases call for use of temporally variable bias adjustments. Further, biases showing significant spatial variance—especially if the watershed size is large relative to the storm size or if the storm structure includes multiple significant cells—warrant a spatially variable bias adjustment procedure.

After completing the radar rainfall data adjustments and judging them consistent with the gage observations, the engineer proceeds to hydrologic analysis of the data. Given the qualitative and subjective nature of this consistency judgment, in practice, hydrologists assess the quality of GARR by comparing hydrologic model performance with GARR to performance with gage data alone.

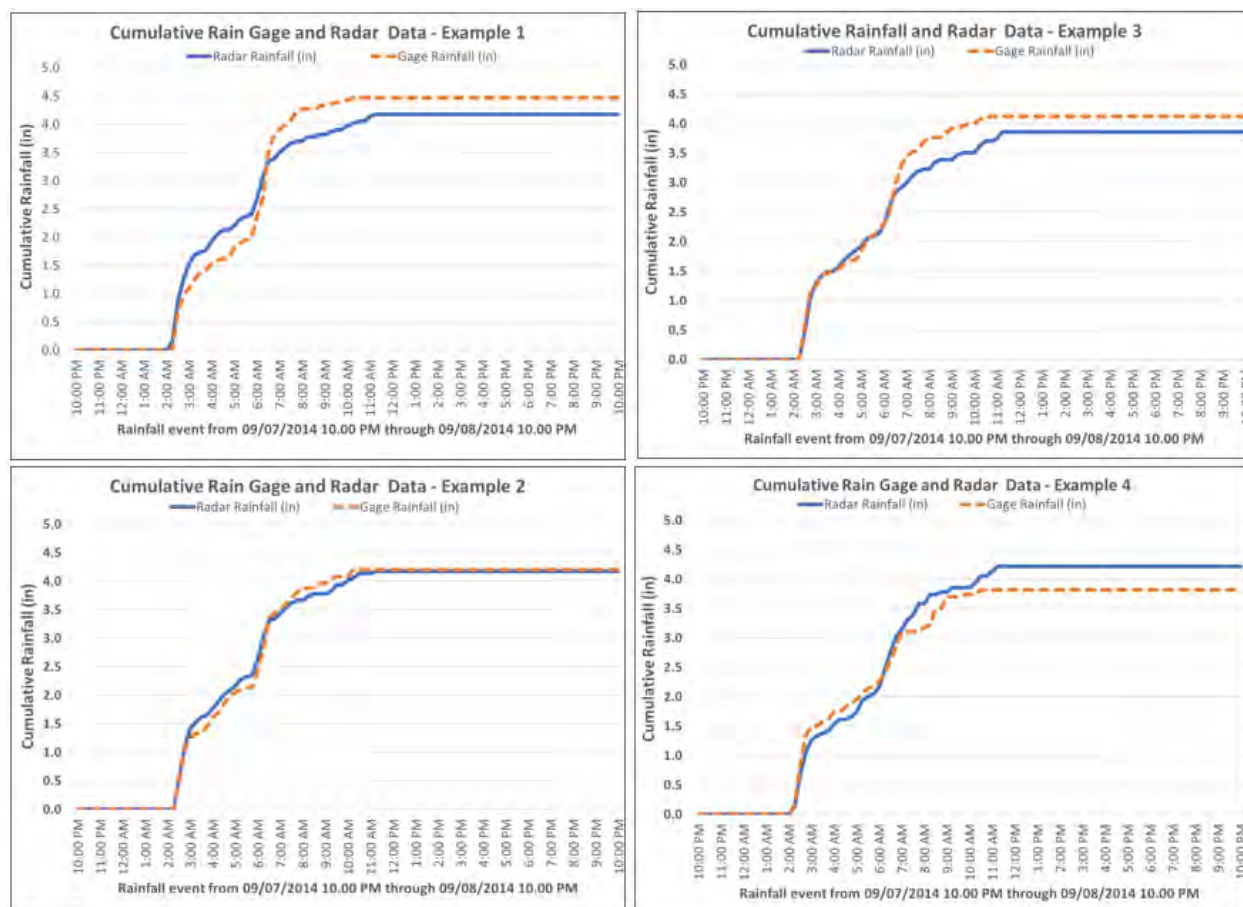


Figure 6.17. Cumulative rainfall comparison (intrastorm).

## 6.5 Design Storm Development Using Gridded Precipitation

For many design applications, hydrologists do not directly use observed data. Instead, they use a statistical representation of a design rainfall depth with assumed spatial and temporal distributions to create a “design storm.” This section focuses on recent developments in design storm development using gridded precipitation data in studies in Colorado (Curtis 2011) and



Nevada (Kimley-Horn 2015). Another study (Kao et al. 2020) reported a nationwide comparison of depth area reduction factors (DARF). Studies for the States of Texas and Arizona report new design storm methodologies derived from gridded precipitation products (Curtis et al. 2022). These studies leverage spatially distributed rainfall databases (i.e., radar rainfall estimates) to develop more appropriate spatial structures for design storms.

### 6.5.1 Creating Design Storms

A design storm typically has three elements:

- Storm depth.
- Temporal distribution.
- Spatial distribution.

Hydrologists commonly take the storm depth from NOAA Atlas 14 for a given return frequency and duration. (e.g., 0.1 Annual Exceedance Probability (AEP), 24-hour). Values from NOAA Atlas 14 represent estimates of rainfall at a specific point.

For modeling applications, engineers use various methods to distribute storm depths over time. As described by the Natural Resources Conservation Service (NRCS 2019), type 1, 2 or 3 storm distributions frequently apply.

Figure 6.18 shows a nested design storm or alternating block method (Mays 1996), another common method for temporal distribution. Engineers construct a 24-hour nested design storm with the maximum rainfall for any duration within the storm equal to the rainfall for that duration at the selected frequency. The table insert in Figure 6.18 shows 0.1 AEP values for each duration (15-min, 30-min, 1-hour...24-hour).

### 6.5.2 Depth Area Reduction Curves

To apply rainfall to a watershed model as indicated in Figure 6.19, engineers distribute the design rainfall spatially over the watershed area. For small watersheds, engineers sometimes assume a uniform distribution of the design rainfall over the watershed. However, simply spreading the point rainfall depth over the watershed may effectively change the rainfall frequency for the watershed. High intensities occur over a larger area more rarely than for a point. Therefore, applying the unadjusted NOAA Atlas 14 estimate over a large watershed area may effectively change the design storm frequency to a rarer event than intended. To maintain the appropriate frequency over a watershed area, the engineer converts from point to area estimates. The conversion reduces a point rainfall amount of a given frequency and duration to an areal estimate of the same frequency and duration. Engineers typically achieve the conversion using a DARF:

$$P_a = \text{DARF}(P_p) \quad (6.1)$$

where:

- $P_p$  = Point rainfall value, inches (mm)
- $P_a$  = Uniform average rainfall depth over the target watershed, inches (mm)
- DARF = Depth area reduction factor

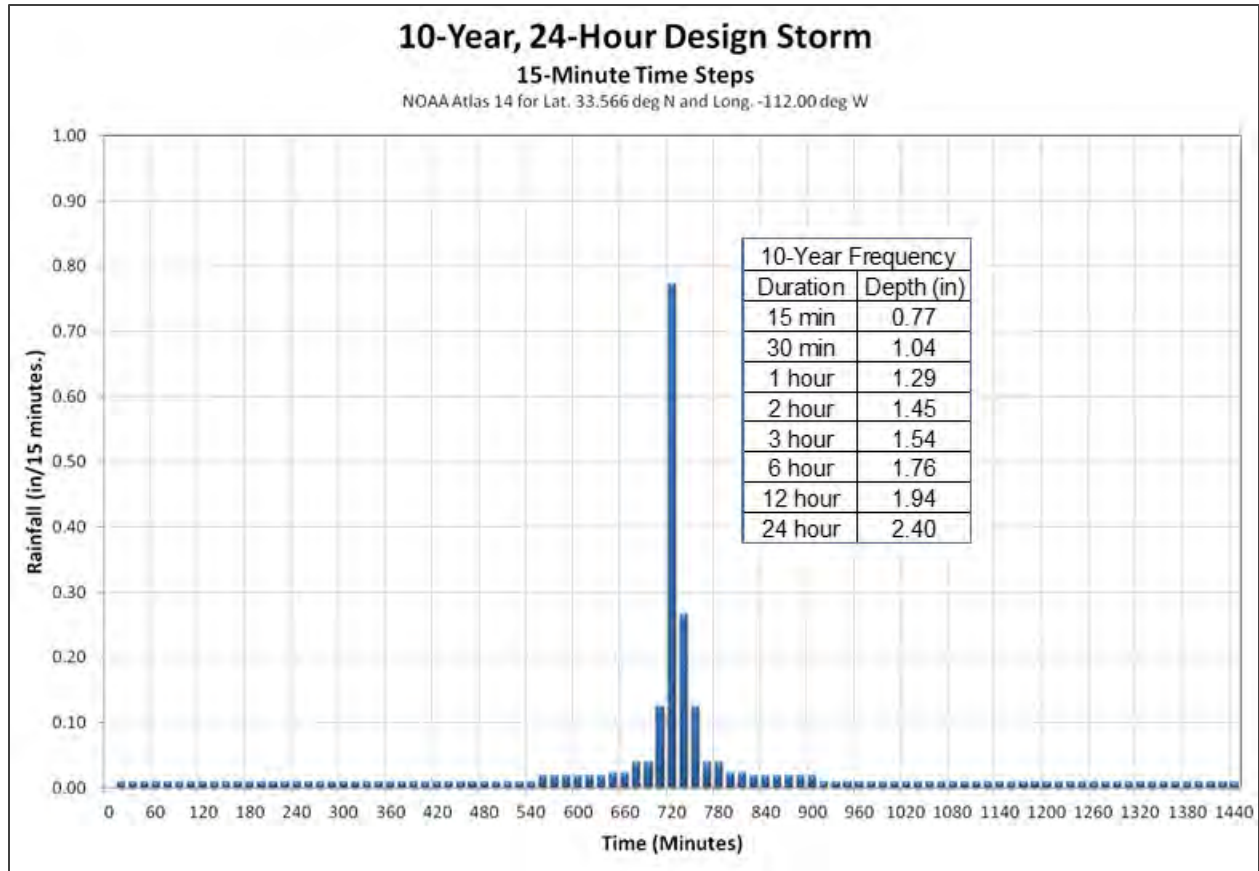


Figure 6.18. Example nested design storm.

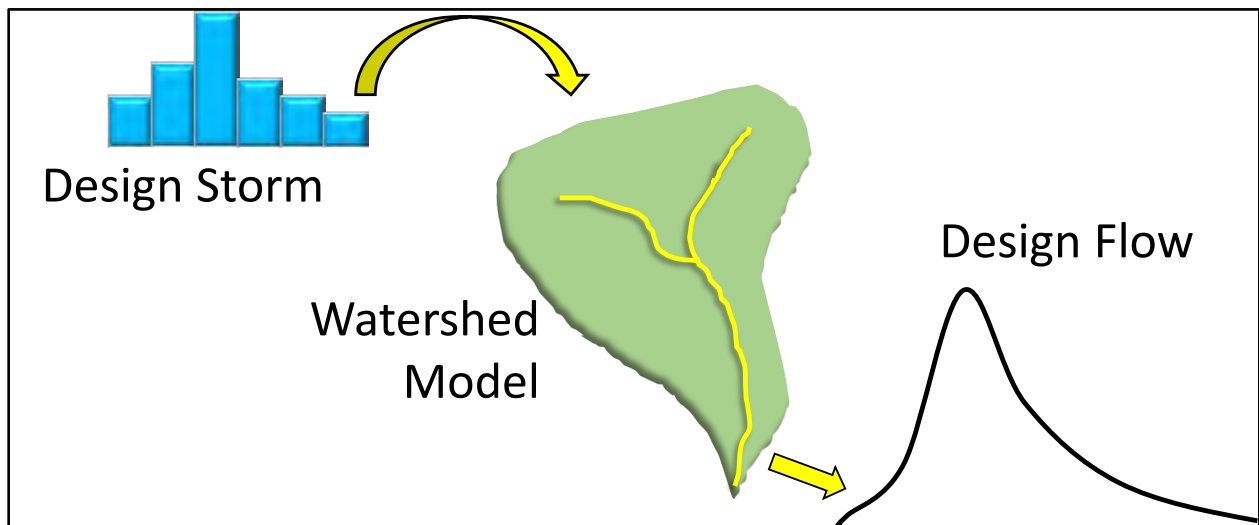


Figure 6.19. Conceptual diagram of hydrologic application to develop design flows.

The U.S. Weather Bureau, now known as the National Weather Service, first published the most widely used DARF in common practice in a series of technical papers in the late 1950s. Figure 6.20 presents the DARF chart reproduced from the U.S. Weather Bureau Technical Paper 29 (TP 29) (U.S. Department of Commerce Weather Bureau 1957). The TP 29 chart relates the percent

of point rainfall (i.e., DARF) for watershed sizes up to 400 mi<sup>2</sup> and durations from 30 minutes to 24 hours.

The U.S. Weather Bureau developed the TP 29 DARFs from very limited datasets (average period of record is approximately 12 years) and for areas primarily in the New England, the mid-Atlantic States, and the Ohio Valley. Despite the limited datasets in both time and geographic locations, the chart's simplicity and the lack of better alternatives have led to widespread use across the United States and abroad.

Studies using spatially distributed rainfall datasets suggest that the DARFs shown in Figure 6.20 do not apply universally (Curtis 2011, Kimley-Horn 2015, Kao et al. 2020). The data show potential variation with frequency, region, season, and storm type. The precipitation products used (i.e., gage vs. radar) affect DARF development. Additional important considerations include storm scales versus watershed size and shape.

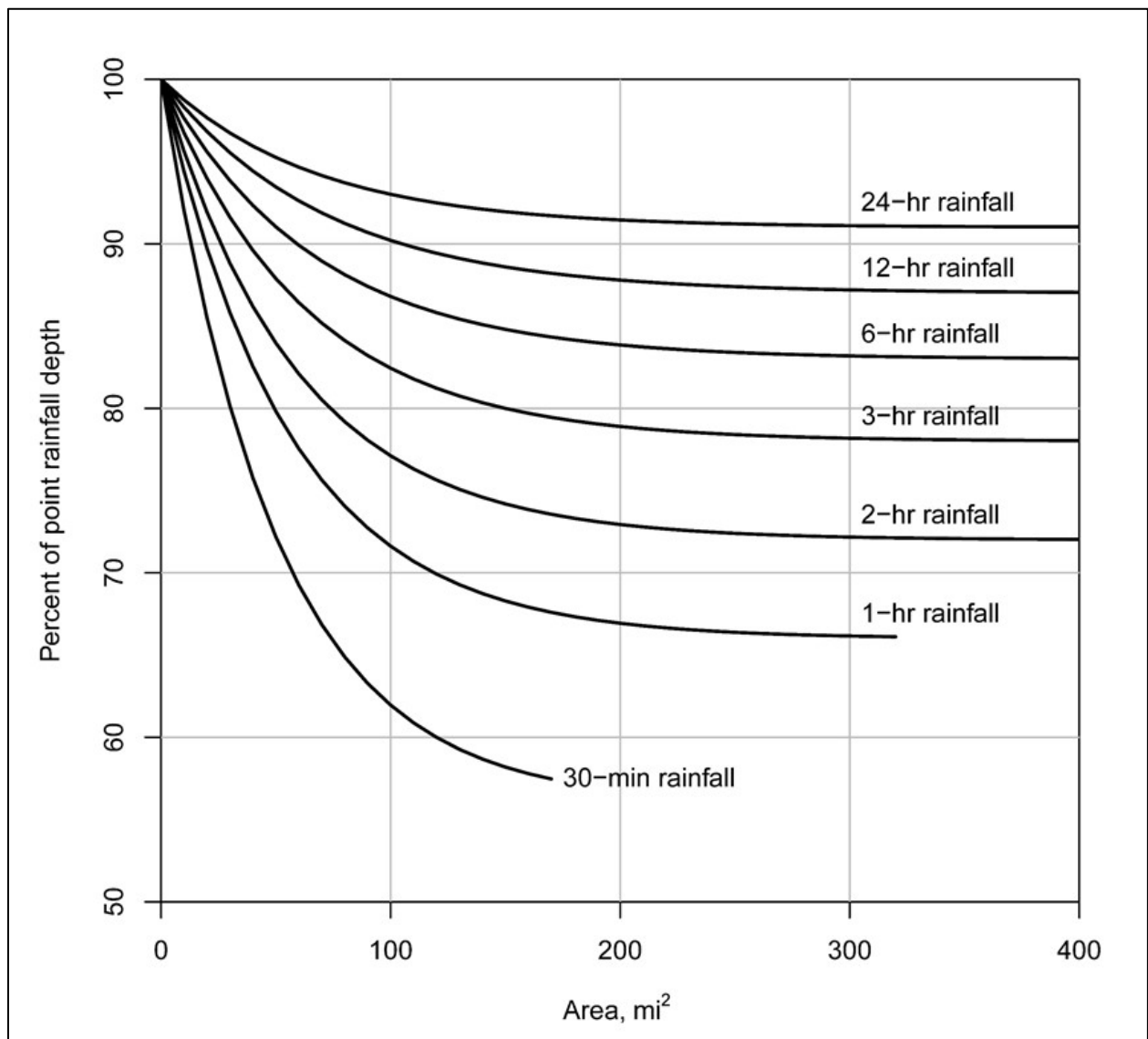


Figure 6.20. Depth area reduction factor from TP 29. Source: NWS.

Figure 6.21 presents a comparison of the TP 29 1-Hour DARF with 1-Hour DARFs derived from radar rainfall data in Colorado Springs, Colorado (Curtis 2011). The radar based DARFs decay much faster than the TP 29 DARF. Further, the radar based DARFs suggest sensitivity to rainfall frequency.

Using the TP 29 DARF effectively places greater design rainfall depths watershed wide which, in turn, produces greater runoff for the same frequency depth than the radar based DARFs. Greater design runoff can lead to increased costs associated with development of facilities to manage larger design flows.

Design for many water conveyance projects uses standard TP 29 DARFs. Practitioners have long suspected that these curves do not represent real rainfall conditions, especially in regions where intense convective storms dominate (Asquith and Famiglietti 2000, Lombardo et al. 2006, Wright et al. 2014). This can result in overly conservative and unnecessarily costly designs. Updated DARFs leveraging high resolution spatially distributed rainfall datasets will significantly impact future hydrologic design standards.

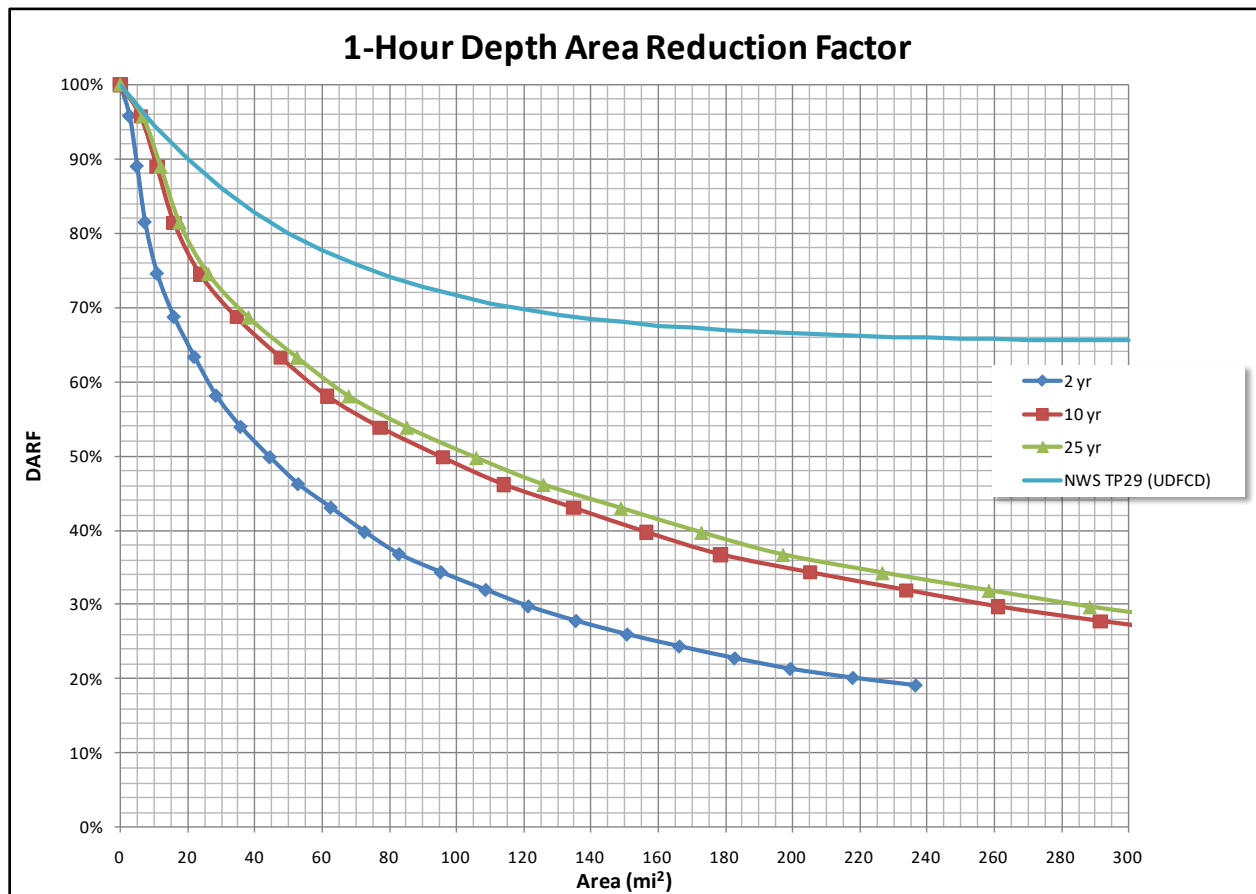


Figure 6.21. Comparison of 1-hour DARFs.

## 6.6 Sources for Historical Precipitation Data

A broad spectrum of public and private entities observes and archives precipitation data. Universities and Federal, regional, State, and local agencies often own and operate hydrometeorological monitoring networks. Water, irrigation, flood control, and power utilities maintain monitoring networks. Many of these entities make their data available publicly. In recent years, private internet-enabled weather stations have emerged and often offer a valuable source

of information. Providing a comprehensive listing of available datasets exceeds the scope of this manual but this section highlights several data sources.

### 6.6.1 National Center for Environmental Information

NOAA's National Center for Environmental Information (NCEI) manages one of the largest environmental data archives in the world. The NCEI developed land-based (in situ) datasets from data collected across the United States and globally. Data availability varies by type and station, and some have periods of record of more than a century. The NCEI provides both manually and automatically recorded data in various time increments. Manually observed data are most commonly recorded at longer time intervals (e.g., daily or six hours). Automated data are available in time increments as small as one minute or less. The NCEI website provides most of these data.

NCEI also maintains several regional climate data centers, shown in Figure 6.22, that may house additional data and offer custom products tailored to individual regions of the United States.

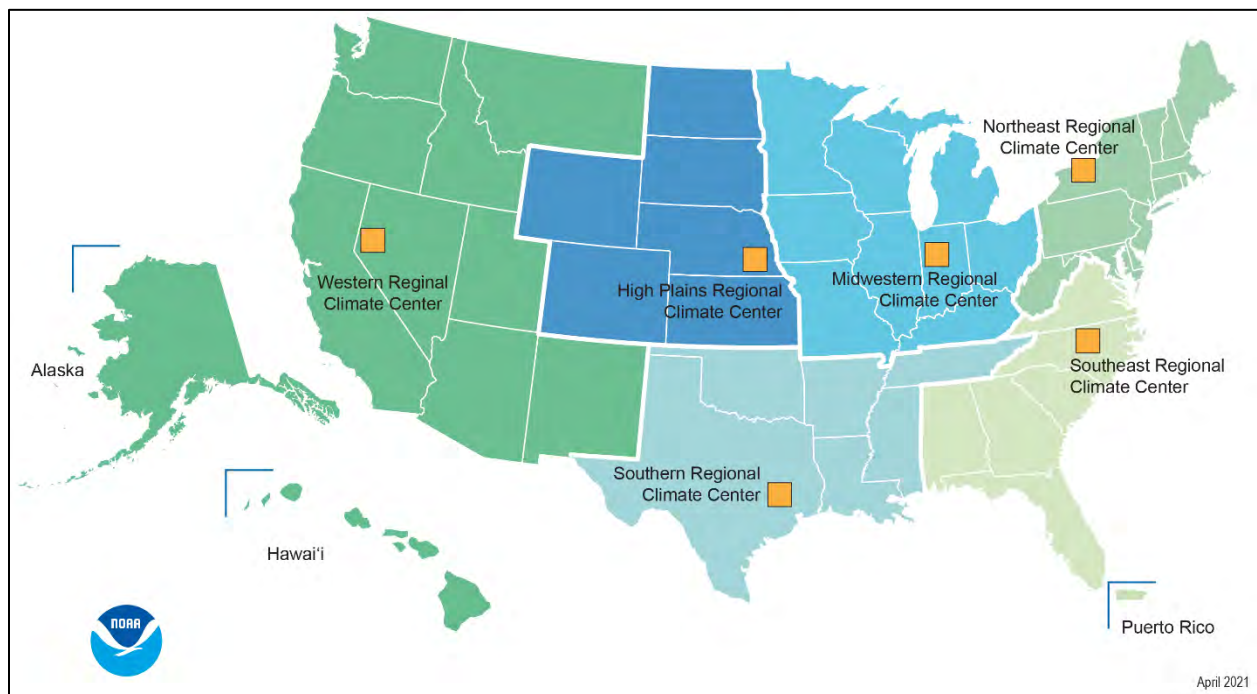


Figure 6.22. Regional climate centers. Source: NOAA.

The NCEI also manages the nation's archive for NEXRAD data. Most of the raw data come from individual radars. To use the data in hydrologic applications, the hydrologist checks them for quality, converts them to appropriate rainfall units (i.e., inches), and adjusts them using gage data as appropriate. For smaller subbasins, the modeler uses the specific radar that adequately observes precipitation over the watershed of interest. The NCEI website provides NEXRAD data.

### 6.6.2 State and Regional Networks

Several State-specific environmental monitoring networks, including several mesonets (mesoscale networks) and regional agencies, provide either point rainfall measurements or radar-based rainfall databases. Table 6.2 lists several statewide mesonets.

Table 6.2. Statewide mesonets. Adapted from Mahmood et al. (2017).

Network	State	Total number of real-time stations
North Alabama Climate Network	Alabama	22
University of South Alabama Mesonet (CHILI)	Alabama	25
Arkansas State Plant Board Weather Network	Arkansas	50
California Irrigation Management Information System	California	152
Colorado Agricultural Meteorological Network	Colorado	75
Delaware Environmental Observing System	Delaware	57
Florida Automated Weather Network	Florida	42
Georgia Automated Weather Network	Georgia	82
Illinois Climate Network	Illinois	19
Iowa Environmental Mesonet	Iowa	17
Kansas Mesonet	Kansas	51
Kentucky Mesonet	Kentucky	66
Louisiana Agroclimatic Information System	Louisiana	9
Enviroweather	Michigan	82
Minnesota Mesonet	Minnesota	8
Missouri Mesonet	Missouri	24
Nebraska Mesonet	Nebraska	68
New Jersey Weather and Climate Network	New Jersey	61
New Mexico Climate Network	New Mexico	6
New York Mesonet	New York	101
North Carolina ECONet	North Carolina	40
North Dakota Agricultural Weather Network	North Dakota	90
Oklahoma Mesonet	Oklahoma	120
South Dakota Mesonet	South Dakota	25
West Texas Mesonet	Texas	98
Utah Agricultural Weather Network	Utah	32
Washington AgWeatherNet	Washington	176

Among the State-specific mesonets, the Oklahoma mesonet includes 120 environmental monitoring stations. This network covers Oklahoma with at least one station in each of Oklahoma's 77 counties. The Oklahoma Climatological Survey automatically receives, verifies,

and provides access to the data. California, Arizona, Texas, Iowa, New York, and North Carolina also provide reliable State-level data.

Florida provides statewide GARR estimates. Figure 6.23 shows the five water management districts maintaining historical GARR databases dating from the mid-1990s. These districts include:

- St Johns Water Management District.
- South Florida Water Management District.
- Southwest Florida Water Management District.
- Suwannee River Water Management District.
- Northwest Florida Water Management District.

The rainfall data have high resolution with estimates on a 2 km x 2 km grid in 15-minute time steps.

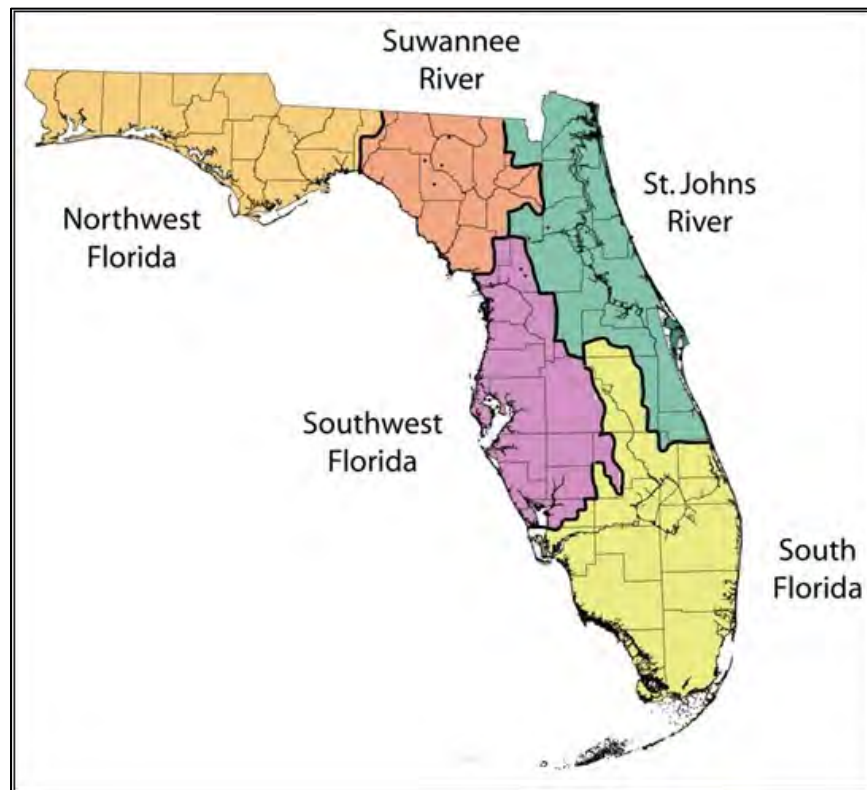


Figure 6.23. Florida water management districts. Source: Florida Department of Environmental Protection.

### 6.6.3 MesoWest

A cooperative project to access and archive weather observations, MesoWest started at the University of Utah with the goal of providing current and archived weather observations online. Today, more than 20,000 weather stations from across the United States actively send observations to MesoWest. The system facilitates the efficient exchange of data from diverse sources to support decision-making by government agencies, businesses, communities, and individuals.



#### 6.6.4 NEXRAD Stage IV Data

The NWS creates hourly nationwide GARR estimates on a 4 km x 4 km grid to support river forecast operations. In areas with poor or no radar coverage, the NWS often considers satellite estimated rainfall. West of the Continental Divide, the NWS plots gage data against long-term precipitation data and interpolates precipitation estimates between gage locations. The NWS provides the data, known as Stage IV Precipitation, for download at their Advanced Hydrologic Prediction Service FTP site.

#### 6.6.5 NWS Analysis of Record for Calibration (AORC) Archive

The NWS developed a nationwide gridded database of precipitation and temperature data to calibrate its own hydrologic forecast models and to support hydrologic modeling in general. The precipitation portion of the database derives from:

- Monthly precipitation totals (Livneh et al. 2013).
- NLDAS-v2 and NEXRAD Stage IV daily precipitation totals.
- Radar based data.
- Climate Prediction Center Morphing Technique satellite-based precipitation (CMORPH) data (Xie et al. 2020).
- Hourly climate forecast system reanalysis data.

Analysis of Record for Calibration Temperature and Precipitation Records (AORC) data cover the period from 1979 to near-present at 4 km x 4 km resolution in hourly time increments. A NOAA FTP site provides the current AORC data archive.

#### 6.6.6 PRISM

The PRISM (Parameter-elevation Regressions on Independent Slopes) interpolation method includes factors accounting for location, elevation, coastal proximity, topographic facet orientation, vertical atmospheric layer topographic position, and orographic effectiveness of the terrain (Daly et al. 2008). The Oregon State University (OSU) PRISM Climate Group develops and maintains a nationwide database of gridded rainfall and temperature data as well as other hydrometeorological data. PRISM data have a native resolution of 800 m on daily time steps. Daily time steps do not provide sufficient granularity for hydrologic modeling for many transportation projects. However, the data may provide useful insights in data poor areas and for watersheds draining complex terrain.

#### 6.6.7 Private Sector

Several private sector sources provide GARR estimates at a range of possible data resolutions for a fee. These firms typically obtain NWS WSR-88D data from NOAA and any available rain gage data for a specific period. They then quality control and merge the gage and radar data to form GARR. Depending on the source data and data merging procedures, resolutions as high as 0.25 km x 0.25 km in 5-minute time steps or higher may be available.

### **6.7 Application of Gridded Precipitation to Hydrology and Hydraulics Models**

Hydrologic engineers and modelers increasingly apply gridded precipitation as inputs to hydrologic and hydraulic models to improve runoff and design flow estimation. Successful

application depends on appropriate sources of gridded precipitation and flexible tools to analyze the information.

Gridded hydrologic models such as HEC-HMS have become commonplace. Gridded hydrologic models employ a specific user-selected method to transform the excess rainfall into a hydrograph at the outlet of the subbasin where it is integrated into a channel routing model.

Rain-on-grid hydraulic models, such as HEC-RAS 6.1, add hydrologic functionality to convert rainfall to runoff. Although these are gridded models, they differ from gridded hydrologic models. Rain-on-grid hydraulic models directly apply rainfall to the 2-D hydrodynamic surface flow grid (i.e., HEC-RAS 6.1) that accounts for infiltration. The runoff process is dynamically connected to the hydraulic flow routing computations at each grid point.

### 6.7.1 Gridded Precipitation Data Sources

Several sources provide gridded precipitation data for use in hydrologic models. Each data source has a unique combination of spatial and temporal coverage, resolution, and accuracy. Sources include:

- Multisensor Precipitation Estimates (MPE), produced by the NOAA.
- North American Land Data Assimilation System version 2 (NLDAS-v2), produced by the National Aeronautics and Space Administration (NASA).
- PRISM, produced by the OSU PRISM Climate Group.
- Livneh (Livneh et al. 2013) daily, near-surface precipitation, a long-term gridded dataset at fine (~6 km) horizontal resolution derived from the National Climatic Data Center (NCDC) Cooperative Observer (COOP) stations across the conterminous United States.

Table 6.3 summarizes the primary attributes of these data sources.

Table 6.3. Gridded precipitation data sources.

Data Source	Format	Spatial Resolution	Temporal Resolution	Spatial Coverage	Period of Record
MPE	Gridded	1 km	1 hour	United States	2003 to present
NLDAS-v2	Gridded	0.125 degrees (~14 km)	1 hour	North America	1979 to present
PRISM	Gridded	4 km	1 day	United States	1981 to present
Livneh	Gridded	0.0625 degrees ~ 6 km	Daily	United States	1915-2012

MPE data provide the finest spatial resolution of all the data sources but have limited spatial coverage and dates for which data is available. NLDAS-v2 and PRISM data cover a longer duration than MPE but have either spatial or temporal resolution limitations. The NCDC data theoretically have the most accuracy as they derive from observed precipitation gage data, but only at discrete locations throughout North America.

After collecting the gridded precipitation data from the applicable source, the engineer checks the compatibility of the dataset to the hydrologic and hydraulic model. Each model uses precipitation data in a specific coordinate system. Typically, the engineer ensures that the data projection and spatial resolution (i.e., grid size) match the model's grid by reprojecting and resampling.

Documentation for commonly available GIS programs describes reprojection and resampling, e.g., Maidment (2002).

### 6.7.2 Application to Hydrologic Models

Hydrologic modelers generally use one of two common approaches to applying spatially distributed rainfall data like GARR to hydrologic models. One is a fully distributed model, and the other is aggregated by subbasin.

Figure 6.24 illustrates a fully distributed model of the Sopori Wash watershed. For a fully distributed and gridded hydrologic model, the hydrologist remaps the gridded GARR data to the hydrologic model grid for each time step using a common GIS procedure or a tool such as HEC-MetVue to prepare GARR for HEC-HMS. With this remapped gridded GARR data prepared in a format compatible with the hydrologic model, the hydrologist proceeds with typical modeling.

Figure 6.25 represents the other common method for using GARR using subbasin averaging. Here, GIS or HEC-MetVue determine average sub-watershed rainfall at each time step. This approach treats each sub-watershed rainfall time series exactly like a traditional rain gage, with one “rain gage” assigned to each sub-watershed.

The rainfall shown produced a major flood on Sopori Wash, well above the 100-year event. Note that U.S. Interstate Route 19 parallels the Santa Cruz River in the north-south direction along the right edge of Figure 6.24 and Figure 6.25. A bridge on I-19 spans the Sopori Wash near its confluence with the Santa Cruz River. This watershed had no recording rain gages. Three gages to the north and east of the watershed, all within five miles of the mouth of Sopori Wash, measured just a fraction of the peak rainfall estimated for the storm and were not representative of rainfall within Sopori Wash. Without radar rainfall estimates, an accurate hydrologic analysis of this event at the I-19 bridge is difficult, if not impossible.

Regardless of the chosen approach, engineers calibrate hydrologic and hydraulic models using historic runoff events. Gridded precipitation can drive these models. After selecting the events, the engineer determines the availability of gridded precipitation. If data exist, the engineer uses them in the model after reprojection and resampling.

Engineers also apply calibrated hydrologic models to synthetic (design) events. An example of a synthetic event is an 0.01 AEP design event or a 0.5 design AEP event. NOAA Atlas 14 provides point precipitation estimates ranging from the 1.0 AEP to the 0.001 AEP event. Engineers adjust these point estimates spatially (i.e., using DARF). Some hydrologic models, e.g., HEC-HMS (USACE 2021a)) perform areal adjustments automatically. See Section 6.5.2 for discussion of areal adjustments.

Generally, the results from a gridded hydrologic model are calibrated by using observed flows at locations within the basin. By calibrating to observed flows the analyst can update basin parameters to reproduce observed flows. If no observed flows are available, then parameters can be based on physical properties that can be measured like soil type or channel cross-section size.

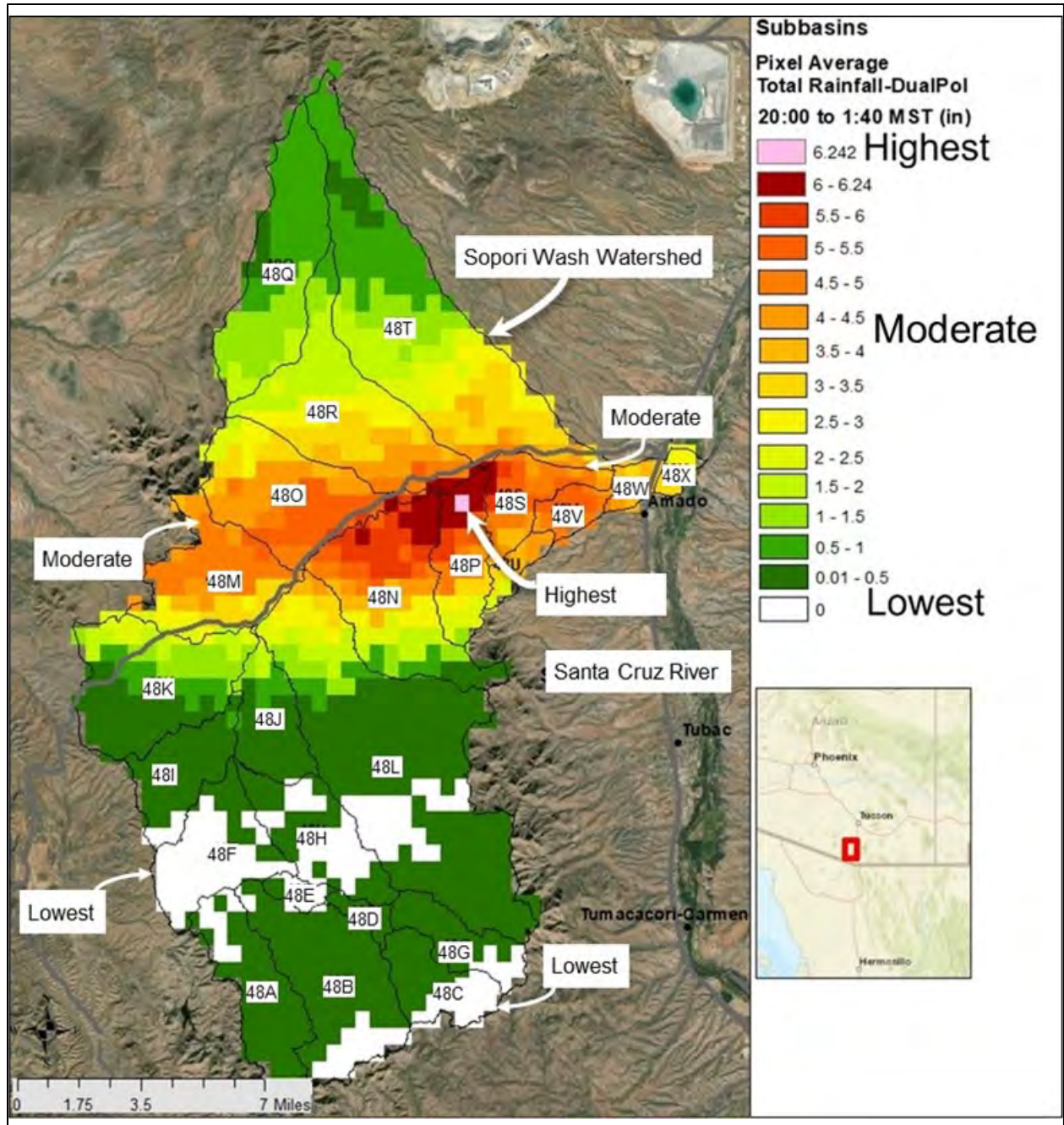


Figure 6.24. Watershed with individual radar pixels shown.



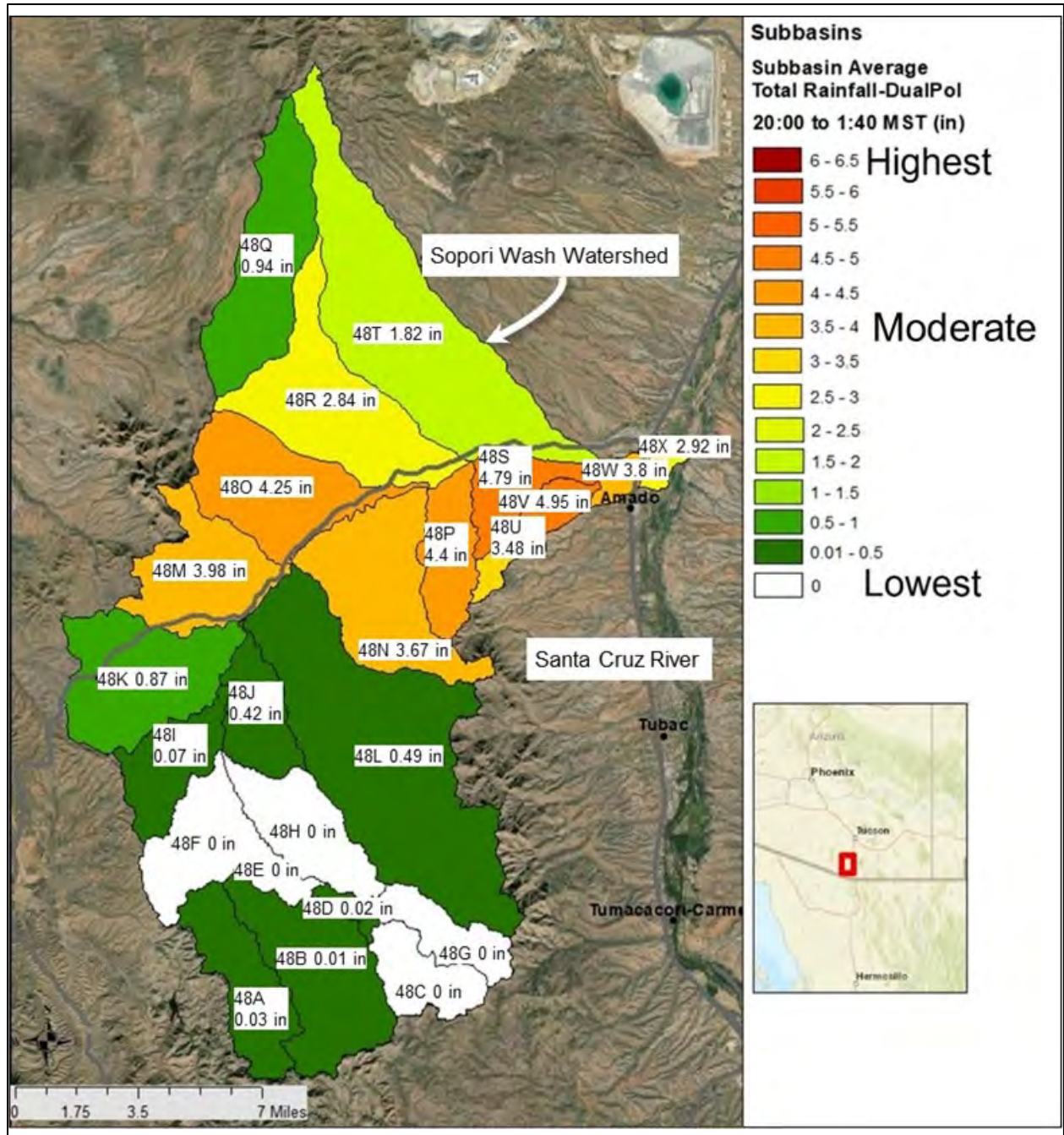


Figure 6.25. Watershed with sub-watershed averages shown.

### 6.7.3 Application to Integrated Hydrologic and Hydraulic Models

The rain-on-grid application approach tightly integrates hydrologic and hydraulic model functionality, facilitates estimation of complex 2D flows, and allows high resolution descriptions of flow behavior. It can eliminate the demand for separate hydrologic modeling within the 2D model domain.

Rain-on-grid modeling involves directly applying rainfall to a 2D hydrodynamic model. The model accounts for infiltration, and routes rainfall excess dynamically to the basin outlet. The analyst verifies the capabilities of the rain-on-grid software selected for use so that the software is able to model the important aspects of the basin such as using a specific loss method or baseflow.

Rain-on-grid models have some challenges. This type of spatially varied, physically based modeling is very complex. For example, a popular method for estimating infiltration losses is the Green and Ampt method because it is physically based and relies on hydraulic conductivity, capillary suction, and the soil moisture deficit. This information relies on the soil surveys which can be inaccurate. In addition, the soil texture changes over a watershed, making it difficult to accurately estimate the spatial variability of infiltration parameters. With the added spatially varying data, the computer power needed to perform the hydrodynamic simulations increases substantially.

Over many years, researchers have sought improved physically based, spatially varied, watershed scale hydrodynamic models. The results of these efforts have been mixed, with some engineers and researchers suggesting simpler models perform better than complex models. A good discussion of this topic is presented by Woolhiser (1996).

HEC-RAS (USACE 2021d) can apply spatially varied precipitation to compute runoff. The modeler can add spatial precipitation to HEC-RAS using three different methods: gridded data, point gage data, or a constant rate. HEC-RAS can read data from a Hydrologic Engineering Center Data Storage System (HEC-DSS) file or from Geospatial Data Abstraction Library (GDAL) raster files. Once the modeler enters gridded precipitation data, HEC-RAS can animate the storm event to show the storm moving over the watershed. Figure 6.26 shows a single time step of gridded precipitation. Additionally, RAS Mapper (USACE 2021e) can show accumulated precipitation. Figure 6.27 shows the accumulated precipitation over the Sopori Wash watershed with the largest amount of accumulated precipitation occurring in the center of the figure as indicated.

#### What to Look for: Rain-on-grid Reviews

Rain-on-Grid modeling is not always transparent for review. Look to:

- Verify that the rainfall is correctly depicted in both space and time (and entered that way in the model), as well as magnitude, e.g., snow is not affecting the rainfall values.
- If infiltration is used, check that the soils used in the model agree with the actual soils in the field. Confirm that infiltration parameters are reasonable.
- Examine available calibration data to compare results (even anecdotal information).
- With or without calibration data, consider the reasonableness of results. In the aggregate is the model providing reasonable precipitation volumes, is the infiltration component removing too much water or not enough water, and are the flow values within a reasonable range of values?



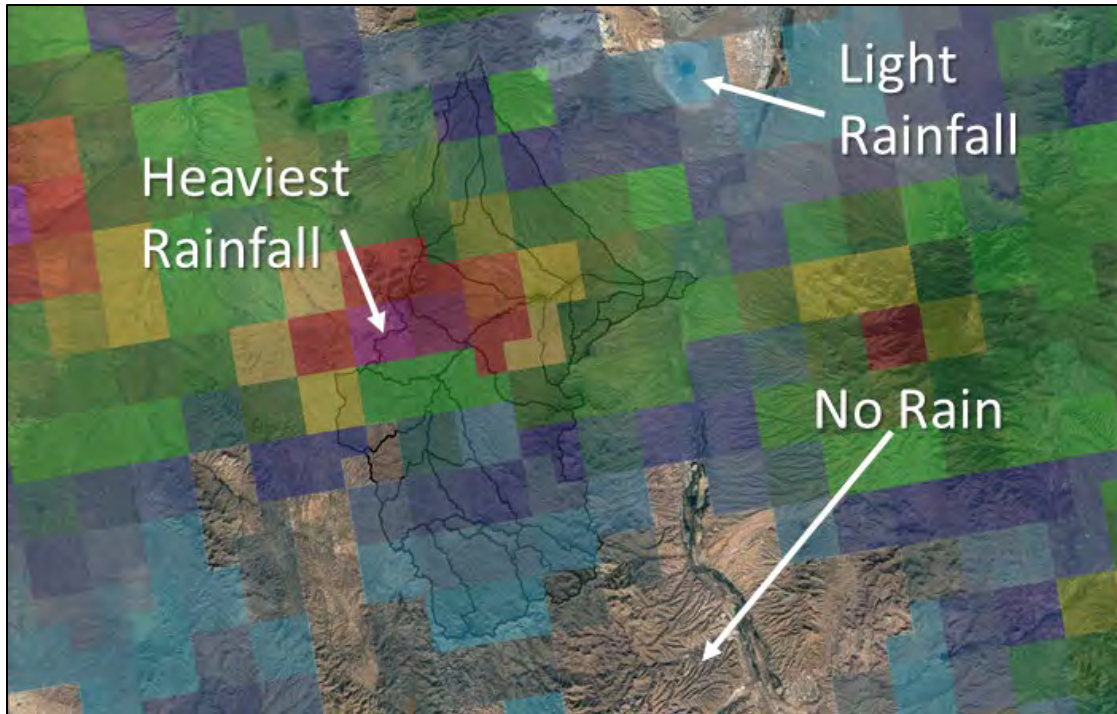


Figure 6.26. Gridded precipitation across the Sopori Wash watershed.

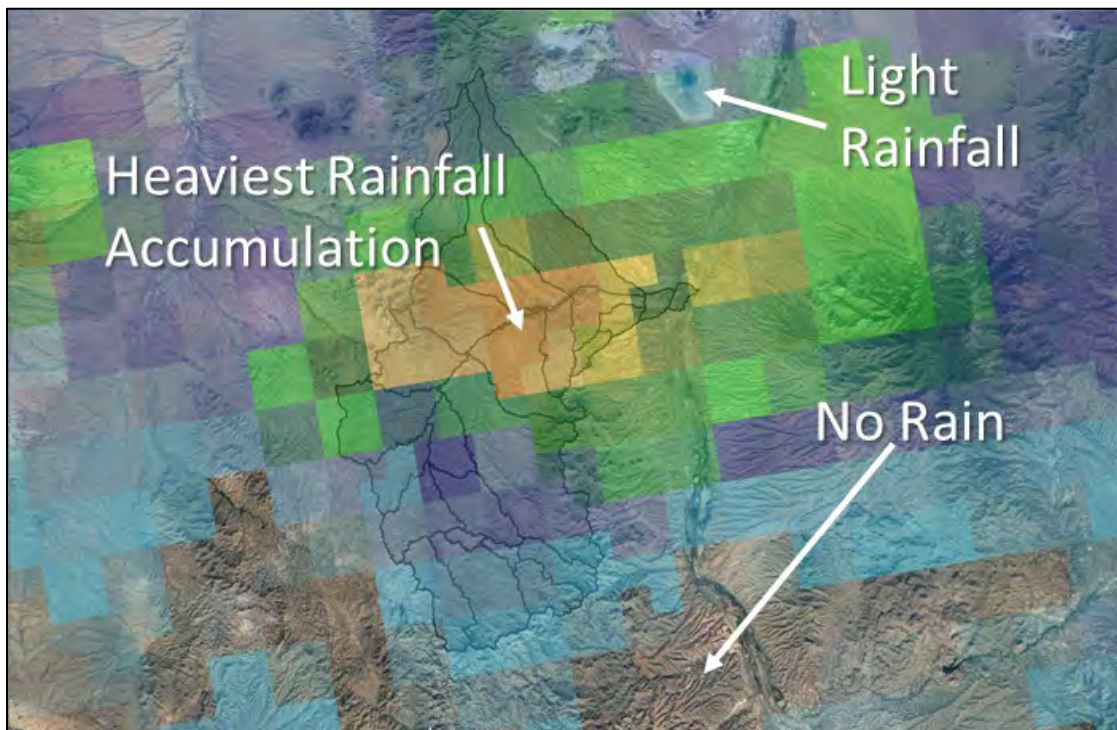


Figure 6.27. Accumulated precipitation across the Sopori Wash watershed.



## Chapter 7 - Special Topics

This chapter introduces special topics that are of particular interest in specific areas of the country including the effects of wildfires on runoff, karst areas, and paleohydrology. The chapter provides an overview to each topic, describes the relevance to transportation related hydrologic analyses, and provides references to additional sources of information.

### 7.1 *Wildfires and Runoff*

In the context of highway drainage design, wildfires influence infiltration, runoff, and sediment concentrations. The effects also vary over time during recovery of the landscape. These changing effects and varied recovery times create uncertainty in flow estimates. This section discusses the effects of wildfire on hydrology, including soil physical properties and fire, the hydrologic cycle and water resources, and watershed rehabilitation.

Wildfires occur naturally and sporadically, most commonly in forested areas of the Western United States. Regions with a Mediterranean or semi-arid climate (Southern California and the Southwest) generally have higher post-wildfire peak flows and annual water yields than those in the highlands (Rocky Mountains and the Pacific Northwest). In these Mediterranean or semi-arid regions, fire-induced changes in hydraulic connectivity along the hillslope result in the delivery of more water, more rapidly to streams (Hallema et al. 2017). Whether natural or human-induced, wildfire can cause extreme changes to the landscape immediately, extensively, and with long-term effects. One of the most significant effects is the removal of protective vegetation, resulting in more rapid runoff. Wildfire frequently inhibits soil infiltration, resulting in larger runoff volumes. The radically changed hydrologic response of burned watersheds causes post-wildfire runoff events that excessively erode streambanks and transport high loads of sediment, large wood, and debris. Therefore, engineers consider wildfire influences on hydrology, which is based on observations of historical storms in burn zones. Post-wildfire runoff potentially increases the flood hazard, therefore, accounting for the resulting higher peak flows in design lends itself to more sustainable infrastructure.

Roads are frequently negatively affected by post-fire flows in burn zones because surface runoff is conveyed under roadways in culverts. Common design practice sizes culverts, curb and gutter and other roadway drainage structures for clearwater flows during unburned watershed conditions. Under burned conditions, runoff burdened with sediment, wood, and debris often exceeds the design capacity of roadway drainage infrastructure. Road replacement costs account for 20 percent of all post-fire rehabilitation costs (Foltz et al. 2009). Hence, a significant portion of burned area emergency response (BAER) treatments relate to roadway projects. In burned zones, post-fire flows become a relevant design consideration for roadway projects.

#### Emergency Stabilization

Emergency stabilization treatments and activities applied soon after a wildfire protect public safety and stabilize and prevent further degradation to affected natural and cultural resources (USDOI and USDA 2006). In response to wildfires on Federal lands, a technical team of specialists, including hydrologists, geotechnical engineers, biologists, and land management specialists, prepares a burned area emergency response (BAER) report. A BAER report provides an emergency stabilization plan.

*Wildland Fire in Ecosystems: Effects of Fire on Soil and Water* compiled the collective knowledge of the Federal agencies that deal with wildfires (Neary et al. 2008). This resource provides land and fire managers with information on the physical, chemical, and biological effects of fire useful for successfully managing ecosystems and informing others about the role and impacts of wildland fire.

Conventional hydrologic design configures drainage structures to have capacity to accommodate the direct runoff resulting from rainfall (clearwater design flow), not including any potential entrained and transported sediment, wood, and debris. However, in watersheds prone to wildfires, designing infrastructure to accommodate only clearwater flow may provide insufficient capacity for potential sediment, wood, and debris laden flows characteristic of historical burn zones. Design for these areas may warrant special care to ensure functionality, resilience, and sustainability by configuring the hydraulic structure to accommodate the post-fire runoff increase.

Figure 7.1 illustrates a typical post-wildfire runoff condition, in this case sediment- and debris-laden runoff from a watershed following the 2004 Foothill wildfire in Los Angeles County, California.



Figure 7.1. Placerita Canyon Road after the Foothill Fire, October 10, 2004. Source: Los Angeles County Department of Public Works.

The Desert Research Institute (DRI) and the U.S. Army Corps of Engineers (USACE) collaborated to develop the Urban Flood Demonstration Program (UFDP) Data Clearing House (<https://ufdp.dri.edu/>), an online tool that provides access to models, data, and literature that may be useful to fire responders and researchers interested in the effects of wildfire on hydrology. The USGS conducts post-fire debris-flow hazard assessments for select fires in the Western United States and documents findings at [https://landslides.usgs.gov/hazards/postfire\\_debrisflow/](https://landslides.usgs.gov/hazards/postfire_debrisflow/). This tool allows practitioners to use geospatial data related to basin morphometry, burn severity, soil properties, and rainfall characteristics to estimate the probability and volume of debris flows that may occur in response to a design storm.

### 7.1.1 Wildfire Effects on Hydrology

Hydrologists and geotechnical engineers evaluate the impacts of the wildfire on flooding and other potential hazards. Wildfires affect runoff, and therefore flooding, in two primary ways. First, fire increases the runoff of water by reducing the infiltration and retention capacity of the watershed. Second, fire increases the sediment yield from the watershed causing surface and channel erosion that “bulks” the flow, further increasing flood volumes. BAER reports may provide useful descriptive information relevant to hydrology analyses such as detailed maps of burn intensity and vegetation types. Engineers use an understanding of the effects of wildfire to establish stabilization plans and protection practices to enable the watershed to recover and return to a stable hydrologic state. The following sections discuss these two wildfire effects on flooding.

#### 7.1.1.1 Infiltration Reduction

Figure 7.2 shows a denuded hillslope after a wildfire. Wildfire removes protective vegetation and frequently inhibits soil infiltration, resulting in larger runoff volumes and higher velocities. Fire destroys the soil structure by causing it to collapse, thereby increasing soil density and reducing its porosity (Neary et al. 2008). Rainfall consolidates soil and ash particles, causing surface soil pores to become sealed.

Hydrologists can model the effects on infiltration of soil hydrophobicity, a tendency to resist wetting or infiltration of moisture, by evaluating the influential parameters of infiltration. To model infiltration, engineers commonly use the Green-Ampt and Natural Resources Conservation Service (NRCS) curve number (CN) methods, discussed in more detail in HDS-2. To account for the reduction in infiltration caused by hydrophobicity, hydrologists can apply one or more options, as appropriate (NRCS 2016):

- Reduce hydraulic conductivity (Green-Ampt method).
- Increase percentage of impervious surface area, e.g., in the Rational method.
- Increase the CN to the high 90s (NRCS CN method).

BAER specialists estimate reduction in infiltration primarily from U.S. Forest Service soil burn severity maps or from field measurements. The hydrologist can consult these maps or geotechnical assessments to estimate the severity of wildfire as it relates to the hydrology. The U.S. Department of Agriculture (USDA) provides a field guide (Parsons et al. 2010) to help BAER teams consistently interpret, field validate, and map soil burn severity. The guide aids identification of soil condition indicators that differentiate soil burn severity classes.





Figure 7.2 Diamond Mountain Road near Antelope Lake, California. Source: U.S. Forest Service.

#### 7.1.1.2 Sediment Bulking

Because of the significant sediment load vegetation-denuded watersheds produce, higher flows and stages characterize post-fire hydrographs. Figure 7.3 shows severe damage caused by sediment laden flood flows. Figure 7.4 depicts clearing of post-wildfire sediment, wood, and debris flows that crossed and closed I-70.

The following equation relates bulk flow to clearwater flow.

$$Q_{\text{bulked}} = Q + Q_s \quad (7.1)$$

where:

$$\begin{aligned} Q &= \text{Water flow, ft}^3/\text{s (m}^3/\text{s)} \\ Q_s &= \text{Sediment flow, ft}^3/\text{s (m}^3/\text{s)} \end{aligned}$$

The following equation, with an empirical bulking factor, applies when estimating sediment bulking in post-wildfire hydrograph analyses (O'Brien and Fullerton 1989). HEC-16 (FHWA 2023) provides similar bulking recommendations.

$$BF = \frac{Q + Q_s}{Q} = \frac{1}{1 - C_v} \quad (7.2)$$

#### Debris Flow Likelihood

The USGS maintains a website estimating the likelihood of sediment/debris flows from current fires:

[https://landslides.usgs.gov/hazards/postfire\\_debrisflow/](https://landslides.usgs.gov/hazards/postfire_debrisflow/)

This site may provide insights for initial assessment of roadway impacts and for property owners in affected watersheds.

where:

- BF = Bulking factor  
 $C_v$  = Maximum sediment concentration by volume, (sediment volume/total volume)



Figure 7.3. Post-wildfire 2010 debris flow from San Gabriel Mountains, California. Source: NRCS (2016).

HEC-16 describes a  $BF < 1.25$  as clearwater flow;  $1.25 < BF < 1.65$  as sediment laden flow; and  $BF > 1.65$  as mud flow (FHWA 2023). The volumetric and weight concentration of sediment laden flow ranges from 20 to 40 percent and 10 to 65 percent, respectively.

For sediment laden runoff hydrographs, the water flow ( $Q$ ), sediment flow ( $Q_s$ ), and bulking factor ( $BF$ ) vary with time. For design, engineers estimate these values at peak conditions, including the maximum sediment concentration ( $C_v$ ), which tends to occur before the peak of the flood hydrograph.

Some jurisdictions, such as Los Angeles County (LACDPW 2006), have developed alternative empirical relationships between sediment production and drainage area and bulking factors and drainage area for the various hydrologic regions. These relationships are based on observed floods as they relate to geologic, topographic, vegetative, and rainfall features. Applying a bulking factor to a clearwater hydrograph produces bulked flow as illustrated in Figure 7.5. This hydrograph plots the relationship between clearwater, sediment, and bulked flows for a hypothetical case.





Figure 7.4. Clearing of a post-wildfire debris flow that closed I-70 in Glenwood Canyon, Colorado, in 2021.

### 7.1.2 Methodologies and Analytical Approaches

To gauge the effects of wildfires on watershed hydrology, specialists conduct BAER assessments in field investigations. In practice based on field observations of post-fire watersheds, BAER specialists use U.S. Geological Survey (USGS) regression methods for larger watersheds (>5 mi<sup>2</sup>) and NRCS curve number methods for smaller watersheds (<5 mi<sup>2</sup>) (Foltz et al. 2009). Methods for estimating pre- and post-fire runoff include:

- USGS regional rural regression equations.
- NRCS peak flow and unit hydrograph (curve number) methods.
- USDA rule of thumb.

The USGS developed nationwide regional rural regression equations, which form the basis for this approach. HDS-2 provides information on applying the regression equations. Engineers most commonly use this methodology, often using StreamStats to estimate the peak flows. As an alternative resource, the USGS publishes the rural regression equations for each State in its scientific investigation report (SIR) series. Each hydrologic region has its set of independent parameters; there, the hydrologist would acquire the relevant data for the applicable equation and determine the appropriate variable to adjust to account for the wildfire effects. Typically, regional guidelines, when available, are the primary source for adjusting hydrologic parameters to account for hydrophobicity. Modifiers account for the increase in runoff based on the high and moderate soil burn severity. Because regional regression equations often have no independent variables that can be adjusted to account for hydrophobicity, BAER specialists rely on regional guidelines for estimating the increase in runoff that may include a simple multiplier adjustment.

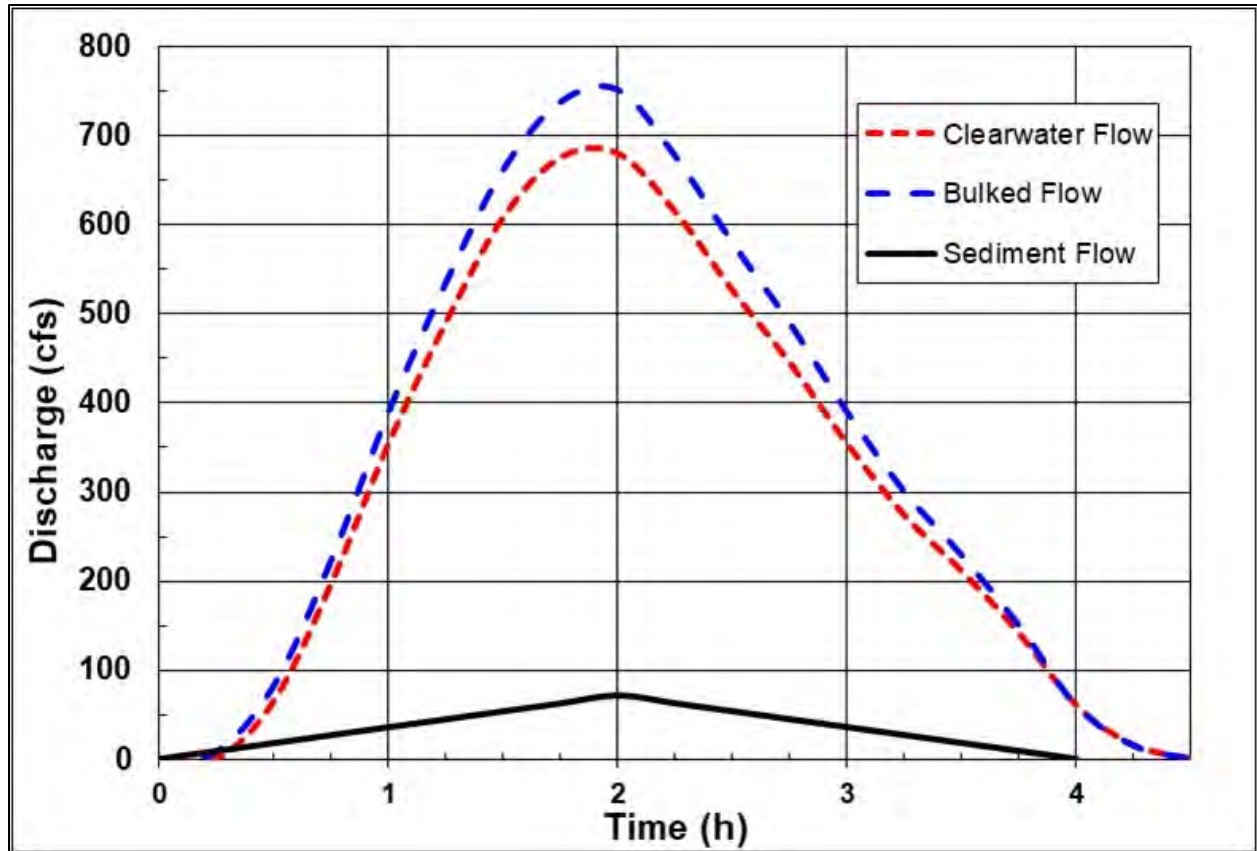


Figure 7.5. Example of bulked flow hydrograph.

The NRCS offers a peak flow and unit hydrograph method, used in practice for estimating pre- and post-wildfire runoff. Adjustment of curve number, which typically increases, and time of concentration, which typically reduces, can account for the change in the hydrologic condition resulting from wildfires. HDS-2 provides a detailed discussion of the NRCS methods, including discussions of appropriate curve number selection and estimation of peak clearwater flows.

Engineers can also estimate wildfire runoff using the USDA rule of thumb method (Foltz et al. 2009). It is a simple and quick approximation that estimates the post-fire peak flow as a function of area, rainfall intensity, and extent of moderate burn severity:

$$Q_p = 300BF A_s I \quad (7.3)$$

where:

- BF = Bulking factor (usually taken as 1.25)
- $A_s$  = Area of high and moderate burn severity area,  $\text{mi}^2$
- I = Rainfall intensity, inches/h



Modeling software tools aid in assessing the effects of wildfire on hydrology. Wildfire hydrology modeling software includes Water Yield and Sediment, WATSED (USDA 1990), Water Erosion Prediction Project, WEPP (Flanagan and Nearing 1995), Rangeland Hydrology and Erosion Model, RHEM (Nearing et al. 2011), Revised Universal Soil Loss Equation, RUSLE (USDA 2008), HEC-HMS (USACE 2021a), and Wildcat5 (Hawkins and Barreto-Munoz 2016). The hydrologic component of these software tools implements the hydrologic methods discussed in the preceding sections. In addition to the hydrologic elements, these tools perform soil loss estimates.

#### Debris Yield Methods in HEC-HMS

Modelers will select tools appropriate for their objectives based on the options available in each software tool. For example, HEC-HMS (version 4.10 at the time of this publication) includes several methods for estimating debris yield including the USGS emergency assessment debris model. Software developers update their products so modelers will review documentation to stay current on software capabilities.

### 7.1.3 Mitigation and Countermeasures

Several approaches exist for mitigation of watersheds whose hydrologic process has been affected by wildfires. Post-fire peak flow estimation provides critical information for selection of road treatments for either emergency or long-term mitigation. Figure 7.6 illustrates emergency placement of a countermeasure to prevent additional flow of sediment and rock onto I-70 in Colorado.



Figure 7.6. Temporary emergency mitigation to prevent further post-wildfire sediment and rock flow onto I-70 in Glenwood Canyon Colorado.

Long-term mitigation can include culvert upgrading and ditch cleaning/armoring, among others. Configuring the countermeasure involves consideration of basin capacity design and sediment, wood, and debris volume estimates. Chapters 5 and 6 of HEC-9 (FHWA 2005) provide detailed information on debris control countermeasures for culvert and bridge structures; engineers can extend these measures to other riverine applications. HEC-16 (FHWA 2023) provides detailed discussion estimating sediment load and post-wildfires debris flows. The Los Angeles Department of Public Works *Sedimentation Manual* (LACDPW 2006) provides several mitigation measures applied in common practice for watersheds with historical burn areas and prone to sediment- and debris-laden flows:

- Debris basins.
- Rail and timber structures.
- Elevated inlets.
- Crib dams.
- Desilting inlets.

**Debris basins** intercept and retain debris—including sediment, gravel, boulders, and uprooted vegetation—washed out of canyons during storms. While trapping debris, the basin releases water into the downstream drainage system, thereby reducing flood risk for communities downstream of the facility. Figure 7.7 provides an aerial view of a debris basin.



Figure 7.7. Debris basin. Source: Los Angeles County Department of Public Works.

Engineers typically implement **rail and timber structures**, as shown in Figure 7.8, for temporary emergency mitigation, constructing them downstream of burned areas with potential for sediment





debris loads ensure a more sustainable design. Part of the maintenance plan is an emergency plan to remove sediment, wood, and debris during a flood event that poses a potential risk to infrastructure and human life. Chapter 7 of HEC-9 (FHWA 2005) discusses maintenance of debris control structures.



Figure 7.9. Crib dam. Source: USGS.

## 7.2 Karst Terrain

Karst terrain can significantly alter the runoff characteristics of a watershed compared with non-karst terrain. This section introduces engineers to the phenomenon of karst terrain, how to identify it, and its implications for roadway design.

“Karst terrain” describes a topography formed from the dissolution of limestone or dolomite and typically consists of **sinks**, **underground streams**, and **caverns**. The karst features include sinkholes, springs, caves, and sinking streams. A sink or natural depression is a natural basin with no surface outlet except for overflows during high water conditions. Sinkholes are surface openings in sinks, which convey surface runoff waters from the sinkhole watershed into the aquifer.

Initial abstraction and rainfall losses tend to be higher in karst terrain because of the additional storage capability of the karst features. Depending on the additional volume of abstraction and storage from karst areas, the runoff effects on more frequent smaller storms may be greater than for larger storms as the abstraction and storage volumes become a decreasing fraction of the total storm volume as storm volume increases for larger storms.

Urbanization in karst areas has the potential for reducing rainfall losses associated with karst terrain by covering the land surface with impervious surfaces and by grading the landscape to fill

sinkholes and other karst features. In these cases, the engineer could anticipate greater increases in post-development runoff volumes and peaks resulting from urbanization in karst areas than would otherwise be expected.

Karst hydrology affects roadway design in areas of a natural depression or sink, near-surface solution channels and vertically inclined bedding planes, or “rock breaks.” In addition to the hydrologic effects, project considerations include stormwater management and erosion control as they specifically relate to the karst terrain and underlying aquifer.

Figure 7.10 and Figure 7.11 show karst and potential karst areas in the United States that comprise approximately 20 percent of ground surface of the United States (Weary and Doctor 2014, Epstein and Johnson 2003). Engineers can use these resources and any available State and local karst inventories and then conduct site investigations and geologic surveys of the watershed area to verify the karst characteristics including drainage patterns, vegetation changes, depressions, and bedrock outcrops.

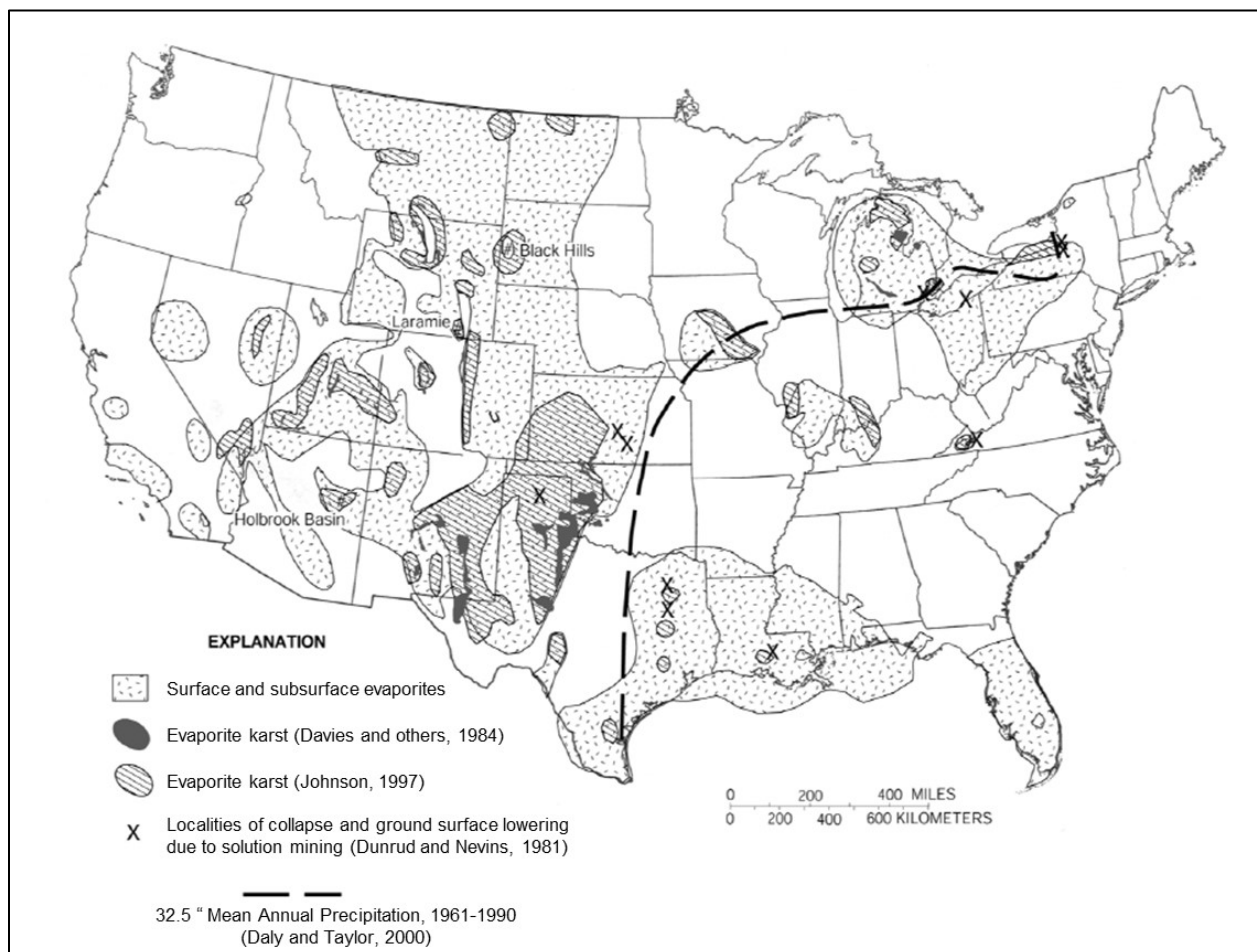


Figure 7.10. Karst and potential karst areas in soluble rock in the contiguous United States.

Source: Epstein and Johnson (2003).

Figure 7.12 is photograph of the Seco sinkhole entrance to the Edwards Aquifer in Medina County, Texas, which illustrates the conveyance of surface water flow through a sinkhole and ultimately into the underlying aquifer.

Figure 7.13 is a photograph of a cave which is part of a karst system in western Texas. Caves, like other karst features, are gateways to groundwater and underlying aquifer, in this case the Edwards Aquifer.

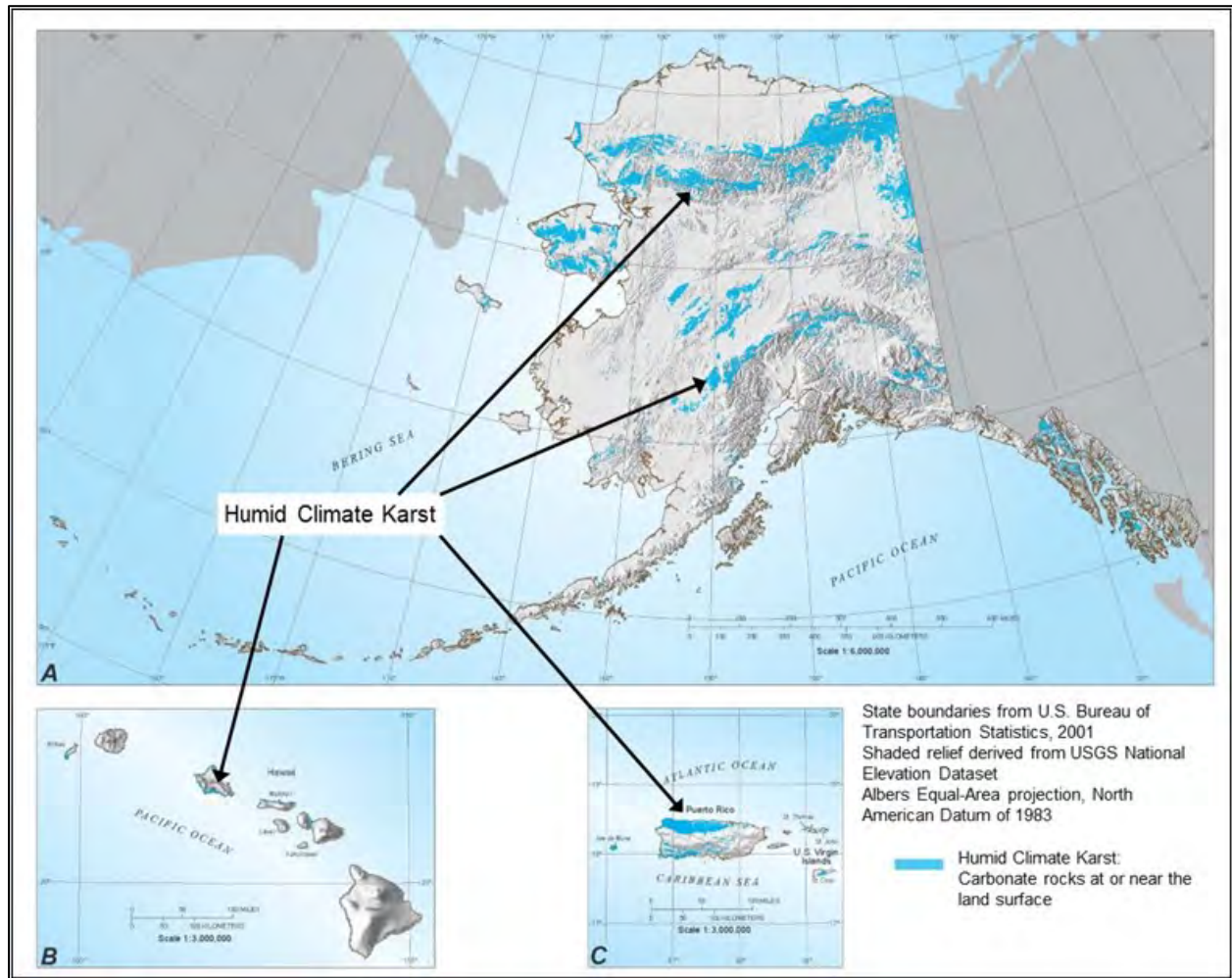


Figure 7.11. Karst and potential karst areas in soluble rock in (A) Alaska, (B) Hawaii, and (C) Puerto Rico and the Virgin Islands. Source: Weary and Doctor (2014).

### 7.2.1 Estimating Runoff

Drainage designers use many methods to account for karst loss on estimates of runoff. These include:

- Adjusting the runoff coefficient in a rainfall-runoff method.
- Using an NRCS Type I rainfall distribution within a Type II area (Laughland 1996).
- Adjusting the curve number values or peak rate factors using the TR-20 method.
- Applying regression equations developed for karst terrain.
- Applying empirical reduction factors.





Figure 7.12. Seco sinkhole entrance, Edwards Aquifer, Texas. Source: Edwards Aquifer Authority (2022).



Figure 7.13. Karst cave system, Texas. Source: Desert Sky Engineering and Hydrology and used by permission.

The first three methods use common hydrologic tools applicable to many circumstances. (See *Highway Hydrology* (FHWA 2022a) for descriptions of these methods). For example, Laughland (1996) notes that a curve number adjustment approach was used in the Pennsylvania State University (PSU-IV) software. Although the NRCS rainfall type distributions are gradually being replaced with newer distributions, the approach of the second method could be adapted to new distributions. Designers rely on engineering judgment and site-specific information to select appropriate adjustments for any given situation.

As an example of the fourth method, the U.S. Geological Service (USGS) (Flippo 1977) studied eight different hydrologic areas and developed regression models using rainfall measurements and stream gage records. Applicable to West Virginia and Pennsylvania, one of the models applied to drainage basins predominantly underlain by limestone or dolomite bedrock is:

$$Q = cA^x \quad (7.4)$$

where:

Q	=	Runoff, ft <sup>3</sup> /s
c	=	Coefficient, variable by AEP
x	=	Exponent, variable by AEP
A	=	Drainage area, mi <sup>2</sup>

Table 7.1 provides the coefficients as a function of the annual exceedance probability (AEP). The drainage area is the portion of the watershed that drains to the outlet. However, the total drainage would deduct areas that drain to streams that terminate or disappear in karst features and any surface areas where the drainage is not conveyed to the outlet but rather can only be transported through the underlying karst (WVDOT 2007). Figure 7.14 illustrates a case when the karst condition reduces the effective watershed area, from 20.0 mi<sup>2</sup> based on surface features as recognized by StreamStats to 3.9 mi<sup>2</sup> based on site-specific evaluation of the karst features. The karst system can cut off surface flow by diverting it to groundwater or other streams, thereby, reducing the effective drainage area.

Figure 7.15 illustrates a converse example where the karst features effectively increase the watershed. Using StreamStats for the Big Spring Creek watershed in south central Pennsylvania, the drainage area is 12.0 mi<sup>2</sup>. But with a site-specific assessment of karst features the effective watershed area increases to 46.6 mi<sup>2</sup>.

Table 7.1. Coefficients for USGS regression equation (Flippo 1977).

AEP	c	x	Standard Error
0.50	23.5	0.880	—
0.10	39.8	0.933	26
0.04	49.1	0.952	27
0.02	56.0	0.970	31
0.01	64.4	0.979	33



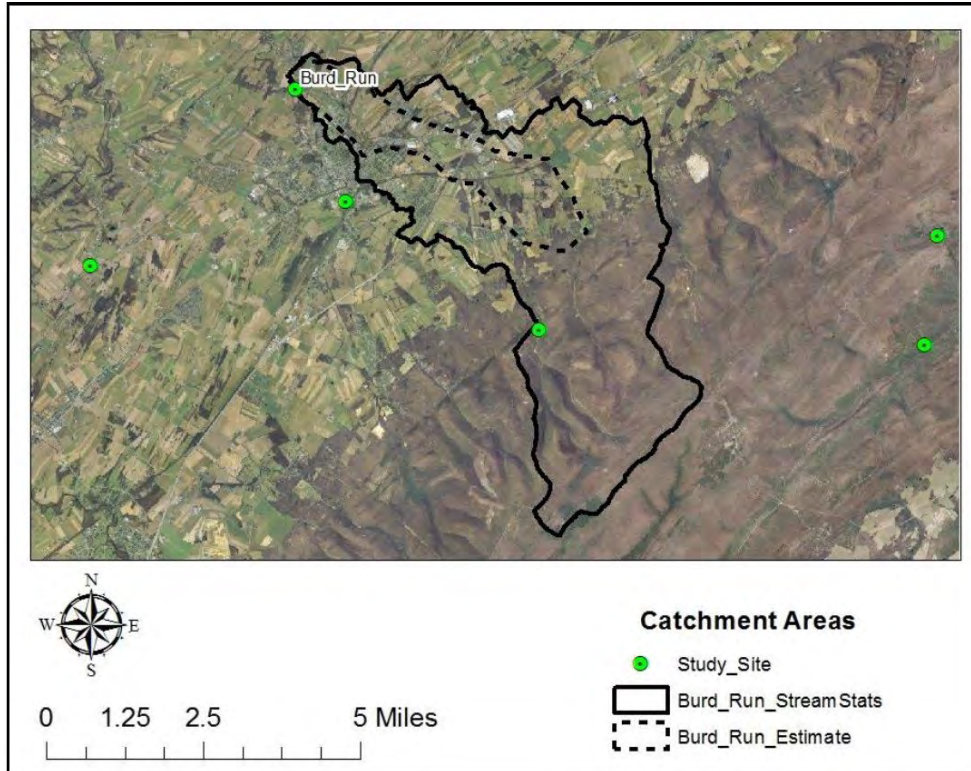


Figure 7.14. Burd Run watershed, south central Pennsylvania. Source: Hawkins and Weichel (2015).

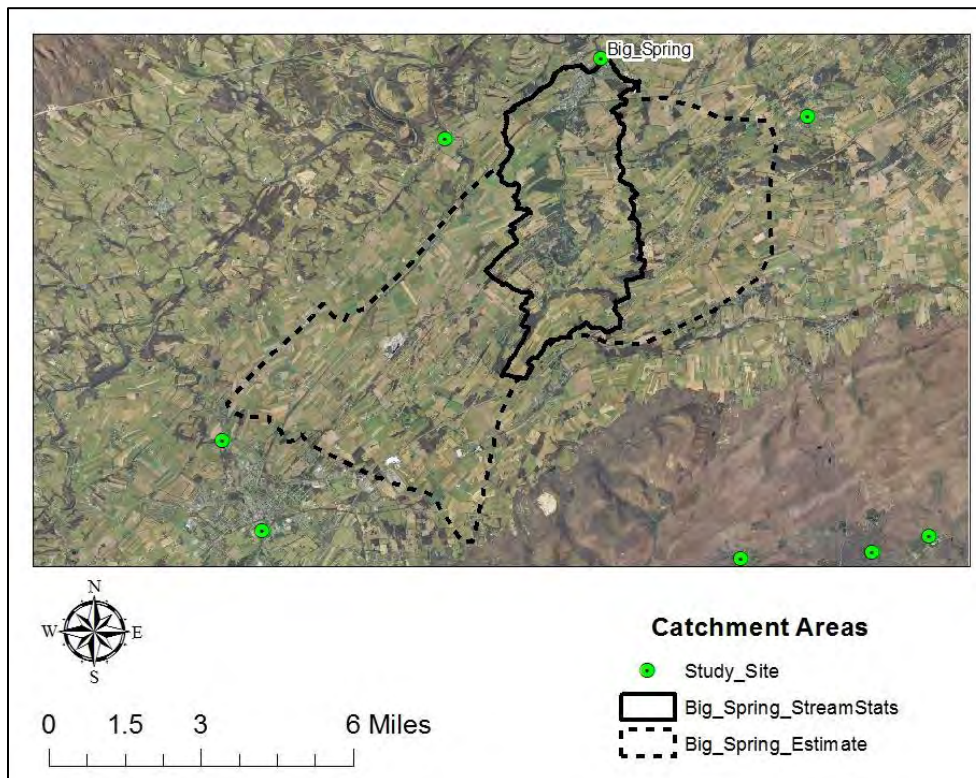


Figure 7.15. Big Spring Creek watershed, south central Pennsylvania. Source: Hawkins and Weichel (2015).

The basis of this methodology is empirical data specific to a region. Since empirical coefficients can vary regionally and hydrologic data are often limited in karst regions, practitioners will consider the evolving technology and associated limitations when applying the method.

The last method estimates runoff using a peak flow method multiplied by an empirical reduction factor or karst loss coefficient. Laughland (1996) developed a karst loss coefficient as a function of the percent of the watershed area with underlying karst, as listed in Table 7.2. The coefficient accounts for the abstraction which is conveyed to the bedrock. Designers may verify and calibrate these coefficients with field observations and measurements, if available.

Table 7.2. Karst loss coefficients (Laughland 1996).

% Karst	Annual Exceedance Probability (AEP)				
	0.50	0.10	0.04	0.02	0.01
100	0.33	0.43	0.44	0.46	0.50
90	0.35	0.46	0.48	0.50	0.56
80	0.38	0.51	0.53	0.56	0.62
70	0.47	0.58	0.60	0.62	0.68
60	0.55	0.66	0.67	0.70	0.74
50	0.64	0.73	0.74	0.76	0.80
40	0.73	0.80	0.81	0.82	0.85
30	0.82	0.86	0.87	0.87	0.89
20	0.91	0.92	0.92	0.92	0.93
10	1.00	0.98	0.98	0.98	0.97
0	1.00	1.00	1.00	1.00	1.00

### 7.2.2 Mitigation

Runoff from roadway projects typically conveys contaminants and sediment. In karst areas, a portion of this urbanized runoff may enter the underlying karst and aquifer. Stormwater management and erosion and sediment control plans protect the groundwater in the aquifer from runoff pollutants. Designers can mitigate the potentially negative impacts of urbanized runoff in karst areas using various design practices.

A filter cap or concrete plug is an effective measure to protect small to moderate sinkholes (Laughland 1996). Figure 7.16 shows a schematic of karst hole plugging with an impervious cover.

A perimeter berm with stone filter or vegetative barrier around a sink protects the sinkhole and underlying karst and aquifer from urbanized runoff. Stormwater management techniques to slow down runoff and allow for settling of sediment and pollutants reduce negative impacts.

An alternative countermeasure for sinkhole repair is a graded filter. The process involves excavation of the sinkhole down to the bedrock, if practicable. Install layers of small stones, gravel, geotextile fabric, sand, and soil. Figure 7.17 illustrates a typical graded filter countermeasure for sinkhole repair. This option allows surface water to enter the groundwater after treatment to mitigate water quality degradation.

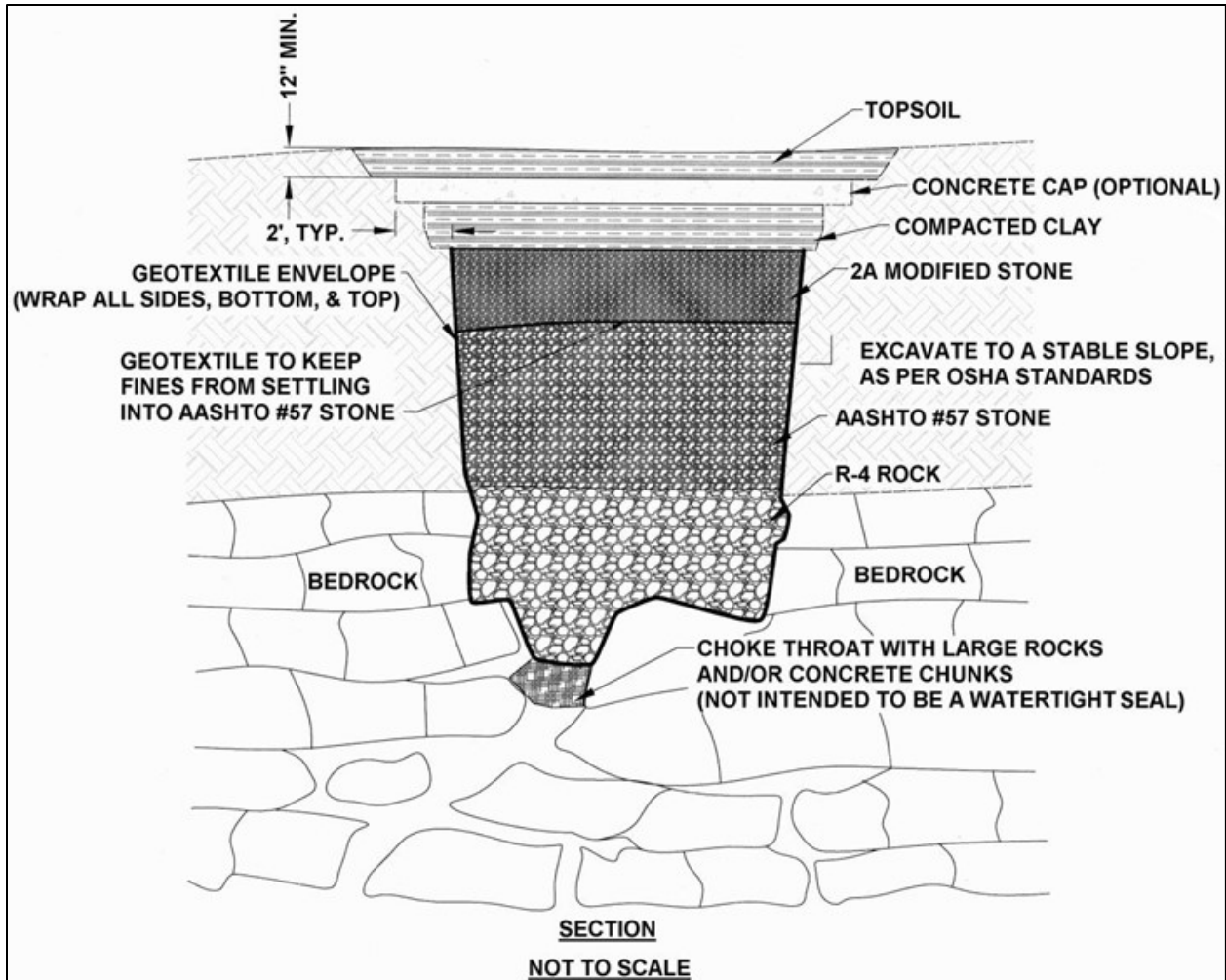


Figure 7.16. Sinkhole repair with an impervious cover. Source: PennDEP (2012).

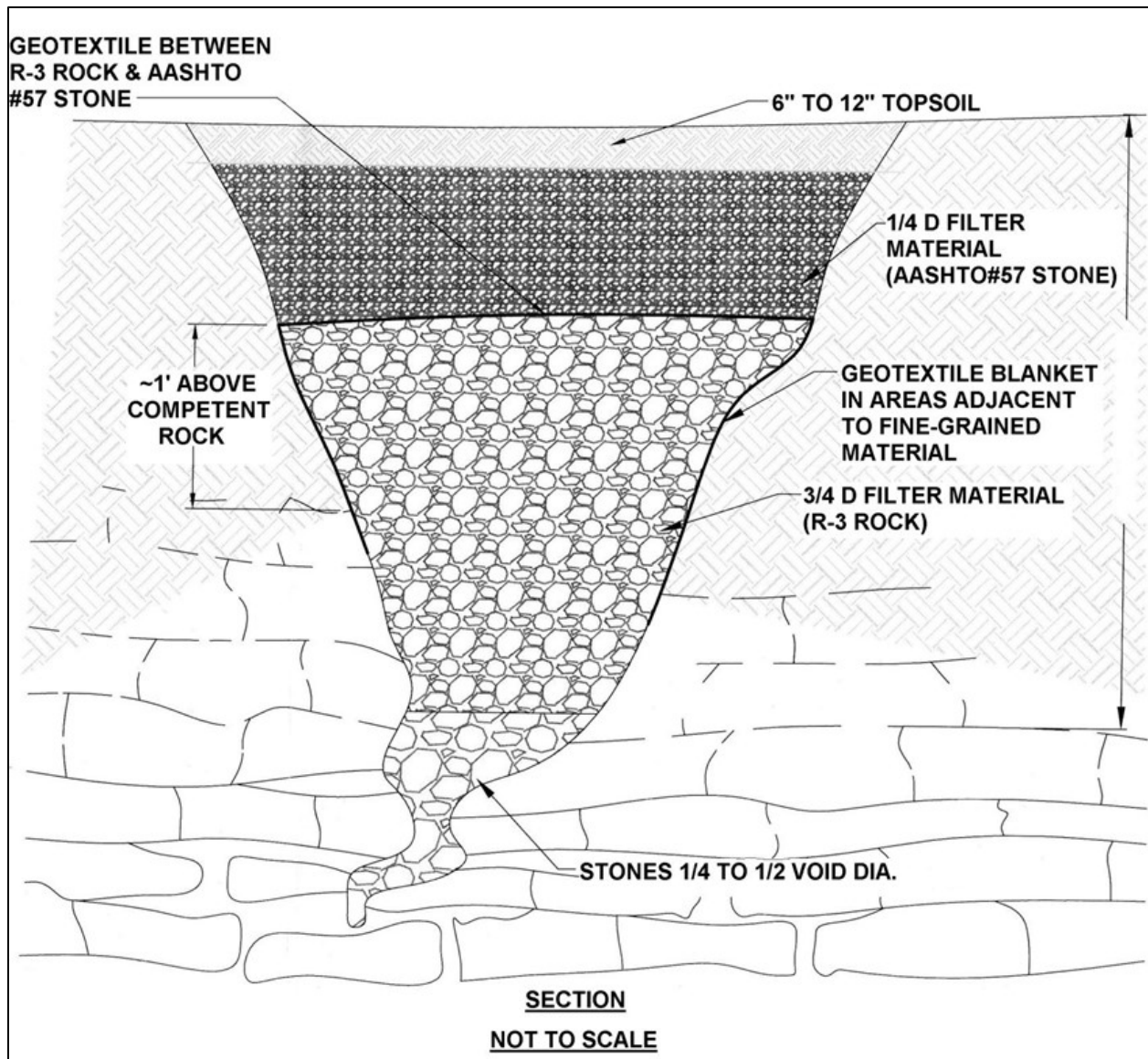


Figure 7.17. Sinkhole repair with a pervious cover. Source: PennDEP (2012).

### 7.3 Paleohydrology

**Paleoflood hydrology** (or **paleohydrology**) studies floods that can be identified from witness accounts or physical evidence but that were not directly measured when they occurred. **Paleohydrologists** search for and validate information about floods that occurred outside of human observation, often prior to human occupation. By placing past flood information from paleohydrology studies in context with respect to both magnitude and time, hydrologists can add depth and breadth to traditional flood studies, primarily by looking more deeply into the past beyond the systematic record.

State Departments of Transportation (DOTs) often rely on the results of statistical analysis of flow gage (systematic) records for design flow and stage at bridges and culverts. Few gage records extend more than 100 years, and most have much shorter duration. Paleohydrology studies can extend the historical records much further back in time thereby improving estimates of design flow and stage for infrequent events. State DOTs may justify paleoflood studies for specific, high-



priority sites, to assess vulnerability, or influence design/management strategy. Bridges or roadways with high commercial traffic volume or that have particular importance for emergency services may warrant site-specific examination. For example, paleoflood studies of the Pecos River in Texas are well documented (Jarrett and England 2002, Webb and Jarrett 2002, Yanofsky and Jarrett 2002). As the science matures and the body of data increases, the practicality of studies is enhanced.

Paleoflood studies also have the potential to add valuable information for statewide or regional flood studies. Because the emphasis is on infrequent (extreme) floods, paleoflood studies can inform the development of generalized skew maps and regional regression equations. (See *HDS-2* for more detailed discussion of these topics.) For example, Kohn et al. (2016) developed regression equations in Colorado using paleoflood information, ultimately supplementing the systematic series on 44 out of 188 gages. The paleoflood information added valuable insights to low-probability flood estimates.

Conducting paleoflood studies involves highly specialized skills. The time, education, and expertise to develop those skills would generally place them outside of reasonable expectation for a design engineer. When needed, a State DOT would generally engage the services of specialists through universities, the USGS, or other organizations to conduct such studies. A large State DOT may have archaeologists on staff for environmental studies that may aid in organizing paleoflood studies. Under most circumstances, a multidisciplinary team of scientists, may best conduct a paleoflood study or studies.

This section provides context to the transportation hydrology and hydraulics (H&H) engineer by describing the science of paleohydrology and how paleohydrology fits within the analytical framework the statistical analysis of gaged flow records. The section also provides an introduction of several scientific techniques useful in paleohydrology studies, as well as some of the limits such studies. Finally, the section provides a case study illustrating the utility of paleohydrology to the H&H engineer.

### 7.3.1 The Science of Paleohydrology

Paleoflood hydrology emerges from the field of fluvial geomorphology, which is the science dealing with the morphology (form) and dynamics of streams and rivers. As the field of fluvial geomorphology grew, and the ability to identify features attributable to floods increased, it became more possible and desirable to place the floods identified by geomorphology appropriately in time. Toward that end, practitioners of the science began to use techniques from hydrology, archaeology, and paleoclimatology to place floods in time. As Figure 7.18 shows, paleoflood hydrology lies at the nexus of these four disciplines adapting and sharing technology with them. Paleoflood hydrology draws from information gathered from these other disciplines and paleoflood studies provide useful information for studies in the other disciplines.

#### Help for Disaster Preparation

Paleoflood studies may provide information helpful in preparing for natural disasters, including floods, fires, storm surges, or even earthquakes. Because catastrophic floods have magnitudes that may be difficult to visualize, disaster preparation and planning may benefit more from knowing that such events occurred in the past than from the abstract concept of probability.

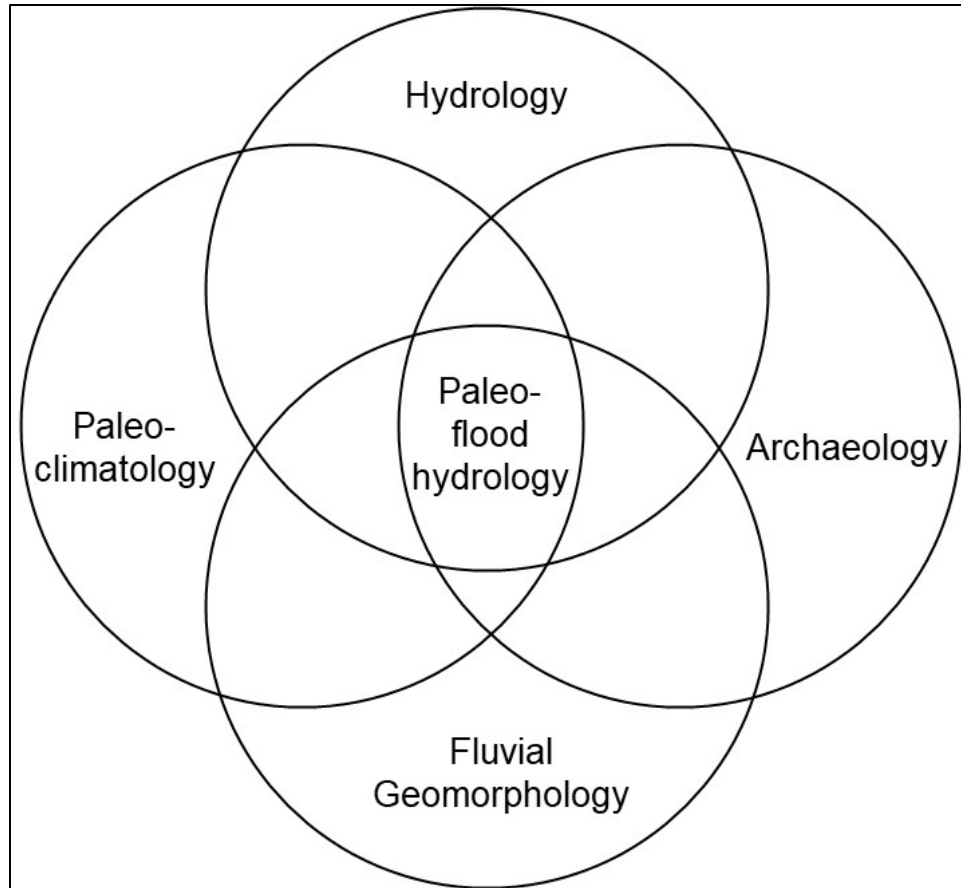


Figure 7.18. Relationship of paleoflood hydrology to related sciences.

Fluvial geomorphologists applied dating techniques from archaeology (the study and reconstruction of past human life and activities). They can use radiocarbon dating where organic matter is present and optically stimulated luminescence (OSL) where there is no organic matter to date sedimentological features. (See section 7.3.3 for information on radiocarbon dating and OSL.) Serendipitously, archaeological sites and paleoflood sites often share locations, concerns, and events, making them mutually supporting. Floods were undoubtedly important events to primitive inhabitants, and flood deposits in occupied sites are often important for the preservation of artifacts, as well as for stratigraphic context.

Paleoclimatology (the study of ancient climates, prior to the widespread availability of instrumental records) uses physical evidence to study past climate and climate change. Paleoclimatology relies heavily on uninterrupted tree ring series to paint a picture of past climate, both globally and regionally. (See section 7.3.3 for information on dendrochronology.) Ocean and lake sediments, soil pedology, ice cores, and other biological evidence also contribute paleoclimate information.

As with fluvial geomorphology, paleoclimatology shares techniques, sites, and important events with archaeology. Climate provides the context for the potential for large floods. Large floods are more likely to be associated with climate episodes involving high rainfall over several years or decades as compared to more arid episodes, although wet episodes do not guarantee the occurrence of large floods, nor do arid episodes preclude them. Paleoflood studies have a primary interest in large flood events because of the greater likelihood that they resulted in evidence that would have been preserved.

Published roughly 20 years apart, two collections of scientific papers—*Flood Geomorphology* (Baker et al. 1988) and *Ancient Floods, Modern Hazards* (House et al. 2002)—document the extension of fluvial geomorphology to paleoflood hydrology. The latter collection reflects research linking fluvial geomorphology to both flood flow and age estimation.

Paleohydrologists identify paleofloods and estimate their magnitude by locating biological or sedimentological evidence of their occurrence and stage. This evidence is called paleostage indicators (PSIs). Examples of biological PSIs include:

- **Tilted trees:** Tilted trees from which vertical sprouts have sprung may indicate that floodwaters pushed over the trees. Paleohydrologists estimate the year in which the flood occurred by comparing the age of the sprouts to the age of the trunk (via dendrochronology).
- **Organic matter in flood-deposited sediment:** Paleohydrologists use radiocarbon techniques to date wood, seeds, animal remains, etc. Figure 7.19 illustrates embedment of organic material.
- **Large wood in sediment:** Branches and tree trunks left in sediment may provide tree ring series. With sufficiently complete series, paleohydrologists may compare them with regional dendrochronological databases to place the series in time.
- **Scarred trees:** Wounds created by flood-born large wood or rocks can provide both temporal information via dendrochronology and stage information by their elevation. Features on trees do not move vertically as the tree grows.

### What Is Dendrochronology?

Each year, trees grow a new layer of wood. These layers are proportional in thickness to the environment the tree endured that year. Scientists can learn much about the weather in past years by studying the nature of the rings. Assembling and correlating the series of years from many trees allows the placement of other (even long-dead) trees in time. This is known as dendrochronology—tree time.

Sedimentological PSIs include:

- **Floodplain terraces:** These geomorphic features indicate past stream banks, possibly during episodes of different climate; they also may indicate changes in channel depth and form over time. Figure 7.20 illustrates flood deposit layers.
- **Slackwater deposits:** These deposits of sediment in areas subject to inundation by stagnant rather than flowing water constitute high water marks. Slackwater deposits usually occur in isolated places protected from erosion and weather (caves, crevices, etc.). These deposits indicate stage. Paleohydrologists may use radiocarbon to date slackwater deposits containing organic material such as wood. Paleohydrologists may use OSL to date undisturbed slackwater deposits with sufficient protection to have remained unexposed to sunlight since deposition.
- **Lake sediment deposits:** Where streams flow into lakes, the sequence and nature of lake bottom sediment layers constitute a time series that can reveal catastrophic flood events. These deposits represent both temporal and relative magnitude of floods, although verifying magnitude by other evidence would be prudent.
- **Speleothems:** Flooded caves and caverns have these geologic formations left by mineral deposits. Paleohydrologists may use changes in the layering of the forming minerals to gather stage and age information.



Figure 7.19. Potential PSI in a flood deposit: a tree branch protruding from a dark sediment layer. Source: Desert Sky Engineering and Hydrology and used by permission.



Figure 7.20. Potential PSI in a flood deposit: interspersed coarse and fine sediment layers indicating different flood deposits. Source: Desert Sky Engineering and Hydrology and used by permission.

### 7.3.2 Historical Floods, Paleofloods, and Statistical Analyses

Hydrologists use the flood history of a stream or region to characterize the flow frequency relationship fundamental in risk-based design. Stream gages and the series of flows that result from gaging constitute a sample of the flood history of the stream on which they are placed. Such systematic records provide important information on the flooding behavior of streams.

Hydrologists know that other sources of flooding information may exist to supplement the gaged (systematic) record. For example, local knowledge of flood events before the placement of a gage or that complement a gage such as high water marks or news reports may exist. Town histories may include records flood events. Both the magnitude and timing of documented floods and the length of time covered by human observation contain valuable information. The latter may be useful by itself. If over a period of 300 years, for example, a town has documented catastrophic floods by noting years and water levels, that knowledge provides the hydrologist with information about the stream's flood characteristics. Before gaged flows were more widely available, communities used anecdotal observations of flood histories to plan and build infrastructure. In some cases, even knowing that catastrophic floods have NOT occurred during a long period of history is valuable information about the stream.

Paleohydrology can extend back further beyond modern history and observation to add information on floods. Paleohydrology focuses on estimating the magnitude and age of floods from the past by identifying indicators of stage or water surface. If paleohydrologists identify a flood that occurred so far in the past that humans did not observe it, it likely had large magnitude. From flood geomorphic features, paleohydrologists can deduce the stage of past floods, and from stage, they can estimate flow. Using tools discussed in this section, paleohydrologist can also estimate when a flood occurred.

Both Bulletin 17B (IACWD 1982) and Bulletin 17C (England et al. 2019) acknowledge the value of anecdotal historical information and paleofloods. Appendix 6 of Bulletin 17B introduced formal methods for using this information. Bulletin 17C states, "historical floods provide probably the most effective data available on which to base flood frequency determinations, and where the data are reliable, this information should be given the greatest weight in constructing the flood frequency graph."

Short systematic records and the reliability of the historical information used limit the traditional methods, such as those described in Bulletin 17B and Bulletin 17C. However, the Expected Moments Algorithm (EMA) for parameter estimation in Bulletin 17C allows the engineer to include in statistical analyses both anecdotal historical peak flows, as well as flows estimated by paleoflood techniques. While engineers may not know the flow associated with a paleoflood with the same precision of measured floods, they can typically estimate a range or interval. The EMA can accommodate interval information.

Because identifiable PSIs tend to represent large, and, thus, rare, events, paleoflood information adds knowledge about the "tail," or rare end, of the flood frequency curve. Paleoflood information does not likely improve estimates of uncertainty, because uncertainty results more from complexity than from simple series length.

The immediate product of paleoflood studies is information about stage. To perform statistical analysis using Bulletin 17C, the engineer uses hydraulic studies to estimate flow from the stage and geometry. A graphical tool connecting water surface elevation and flow (called a rating curve) is often developed, based on a model like Manning's equation, to visualize the relationship between quantities.



### 7.3.3 Scientific Techniques

This section describes some of the basic techniques used in paleoflood studies and related fields. In *Quantitative Paleoflood Hydrology*, Benito et al. (2020) outlines field techniques useful in paleohydrology. Field investigation provides information for laboratory analysis, flow estimation, and for conclusions to relevant archaeological or climatological objectives.

Universities and scientific organizations such as the U.S. Geological Survey (USGS) have the capacity to conduct laboratory analysis for dendrochronology and sediment dating (through OSL or radiocarbon). Laboratory procedures to accomplish these tasks are well documented, and not specific to paleohydrology.

#### 7.3.3.1 Dendrochronology

Dendrochronology is the study of trees, primarily through the annual growth rings, for deducing a time series of prevailing weather. Broadly, in years of weather favorable to tree growth (e.g., high rainfall years), trees have wide annual rings, whereas in years when the tree experienced stress (drought years), trees have narrow rings. Within a region, dendrochronologists can correlate specimens of tree rings from trees that grew in overlapping series of years to extend the record of prevailing annual weather into the past, in some cases, to several thousand years. Online dendrochronology data repositories accumulate information to reconstruct historical timelines associated climates. Using those repositories, almost any piece of wood with tree rings (as can be found in flood sediments) can be placed in temporal context in almost any area of the world.

Dendrochronology involves extensive training and experience in collection, preparation, and laboratory examination of samples from both living and “fossil” wood.

#### 7.3.3.2 Radiocarbon Dating

Scientists can date sedimentological information using radiocarbon (carbon-14) dating developed in the 1950s. Radiocarbon dating applies only to organic material such as charcoal, wood, or seeds, which may be indicators of high water marks of paleofloods. It cannot be used to date inorganic minerals such as sediment grains.

Carbon-14 occurs naturally as a radioactive isotope of ordinary carbon. Scientists believe carbon-14 forms naturally in the upper levels of the atmosphere when cosmic rays interact with other carbon isotopes.

All organic life, as well as organic non-living materials like seashells, contains carbon. Living creatures have the same ratio of carbon-14 to carbon-12 as the atmosphere during their life. However, once a living creature dies, the carbon is no longer replaced. Naturally

#### Stable and Radioactive Carbon

The most common carbon isotope is carbon-12. Ratios to other carbon isotopes include:

- Carbon-13: approximately 1:93 with carbon-12.
- Carbon-14: approximately 1:1,000,000,000,000 with carbon-12.

The ratio of carbon-14 to carbon-12 in the environment varies over time. For instance, because of the combustion of fossil fuels, which lack carbon-14, a larger fraction of carbon-12 exists in the atmosphere today than 100 years ago. Conversely, during the era of atmospheric nuclear testing, the fraction of carbon-14 was higher than before because of the carbon-14 generated by nuclear explosions.



radioactive, and therefore unstable, carbon-14 begins to diminish immediately by radioactive decay, changing the carbon ratio. Eventually, no carbon-14 is detectable.

Scientists estimate the half-life of carbon-14 at 5,730 years, plus or minus 40 years. Whatever carbon-14 a creature contains when it dies, after approximately 5,730 years, only half of the original carbon-14 remains. Measuring the carbon ratio in organic material allows scientists to estimate the time since the death of the creature or plant from which the material came, up to an age of about 55,000 years; beyond that, insufficient carbon-14 remains for reliable dating.

The most common techniques for carbon dating include gas proportional counting (via carbon dioxide gas), liquid scintillation counting (liquid containing carbon), and accelerator mass spectrometry (AMS) (solid carbon-containing material). Carbon ratio measurement techniques may involve elaborate sample preparation including conversion of the carbon to a gas, liquid, or altered solid form. Sample handling for carbon dating involves removal of possible in situ contamination such as rootlets or microorganisms and prevention of contamination in the lab. Both commercial labs and research institutions conduct radiocarbon dating.

### 7.3.3.3 Optically Stimulated Luminescence

Paleohydrologists use optically stimulated luminescence (OSL) to estimate the time since sediment was last exposed to light. OSL assumes the regular decay of radioactive elements in minerals. When decay occurs, electrons are released; flaws in the crystal structure of minerals often “trap” those electrons.

The electrons trapped in the crystal structure of a mineral grain can be released from the flaws that they are trapped in by exposure to light, particularly specific, known wavelengths of light (optical stimulation). When released, the electrons cause the mineral to luminesce (glow) with light in other, known wavelengths. The intensity of the stimulated glow is proportional to the quantity of electrons released. Under carefully controlled laboratory conditions, the stimulated light can be measured, and the time elapsed since the trapped electrons began accumulating can be estimated.

While fluvially deposited sediments are of particular interest in paleoflood studies, they are among the more difficult materials to date using OSL. A sample can only provide a valid age if it has been completely “bleached” by exposure to sunlight prior to deposition. Bleaching releases trapped electrons from the crystal structure of the minerals, and in that way “resets” the dosimeter on the crystal, and thus resets the dosimeter clock. Incomplete bleaching, which may occur when turbid water transports the sediment, leaves residual electrons trapped, and can result in erroneously long estimates of burial time. Crystals can also become “saturated,” with all available capacity of crystal traps filled. When this occurs, the dosimeter clock stops recording time, giving erroneously short burial times. OSL laboratories, most often located at research institutions and universities, conduct tests on each sample to calibrate the process for dose rate, and to check for incomplete bleaching or saturation.

#### Trapped Electrons

When certain minerals, such as quartz and feldspar, are exposed to natural radioactivity, they can “trap” the electrons resulting from the radioactivity (beta particles) in flaws in their crystal structures. The trapped electrons act as a “dosimeter,” measuring the amount of natural radioactivity that the crystal has been exposed to. If the time rate of exposure can be measured, the dosimeter can be considered a clock, measuring the time since the crystal began trapping electrons.

Effective use of OSL involves careful planning, sampling, and sample handling, including carefully controlling light exposure. Providing temporal scale to the dose rate and resulting accumulation of trapped electrons involves additional field measurements of in situ background radioactivity. Given these factors, a State DOT wishing to use OSL will select and engage a lab prior to beginning the study. The lab and associated experts will have insight and input into the effectiveness of OSL for a particular study and can assist in the planning and documentation of the samples and the study. Early planning is also important both because laboratory effort can be large, with corresponding cost and because turnaround time may be in the range of six months.

An associated technique, known as thermal luminescence (TL), can augment OSL on fluvial sediments. Like OSL, TL measures the release of trapped electrons, but in TL the “clock” measures the time since an object experienced relatively high heat, like that of a fire. For example, TL may be useful dating sediments collocated with fire-exposed artifacts such as flint or pottery shards.

OSL and TL can provide ages 50,000 to 150,000 years into the past, depending on the minerals, conditions, and background dose rates. Higher dose rates result in earlier saturation, after which the dosimeter does not record more dose. Low dose rates may bring errors caused by the decay of the background radioactive elements over long periods of time.

#### 7.3.3.4 Speleothems

Mineral formations in caves and caverns represent another possible source of stage and age information for paleohydrologists. Created when minerals carried by water accumulate in the form of speleothems, these deposits may be subject to occasional flooding from adjacent streams. Speleothems, including the most recognized stalagmites and stalactites, often retain evidence of floods in the form of sediment coatings or differences in mineral composition. Changes in the layering of the forming minerals can accurately record stage. Similar to tree rings, the growth rate and layering observable in speleothems represent age. The use of speleothems as PSIs is relatively new but has the potential to render very high resolution paleoflood data where they are available.

Figure 7.21 illustrates several of these features. Although the particular small cavern in the photo is not currently subject to flooding, the photo helps visualize how speleothems can provide a stage indication if floodwaters enter a cave. Sediment or water of different geochemistry could indicate the maximum level on the vertical structures of the speleothems.

#### 7.3.4 Limitations and Conditions

Certain environments present unique conditions and limits for paleohydrology. In general, paleoflood studies most often treat rural environments. Remote uncultivated areas best suit paleoflood studies because they minimize the chance of obliteration of PSIs and sites of archaeological interest. Certain features enhance PSI preservation and the potential for identifying paleoflood information, among them caves and areas protected from erosion and topographically steep canyons.

Forested areas and humid environments enhance the probability of finding preserved dendrochronological evidence yet may make sedimentological evidence harder to detect. Dense vegetation makes access to, and visual assessment of, sediment deposits difficult. Vegetation roots may disrupt and chemically alter sediment deposits. Paleoflood studies in arid environments more often focus on sediment PSIs and sedimentology.

Human activities have invariably heavily disrupted urban environments, obliterating or rendering ambiguous the PSIs on which paleoflood studies focus. Urban areas occupied for centuries may exhibit other signs of historical floods, such as high water marks on buildings and records in

church or city archives. Studies in rural areas upstream and downstream may fill in urban area flood history.



Figure 7.21. Speleothems, stalagmites, and stalactites. Source: Desert Sky Engineering and Hydrology and used by permission.

### 7.3.5 Case Study

Because each situation includes unique features and each study may have unique objectives, paleohydrology studies do not follow a standardized series of steps. This section provides a case study to illustrate the types of information and analysis an actual paleohydrology assessment uses. It also illustrates the relationship between archaeology, paleoflood hydrology, and PSIs. This discussion does not reveal the location to protect the archaeological features, in particular the rock shelters.

The objective of the assessment was to determine the source of sediment in several rock shelters perched in canyon walls. Investigators proposed two hypotheses: 1) backwater flow conditions in the channel deposited the sediment, and 2) humans carried the sediments to the rock shelters. Related to the first hypothesis, investigators explored the magnitude of historical flow rates in the canyon. General information regarding the site includes:

- The site is a rugged, remote, and arid environment (mean annual precipitation approximately 18 inches currently) near the confluence of two rivers.
- The main river flows through a deeply incised, sheer-walled canyon. It drains an area of several States in two countries, with widely varying geology including both sedimentary and igneous rock.
- A similarly incised tributary canyon has a contributing area of approximately 11 square miles with relatively uniform carbonate sedimentary geology.
- The tributary canyon contains three “rock shelter” archaeological sites within less than 0.5 miles of the mouth of the canyon. Formal studies suggest these sites were intermittently occupied by humans for approximately 12,000 years.
- Sediment in the main river and sediment in the tributary canyon are mineralogically distinct from one another, and thus readily identifiable.
- Layers of sediment identifiable as being sediment from the main river occasionally interrupt layers of human-generated detritus (primarily ash) in the rock shelters. These layers are consistent with “slackwater” deposits from large-magnitude floods on the main river.
- Organic matter in the human detritus (seeds, charcoal, plant fiber) can be dated by radiocarbon techniques. The stratigraphic principle of superposition (that younger deposits overlay older deposits) allows analysts to date the slackwater deposits by placing them in time between the human layer below and the human layer above.
- A stream gage existed on the main river for many years, within less than 0.5 miles of the mouth of the tributary canyon. The gage records contain flow for 71 years, and both stage and flow for 42 years. The canyon in this reach has near vertical walls such that it can be approximated as a rectangular channel of reasonably well-behaved stage-discharge nature.

Investigators expect that human occupation caused some disturbance of the sediment in the rock shelters, but the rugged texture of the canyon walls provides ample possibility of undisturbed deposits in inaccessible areas. The elevation of the sediment layers within the shelters provides information for finding those undisturbed flood deposits in smaller caves, crevices, and ledges.

Figure 7.22 shows a view of the lower rock shelter (shelter 1). Note the sheer, nearly vertical cliff face, and the rugged appearance of the terrain. Figure 7.23 provides a view of rock shelter 2, including the material inside the shelter (a mix of sediment and the detritus of human habitation). The archaeologists studying these sites have managed the work to ensure the preservation of undisturbed parts for future study. Figure 7.24 shows a view of the canyon wall, including an inaccessible ledge, and crevices and unoccupied shelters with overhangs. Investigation of these features may reveal slackwater deposits. The ledge contains desert vegetation, and, therefore, the soil to support it. That soil could likely contain slackwater sediment. The inaccessibility of the ledge adds to the likelihood that deposits there have not been disturbed. However, that inaccessibility poses challenges to collecting samples for the paleoflood study.





Figure 7.22. View of the lower of the rock shelters (#1). Image used by permission of Desert Sky Engineering and Hydrology.



Figure 7.23. Rock shelter #2. Image used by permission of Desert Sky Engineering and Hydrology.





Figure 7.24. Canyon wall, including an inaccessible ledge, and showing crevices and unoccupied shelters with overhangs. Image used by permission of Desert Sky Engineering and Hydrology.

Investigators collected the rock shelter elevations in the tributary canyon and estimated the flows that would result in water surface elevations reaching those elevations. Table 7.3 summarizes the associated elevations and flows. The flow that would inundate the highest level of the highest rock shelter is approximately 750,000 ft<sup>3</sup>/s and a stage of over 106 ft. Approximately 260,000 ft<sup>3</sup>/s would completely inundate the lower shelter. A flood approaching that magnitude (202,000 ft<sup>3</sup>/s) occurred during the gaging period, although a gage height was not preserved for that flow.

Investigators calculated the water surface elevations at the gage that would correspond to various elevations in the rock shelters in the tributary canyon by using the river slope indicated in the gage information. They also estimated the flows on the main river that would cause slackwater elevations at the rock shelters and deposition of river sediment in the shelters. Figure 7.25 presents the resulting relationship between stage and flow for the measured flow values as well as the extrapolated estimated flow and elevation information for the rock shelters.

On a tributary river of similar length to the main river, another gaging station existed approximately 14 miles away. This station recorded an annual peak flow of just under 1,000,000 ft<sup>3</sup>/s in the middle part of the twentieth century. That flow was generated from a storm on only a portion of the river watershed that was approximately 5,000 square miles. This measured flood demonstrates that flows in the range that would reach the highest level in the highest rock shelter have occurred under current climatic conditions.



Table 7.3. Gage heights and flows.

Shelter/Elevation	Gage Height at Gage (ft)	Flow (ft <sup>3</sup> /s)
#1/Bottom	57.39	220,000
#1/Top	63.29	260,000
#2/Bottom	75.43	370,000
#2/Top	82.98	450,000
#3/Bottom	98.89	640,000
#3/Top	106.60	750,000

Further study of the tributary canyon would likely reveal undisturbed slackwater deposits that radiocarbon or OSL could date. Based on the information about the rock shelters from archaeological studies, floods of catastrophic magnitude could possibly be identified as far back in time as 12,000 years. Paleoclimate indicators (biologic and geologic) might give them further context.

This limited case study gives a view into the relationship among the parent sciences and how they complement one another to allow the identification and documentation of paleofloods. It also illustrates a small fragment of what a complete study might include. Other than the stream gage information, the information shown is from archaeological studies only. However, the presence of river-born sediment in all three shelters indicates that catastrophic floods have reached them. Past archaeological studies have understandably focused on the layers representing human occupation. Only in recent years have the roles of paleoclimate and paleofloods in the lives of the occupants been of interest. The convenience of the hydraulic aspects of the topography and the existence of gage data makes this case unique.

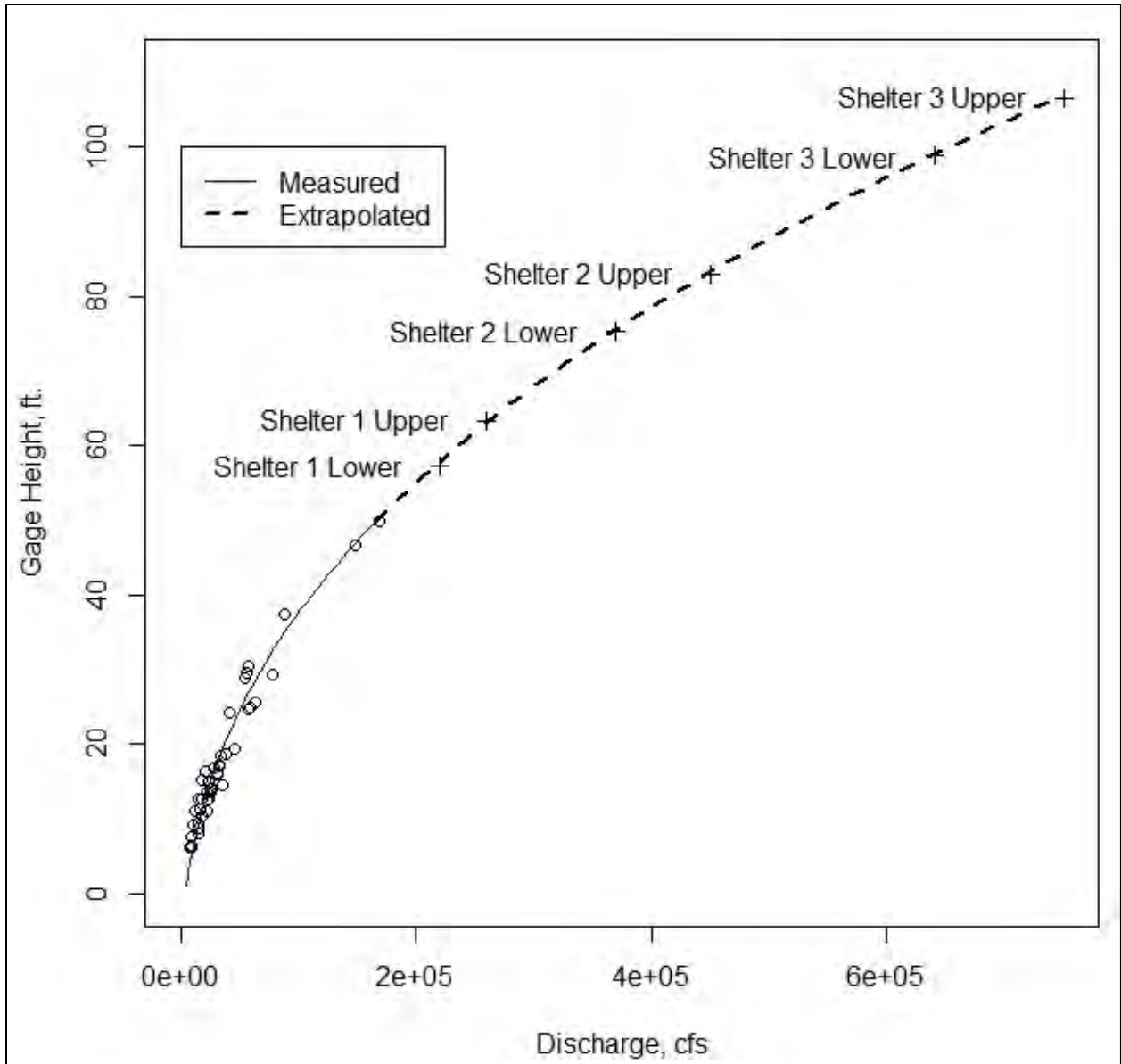


Figure 7.25. Stage/discharge curve at the former gage location, with stage translated from the tributary canyon to the gage. Source: Desert Sky Engineering and Hydrology and used by permission.

*Page Intentionally Left Blank*

## Literature Cited

- Andrews, E.D. 1980. "Effective and Bankfull Discharge of Streams in the Yampa Basin, Western Wyoming," *Journal of Hydrology*, 46, 311-330.
- Asquith, W.H. and J.S. Famiglietti 2000. "Precipitation Areal-reduction Factor Estimation Using an Annual-maxima Centered Approach," *Journal of Hydrology*, 230(1-2), 55-69.
- Baker, V.R., R.C. Kochel, and P.C. Patton (eds.) 1988. *Flood Geomorphology*, John Wiley and Sons.
- Barnard, R.J., J. Johnson, P. Brooks, K.M. Bates, B. Heiner, J.P. Klavas, D.C. Ponder, P.D. Smith, and P.D. Powers 2013. *Water Crossing Design Guidelines*, Washington Department of Fish and Wildlife, Olympia, WA.
- Benito, G., T. Harden, and J. O'Connor 2020. "Quantitative Paleoflood Hydrology," in *Reference Module in Earth Systems and Environmental Sciences*.
- Bensi, M., S. Mohammadi, S-C. Kao, S. DeNeale, M. Carr, and J. Kanney 2019. "A Review of Available Methods for the Probabilistic Treatment of Coincident and Correlated Flood Mechanisms," *Transactions*, SMiRT-25, Charlotte, NC, August 4-9.
- Biedenharn, D.S., R.R. Copeland, C.R. Thorne, P.J. Soar, R.D. Hey, and C.C. Watson 2000. *Effective Discharge Calculation: A Practical Guide*, ERDC/CHL TR-00-15, U.S. Army Engineer Research and Development Center, Vicksburg, MS.
- Bledsoe, B., D. Baker, P. Nelson, T. Rosburg, J. Sholtes, and T. Stroth 2017. *Guidance for Design Hydrology for Stream Restoration and Channel Stability*, NCHRP Research Report 853, The National Academies Press, Washington, DC.
- Bringi, V.N. and V. Chandrasekar 2001. *Polarimetric Doppler Weather RADAR*, Cambridge University Press.
- Cohn, T.A. and H.F. Lins 2005. "Nature's Style - Naturally Trendy," *Geophysical Research Letters*, 32(23).
- Cohn, T.A., J.F. England, C.E. Berenbrock, R.R. Mason, J.R. Stedinger, and J.R. Lamontagne 2013. "A Generalized Grubbs-Beck Test Statistic for Detecting Multiple Potentially Influential Low Outliers in a Flood Series," *Water Resources Research*.
- Copeland, R.R., D.S. Biedenharn, and J.C. Fischenich 2000. *Channel-Forming Discharge*, ERDC/CHL CHETN-VIII-5, December 2000.
- Curtis, D.C. 2011. "Fountain Creek Watershed Rainfall Characterization Study," Carlton Engineering, Shingle Springs, CA.
- Curtis, D.C., S. Benson, L. Cunha, N. Fang, J. Nielsen-Gammon, and P. Bedient 2022. "Improving Design Storm Concepts for Large Watersheds in Texas, presented at the 10th SSPEED Conference, Rice University, Houston, TX, April 28-29.
- Daly, C., M. Halbleib, J.I. Smith, W.P. Gibson, M.K. Doggett, G.H. Taylor, J. Curtis, and P.P. Pasteris 2008, "Physiographically Sensitive Mapping of Climatological Temperature and Precipitation Across the Conterminous United States," *International Journal of Climatology*.
- DHI 2003. *MOUSE Version 2003 User Guide*, Danish Hydraulic Institute, Hørsholm, Denmark

- Dudley, R.W., R.M. Hirsch, S.A. Archfield, A.G. Blum, and B. Renard 2019. "Low-streamflow Trends and Basin Characteristics for 2,482 U.S. Geological Survey Streamgages in the Conterminous U.S." (ver. 2.0, February 2019): U.S. Geological Survey data release, <https://doi.org/10.5066/P9LO24MG>.
- Dudley, R.W., S.A. Archfield, G.A. Hodgkins, B. Renard, and K.R. Ryberg 2018. "Peak-streamflow Trends and Change-points and Basin Characteristics for 2,683 U.S. Geological Survey Streamgages in the Conterminous U.S." (ver. 2.0, October 2018): U.S. Geological Survey data release, <https://doi.org/10.5066/P9AEGXY0>.
- Dunne, T. and L.B. Leopold 1978. *Water in Environmental Planning*, W.H. Freeman and Co., New York, NY.
- Dyhouse, G.R. 1985. "Stage Frequency Analysis at a Major River Junction," *Journal of Hydraulic Engineering*, American Society of Civil Engineers, 111(4), 565-583.
- Edwards Aquifer Authority 2022. "Edwards Aquifer Maps and GIS" (website), San Antonio, TX available online: <https://www.edwardsaquifer.org/science-maps/maps/>, last accessed June 30, 2022.
- England, J.F., Jr., T.A. Cohn, B.A. Faber, J.R. Stedinger, W.O. Thomas, Jr., A.G. Veilleux, J.E. Kiang, and R.R. Mason, Jr. 2019. "Guidelines for determining flood flow frequency—Bulletin 17C" (version 1.1), *U.S. Geological Survey Techniques and Methods, Book 4*, Chapter B5.
- Epstein, J.B. and K.S. Johnson 2003. "The Need for a National Evaporate Karst Map," Oklahoma Geological Survey, Circular 109, 21-30.
- Erickson, E. 1962. *Bridge Failure Report – South Dakota - Iowa - Project I-29, Big Sioux River, Sioux City, Iowa*, Federal Highway Administration.
- Fadhel, S., M.A. Rico-Ramirez, and D. Han 2017. "Uncertainty of Intensity-Duration-Frequency (IDF) curves due to varied climate baseline periods," *Journal of Hydrology*, 547, 600-612.
- FHWA 2002. *Highway Hydrology*, Hydraulic Design Series No. 2 (HDS-2), Second Edition, FHWA-NHI-02-001, Federal Highway Administration, Washington, DC.
- FHWA 2005. *Debris Control Structures, Evaluation and Countermeasures*, Hydraulic Engineering Circular No. 9 (HEC-9), FHWA-IF-04-016, Federal Highway Administration.
- FHWA 2010. *Culvert Design for Aquatic Organism Passage*, Hydraulic Engineering Circular No. 26, (HEC-26) First Edition, Federal Highway Administration, Washington, DC.
- FHWA 2014. "FHWA Order 5520: Transportation System Preparedness and Resilience to Climate Change and Extreme Weather Events," Federal Highway Administration, Washington, DC.
- FHWA 2015. *FHWA Environmental Justice Reference Guide*, Federal Highway Administration, Washington, DC, available online: [http://www.ncfrpc.org/mtpo/FullPackets/MTPO/2021/ej\\_guide\\_fhwahep15035.pdf](http://www.ncfrpc.org/mtpo/FullPackets/MTPO/2021/ej_guide_fhwahep15035.pdf).
- FHWA 2016. *Highways in the River Environment — Floodplains, Extreme Events, Risk, and Resilience*, Hydraulic Engineering Circular No. 17 (HEC-17), Second Edition, FHWA-HIF-16-018, National Highway Institute, Federal Highway Administration, Arlington, VA.
- FHWA 2020. *Highways in the Coastal Environment*, Hydraulic Engineering Circular No. 25 (HEC-25), Third Edition, Federal Highway Administration, Washington, DC.
- FHWA 2021a. "Policy on Using Bipartisan Infrastructure Law Resources to Build a Better America," Federal Highway Administration, Washington, DC.



- FHWA 2021b. *Coupled Model Intercomparison Project (CMIP) Data Processing Tool, Version 2.1, User Guide*, FHWA-HIF-21-016, Washington DC.
- FHWA 2022a. "Sustainable Highways Initiative, Overview" (website), Federal Highway Administration, Washington, DC, available online: <https://www.sustainablehighways.dot.gov/overview.aspx#quest1>, last accessed June 1, 2022.
- FHWA 2022b. "FHWA State Asset Management Plan Under BIL," May 5, 2022, Federal Highway Administration, Washington, DC.
- FHWA 2023. *Highways in the River Environment: Roads, Rivers, and Floodplains*, Hydraulic Engineering Circular No. 16 (HEC-16), First Edition, Federal Highway Administration, Washington, DC.
- FISRWG 1998. *Stream Corridor Restoration: Principles, Processes, and Practices*, by the Federal Interagency Stream Restoration Working Group (FISRWG)(15 Federal agencies of the U.S. government).
- Flanagan, D.C. and M.A. Nearing (eds.) 1995. *USDA Water Erosion Prediction Project (WEPP): hillslope profile and watershed model documentation*, NSERL Report No. 10., USDA-ARS National Soil Erosion Research Laboratory, West Lafayette, IN.
- Flippo, H.N., Jr. 1977. *Floods in Pennsylvania: A Manual for Estimation of Their Magnitude and Frequency*, Bulletin 13, Pennsylvania Department of Environmental Resources.
- Flynn, K.M., W.H. Kirby, and P.R. Hummel 2006. "User's manual for program PeakFQ, Annual Flood Frequency Analysis Using Bulletin 17B Guidelines," *U.S. Geological Survey Techniques and Methods, Book 4*, Chapter B4.
- Foltz, R.B., P.R. Robichaud, and H. Rhee 2009. *A Synthesis of Postfire Road Treatments for BAER Teams: Methods, Treatment Effectiveness, and Decision-making Tools for Rehabilitation*, Gen. Tech. Rep. RMRS-GTR-228, U.S. Department of Agriculture, Forest Service, Rocky Mountain Research Station, Fort Collins, CO.
- Friedman, D., J. Schechter, B. Baker, C. Mueller, G. Villarini, and K.D. White 2016. *U.S. Army Corps of Engineers Nonstationarity Detection Tool User Guide*, U.S. Army Corps of Engineers, Washington, DC.
- Genest, C. and A.C. Favre 2007. "Everything You Always Wanted to Know about Copula Modeling but Were Afraid to Ask," *Journal of Hydrologic Engineering*, American Society of Civil Engineers, 12(4), 347-368.
- Gori, A., N. Lin, and J. Smith 2020. "Assessing Compound Flooding from Landfalling Tropical Cyclones on the North Carolina Coast," *Water Resources Research*, 56(4).
- Granato, G.E. 2013. *Stochastic Empirical Loading and Dilution Model (SELDL)*, U.S. Geological Survey.
- Gustard, A., A. Bullock, and J.M. Dixon 1992. *Low Flow Estimation in the United Kingdom*, Institute of Hydrology, Wallingford, Oxfordshire, UK.
- Hallema D.W., G. Sun, K.D. Bladon, S.P. Norman, P.V. Caldwell, Y. Liu, and S.G. McNulty 2017. "Regional Patterns of Post Wildfire Streamflow Response in the Western United States: The Importance of Scale-specific Connectivity," *Hydrological Processes*, 31, 2582-2598.
- Hamed, K.H. 2008. "Trend detection in hydrologic data: The Mann-Kendall trend test under the scaling hypothesis," *Journal of Hydrology*, 349, 350-363.

- Hamed, K.H. and R. Rao 1998. "A modified Mann-Kendall trend test for autocorrelated data," *Journal of Hydrology*, 204, 182-196.
- Hao, Z. and V.P. Singh 2020. "Compound Events under Global Warming: A Dependence Perspective," *Journal of Hydrologic Engineering*, American Society of Civil Engineers, 25(9), September.
- Hawkins, R.H., and A. Barreto-Munoz 2016. *Wildcat5 for Windows, A Rainfall-Runoff Hydrograph Model: User Manual and Documentation*, Gen. Tech. Rep. RMRS-334, U.S. Department of Agriculture, Forest Service, Rocky Mountain Research Station, Fort Collins, CO.
- Hawkins, S. and D. Weichel 2015. *Estimating Catchment Zones for Streams Located in Karst Systems in South-central Pennsylvania*, Shippensburg University, PA.
- Helsel, D.R., R.M. Hirsch, K.R. Ryberg, S.A. Archfield, and E.J. Gilroy 2020. "Statistical methods in water resources," *U.S. Geological Survey Techniques and Methods, Book 4*, Chapter A3.
- Hendry, A., I.D. Haigh, R.J. Nicholls, H. Winter, R. Neal, T. Wahl, A. Joly-Laugel, and S.E. Darby 2019. "Assessing the Characteristics and Drivers of Compound Flooding Events around the UK Coast," *Hydrology and Earth System Sciences*, 23(7), 3117-3139.
- Herdman, L., L. Erikson, and P. Barnard 2018. "Storm Surge Propagation and Flooding in Small Tidal Rivers during Events of Mixed Coastal and Fluvial Influence," *Journal of Marine Science and Engineering*, 6(4).
- Hey, R.D. (1975). "Design Discharge for Natural Channels," *Science, Technology and Environmental Management*, R.D. Hey and T.D. Davies (eds.), Saxon House, 73-88.
- House, P.K., R.H. Webb, V.R. Baker, and D.R. Levish (eds.) 2002. *Ancient Floods, Modern Hazards: Principles and Applications of Paleoflood Hydrology*, American Geophysical Union.
- IACWD 1982. *Guidelines for Determining Flood Flow Frequency Bulletin 17B*, Interagency Advisory Committee on Water Data, U.S. Department of Interior, Reston, VA.
- Jarrett, R.D. and J.F. England, Jr. 2002. "Reliability of Paleostage Indicators for Paleoflood Studies," *Ancient Floods, Modern Hazards* (House, P.K., R.H. Webb, V.R. Baker, and D.R. Levish, eds.).
- Kao, S., S.T. Deneale, E. Yegorova, J. Kanney, and M. Carr 2020, "Variability of precipitation areal reduction factors in the conterminous United States," *Journal of Hydrology X*, 9.
- Karim, F., M. Hasan, and S. Marvanek 2017. "Evaluating Annual Maximum and Partial Duration Series for Estimating Frequency of Small Magnitude Floods," *Water*, June.
- Kilgore, R.T., D.B. Thompson, and D.T. Ford 2013. *Estimating Joint Probabilities of Design Coincident Flows at Stream Confluences*, National Cooperative Research Program (NCHRP) Web-Only Document 199, Transportation Research Board of the National Academies, Washington, DC.
- Kilgore, R.T., W.O. Thomas, Jr., S. Douglass, B. Webb, K. Hayhoe, A. Stoner, D.B. Thompson, G.R. Herrmann, E. Douglas, and C. Anderson 2019. *Applying Climate Change Information to Hydrologic and Coastal Design of Transportation Infrastructure, Design Practices*, NCHRP 15-61, The National Cooperative Highway Research Program, Transportation Research Board, Washington DC.
- Kimley-Horn 2015. *Final Technical Memorandum (TM #5) – Streamlining Hydrologic Prediction Processes (P530-13-803)*, Nevada Department of Transportation (NDOT) Technical Advisory Panel, Carson City, NV.

- Knighton, D. 1984. *Fluvial Forms and Processes*, Edward Arnold, London.
- Kohn, M.S., M.R. Stevens, T.M. Harden, J.E. Godaire, R.E. Klinger, and A. Mommandi 2016. *Paleoflood Investigations to Improve Peak-Streamflow Regional-Regression Equations for Natural Streamflow in Eastern Colorado, 2015*, U.S. Geological Survey, SIR 2016-5099.
- Konrad, C. and D. Restivo (2021). "Assessment and significance of the frequency domain for trends in annual peak streamflow," *Journal of Flood Risk Management*, e12761.
- Kumbier, K., R.C. Carvalho, A.T. Vafeidis, and C.D. Woodroffe 2018. "Investigating Compound Flooding in an Estuary using Hydrodynamic Modelling: A Case Study from the Shoalhaven River, Australia," *Natural Hazards and Earth System Sciences*, 18(2), 463-477.
- LACDPW 2006. *Sedimentation Manual*, Second Edition, Los Angeles County Department of Public Works, Los Angeles, CA.
- Laughland, J.C. 1996. "Stormwater Management Design in Karst Terrane: Adjusting Hydrology Models and Using Karstic Features," County Engineer, Jefferson County, Charles Town, WV.
- Leopold, L.B. 1994. *A view of the river*, Harvard University Press, Cambridge.
- Livneh, B., E.A. Rosenberg, C. Lin, B. Nijssen, V. Mishra, K.M. Andreadis, E.P. Maurer, and D.P. Lettenmaier 2013. "A Long-Term Hydrologically Based Dataset of Land Surface Fluxes and States for the Conterminous United States: Update and Extensions," *Journal of Climate*, 26, 9384-9392.
- Lombardo, F., F. Napolitano, and F. Russo 2006. "On the use of radar reflectivity for estimation of the areal reduction factor," *Natural Hazards and Earth Systems*, 6, 377-386.
- Mahmood, R., R. Boyles, K. Brinson, C. Fiebrich, S. Foster, K. Hubbard, D. Robinson, J. Andresen, and D. Leathers 2017. "Mesonets: Mesoscale Weather and Climate Observations for the U.S.," *Bulletin of the American Meteorological Society*, 98(7), 1349-1361.
- Maidment, D.R. 2002. *Arc Hydro: GIS for Water Resources*, ESRI Press, Redlands CA.
- Mays, L.W. (ed.) 1996. *Water Resources Handbook*, McGraw-Hill, New York, NY.
- Miro, M., A. DeGaetano, C. Samaras, K. Romita Grocholski, T. López-Cantú, M. Webber, B. Eck 2021. "Projected Intensity-Duration-Frequency (IDF) Curve Tool for the Chesapeake Bay Watershed and Virginia," (website) ,Northeast Regional Climate Center, available online: <https://midatlantic-idf.rcc-acis.org/>, last accessed May 4, 2022.
- Nadal-Caraballo, N.C., M.C. Yawn, L.A. Aucoin, M.L. Carr, A.A. Taflanidis, A.P. Kyprioti, V.M. Gonzalez, E. Ramos-Santiago, T.C. Massey, Z. Cobell, and A.T. Cox 2022. *Coastal Hazards System (CHS): Louisiana*, ERDC/CHL TR-22-16, Vicksburg, MS, U.S. Army Engineer Research and Development Center.
- NASEM 2006. *Evaluation of Best Management Practices for Highway Runoff Control*, Report Number 565, National Academies of Sciences, Engineering, and Medicine, Washington, DC.
- NASEM 2017. *Guidance for Design Hydrology for Stream Restoration and Channel Stability*, National Academies of Sciences, Engineering, and Medicine, The National Academies Press, Washington, DC.

- Nearing, M.A., H. Wei, J.J. Stone, F.B. Pierson, K.E. Spaeth, M.A. Weltz, D.C. Flanagan, and M. Hernandez 2011. *A Rangeland Hydrology and Erosion Model (RHEM)*, U.S. Department of Agriculture, USDA-ARS Southwest Watershed Research Center, Tucson, AZ.
- Neary, D.G., K.C. Ryan, and L.F. DeBano (eds.) 2008 (revised). *Wildland Fire in Ecosystems: Effects of Fire on Soils and Water*, Gen. Tech. Rep. RMRS-GTR-42-vol.4, U.S. Department of Agriculture, Forest Service, Rocky Mountain Research Station, Ogden, UT.
- Nelsen, R.B. 2006. *An Introduction to Copulas*, Second Edition, Springer Series in Statistics, Springer-Verlag, New York, NY.
- NOAA 2022. *Analysis of Impact of Nonstationary Climate on NOAA Atlas 14 Estimates, Assessment Report*, National Weather Service, Office of Water Prediction, National Oceanic and Atmospheric Administration, January.
- NRCS 2016. *Hydrologic Analyses of Post-Wildfire Conditions, Hydrology Technical Note No. 4*, U.S. Department of Agriculture, Natural Resources Conservation Service Washington, DC, August.
- NRCS 2019. "Storm Rainfall Depth and Distribution," *National Engineering Handbook*, Natural Resource Conservation Service, U.S. Department of Agriculture.
- O'Brien, J.S., and W.T. Fullerton 1989. *Hydraulic and Sediment Transport Study of Crown Pointe Flood Wall: Breckenridge, Colorado*, Lenzotti and Fullerton Consulting Engineers, Inc.
- ODFW 2004. *Fish Passage Criteria*, Oregon Department of Fish and Wildlife, Salem, OR.
- Parsons, A., P.R. Robichaud, S.A. Lewis, C. Napper, and J.T. Clark (eds.) 2010. *Field Guide for Mapping Post-fire Soil Burn Severity*, Gen. Tech. Rep. RMRS-GTR-243, U.S. Department of Agriculture, Forest Service, Rocky Mountain Research Station, Ft. Collins, CO.
- PennDEP 2012. *Erosion and Sediment Pollution Control Program Manual*, Technical Guidance Number 363-2134-008, Pennsylvania Department of Environmental Protection, March.
- Petroliagkis, T.I., E. Voukouvalas, J., Disperati, and J. Bildot 2016. *Joint Probabilities of Storm Surge, Significant Wave Height and River Discharge Components of Coastal Flooding Events*, EUR 27824.
- Pettitt, A.N. 1979. "A Non-Parametric Approach to the Change-Point Problem," *Applied Statistics*, 28(2), 126-135.
- Pickup, G. and R.F. Warner 1976. "Effects of hydrologic regime on magnitude and frequency of dominant discharge," *Journal of Hydrology*, 29, 51-75.
- Pingel, N. and D. Ford 2004. "Interior Floodplain Flood-Damage Reduction Study," *Journal of Water Resources Planning and Management*, American Society of Civil Engineers, 130(2), 123-130.
- Read, L.K. and R.M. Vogel 2015. "Reliability, Return Periods, and Risk Under Uncertainty," *Water Resources Research*, 51(8), 6381-6398.
- Rinehart, R.E. 2010. *RADAR for Meteorologists*, Rinehart Publications.
- Rossmann, L.A. 2015. *Storm Water Management Model, User's Manual Version 5.1*, U.S. Environmental Protection Agency.
- Salvadori, G., C. De Michele, N.T. Kottegoda, and R. Rosso 2007. *Extremes in Nature, An Approach Using Copulas*, Volume 56 of Water Science and Technology Library, Springer.

- Santos, V.M., T. Wahl, R. Jane, S.K. Misra, and K.D. White 2021. "Assessing Compound Flooding Potential with Multivariate Statistical Models in a Complex Estuarine System under Data Constraints," *Journal of Flood Risk Management*, 14(9).
- Sarhadi, A. and E.D. Soulis 2017. "Time-varying extreme rainfall intensity-duration-frequency curves in a changing climate," *Geophysical Research Letters*, 44(5), 2454-2463.
- Serago, J.M. and R.M. Vogel 2018. "Parsimonious nonstationary flood frequency analysis," *Advances in Water Resources*, 112, 1-16.
- Serinaldi, F., C.G. Kilsby, and F. Lombardo 2018. "Untenable nonstationarity: An assessment of the fitness for purpose of trend tests in hydrology," *Advances in Water Resources*, 111, 132-155.
- Shiau, J.T., H.Y. Wang, and C.T. Tsai 2006. "Bivariate Frequency Analysis of Floods Using Copulas," *Journal of the American Water Resources Association*, 42(6), 1549-1564.
- Stenstrom, M.K. and M. Kayhanian 2005. *First Flush Phenomenon Characterization*, California Department of Transportation, Sacramento, CA.
- Sumioka, S.S., D.L. Kresch, and K.D. Kasnick 1998. *Magnitude and Frequency of Floods in Washington*, USGS Water Resources Investigations Report 97-4277.
- Thomas, W., D. Newell, E. Bernzott, D. Szekeres, J. Harris, C. Tabb, F. Siddiquee 2020. *Development of Site-Specific Hydrologic and Hydraulic Analyses for Assessing Transportation Infrastructure Vulnerability & Risks to Climate Change*, FHWA-HEP-21-025.
- U.S. Department of Commerce Weather Bureau 1957. *Rainfall Intensity-Frequency Regime, Part 1-The Ohio Valley*, Technical Paper No. 29, Washington, DC.
- USACE 1993. *Hydrologic Frequency Analysis*, Engineer Manual 1110-2-1415, U.S. Army Corps of Engineers, Washington, DC.
- USACE 2019. *HEC-SSP Statistical Software Package User's Manual*, CPD-86, Hydrologic Engineering Center, Davis, CA.
- USACE 2021a. *HEC-HMS Hydrologic Modeling System*, Hydrologic Engineering Center, Davis, CA.
- USACE 2021b. *Gridded Surface Subsurface Hydrologic Analysis*, Engineer and Research Development Center, Vicksburg, MS.
- USACE 2021c. *HEC-RAS River Analysis System*, Hydrologic Engineering Center, Davis, CA.
- USACE 2021d. *HEC-RAS 2D Modeling User's Manual*, U.S. Army Corps of Engineers, Hydrologic Engineering Center, Davis CA, April.
- USACE 2021e. *HEC-RAS Mapper User's Manual*, U.S. Army Corps of Engineers, Hydrologic Engineering Center, Davis CA, April.
- USBR 2020. *SRH-2D, Sedimentation and River Hydraulics – Two-Dimensional River Flow Modeling*, U.S. Bureau of Reclamation.
- USDA 1990. *Water Yield and Sediment (WATSED) Model*, Region 1 water and sediment model, U.S. Department of Agriculture, Forest Service, Montana Region, Missoula, MT.
- USDA 2008. *Revised Universal Soil Loss Equation Version 2 (RUSLE2)*, U.S. Department of Agriculture (USDA) – Agricultural Research Service (ARS).
- USDOI and USDA 2006. *Interagency Burned Area Emergency Response Guidebook: Interpretation of Department of the Interior 620 DM 3 and USDA Forest Service Manual*

- 2523 *For the Burned Area Rehabilitation of Federal and Tribal Trust Lands*, version 1.3, U.S. Department of the Interior.
- USDOT 2021. *Climate Action Plan: Revitalizing Efforts to Bolster Adaptation and Increase Resilience*, U.S. Department of Transportation, Washington, DC.
- USDOT 2022. *Equity Action Plan*, U.S. Department of Transportation, Washington, DC.
- USEPA 1986. *Technical Guidance Manual for Performing Wasteload Allocations, Book VI: Design Conditions, Chapter 1: Stream Design for Steady State Modeling*, U.S. Environmental Protection Agency, Washington, DC.
- USEPA 2011. *Summary of State Stormwater Standards*, U.S. Environmental Protection Agency, Washington, DC.
- USEPA 2018. *Low Flow Statistics Tools, A How-To Handbook for NPDES Permit Writers*, EPA-833-B-18-001, Washington, DC.
- USEPA 2020. *Storm Water Management Model*, U.S. Environmental Protection Agency, Washington, DC
- USEPA 2021. "Definition and Characteristics of Low Flows" (website) U.S. Environmental Protection Agency, Washington, DC, available online: <https://www.epa.gov/ceam/definition-and-characteristics-low-flows>, last accessed June 26, 2021.
- USGS 2006. *User's Manual for Program PeakFQ, Annual Flood Frequency Analysis Using Bulletin 17B Guidelines, Techniques and Methods 4-B4*, U.S. Geological Survey, Reston, VA.
- USGS 2017a. *StreamStats, version 4*, K. G. Ries III, Newson J.K., Smith, M.J., Guthrie, J.D., Steeves, P.A., Haluska, T.L., Kolb, K.R., Thompson, R.F., Santoro, R.D., and Vraga, H.W., 2017, U.S. Geological Survey Fact 2017-3046 [Supersedes USGS Fact Sheet 2008–3067.], Reston, VA.
- USGS 2017b. *WREG*, U.S. Geological Survey, Reston, VA.
- USGS 2019a. *SWToolbox*, U.S. Geological Survey, Reston, VA.
- USGS 2019b. *National Streamflow Statistics Program, NSS*, U.S. Geological Survey, Reston, VA.
- USGS 2021. *Precipitation Runoff Modeling System (PRMS)*, U.S. Geological Survey, Reston, VA.
- Viessman, W. and G. Lewis 2003. *Introduction to Hydrology*, Pearson Education, Inc., Upper Saddle River, NJ.
- Villarini, G., F. Serinaldi, J.A. Smith, and W.F. Krajewski 2009. "On the Stationarity of Annual Flood Peaks in the Continental United States During the 20th Century," *Water Resources Research*, 45(8).
- Vogel, R.M., C. Yaindl, and M. Walter 2011. "Nonstationarity: Flood Magnification and Recurrence Reduction Factors in the United States," *Journal of the Water Resources Association (JAWRA)* 47(3), 464-474.
- Wahl, T., S. Jain, J. Bender, S.D. Meyers, and M.E. Luther 2015. "Increasing Risk of Compound Flooding from Storm Surge and Rainfall for Major US Cities," *Nature Climate Change*, 5(12), 1093-1097.
- Wang, X., X. Yang, and Z. Cai 2019. *Next-Generation Rainfall IDF Curves for the Virginian Drainage Area of Chesapeake Bay*, Department of Defense Strategic Environmental



- Research and Development Program (SERDP), Project No. RC18-1569, Old Dominion University, Norfolk, VA.
- Watson, C.C., D. Dubler, and S.R. Abt 1997. *Demonstration erosion control project report*, Design Hydrology Investigations, Fort Collins, Colorado, submitted to U.S. Army Engineer Waterways Experiment Station, Vicksburg, MS.
- Watson, K.M. and R.D. Schopp 2009. *Methodology for Estimation of Flood Magnitude and Frequency for New Jersey Streams*, U.S. Geological Survey Scientific Investigations Report 2009-5167, Reston, VA.
- Weary, D.J. and D.H. Doctor 2014, *Karst in the United States: A Digital Map Compilation and Database*, U.S. Geological Survey Open-File Report 2014-1156.
- Webb, R.H. and R.D. Jarrett 2002. "One-Dimensional Estimation Techniques for Discharges of Paleofloods and Historical Floods," *Ancient Floods, Modern Hazards* (House, P.K., R.H. Webb, V.R. Baker, and D.R. Levish, eds.).
- Williams, G.P. 1978. "Bankfull discharge of rivers," *Water Resources Research*, 14(6), 1141-1154.
- WMO 1974. *International glossary of hydrology*, World Meteorological Organization, Geneva, Switzerland.
- WMO 2009. *Manual on Low-flow Estimation and Prediction, Operational Hydrology Report No. 50*, WMO-No. 1029, Koblenz, Germany.
- Wolman, M.G. and L.B. Leopold 1957. *River flood plains: Some observations on their formation*, Geological Survey Professional Paper 282-C, U.S. Government Printing Office, Washington, DC.
- Wolman, M.G. and J.P. Miller 1960. "Magnitude and frequency of forces in geomorphic processes," *Journal of Geology*, 68, 54-74.
- Woolhiser, D.A. 1996. "Search for Physically Based Runoff Model – A Hydrologic El Dorado?" *Journal of Hydraulic Engineering*, 122(3), 122-129.
- Wright, D.B., J.A. Smith, and M.L. Baeck 2014. "Critical Examination of Area Reduction Factors," *Journal of Hydrologic Engineering*, 19(4), 769-776.
- WSDOT 2019. *Hydraulics Manual*, Washington Department of Transportation, M 23-03.06.
- WV DOT 2007. "Influence of Karst Topography," *Drainage Manual* (Section 4.2.8), Third Edition, West Virginia Department of Transportation, Division of Highways, Engineering Division.
- Xie, P., R. Joyce, S. Wu, S.-H. Yoo, Y. Yarosh, F. Sun, and R. Lin 2020 (updated daily). *NOAA Climate Data Record (CDR) of CPC Morphing Technique (CMORPH) High Resolution Global Precipitation Estimates, Version 1*, Research Data Archive at the National Center for Atmospheric Research, Computational and Information Systems Laboratory, <https://doi.org/10.5065/OEFN-KZ90>, last accessed January 12, 2022.
- Yanosky, T.M. and R.D. Jarrett 2002. "Dendrochronologic Evidence for the Frequency and Magnitude of Paleofloods," in *Ancient Floods, Modern Hazards* (House, P.K., R.H. Webb, V.R. Baker, and D.R. Levish, eds.).
- Yu, X. and J.R. Stedinger 2018. "LP3 Flood Frequency Analysis Including Climate Change," *World Environmental and Water Resources Congress 2018: Watershed Management, Irrigation and Drainage, and Water Resources Planning and Management*, American Society of Civil Engineers, Reston, VA, 459-467.

- Yue, S., T. Ouarda, B. Bobee, P. Legendre, and P. Bruneau 1999. "The Gumbel Mixed Model for Flood Frequency Analysis," *Journal of Hydrology*, American Society of Civil Engineers, 226(1-2), 88-100.
- Zhang, L. and V.P. Singh 2006. "Bivariate Flood Frequency Analysis Using the Copula Method," *Journal of Hydrologic Engineering*, American Society of Civil Engineers, 11(2), 150-164.

# Appendix A - Units

<b>SI* (MODERN METRIC) CONVERSION FACTORS</b>				
<b>APPROXIMATE CONVERSIONS TO SI UNITS</b>				
<b>Symbol</b>	<b>When You Know</b>	<b>Multiply By</b>	<b>To Find</b>	<b>Symbol</b>
<b>LENGTH</b>				
in	inches	25.4	millimeters	mm
ft	feet	0.305	meters	m
yd	yards	0.914	meters	m
mi	miles	1.61	kilometers	km
<b>AREA</b>				
in <sup>2</sup>	square inches	645.2	square millimeters	mm <sup>2</sup>
ft <sup>2</sup>	square feet	0.093	square meters	m <sup>2</sup>
yd <sup>2</sup>	square yard	0.836	square meters	m <sup>2</sup>
ac	acres	0.405	hectares	ha
mi <sup>2</sup>	square miles	2.59	square kilometers	km <sup>2</sup>
<b>VOLUME</b>				
fl oz	fluid ounces	29.57	milliliters	mL
gal	gallons	3.785	liters	L
ft <sup>3</sup>	cubic feet	0.028	cubic meters	m <sup>3</sup>
yd <sup>3</sup>	cubic yards	0.765	cubic meters	m <sup>3</sup>
NOTE: volumes greater than 1000 L shall be shown in m <sup>3</sup>				
<b>MASS</b>				
oz	ounces	28.35	grams	g
lb	pounds	0.454	kilograms	kg
T	short tons (2000 lb)	0.907	megagrams (or "metric ton")	Mg (or "t")
<b>TEMPERATURE (exact degrees)</b>				
°F	Fahrenheit	5 (F-32)/9 or (F-32)/1.8	Celsius	°C
<b>ILLUMINATION</b>				
fc	foot-candles	10.76	lux	lx
fl	foot-Lamberts	3.426	candela/m <sup>2</sup>	cd/m <sup>2</sup>
<b>FORCE and PRESSURE or STRESS</b>				
lbf	poundforce	4.45	newtons	N
lbf/in <sup>2</sup>	poundforce per square inch	6.89	kilopascals	kPa
<b>APPROXIMATE CONVERSIONS FROM SI UNITS</b>				
<b>Symbol</b>	<b>When You Know</b>	<b>Multiply By</b>	<b>To Find</b>	<b>Symbol</b>
<b>LENGTH</b>				
mm	millimeters	0.039	inches	in
m	meters	3.28	feet	ft
m	meters	1.09	yards	yd
km	kilometers	0.621	miles	mi
<b>AREA</b>				
mm <sup>2</sup>	square millimeters	0.0016	square inches	in <sup>2</sup>
m <sup>2</sup>	square meters	10.764	square feet	ft <sup>2</sup>
m <sup>2</sup>	square meters	1.195	square yards	yd <sup>2</sup>
ha	hectares	2.47	acres	ac
km <sup>2</sup>	square kilometers	0.386	square miles	mi <sup>2</sup>
<b>VOLUME</b>				
mL	milliliters	0.034	fluid ounces	fl oz
L	liters	0.264	gallons	gal
m <sup>3</sup>	cubic meters	35.314	cubic feet	ft <sup>3</sup>
m <sup>3</sup>	cubic meters	1.307	cubic yards	yd <sup>3</sup>
<b>MASS</b>				
g	grams	0.035	ounces	oz
kg	kilograms	2.202	pounds	lb
Mg (or "t")	megagrams (or "metric ton")	1.103	short tons (2000 lb)	T
<b>TEMPERATURE (exact degrees)</b>				
°C	Celsius	1.8C+32	Fahrenheit	°F
<b>ILLUMINATION</b>				
lx	lux	0.0929	foot-candles	fc
cd/m <sup>2</sup>	candela/m <sup>2</sup>	0.2919	foot-Lamberts	fl
<b>FORCE and PRESSURE or STRESS</b>				
N	newtons	0.225	poundforce	lbf
kPa	kilopascals	0.145	poundforce per square inch	lbf/in <sup>2</sup>

\*SI is the symbol for the International System of Units. Appropriate rounding should be made to comply with Section 4 of ASTM E380. (Revised March 2003)

*Page Intentionally Left Blank*

## Appendix B - Introduction to Multivariate Analysis

Multivariate analysis provides expanded analytical tools to explore the interrelationships between variables useful for analyzing numerous engineering problems including flooding at river confluences and compound flooding. This appendix provides a brief introduction to multivariate analysis including a general formulation of the problem followed by descriptions of two multivariate tools: multivariate distributions and copulas.

### B.1 General Formulation of the Problem

Multivariate analysis typically includes two components: 1) establishing the marginal distributions of each variable and 2) describing the dependence between variables. The marginal distribution of a random variable is the probability distribution of that variable independent of any other value. That is, it is the univariate distribution. As described previously, the dependence relates to how one variable contributes to the other variable or how both variables can result from a common source.

Salvadori et al. (2007) discussed the multiple cases that can arise in hydrologic applications of multivariate statistics but can be described with the same formulation. First, consider the expression for an extreme event on one of the confluent streams (the marginal event) where “extreme” means exceeding a threshold value:

$$E_{X,x}^> = \{X > x\} \quad (\text{B.1})$$

where:

$$\begin{aligned} E_{X,x}^> &= \text{Event where the occurrence, } X, \text{ is greater than a threshold value } x \\ X &= \text{Magnitude of the event} \\ x &= \text{Threshold value for defining an event} \end{aligned}$$

Similarly, on the confluent stream:

$$E_{Y,y}^> = \{Y > y\} \quad (\text{B.2})$$

where:

$$\begin{aligned} E_{Y,y}^> &= \text{Event where the occurrence, } Y, \text{ is greater than a threshold value } y \\ Y &= \text{Magnitude of the event} \\ y &= \text{Threshold value for defining an event} \end{aligned}$$

These expressions represent an event where exceedance of a threshold value occurs on each stream individually. Depending on the objective of the analysis, the engineer may be interested in an extreme event occurring on X and Y simultaneously or, alternatively, an extreme event occurring on X or Y. The coincident extreme events for the “and” and “or” formulation, respectively, are:

$$E_{x,y}^{\cap} = \{X > x\} \cap \{Y > y\} \quad (\text{B.3})$$

$$E_{x,y}^{\cup} = \{X > x\} \cup \{Y > y\} \quad (\text{B.4})$$

The probability of the coincident extreme events shown in equations B.3 and B.4 are expressed as:

$$P_{x,y}^{\cap} = P(E_{x,y}^{\cap}) = P(X > x \cap Y > y) \quad (\text{B.5})$$

$$P_{x,y}^{\cup} = P(E_{x,y}^{\cup}) = P(X > x \cup Y > y) \quad (\text{B.6})$$

Let  $H(x, y)$  denote a joint bivariate distribution of two random variables,  $X$  and  $Y$ . The joint probability distribution function is:

$$H(x, y) = P[X < x, Y < y] \quad (\text{B.7})$$

If the marginal distributions of the random variables  $X$  and  $Y$  are given by  $F_x(x)$  and  $F_y(y)$ , then:

$$P_{x,y}^{\cap} = 1 - F_x(x) - F_y(y) + H(x, y) \quad (\text{B.8})$$

$$P_{x,y}^{\cup} = 1 - H(x, y) \quad (\text{B.9})$$

Equation B.8 expresses exceedance probability with the “and” formulation while equation B.9 expresses exceedance probability with the “or” formulation. As is apparent from these equations, the two formulations are related by the joint probability distribution  $H(x, y)$ . Salvadori et al. (2007) and Shiau et al. (2006) discuss use of these probability statements in substantial detail. The “and” formulation, as expressed in equation B.8, applies to the objectives of this chapter.

## ***B.2 Multivariate Distributions***

Bivariate distributions are a subset of multivariate distributions involving two random variables. A bivariate distribution is characterized by a distribution function, which is a scalar-valued function of a vector-valued random variable (in this case two random variables). In the limit of each random variable, a univariate distribution function results, termed the marginal distribution. So, for a distribution function  $H(x, y)$  there are two marginal distributions,  $F(x)$  and  $G(y)$ . Bivariate distributions have the same type of marginal distributions, that is, the same distribution function, although with different parameter values. Examples of bivariate distributions include the bivariate normal distribution and the bivariate Gumbel distribution. The latter can be developed in several forms.

As an example, Yue et al. (1999) presents results from application of the bivariate mixed-model Gumbel distribution to hydrologic problems. The bivariate mixed-model Gumbel distribution is:

$$H(x, y) = F(x)F(y) \exp \left\{ -\theta \left[ \frac{1}{\ln F(x)} + \frac{1}{\ln F(y)} \right]^{-1} \right\} \quad (\text{B.10})$$



where:

- $F(x)$  = The marginal Gumbel distribution on  $x$   
 $F(y)$  = The marginal Gumbel distribution on  $y$   
 $\theta$  = A dependence parameter

The dependence parameter is estimated as:

$$\theta = 2 \left[ 1 - \cos \left( \pi \sqrt{\frac{\rho}{6}} \right) \right] \quad (\text{B.11})$$

The dependence parameter,  $\theta$ , is a function of Pearson's correlation coefficient ( $\rho$ ) and reaches unity when  $\rho$  is  $2/3$ , indicating complete dependence in the Gumbel model. For values of  $\rho$  exceeding  $2/3$ , the bivariate mixed-model Gumbel distribution does not apply because the dependence parameter is undefined.

Multivariate distributions may include two (bivariate), three (trivariate), or more variables. They are characterized by fitting each of the variables with the same marginal distribution and linking the distributions with a dependence parameter. Kilgore et al. (2013) provides additional detail on bivariate distributions commonly used in hydrology.

### B.3 Copulas

Copulas are a more general approach to bivariate (or multivariate) problems. The term copula refers to a function, called the dependence function, used to link two univariate distributions in such a way as to represent the bivariate (or multivariate) dependence between the two random variables.

The potential of a copula is realized in that the copula is independent from the form of the univariate marginal distributions. That is, the marginal distributions of a copula are uniformly distributed on the interval (0,1). Therefore, the marginal distributions can be chosen such that they provide a best-fit of the univariate random variables, with the copula used to model the dependence behavior. Engineers can apply many copulas to bivariate (and multivariate) random variables. Hydrologists are typically most interested in those in the *Archimedean* family of copulas.

Bivariate copulas link two random variables,  $X$  and  $Y$ , with cumulative distribution functions of  $F_X(x)$  and  $F_Y(y)$ , respectively, by setting  $U = F_X(X)$  and  $V = F_Y(Y)$ . Then,  $U$  and  $V$  are uniformly distributed random variables and  $u$  will denote a specific value of  $U$  and  $v$  will denote a specific value of  $V$ . As described by Zhang and Singh (2006) the one-parameter Archimedean copula is:

#### Copula Families

Copulas are grouped in families based on common characteristics. The Archimedean family includes:

- Gumbel–Hougaard
- Clayton
- Ali–Mikhail–Haq
- Frank

Another family used in hydrology is the elliptical family which includes:

- Gaussian
- Student's  $t$

$$C_{\theta}(u,v) = \varphi^{-1}\{\varphi(u) + \varphi(v)\} \quad 0 < u,v < 1 \quad (\text{B.12})$$

where:

- $C_{\theta}(u,v)$  = Copula function with  $\theta$  representing the dependence parameter
- $\varphi$  = Copula generating function
- $u,v$  = Specific values of the uniformly distributed random variable U and V

Figure B.1 illustrates the probability surface for a copula with two variables. The variables U and V are distributed uniformly along the axes in the bottom plane. The copula (C) describes the joint probability. The **level curves** describe isoprobability lines increasing up to a value of 1 and the top of the surface. The shape of the surface varies with different copula generating functions and with alternative copula types.

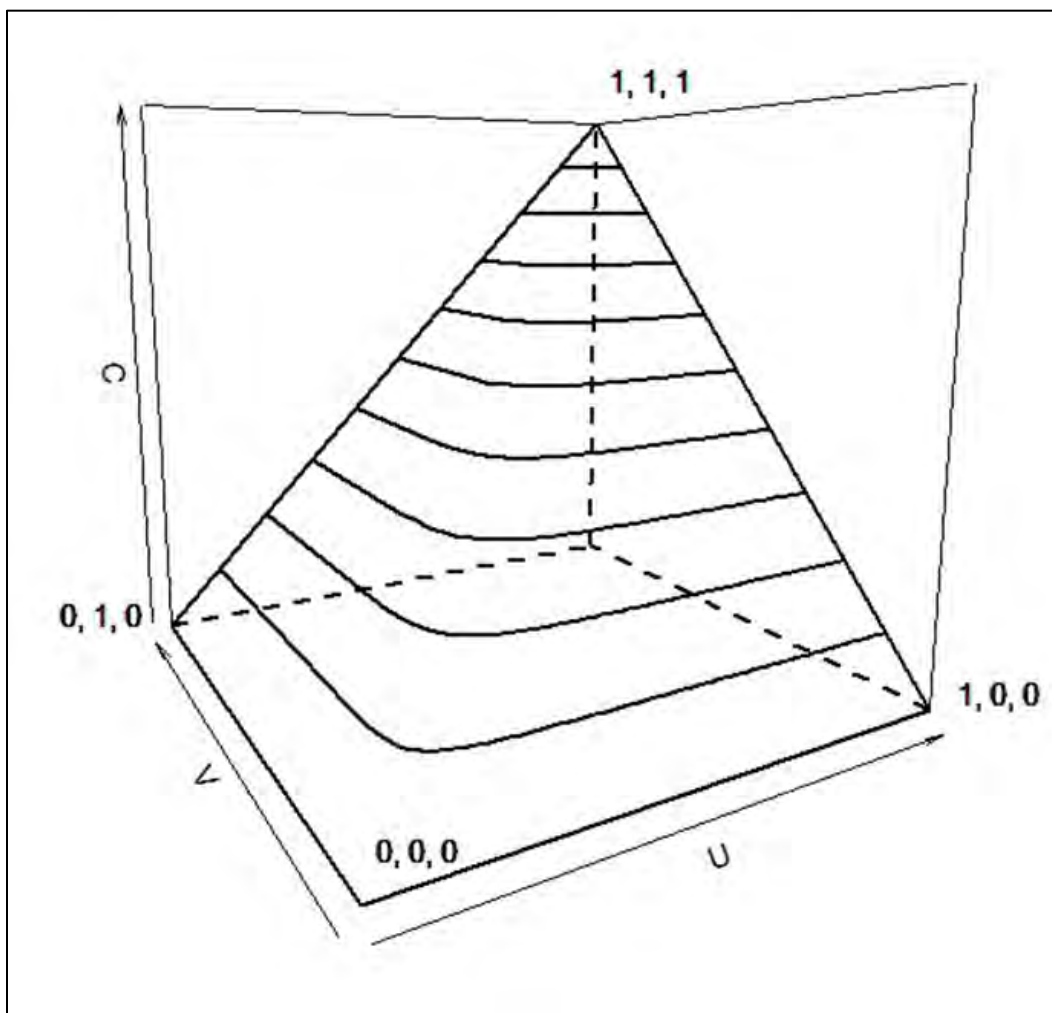


Figure B.1. Example of a joint probability surface for the Gumbel-Hougaard copula.

The copula,  $C_{\theta}(u,v)$ , is analogous to the distribution function,  $H(x,y)$  discussed in section B.2. Genest and Favre (2007) use the concept of a bivariate probability integrated transform (BPIT) to evaluate suitability of a given copula for a given application:

$$K(t) = t - \frac{\varphi(t)}{\varphi'(t)} \quad (\text{B.13})$$

where  $\varphi'$  is the derivative of  $\varphi$ .

As an example of a copula, the generating function for the Gumbel-Hougaard copula (Nelsen 2006) is:

$$\varphi(t) = -\ln(t)^\theta \quad (\text{B.14})$$

The corresponding copula is:

$$C_\theta(u, v) = \exp\left\{-\left[(-\ln(u))^\theta + (-\ln(v))^\theta\right]^{1/\theta}\right\} \quad \theta \in [1, \infty] \quad (\text{B.15})$$

where:

$\theta$  = The dependence parameter

The relation between Kendall's  $\tau$  and  $\theta$  is:

$$\tau = 1 - \theta^{-1} \quad (\text{B.16})$$

To develop the BPIT, determine the derivative of  $\varphi$ :

$$\varphi'(t) = -\frac{\theta}{t}(-\ln t)^{\theta-1} \quad (\text{B.17})$$

Like multivariate distributions, multivariate copulas may include two (bivariate), three (trivariate), or more variables. Each variable can be fit to its own marginal distribution with the marginal distributions linked by a dependence parameter. Kilgore et al. (2013) presents additional detail on copulas commonly used in hydrology. Genest and Favre (2007) provide an overview of the use of copulas for many hydrology applications.